The role of α-synuclein in the pathology of murine Mucopolysaccharidosis type IIIA

Kyaw Kyaw Soe

(MBBS, MSc)

Lysosomal Diseases Research Unit

South Australian Health and Medical Research Institute

and

Department of Paediatrics

School of Medicine, Faculty of Health Sciences

University of Adelaide

Thesis submitted for the degree of

Doctor of Philosophy

January 2017

TABLE OF CONTENTS

Chapter (3): Generation and characterisation of MPS IIIA mice deficient in α-synuclein

Chapter (4): Behavioural assessment of MPS IIIA mice deficient in α-synuclein

Chapter (7): Conclusions, Implications and Future directions

List of abbreviations

Autophagy	macroautophagy
CD-MPR	cation-dependent M6P receptor
CI-MPR	cation-independent M6P receptor
D31N	aspartic acid to asparagine change at codon 31
ELISA	enzyme-linked immunosorbent assay
G_{M2}	monosialoganglioside 2
G_{M3}	monosialoganglioside 3
HS	heparan sulphate
hr	hour(s)
IGF-II	insulin-like growth factor II receptor
Kb	kilobase (1000 base pairs of DNA or RNA)
kDa	kilodalton (unified atomic mass unit)
LC-MS/MS	liquid chromatography- tandem mass spectrometry
LSDs	lysosomal storage disorders
min	minute(s)
MPS	mucopolysaccharidoses
MPS IIIA	mucopolysaccharidosis type IIIA
MPS IIIA-$SNCA^{+/+}$	mucopolysaccharidosis type IIIA with intact α-synuclein
MPS IIIA-$SNCA^{+/-}$	mucopolysaccharidosis type IIIA with heterozygous α-synuclein
MPS IIIA-$SNCA^{-/-}$	mucopolysaccharidosis type IIIA with an absence of α-synuclein
MPTP	1-methyl-4-phenyl-1,2,3,6-tetrahydropyridine
NACP	precursor of non-Aβ component of Alzheimer disease amyloid
Normal mice	wild type mice ($SGSH^{+/+}$ $SNCA^{+/+}$)
PBS	phosphate buffered saline
PC12	pheochromocytoma cells of the rat adrenal medulla
sec	seconds
SGSH	sulphamidase
SNARE	soluble N-ethylmaleimide-sensitive factor attachment protein receptor
SNCA	α-synuclein

Thesis abstract

Lysosomal storage disorders are a heterozygous group of inherited metabolic disorders caused by a deficiency in one or more lysosomal enzymes, resulting in the accumulation of undegraded substrates in cells. Although specific enzymes deficits are the primary cause of specific lysosomal storage disorders, the underlying pathological mechanisms responsible for subsequent clinical features are largely unknown. About two-thirds of affected cases are associated with neurodegeneration with no effective therapies available due to the lack of understanding of the pathological mechanisms in the brain.

One of the foremost pathological events in several lysosomal storage disorders is the progressive accumulation of α-synuclein in the affected brain (Hamano et al., 2008a). α-Synuclein has long been known for its pathological involvement in Parkinson's disease and other neurological disorders, collectively known as 'synucleopathies'. Moreover, wild-type α-synuclein at physiological levels can impair lysosomal autophagy both *in vitro* and *in vivo*, but deletion of α-synuclein improves autophagy and clinical features in Huntington's disease mice (Corrochano et al., 2012; Tomás-Zapico et al., 2012).

Few studies have investigated the pathophysiological role of endogenous α-synuclein in lysosomal storage disorders *in vivo*. To address this issue, this study utilised a naturally occurring murine model of the neurological lysosomal storage disorder, mucopolysaccharidosis type IIIA (MPS IIIA; Sanfilippo syndrome type A) to investigate the role of α-synuclein in disease pathogenesis. MPS IIIA is an autosomal recessive disorder caused by the lysosomal deficiency of sulphamidase and the subsequent accumulation of heparan sulphate and secondary ganglioside substrates. Due to an inefficient degradation process, accumulation of aggregate-prone proteins such as α-synuclein was observed in MPS IIIA mouse brain as early as three-weeks of age and in humans with the disorder (Beard et al., unpublished).

In this study, MPS IIIA mice were crossed with α-synuclein knockout mice to create a colony of MPS IIIA mice deficient in α-synuclein. The progeny of these MPS IIIA mice (MPS IIIA-SNCA$^{+/+}$, MPS IIIA-SNCA$^{+/-}$ and MPS IIIA-SNCA$^{-/-}$) showed a similar clinical phenotype, such as coarse, apathetic facial features, hunched posture and aggressiveness toward cage mates. The α-synuclein-deficient MPS IIIA mice showed significant hypoactivity, increased anxiety, motor gait impairment, and reduced learning and memory abilities compared to normal

littermates in a battery of behavioural tests. Histopathological investigations confirmed the deposition of both primary and secondary substrates in the brains of MPS IIIA mice with or without the deficiency of α-synuclein. Moreover, preliminary studies have shown increased amounts of α-synuclein in native forms, instead of toxic oligomers, in congenic MPS IIIA brains and skin fibroblasts compared to wild-type normal tissues, possibly a result of a defect in lysosomal autophagy.

All MPS IIIA mice showed more than 30% loss in dopamine levels compared to normal mice, regardless of α-synuclein *SNCA* gene composition. This shows a possible functional link between MPS IIIA and the abnormal motor phenotypes observed. The results suggest that lysosomal dysfunction in the MPS IIIA brain may lead to impaired synthesis or trafficking of dopamine, or may result in selective loss of dopaminergic neurons in the substantia nigra. Further studies are needed to determine which of these scenarios underlie the observations made here.

Modification of α-Synuclein expression did not change the progressive proteinaceous accumulation (e.g. ubiquitin, phosphorylated-tau) or that of endo/lysosomal proteins (lysosomal integral membrane protein II) and neuroinflammatory proteins (glial fibrillary acidic protein) in MPS IIIA mice. It was also demonstrated that failure of fusion between autophagosomes and lysosomes in MPS IIIA mice resulted in the accumulation of ubiquitin-positive inclusions and toxic substrates (Settembre et al., 2008). Consequently, impaired lysosomal autophagy can also disrupt the continuous clearance of cytosolic proteins by the ubiquitin-proteasome system (Hara et al., 2006; Komatsu et al., 2006).

The major conclusion from this study is that deletion or deficiency of α-synuclein made little or no contribution to the clinical and neuropathological disease progression in MPS IIIA mice. The data suggest that defects in autophagy and/or ubiquitin-proteasome system may play the main pathological mechanism, and α-synuclein accumulation is a secondary downstream event and of itself is unlikely to contribute significantly to the pathogenesis of MPS IIIA.

Declaration

I certify that this work contains no material which has been accepted for the award of any other degree or diploma in my name, in any university or other tertiary institution and, to the best of my knowledge and belief, contains no material previously published or written by another person, except where due reference has been made in the text. In addition, I certify that no part of this work will, in the future, be used in a submission in my name, for any other degree or diploma in any university or other tertiary institution without the prior approval of the University of Adelaide and where applicable, any partner institution responsible for the joint-award of this degree.

I give consent to this copy of my thesis, when deposited in the University Library, being made available for loan and photocopying, subject to the provisions of the Copyright Act 1968. I also give permission for the digital version of my thesis to be made available on the web, via the University's digital research repository, the Library Search and also through web search engines, unless permission has been granted by the University to restrict access for a period of time.

Signed: …… **Date: ……**

Acknowledgements

I would like to express deepest gratitude to my supervisors, Dr. Kim Hemsley, and Professor John Hopwood, for their full support, expert guidance, understanding and encouragement throughout my research years. I am also thankful to them for bringing me to the world of research on lysosomal storage disorders and for giving me the opportunity to complete a fascinating and at times challenging Ph.D. journey at the Lysosomal Diseases Research Unit. Without their incredible patience and timely wisdom and counsel, my thesis work would have been a frustrating and overwhelming pursuit.

Many thanks to Dr. Adeline Lau for demonstrating standard techniques and procedures required for toe tagging and behavioural studies of mice. I would also like to thank Meghan Setford, Andrew Shoubridge, Sarah Tamang and Carly Thorsen for their invaluable input, thoughts and advice on animal monitoring, data recording and perfusion fixation technique; Lynn Garrard and her team for the daily care of the mouse colony (especially on weekends), and for helpful assistance with mouse handling and experimentation.

I wish to thank Helen Beard and Sofia Hassiotis for their insightful advice and guidance with the processing of brain tissues for immunostaining and protein quantification; Jim Manavis at IMVS and Ricky Williams for helping me with tissue embedding and image scanning. My histological work would not be possible without their expert help. I would also like to thank Dr. Stuart Howell for his expert statistical analysis of the data.

I gratefully acknowledge Barbara King for her patient demonstration and helpful advice on protein quantification and preparing tissue samples for Mass Spectrometry analysis; Leanne Winner for helping me in cell culturing and providing me skin fibroblast cells for biochemical analyses. I also would like to thank Lauren Whyte for demonstrating cell-based biochemical methods and for being a great PhD friend. I would like to express my sincere gratitude to Dr. Marten Snel, Dr. Paul Trim and Stephen Duplock for their expert guidance and technical help with Mass Spectrometry analysis.

I take this opportunity to record my sincere thanks to Dr. Anthony Fedele, Sandra Isenmann, Kathryn Hattersley, Tina Rozaklis, and Leanne Hein for their assistance, particularly with immunoblotting and general laboratory protocols; Dr. Tim Sargeant, Dr. Makoto Kamei, Dr.

Litsa Karageorgos and Dr. Lungisa Bickle for sharing their experience and advice on both work and non-work related matters. Their friendship, support, smiles and good humour made the working place truly enjoyable and lively.

I am greatly indebted to my family and friends outside of work for their constant encouragement, unconditioned love, care and support throughout the years, especially during difficult times when I was not well or home sick. Without their mental support and kind companionship in this long and challenging journey, I would not have been able to finish my study.

Last but not least, I would like to acknowledge the financial and technical support from the University of Adelaide to make it possible to finish. I am thankful to the South Australian Health and Medical Research Institute for providing me this opportunity to study in excellent research facilities.

Chapter (1)

Introduction and preliminary review

1.1 General introduction

Lysosomal storage disorders (LSDs) are a heterogeneous group of inherited metabolic diseases, which result from a defect in a lysosomal hydrolase, or an associated protein required for a cellular turnover. A sub-group of the LSDs, the mucopolysaccharidoses (MPS), represent 25% of all LSDs and are caused by a deficiency of one of the several lysosomal enzymes involved in the degradation of sulphated components of connective tissue known as mucopolysaccharides or glycosaminoglycans. The MPS disorders comprise MPS type I (Hurler/Scheie syndrome), MPS II (Hunter syndrome), MPS IIIA-E (Sanfilippo syndrome types A to E), MPS IVA-B (Morquio syndrome types A and B), MPS VI (Maroteaux-Lamy syndrome), MPS VII (Sly syndrome), and MPS IX (Natowicz syndrome).

MPS III refers to a group of five disorders arising from lysosomal deficiencies in different enzymes. Deficiencies of heparan-N-sulphamidase, α-N-acetylglucosaminidase, α-glucosaminide N-acetyltransferase, N-acetylglucosamine 6-sulphatase and N-sulphoglucosamine 3-O-sulphatase cause MPS IIIA, B, C, D, and E, respectively. Clinically, all five share similar features, most predominantly affecting the central nervous system leading to progressive neurological dysfunction, developmental regression, mental retardation, aggressive behaviour, and loss of learning ability, with premature death generally occurring in the second or third decade of life.

Although it is recognised that deficiency in the respective enzymes is the primary cause of MPS III, subsequent pathological cascades that lead to the development of clinical signs and symptoms are still unknown. Current therapeutic approaches are primarily symptomatic, and the development of effective treatments to alleviate the neuropathology has been hampered due to a lack of understanding of the complex pathophysiological processes involved, although human clinical trials of enzyme replacement and gene therapy are in progress for MPS IIIA.

Previous studies have demonstrated the accumulation of α-synuclein in the brains of MPS IIIA and other neurological disorders before clinical characteristics become visible. This study utilises these findings to investigate further and evaluate the role that α-synuclein accumulation plays in the development of pathology in MPS IIIA.

The literature review introduces the background of lysosomes and their functions, and discusses the biochemistry and clinical features of MPS IIIA. It also explores the primary and secondary substrate storage in MPS IIIA, with a particular focus on α-synuclein pathology and its role in several neurodegenerative disorders, especially lysosomal storage disorders.

1.2 The lysosome and its functions

Lysosomes were first identified and described as cytoplasmic particles containing acid hydrolases (De Duve et al., 1955). These dense, granular membranous sacs were named 'lysosomes' to reflect their primary digestive properties inside the cytoplasm. Using advanced electron microscopy, Novikoff et al. (1960) characterised lysosomes as membrane-bound intracellular organelles in the endocytic pathway. The diameter of these ubiquitous organelles ranges from 0.1-1.2 μm, and they can be further distinguished from other organelles by their acidic properties: (1) average pH 4.8 by a membrane ATP-driven H^+ pump; (2) their high density on Percoll gradients; and (3) the presence of lysosomal proteins (Hopwood and Brooks, 1997).

The three most important intracellular functions of lysosomes are endocytosis, phagocytosis, and autophagy **(Fig 1.1)**. Lysosomes digest the macromolecules taken by endocytosis or macropinocytosis and engulf extracellular pathogens such as microorganisms by phagocytosis (Saftig and Klumperman, 2009). They also degrade unused or expired intracellular components by autophagy (Shen and Mizushima, 2014). In the latter process, cytosolic proteins and entire organelles are encircled by a membrane to form an autophagosome, which later fuses with late endosomes to give rise to lysosomes (Shen and Mizushima, 2014). Cellular waste products such as proteins, carbohydrates, fats and other cytoplasmic macromolecules are broken down into simple compounds to generate building blocks in the cytoplasm (Appelqvist et al., 2013).

Accumulating evidence suggests that lysosomes have more complex functions than simply waste catabolism. Together with lysosome-related organelles such as melanosomes, lytic granules, and platelet-dense granules, they may play significant roles in plasma membrane repair, cholesterol homoeostasis, tissue remodelling, microorganism defence, cell signalling and death (Saftig and Klumperman, 2009). They are also involved in regulating ion homoeostasis, energy metabolism, autophagy and organelle biogenesis, antigen processing, and the immune system (Johnson et al., 2016).

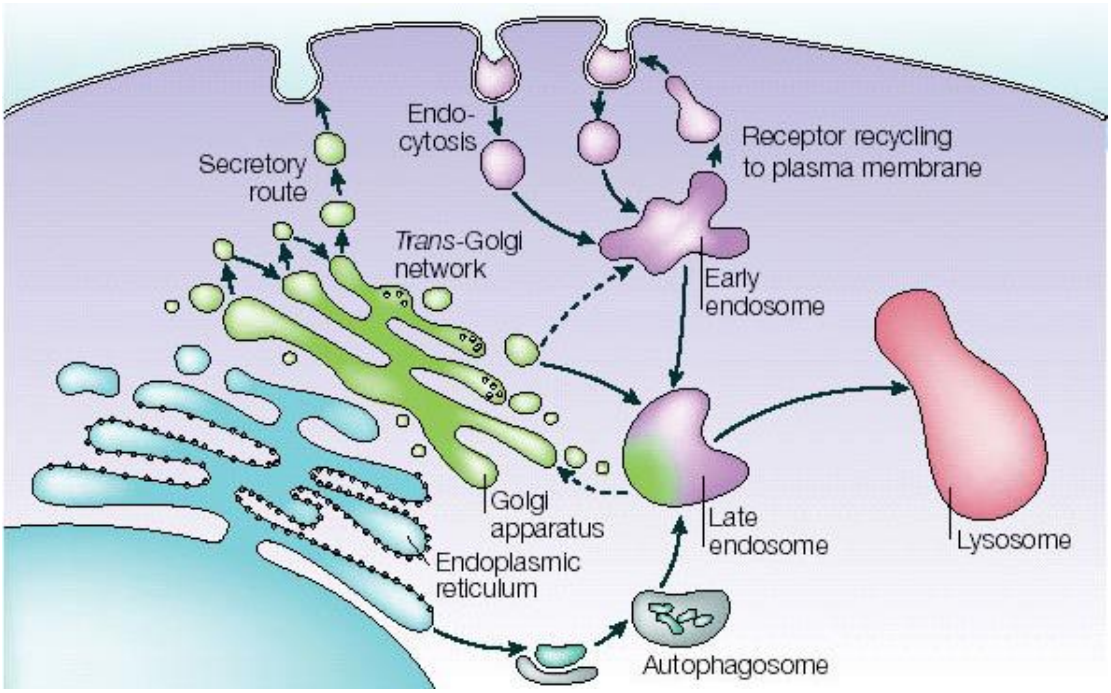

Figure 1.1: Endosomal-lysosomal system. Early endosomes are involved in receptor recycling and endocytosis pathways, while late endosomes are responsible for the breakdown of endocytosed components and connection with the trans-Golgi network.
Source: Jeyakumar et al., 2005

1.3 Biosynthesis of lysosomal enzymes

There are over 60 soluble enzymes in lysosomes for cellular digestion, which are manufactured in the rough endoplasmic reticulum and transported to the trans-Golgi network via the Golgi apparatus (Coutinho et al., 2012). The asparagine-linked oligosaccharides of these enzyme hydrolases sequentially react with UDP-N-acetylglucosamine 1-phosphotransferase (GlcNAc-1-phosphotransferase) and N-acetyl glucosamine-1-phosphodiester α-N-acetyl-glucosaminidase to generate the mannose 6-phosphate marker on the enzymes in the secretory pathway (Coutinho et al., 2012). It is where post-translational modifications such as phosphorylation, glycosylation, and proteolysis occur: for example, terminal mannose-6-phosphate residues are phosphorylated, which are highly attracted to mannose-6-phosphate receptors (Hopwood and Brooks, 1997).

1.4 Functions of mannose-6-phosphate receptors

These residues are recognised and bound by type I transmembrane mannose-6-phosphate glycoprotein receptors at pH 6.5-6.7 in the trans-Golgi network and release the enzymes as small clathrin-coated vesicles in late endosomes at pH 6 (Coutinho et al., 2012). When the hydrolases reach lysosomal pH 5 during endosomal maturation, they start to digest materials by endocytosis. Two types of extracytoplasmic mannose-6-phosphate receptors have been identified: (1) the 300-kDa cation-independent mannose-6-phosphate (CI-MPR)/-insulin-like growth factor II receptor (IGF-II) as a dimer in membranes; and (2) the 46-kDa cation-dependent mannose-6-phosphate receptor (CD-MPR) as a homodimer in membranes (Ghosh et al., 2003). Therefore, the mannose-6-phosphate-dependent targeting pathway is essential for translocating lysosomal acid hydrolases into the endo-lysosomal pathway for proper functioning.

In addition to binding to lysosomal enzymes, mannose-6-phosphate receptors have many diverse physiological functions and processes. CI-MPR binds to IGF-II and internalises it for degradation to prevent early accumulation of this hormone in embryonic development (Ghosh et al., 2003); it also promotes the maturation of transforming growth factor-1 and granzyme B uptake, which is necessary for cytotoxic-mediated apoptosis and takes part in tumour suppression (Ghosh et al., 2003). While mutant mice lacking both CI-MPR and IGF-II are viable, mice with only CI-MPR knockout accumulate IGF-II and die perinatally (Sohar et al., 1998). Primary skin fibroblasts lacking both mannose-6-phosphate receptors contain

undegraded materials in their endo-lysosomal pathway due to total impairment of lysosomal enzyme sorting.

1.5 Lysosomal storage disorders

LSDs are a heterogeneous group of inherited, congenital metabolic diseases, which result from a defect in a lysosomal hydrolase, or an associated protein required for cellular turnover (Pastores, 2011). Dr. Pompe described the first LSD in a seven-month old infant who presented with severe cardiomyopathy and massive glycogen storage in all tissues examined (Limongelli and Fratta, 2011). It was designated as Pompe disease or glycogen storage disease type II when it was shown to be caused by a deficiency of the lysosomal enzyme α-glucosidase (Hers, 1963).

At least 50 distinct LSDs are known, which are classified in groups according to the biochemical composition of the storage material. These groups are the mucopolysaccharidoses (MPS), sphingolipidoses, mucolipidoses, oligosaccharidoses, sialidoses and others (Pastores, 2011). The combined prevalence of LSDs is relatively high, with a reported incidence of 1 in 7700 live births in Australia (Meikle et al., 1999). The occurrence of Gaucher disease and Tay-Sachs disease in the Ashkenazi Jewish population is reported to be much higher with 1:855 (Felson, 2001) and 1:3900, respectively (Petersen et al., 1983).

The majority of LSDs are inherited in an autosomal recessive manner, except for Fabry disease and Hunter syndrome which are X-linked recessively inherited (Meikle and Hopwood, 2003). In all cases, however, the deficient or inactive function of a lysosomal enzyme or protein leads to the progressive accumulation of one or more substrates within the endo-lysosomal system, resulting in a gradual increase in size and number of these organelles. Deterioration in the functions of affected organs then occurs, including the central nervous system in some disorders, and subsequent progressive clinical symptoms (Neufeld, 1991).

1.6 The mucopolysaccharidoses (MPS)

Eleven enzymatic deficits are responsible for seven different mucopolysaccharidoses (MPS I, II, III, IV, VI, VII, and IX) **(Table 1.1)**. The MPS represent 25% of all LSDs, and are caused by deficiencies of lysosomal enzymes involved in the degradation of sulphated components of connective tissue known as glycosaminoglycans or mucopolysaccharides (Neufeld and Muenzer, 2001; Muenzer, 2004). The overall incidence of MPS may be as high as 1 in 22,000

individuals (Meikle et al., 1999). With the exception of X-linked recessive MPS II (Hunter syndrome), all the other MPS disorders are inherited in autosomal recessive manner and affect both males and females equally (Pastores, 2011).

The defective enzymes are responsible for the step-wise degradation of glycosaminoglycans, such as heparan sulphate (HS) (MPS I, II, III, VII), dermatan sulphate (MPS I, II, VI, VII), keratan sulphate (MPS IV), chondroitin sulphate (MPS IVA, VI), and hyaluronan (MPS IX), singly or in combination (Albano et al., 2000). Thus, glycosaminoglycan substrates accumulate within all lysosomes of different organs of the body, with increased amounts of these glycosaminoglycans detectable in the various biological samples used for diagnostic testing, for example: urine, blood, cultured skin fibroblasts and cerebrospinal fluid of affected patients (Neufeld and Muenzer, 2001). This storage leads to lysosomal dysfunction and subsequent cellular and tissue damage (Muenzer, 2011). A single enzyme deficiency can have a complex and high impact on individuals, with symptoms ranging from subtle somatic features, organomegaly, skeletal and vascular abnormalities to severe mental impairment.

The first literature on the MPS traces back to 1917 when Dr. Charles Hunter described two male siblings with coarse facial features, large abdomen, and bone dysplasia amongst other clinical symptoms (Hunter, 1917). A few years later, two unrelated boys with a similar disease morphology were reported by Dr. Gertrud Hurler (Hurler, 1920). Scheie syndrome was identified in 1962 when an American ophthalmologist described corneal opacity in an adult patient; found to result from the same lysosomal enzyme deficiency, it was recognised as an attenuated form of Hurler syndrome (Gifford et al., 1962).

In 1929, Dr. Luis Morquio (1929) reported a new form of congenital skeletal dystrophy, affecting four of five children born to Swedish consanguineous parents. This report, along with another publication on similar cases by Dr. Brailsford (1929), led to the identification of a new skeletal dystrophy with no organomegaly or cognitive impairment, which was later termed Morquio syndrome (MPS IV).

Table 1.1: Classification of the MPS disorders. HS = heparan sulphate; DS = dermatan sulphate; KS = keratan sulphate; CS = chondroitin sulphate; AR = autosomal recessive; XR = X-linked recessive. Table adapted from (Hopwood and Morris, 1990; Bhaumik et al., 1999; Albano et al., 2000; Giugliani, 2012; Kowalewski et al., 2012)

MPS type	Eponym	Stored substrates	Enzyme deficiency	Gene location (Inheritance)	Major clinical features	Prevalence in Australia
I	Hurler, Hurler-Scheie or Scheie	HS, DS	α-Iduronidase	4p16.3 (AR)	Mental retardation Skeletal deformities Short stature Hepatosplenomegaly	1: 88,000
II	Hunter	HS, DS	Iduronate-2-sulphatase	Xq28 (XR)	Mental retardation Skeletal deformities Short stature Hepatosplenomegaly	1: 136,000
III A	Sanfilippo A	HS	Heparan-N-sulphatase	17q25.3 (AR)	Mental retardation Hepatosplenomegaly	1: 114,000
III B	Sanfilippo B	HS	α-N-acetyl-α-glucosaminidase	17q21.1 (AR)	Mental retardation Hepatosplenomegaly	1: 211,000
III C	Sanfilippo C	HS	AcetylCoA α-glucosamine acetyltransferase	14p21 (AR)	Mental retardation Hepatosplenomegaly	1: 1,407,000
III D	Sanfilippo D	HS, KS	N-acetyl-glucosamine 6-sulphatase	12q14 (AR)	Mental retardation Hepatosplenomegaly	1: 1,056,000
III E	Sanfilippo E	HS	Arylsulphatase G	17q24.2 (AR)	No human case yet Learning difficulty in murine model	Unknown
IV A	Morquio A	KS, CS	D Galactosamine-6-sulphate sulphatase	16q24.3 (AR)	Skeletal deformities Short stature	1: 169,000
IV B	Morquio B	KS	β-Galactosidase	3p21.3 (AR)	Skeletal deformities Short stature	Unknown
VI	Maroteaus-Lamy	DS + CS	N-acetyl galactamine 4-sulphatase	5q11-q13 (AR)	Skeletal deformities Short stature Hepatosplenomegaly	1: 235,000
VII	Sly	HS, DS	β-Glucuronidase	7q21.11 (AR)	Mental retardation Skeletal deformities Short stature Hepatosplenomegaly	1: 2,111,000
IX	Natowicz	Hyaluronan	Hyaluronidase 1	3p21.3 (AR)	Skeletal deformities Hepatosplenomegaly	Unknown

The following year in France, a new form of bone deformity with the urinary elimination of chondroitin sulphate but without mental retardation was described by Maroteaux et al. (1963), and later termed Maroteaux-Lamy syndrome (MPS VI). Sly syndrome (MPS VII) was reported a decade later in an American boy with coarse facial features, multiple hernias, skeletal changes, hepatosplenomegaly, haematological abnormalities and mental retardation (Sly et al., 1973). A single hyaluronidase deficiency (MPS IX) case was reported in 1996 in a 14-year-old girl with short stature, bone deformities and multiple periarticular soft tissue masses (Natowicz et al., 1996). There were three new cases of MPS IX with joint deformities described in 2011 (Imundo et al., 2011).

Central nervous system pathology is also present with varying degrees in eight MPS disorders: MPS I, II, IIIA-E, and VII **(Table 1.1)** (Neufeld and Muenzer, 2001; Kowalewski et al., 2012). The neurodegenerative manifestations are devastating on patient quality of life and lifespan, and on families. Current treatments (primarily enzyme replacement therapy) to ameliorate the neurodegenerative features have not been successful due to the limited ability of replacement enzyme to penetrate the blood-brain barrier (Neufeld and Muenzer, 2001). Other forms of treatment are being researched and are discussed below.

1.7 Sanfilippo syndrome

Sanfilippo syndrome is the clinical name given to the MPS III group of disorders. They are the most common of the MPS disorders (de Ruijter et al., 2011), with an average incidence rate of 1 in 66,000 births in Australia (Meikle et al., 1999), 1.89 in 100,000 births in The Netherlands (Poorthuis et al., 1999) and 1.57 in 100,000 births in Germany (Baehner et al., 2005). MPS IIIA is more prevalent in Australia, UK, Canada, The Netherlands, and Germany, while type B is more common in South-Eastern Europe, in countries such as Italy and Greece (Whitley, 1993). Whilst MPS III patients have characteristic mild somatic features, the primary clinical feature is progressive neurodegeneration; diagnosis is still challenging, and many cases are likely to remain undiagnosed or misdiagnosed (Albano et al., 2000).

Sanfilippo syndrome was first reported by Sanfilippo et al. (1963), who studied eight patients with varying degrees of mental retardation, hepatosplenomegaly, and HS-uria; five of the children were girls, and three were boys ranging in age from 1.5 to 10 years. Only three exhibited characteristic coarse facial features while five others had a non-specific or healthy

appearance. While hepatomegaly was observed in seven out of eight, only two patients presented with short stature. Liver biopsy, bone marrow biopsy, and inflammatory cycle studies demonstrated signs of an MPS disorder, such as excessive metachromatic staining. These studies were the first reports of a new disorder of mucopolysaccharide metabolism, which was later termed “MPS III or Sanfilippo syndrome”.

The five sub-types of Sanfilippo syndrome (MPS types A to E; **Table 1**) are caused by a deficiency of one of four lysosomal enzymes involved in the degradation of HS (Pastores, 2011), except for MPS III type C, which results from a deficiency in the lysosome transmembrane protein α-glucosaminide acetyltransferase. Thus, HS is the only glycosaminoglycan stored in Sanfilippo patients. MPS IIIE was recently identified in mice to result from a deficiency of arylsulphatase G (Kowalewski et al., 2012): affected mice showed HS accumulation in visceral organs and the central nervous system, causing neuronal cell death and behavioural problems (Kowalewski et al., 2012); humans with MPS IIIE are yet to be reported.

1.8 Sanfilippo syndrome type A (MPS type IIIA)

MPS IIIA is caused by a mutation in the N-sulphoglucosamine sulphohydrolase gene on chromosome 17q25.3, which encodes lysosomal heparan N-sulphatase (sulphamidase; or N-sulphoglucosamine sulphohydrolase, SGSH) (EC 3.10.1.1) (Kresse and Neufeld, 1972; Scott et al., 1995; Lee and Kamitani, 2011; Muenzer, 2011). The prevalence of MPS IIIA is around 1 per 114,000 live births in Australia (Meikle et al., 1999). The functional defect in SGSH leads to the progressive accumulation of HS in lysosomes, and its excretion in body fluids such as urine (Kresse, 1973). Profound SGSH deficiency was first documented in cultured skin fibroblasts and leucocytes in affected patients, whereas only a partial reduction in enzyme activity was found in heterozygous carriers (Kresse and Neufeld, 1972).

SGSH belongs to the sulphatase family, whose members share similar physical structures and active site characteristics such as a divalent metal binding site, a catalytic formylglycine site and a sulphate-binding site (Sidhu et al., 2014). There are more than 100 mutations reported to cause MPS IIIA (Sidhu et al., 2014). Some, however, are of particular interest as they replace highly conserved amino acid residues that involve catalytic function. For example, the replacement of a highly conserved lysine with arginine (Arg 282) disrupts the binding site for

the N-linked sulphate substrate with a SGSH (Sidhu et al., 2014). SGSH acts to cleave the N-linked sulphate group from the non-reducing terminal glucosamine residues of HS and heparin in mammalian cells (Sidhu et al., 2014).

The enzymatically active sequence of SGSH consists of an open reading frame of 1506 nucleotides, encoding 502 amino acid proteins (Scott et al., 1995). Cleavage of signal peptide occurs after amino acid 20, immediately before the start of the N-terminal amino acid sequence of the mature enzyme (Scott et al., 1995).

The *SGSH* gene spans approximately 11 kb and can be split into eight exons (Karageorgos et al., 1996) **(Fig 1.2 A)**. Northern blots on different somatic tissues have shown that the *SGSH* gene produces a 3.1 kb mRNA transcript in most tissues, along with 4.3 kb and 7.1 kb transcripts. The mature enzyme is predicted to have a molecular mass of 54,679 Da, consistent with the estimated 56 kDa from purified human liver SGSH (Scott et al., 1995). SGSH was purified from human urine and shown to efficiently degrade stored $^{35}SO_4^{=}$-labelled HS in MPS IIIA cultured skin fibroblasts (Kresse and Neufeld, 1972).

Human SGSH consists of monomeric and dimeric forms. The monomeric enzyme comprises a larger N-terminal domain 1 and a smaller C-terminal domain 2, centred on a β-sheet **(Fig 1.2 B)**. Domain 1 is formed by eight β-strands and nine α-helices on each side of the core, while domain 2 is made up of a four-stranded antiparallel β-sheet surrounded by four α-helices (Sidhu et al., 2014). Two monomers covalently bind to form a butterfly-shaped dimer **(Fig 1.2 C)**.

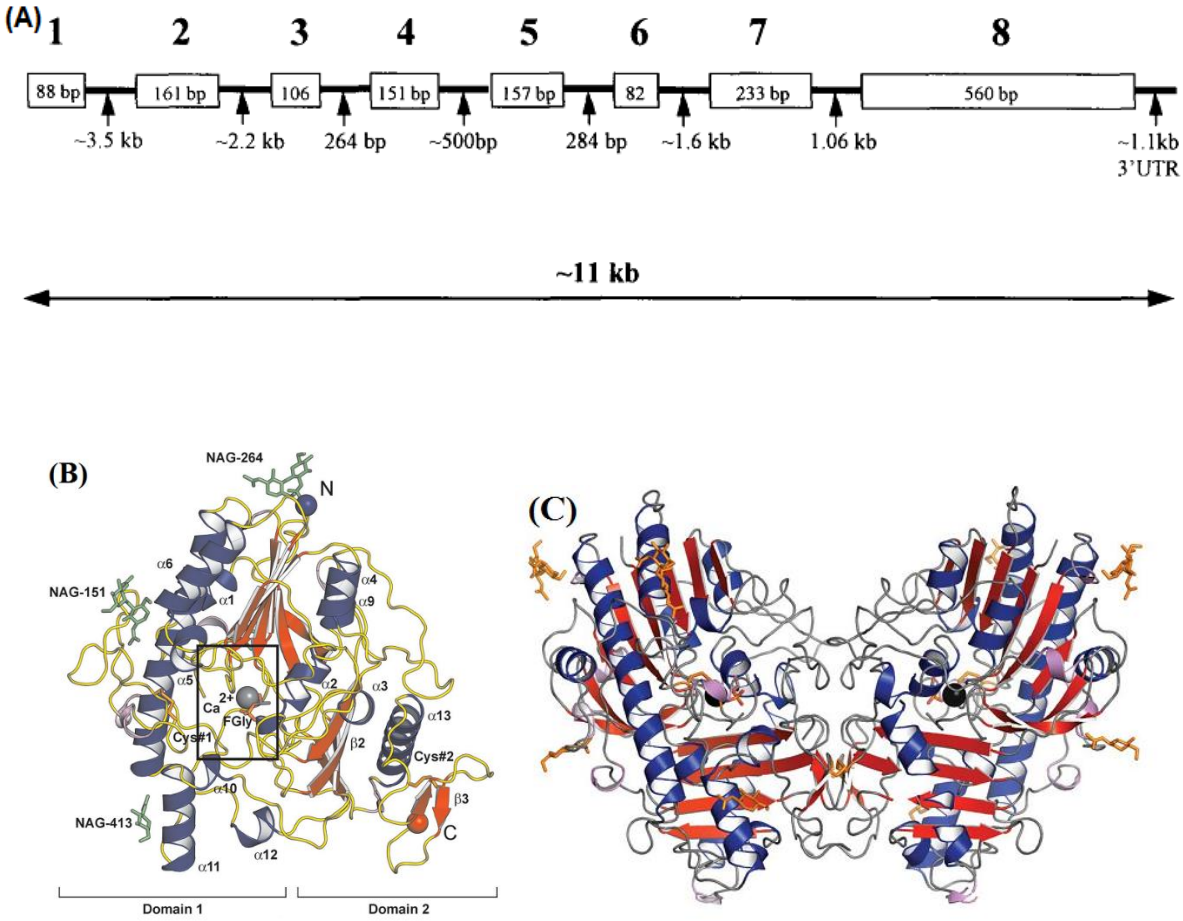

Figure 1.2: (A) The human sulphamidase gene. Source: Karageorgos et al., 1996

(B) The monomeric form, and (C) dimeric form of sulphamidase.

Source: Sidhu et al., 2014

1.9 Clinical presentations of Sanfilippo syndrome

Sanfilippo syndrome patients typically develop mild phenotypic features with severe progressive neurological dysfunction after a period of normal development for one- to two-years (Valstar et al., 2008). As seen in **Table 1.2**, the most frequent clinical symptoms in MPS III patients are behavioural problems and sleep disturbances (Valstar et al., 2010). Early developmental failure can be observed between the ages of three- to five-years, along with upper respiratory tract infections (Valstar et al., 2010).

Clinically, disease progress is generally divided into three phases, even though marked variation can exist between individuals **(Table 1.3)**. The first phase (between the ages of one- to four-years) is associated with regression in language ability and delay in general development (Cleary and Wraith, 1993); the second phase (between the ages of three- to four-years) is associated with the development of neurocognitive signs such as (Cleary and Wraith, 1993); the third or final phase is associated with profound motor retardation, inability to feed, toilet or communicate, and patients are generally confined to a wheelchair. Premature death is common – usually in the second or third decade of life - usually due to respiratory infections (Valstar et al., 2008).

Table 1.2: Frequency of clinical signs in Sanfilippo patients.

Source: Valstar et al., 2010

Symptom	Frequency (ratio of number of patients/ total number)	Percentage
Development		
- Delay < 3 years	39/76	51%
- Delay < 5 years	72/76	95%
Behaviour		
- Behavioural problems	84/87	97%
- Sleep problems	76/79	96%
- Recurrent ear, nose and throat infections	61/70	88%
- Diarrhoea	59/72	82%
Hernias		
- Umbilical hernia	15/45	33%
- Inguinal hernia	26/53	49%

Table 1.3: Three phases of clinical presentation in Sanfilippo syndrome.

Table adapted from Cleary and Wraith, 1993; Valstar et al., 2010

First phase (~1 - 4 years of age)	**Second phase (~3 - 4 years of age)**	**Third phase (> 5 years onwards)**
- Developmental delay - Delayed acquisition of speech - Regression of language abilities	- Temper tantrums - Hyperactivity - Attention deficit - Aggressive behaviour - Panic attacks in unfamiliar environments - Sleep disturbance - Severe dementia	- Ataxia, spasticity - Confinement to wheelchair - Swallowing problems - Seizures - Age of death ~ 18 years (range 6–59 years)

1.10 Diagnosis and therapeutic approaches for MPS disorders

The quantitation of isolated urinary HS is used as a screening process for the detection of MPS III disorders, but it has been reported to have high false-negative and false-positive results (Mahalingam et al., 2004). Therefore, qualitative analysis by multi-solvent sequential thin layer chromatography should also be coupled to assist the diagnosis (Mahalingam et al., 2004). The gold standard for diagnosis of all MPS III types is the measurement of enzyme activity in cultured fibroblasts, plasma or leucocytes (Muenzer, 2011). Early and accurate diagnosis is undoubtedly essential to identify patients before irreversible damage has occurred, particularly neurological (Hassiotis et al., 2014), as well as to identify other affected siblings in the family and to offer accurate prenatal counselling (Staretz-Chacham et al., 2009).

No curative therapy is currently available for MPS III, so regular follow-up, palliative surgeries and supportive care under a multidisciplinary clinical team are the primary symptomatic treatments (Muenzer, 2011). Several therapeutic strategies have been proposed to improve or reverse the natural course of disease pathology. Bone marrow stem cell transplantation, enzyme replacement therapy, gene therapy and substrate reduction therapy are amongst the most common.

Bone marrow transplantation is being used to treat neurological MPS I but it must be applied before clinical symptoms are evident to improve chances of success (Hopwood et al., 1993; Staba et al., 2004); enzyme replacement therapy is being used for the non-neurological forms of MPS I, II and MPS VI (Peters and Steward, 2003; Muenzer, 2011). Both forms of treatment have been effective (with some limitations in the effective treatment of some areas of pathology such as bone and joints) particularly if it is initiated early in the disease course (Muenzer, 2011). Although bone marrow transplantation has been successfully used to treat some LSDs such as MPS I, MPS IVA, MPS VI, metachromatic leucodystrophy and Krabbe disease (Boelens et al., 2010; Chinen et al., 2014), its therapeutic application to neurological MPS II and the MPS III group of disorders is still limited (Sivakumur and Wraith, 1999; Vellodi et al., 1999; Lau et al., 2010). The effective delivery of enzyme replacement to the central nervous system remains a major challenge, and human clinical trials of regular long-term administration of enzyme directly into the cerebrospinal fluid in MPS II and MPS IIIA patients are underway (www.clinicaltrials.gov identifiers: NCT02055118 and NCT01299727). However, there are

significant side-effects from both treatments such as graft-versus-host disease and life-threatening anaphylaxis (Muenzer, 2011).

Other therapeutic strategies for MPS are also being researched, and include substrate reduction therapy, gene therapy, and molecular chaperones. Substrate reduction, which aims to inhibit the synthesis of substrates, has been trialled in other LSDs such as Gaucher disease and Niemann-Pick disease type C patients as a secondary intervention (Schiffmann et al., 2008; Patterson et al., 2010). Inhibition of glycosaminoglycan synthesis by genistein and subsequent reduction in liver lysosome compartment size in MPS IIIB mice until 8-weeks of age has been reported (Malinowska et al., 2009). However, no changes in lysosomal size, total glycosaminoglycan level, or astrogliosis were observed in the brain cortex after 8 weeks of treatment, possibly due to the short-term study (Malinowska et al., 2009).

Intraparenchymal administration of adeno-associated viral vectors carrying the sulphamidase gene in both newborn and adult MPS IIIA mice and MPS IIIA dogs significantly reduced substrate accumulation in regional brain areas, and mediated behavioural improvements (Fraldi et al., 2007; Haurigot et al., 2013; Winner et al., 2016); preliminary clinical trial data demonstrates the safety of an AAVrh10-based gene therapy approach in MPS IIIA patients (Tardieu et al., 2014). Moreover, intravenous injection of AAVrh74 vector carrying the human sulphamidase gene into 4-6 week old MPS IIIA mice resulted in significant restoration of sulphamidase activity with subsequent clearance of CNS and somatic heparan sulphate storage, improved behaviour performance, and significantly extended survival (Duncan et al., 2015). Sorrentino et al. (2013) have also recently shown that intravenous injection of an AAV2/8-vector carrying modified SGSH to adult MPS IIIA mice corrected both brain pathology and behavioural manifestations.

1.11 MPS IIIA animal models

Studying animal models of human disease is useful for a better understanding of disease pathogenesis, severity and progression. Small animals such as rodents are advantageous as they genetically homogenous, are easy to breed and can be tested in large sample sizes for statistical analysis. Large animals such as dogs can also be useful for their longer lifespan and increased size which may better reflect human disease pathology.

Several animal models for MPS III have been identified and studied, but this thesis focuses on models of MPS IIIA. Two naturally-occurring canine models of MPS IIIA - Huntaway dogs (Jolly et al., 2000) and Dachshund dogs (Fischer et al., 1998; Jolly et al., 2000) - and a naturally-occurring murine model of MPS IIIA (Bhaumik et al., 1999) have been identified. The murine model was selected for this study because it replicates many of the clinical features in human MPS IIIA and it has been extensively characterised and studied both behaviourally and histo-biochemically.

The murine model was first described by Bhaumik et al. (1999), and was identified in a collaborative study between the Albert Einstein College of Medicine in New York, USA, and the Lysosomal Diseases Research Unit at the Women's and Children's Hospital in Adelaide, Australia (Bhaumik et al., 1999). The murine mutation arose spontaneously during attempts to produce a targeted mutation in the $Mgat_3$ gene (Bhaumik et al., 1999).

The MPS IIIA mice were originally on a mixed genetic background, predominantly 129SvJ and CD1, with some involvement of C57BL/6 and SJL strains (Bhaumik et al., 1999). A single point mutation (G to A) was identified at nucleotide position 91 (G91A) with a corresponding amino acid change from aspartic acid to asparagine (D to N) at position 31 (D31N) (Bhattacharyya et al., 2001). In consequence, the catalytic function of SGSH is severely affected. However, when the mutation was expressed in CHO-K1 cells, approximately 3% residual SGSH activity was present (Bhattacharyya et al., 2001).

The mixed strain was crossed with the stable and defined C57BL/6 strain to obtain offspring with long-term stability and genetic homogeneity (Crawley et al., 2006). Heterozygotes were backcrossed to C57BL/6 mice for 10 generations to create a congenic colony (B6.Cg-$Sgsh^{mps3a}$), whose phenotype and neuropathological changes have since been extensively studied (Crawley et al., 2006). Congenic MPS IIIA mice display similar disease characteristics to those described in humans **(Fig 3.1)**. At birth, they are indistinguishable from normal. They start to exhibit a unique phenotype by seven- to eight-weeks of age, with facial dysmorphism, skin thickening, dishevelled fur, and hepatosplenomegaly (Crawley et al., 2006). Moreover, a distinct hunched posture due to a mild skeletal deformity can be observed with increasing age.

Congenic MPS IIIA mice become hypoactive by 12- to 15-weeks of age in an Open Field test, and show less anxiety by exploring open arms more often than their normal counterparts in an

Elevated Plus maze test by 18-weeks of age (Lau et al., 2008). Their neuromuscular grip strength and negative geotaxis are affected as early as six-weeks of age (Crawley et al., 2006). Moreover, severe memory and spatial learning impairments become evident by 20-weeks of age, determined by the Morris water maze test (Crawley et al., 2006). Pathologically, accumulation of HS, ubiquitin-positive spheroids, and GM_2 ganglioside can be detected in various brain regions (Crawley et al., 2006). The lifespan of MPS IIIA congenic mice is approximately nine- to 12-months of age (Crawley et al., 2006).

The naturally occurring congenic C57BL/6 MPS IIIA mouse strain has many advantages over engineered and mixed strains. Most other MPS murine models are also on a C57BL/6J background (for example, MPS I, MPS II, MPS IIIB, MPS IVA and MPS VII), which allows direct comparisons with the congenic MPS IIIA model. Moreover, the C57BL/6 strain is the most widely used inbred strain, with a long lifespan, easy breeding, and robustness. However, it is predisposed to certain clinical features such as age-related hearing loss, cataracts, dermatitis, microphthalmia, anophthalmia, malocclusion, barbering, ulcerative dermatitis and hydrocephalus (Burkholder et al., 2012). The congenic MPS IIIA mouse model was utilised in this study.

1.12 Primary storage pathology: glycosaminoglycans

1.12.1 Structure and functions of glycosaminoglycans

The most important pathological feature in the MPSs is the primary accumulation of glycosaminoglycans (or mucopolysaccharides) in cells. Glycosaminoglycans are a group of negatively-charged hetero-polysaccharides ubiquitous in all mammalian tissues (Miller et al., 2014). The glycosaminoglycans consist of sulphated compounds such as chondroitin sulphate, HS, dermatan sulphate, keratan sulphate, and non-sulphated hyaluronan (Miller et al., 2014). The polysaccharide chains in dermatan sulphate, HS, and chondroitin sulphate are composed of alternating residues of uronic acid and sulphated hexosamine, while galactose replaces uronic acid residues in keratan sulphate (Miller et al., 2014). Glycosaminoglycans have numerous vital cellular functions such as maintaining hydrostatic pressure to stabilise connective tissues, binding covalently with proteoglycans to regulate cellular function, and acting together with cell surface proteins via receptors to modulate the surrounding biological area (Miller et al., 2014).

Proteoglycans are a group of mixed species which possess a protein core upon which one or more glycosaminoglycans are covalently bound (Schaefer, 2014). In addition to being integral components of connective tissues, glycosaminoglycan-proteoglycan complexes can also be found ubiquitously in the nucleus, extracellular matrix and cell membrane (Kjellén and Lindahl, 1991). They play several roles in cell proliferation, cell-cell recognition and adhesion, matrix formation and cell-matrix interactions (Schaefer, 2014).

1.12.2 Degradation of glycosaminoglycans

Proteoglycans and their fragments are completely degraded into monosaccharides, sulphate and amino acids in the lysosome. The first degradation occurs at the cell surface, matrix or in endosomes by proteases into peptides, and by endoglycosidases into oligosaccharide fragments (Hopwood and Morris, 1990). When translocated to lysosomes, these glycosaminoglycan fragments are further degraded sequentially by a series of exohydrolases (glycosidases and sulphatases), beginning at the non-reducing end of the sugar chain, into free monosaccharides and sulphate (Hopwood and Morris, 1990).

Deficient activity of any single glycosidase, N-acetyltransferase or sulphatase in lysosomes can cause lysosomal storage and urinary excretion of partially-degraded glycosaminoglycan products in MPS disorders (Hopwood and Morris, 1990). HS degradation is affected in MPS types I, II, III and VII. The synthesis, degradation and abnormal deposition of HS due to enzyme deficiency are discussed below.

1.12.3 Heparan sulphate metabolism

HS is made up of repeating disaccharide units of uronic acid alternating with α-linked glucosamine residues, and is bound to various proteins at the cell surface and in the extracellular matrix (Miller et al., 2014). HS is present in many tissues and is a major component of proteoglycans such as perlecan and agrin, which are secreted into the extracellular matrix (Miller et al., 2014). Similar to other glycosaminoglycans, HS is functionally involved in cell growth and development, cell-cell interactions, infection, coagulation, and lipid metabolism by binding with proteases, growth factors and chemokines (Clarke et al., 2012).

HS degradation is the most complex of the glycosaminoglycans, and involves the sequential action of three glycosidases, three sulphatases and one acetyltransferase **(Fig 1.2)** (Neufeld and

Muenzer, 2001). Deficiency in any of these enzymes leads to massive storage of HS as well as secondary metabolites in the central nervous system, leading to profound and progressive neurodegeneration in affected patients (Neufeld and Muenzer, 2001).

Lysosomal storage of numerous cytoplasmic membrane-bound vacuoles filled with undegraded whorl-like granular materials can be seen in a cerebral cortical neurone in congenic MPS IIIA mice by electron microscopy **(Fig 1.3 A, B, C)** (Crawley et al., 2006). Small to large lysosomal inclusions containing packed granular material can also be observed in cerebellar Purkinje cells in young MPS IIIA mice **(Fig 1.3 D, E)** (Crawley et al., 2006). These granular structures are gangliosides G_{M2} and G_{M3} (Crawley et al., 2006).

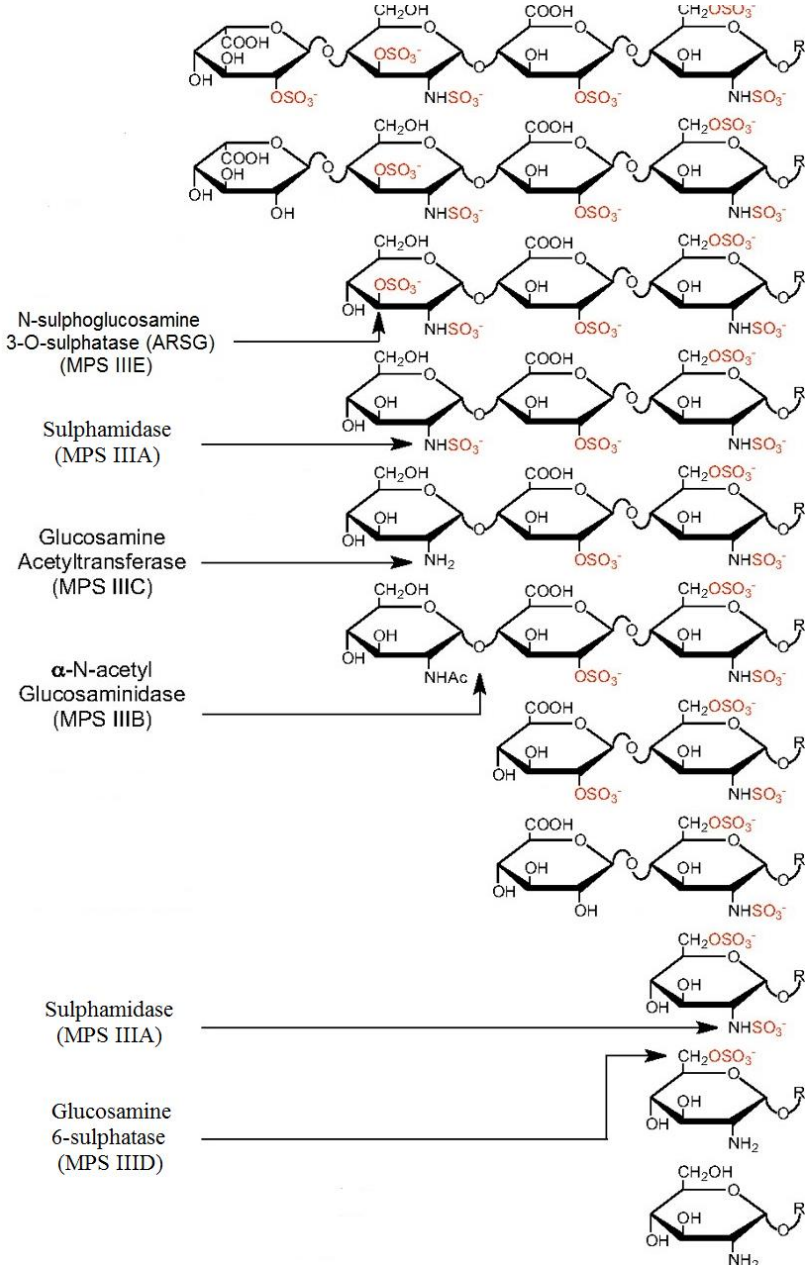

Figure 1.2: Step-wise sequential degradation of heparan sulphate.

The diagram shows the sequential catabolism of a non-reducing end tetrasaccharide-containing N-sulphoglucosamine-3-O-sulphate by nine different enzymes. The disorders caused by the respective enzyme deficiencies are indicated.

Source: Kowalewski et al., 2012

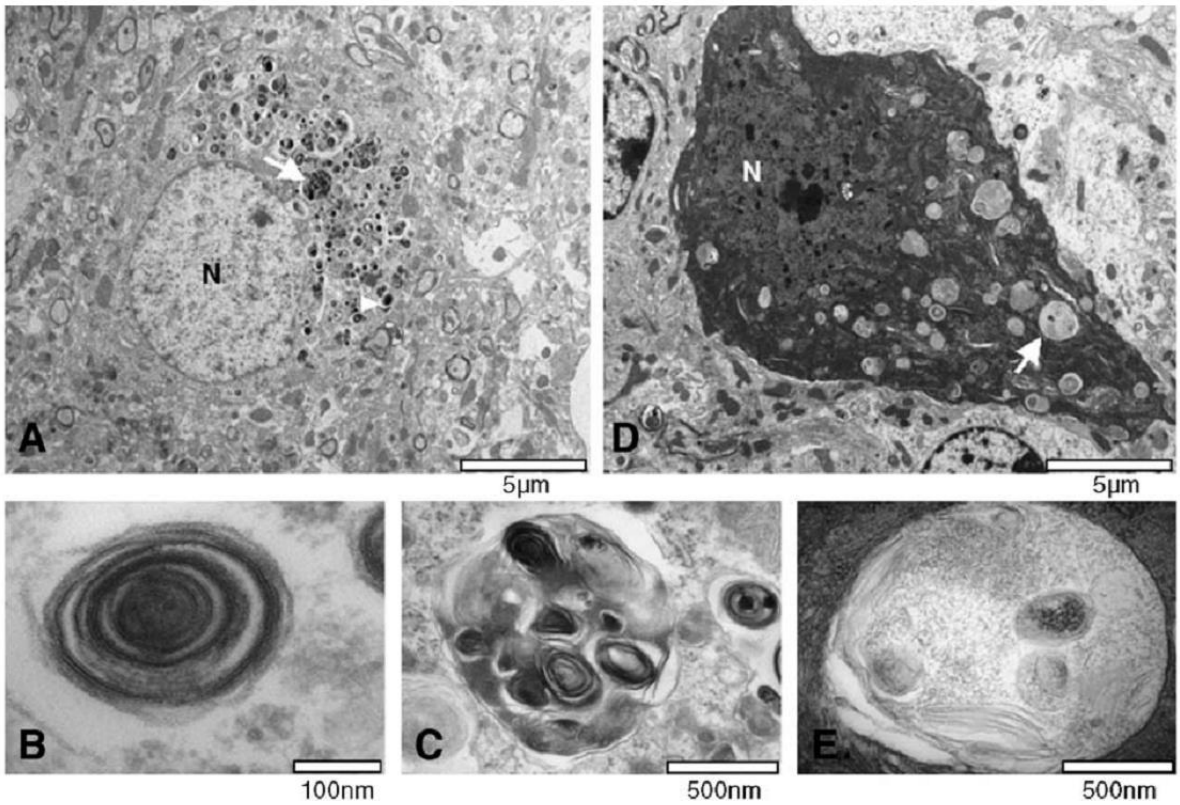

Figure 1.3: Electron micrographs showing cytoplasmic inclusions in brain cells.

(A) Electron-dense inclusions of various sizes, from small membranous whorls (enlarged in B) to large multivesicular bodies (enlarged in C) of a neurone are seen in the cerebral cortex of a six-month old congenic MPS IIIA mouse. (D) Large cytoplasmic inclusions (enlarged in E) containing packed granular material in a Purkinje cell are seen in the cerebellum of a six-week old congenic MPS IIIA mouse.

Source: Crawley et al., 2006

1.13 Secondary pathology

1.13.1 Gangliosides, microglia, neuroinflammation and cell death

Besides HS accumulation, accompanying sequestration of glycosphingolipids such as G_{M2} and G_{M3} gangliosides have been documented in MPS I, II, MPS IIIA-E and MPS VII (Constantopoulos and Dekaban, 1978; Constantopoulos et al., 1980; McGlynn et al., 2004). Glycosphingolipid deposition is believed to be caused by secondary inhibition of glycosphingolipid-degradative enzymes (neuraminidase and sialidase) by intracellular glycosaminoglycan accumulation (McGlynn et al., 2004). Glycosphingolipids and cholesterol are usually co-localised to specialised microdomains known as 'membrane rafts', which are crucial in neuronal signal transduction (Lozano et al., 2013).

Glycosphingolipid accumulation may also contribute to neuronal dysfunction in MPS because of defects in the composition, trafficking, and recycling of lipid raft components (McGlynn et al., 2004). As the accumulation of gangliosides has been shown to precede behavioural abnormalities in MPS IIIA and MPS VII mice, secondary substrate storage may be a precursor to neuroinflammation and brain degeneration (Kaidonis et al., 2016). Inhibiting the synthesis of glycosphingolipids in the brain with N-butyldeoxynojirimycin reduced cytokine gene expression, neuroinflammation and improved the learning ability in MPS IIIA mice (Kaidonis et al., 2016).

Accumulation of HS and gangliosides may also predispose activation of microglia and astrocytes. Increased isolectin B4-positive microglial activation has been observed in MPS IIIA (Hemsley et al., 2007), MPS I and MPS IIIB (Ohmi et al., 2003; Ausseil et al., 2008), Sandhoff disease (Wada et al., 2000) and MPS VII (Richard et al., 2008). Also, activated glial fibrillary acidic protein showing astrogliosis has been reported in MPS IIIA (Savas et al., 2004), and human and murine MPS IIIB (Villani et al., 2007; Hamano et al., 2008a). The cellular burden of storage substrates may recruit more microglia for clearing damaged neurones (Ausseil et al., 2008).

Time-dependent neuroinflammation was also confirmed in MPS IIIB mice by significantly increased levels of glial fibrillary acidic protein-positive astrocytes, monocyte chemoattractant protein, macrophage inflammatory protein and interleukin-1α (Wilkinson et al., 2012). Neurons in the brains of the MPS IIIC mouse model displayed increased storage of

gangliosides, phosphorylated tau, and β-amyloid and subsequent progressive neuroinflammation, abnormal mitochondrial energy metabolism in the neurons and neuronal loss (Martins et al., 2015).

A reduction in activated isolectin B4-positive microglia and glial fibrillary acidic protein-positive astrocytes was observed after direct injection of human SGSH into cerebrospinal fluid in MPS IIIA mice (Hemsley et al., 2008). Moreover, treating either Niemann-Pick disease type C1 or MPS IIIA mice with aspirin improves disease pathology and clinical features (Jeyakumar et al., 2004; Jeyakumar et al., 2005; Smith et al., 2009; Arfi et al., 2011). Treatment with prednisolone to suppress inflammation and autoimmune responses also slowed down neurological disease progression in MPS IIIB mice (DiRosario et al., 2009).

Oxidative stress is another cellular response to neuronal damage due to disruption of lysosomal homoeostasis (Wei et al., 2008). The involvement of reactive oxygen species, cytokines and cytotoxic cells with DNA oxidation was observed in young MPS IIIB mouse brains (Villani et al., 2007; Villani et al., 2009). DNA fragmentation, single-stranded DNA and reduced density of gamma-aminobutyric acid interneurons in the cerebral cortex have also been recorded in post-mortem MPS IIIB human brains (Hamano et al., 2008a).

1.13.2 Secondary proteinaceous accumulation

Previous studies have demonstrated the deposition of polyubiquitinated proteins in MPS IIIA brains (Kiselyov et al., 2007; Settembre et al., 2008). Ubiquitin-positive inclusions in MPS IIIA mouse brains were reported in both mixed strain and congenic MPS IIIA mice (Savas et al., 2004; Crawley et al., 2006). The finding of intracellular filamentous inclusions or hyperphosphorylated tau with paired helical filaments in the medial entorhinal cortex and dentate gyrus of MPS IIIB mice reinforced the concept of tauopathy in MPS III (Ohmi et al., 2009; Ohmi et al., 2011); in addition, accumulation of β-amyloid, cholesterol, and ubiquitin was evident in those cells (Ohmi et al., 2011).

Tau is a microtubule-associated cytosolic protein predominantly expressed in axonal nerve cells that are involved in anterograde axonal transport, and microtubule assembly and stabilisation (Hernandez and Avila, 2007). The abnormal aggregation of tau that occurs when its metabolism is perturbed - as arises from alterations in the amount of the protein, missense mutations or

post-transcriptional phosphorylation – coincides with the appearance of neurodegeneration clearly evident in the brain of patients and animal models (Hernandez and Avila, 2007). Under pathological conditions, hyperphosphorylated-tau accumulates in neurones as paired helical filaments which subsequently form neurofibrillary tangles or Pick's bodies (Brion et al., 1985). Collectively known as 'tauopathies', the group includes Alzheimer's disease, Pick's disease, and Niemann-Pick disease type C (Hernandez and Avila, 2007). Tau clearance was delayed and resulted in the formation of insoluble aggregates when lysosomal autophagy was pharmacologically blocked (Hamano et al., 2008b).

It has been reported that a high protein concentration is required for tau to polymerise, suggesting that other compounds could be necessary to facilitate tau assembly (Crowther et al., 1992). Dementia with Lewy bodies, Alzheimer's disease, and Parkinson's disease human brains have been shown to contain high levels of S396 phosphorylated-tau and phosphorylated α-synuclein (Muntane et al., 2008). Therefore, tau and α-synuclein may interact with each other and promote the fibrillisation processes and contribute to the onset and progression of neurodegeneration.

Similarly, a previous report revealed the progressive accumulation of ubiquitin-positive inclusions in various regions of the MPS IIIA mouse brain (Savas et al., 2004). As a marker of protein catabolism, increased ubiquitination may result from an inability of cells to degrade ubiquitinated proteins, due to either a change in protein structure or a failure within the ubiquitin-proteasome degradative pathway itself. Moreover, ubiquitin is one of the major components of Lewy bodies (Spillantini et al., 1997), indicating an association with Parkinson's disease and its related pathogenesis.

1.13.3 α-Synuclein accumulation in lysosomal storage disorders

Secondary accumulation of α-synuclein (SNCA) has been documented in the brains of several LSDs **(Table 1.4)**. Hamano et al. (2008a) reported the appearance of phosphorylated SNCA inclusions in swollen neurones of the temporal cortex, hippocampus, periaqueductal grey matter and substantia nigra in human MPS IIIB **(Fig 1.4 A,B)**, and of the thalamic nuclei in human MPS II brains. Most of the phosphorylated SNCA seemed to be ubiquitinated in the cerebral cortex and mid-brain. A similar accumulation of SNCA has also been recorded in the perikarya of cortical brain sections from two MPS IIIA patients (Winder-Rhodes et al., 2012). Moreover,

spherical SNCA-positive inclusions have been noted as early as three-weeks of age in the corpus callosum, inferior colliculus, and periaqueductal grey in MPS IIIA mouse brain, and these lesions rapidly progress to other brain regions in congenic C57Bl/6J MPS IIIA mice (Beard et al., unpublished) **(Fig 1.4 C, D)**.

A blockage of autophagy in multiple sulphatase deficiency and MPS IIIA mice was suggested to result in the accumulation of both ubiquitin- and SNCA-positive inclusions (Settembre et al., 2008). Therefore, impaired degradation of SNCA may lead to an overabundance of this protein and reach a critical concentration to facilitate accumulation into pathological inclusions.

Taken together, the breakdown of SNCA and other aggregation-prone proteins is disrupted in many neurodegenerative LSDs **(Table 1.4)**; moreover, mitochondrial dysfunction, altered calcium homoeostasis, increased oxidative stress, and alterations in lipid composition, metabolism and rafts have also been documented (Shachar et al., 2011). It is now recognised that the clinical manifestations of LSDs are not simply a consequence of substrate storage. The perturbation to complex cell signalling mechanisms likely plays a key role. However, the molecular mechanisms by which protein inclusions may lead to symptom expression remain elusive.

1.14 Cellular protein degradation pathways

Intracellular proteins are typically catabolised by the ubiquitin-proteasome and lysosomal autophagy systems (Burman and Ktistakis, 2010). In the ubiquitin-dependent pathway, ubiquitin-activating, conjugating, and ligase enzymes catalyse short-lived soluble proteins to generate a polyubiquitin chain (Glickman and Ciechanover, 2002). The chain is recognised by the 26S proteasome and then degraded into defined oligopeptides and free ubiquitin (Glickman and Ciechanover, 2002). Proteasome degradation is tightly regulated by the ATPase subunits of the 19S complex (DeMartino and Gillette, 2007). Alternatively, ubiquitin-independent proteolysis may take place without the addition of polyubiquitin chains to target proteins with the help of regulatory non-ATPase complexes (DeMartino and Gillette, 2007).

Lysosomal autophagy degrades longer-lived macromolecules, cytosolic proteins, and dysfunctional organelles, and has three different degradation pathways: microautophagy; chaperone-mediated autophagy (CMA); and macroautophagy (hereafter termed autophagy)

(Levine and Klionsky, 2004). While some substrates (lipids, organelles or proteins) directly invaginate the lysosomal lumen through the membrane in the microautophagy pathway, some bind to lysosomal associated membrane protein-2a to insert into the lysosomes in the CMA pathway that depends on the heat-shock cognate 70 protein (Levine and Klionsky, 2004). In the autophagy pathway, cytosolic proteins, lipids, and organelles are engulfed by double-membrane vesicles (forming autophagosomes or autophagic vacuoles) and degraded after fusion with lysosomes (Burman and Ktistakis, 2010). Thus, efficient functioning of the autophagy pathway requires an efficiently functioning cellular transport system.

Both proteolytic systems are functionally connected, such that impairment of one influences the other. Many aggregation-prone proteins such as SNCA, β-amyloid and huntingtin proteins, which are involved in neurodegenerative disorders such as Parkinson's, Alzheimer's and Huntington's diseases, respectively, are degraded in the autophagy pathway (Rubinsztein, 2006). It has also been shown that an increase in mutant huntingtin aggregates resulted when autophagy was blocked (Ravikumar et al., 2002). Induction of autophagy with rapamycin or rilmenidine improved disease phenotype in Huntington mice (Ravikumar et al., 2004; Rose et al., 2010). Both lysosomal autophagy and ubiquitin-proteasome system activity decline with age, suggesting that ageing may play a major role in many neurodegenerative disorders (Xilouri et al., 2013).

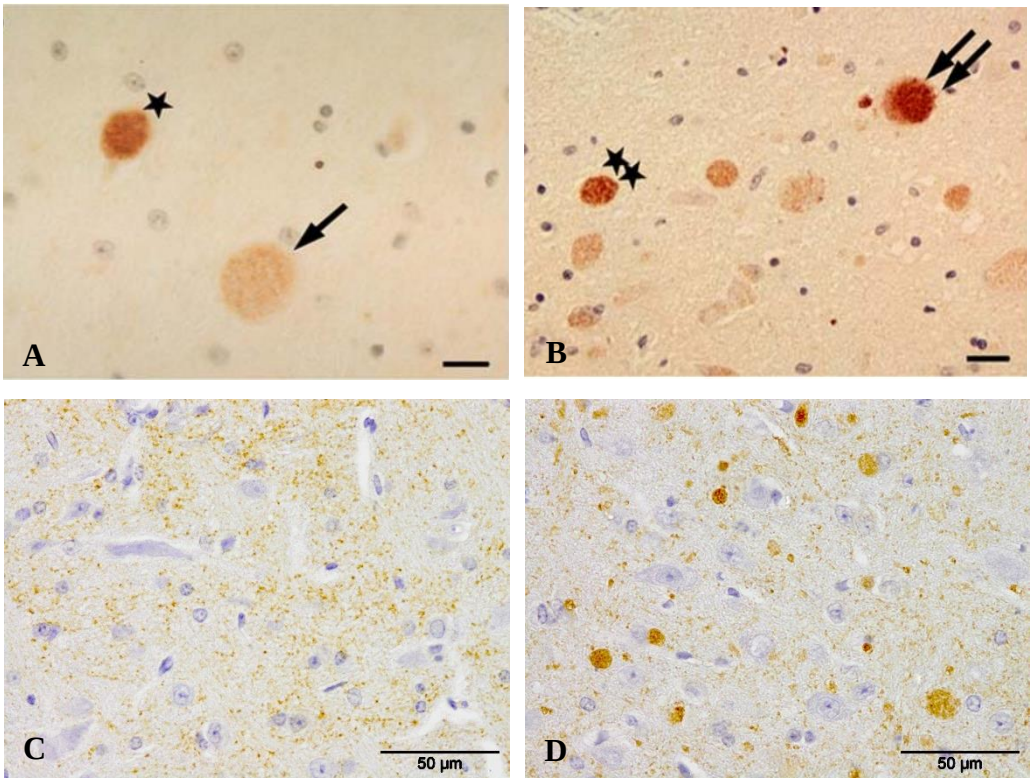

Figure 1.4: α-Synuclein accumulation in the cytoplasms of neurons in the hippocampus (A) and anteroventral nucleus of the thalamus (B) in two human MPS IIIB brains (stars and arrows); bar = 20 µm. Comparison of the extent of α-synuclein inclusions in the brainstem of an unaffected mouse (C) and a MPS IIIA mouse (D) at 30-weeks of age; bar = 50 µm. Sources: Hamano et al., 2008a; Beard et al., unpublished

Table 1.4: The documented list of LSDs associated with SNCA-positive inclusions.

SNCA= α-synuclein, UQ= ubiquitin. Table adapted from (Shachar et al., 2011); [1](Sardi et al., 2013); [2](Saito et al., 2004)

LSDs	Deficient protein	Storage substrates	Protein inclusions
Gaucher disease	β-Glucosidase	Glucocerebroside (glucosylceramide)	SNCA, UQ, Tau[1]
GM2 gangliosidosis	β-Hexosaminidase A (Tay–Sachs)	GM_2	SNCA
MPS II	Iduronate-2-sulphatase	HS, DS	SNCA, UQ
MPS IIIA	Sulphamidase	HS	SNCA, UQ
MPS IIIB	N-Acetyl-α-glucosaminidase	HS	SNCA, UQ
Niemann-Pick type C	NPC1 and 2	Cholesterol and sphingolipids	SNCA, Tau[2]
Cathepsin D deficiency	Cathepsin D	Saposins A and D	SNCA
Metachromatic leucodystrophy	Arylsulphatase A	Sulphated glycolipids	SNCA
β-Galactosialidosis	Cathepsin A	Sialyl-oligosaccharides	SNCA
Multiple sulphatase deficiency	Formylglycine-generating enzyme	Sulphatides	SNCA, UQ

1.15 The synuclein family

Synucleins are a vertebrate-specific family of closely-related neuronal proteins which consist of α, β-, and γ-synuclein (Maroteaux and Scheller, 1991). They have a similar domain organisation and are, therefore, 55-62% identical in sequence to each other (Lavedan, 1998). The protein length may differ in size from 127 to 140 amino acids (Lavedan, 1998). Synucleins can adopt the two-helix conformational changes upon membrane lipid binding (Rivers et al., 2008). The similarities between synucleins suggest overlapping synaptic functions (Greten-Harrison et al., 2010).

Maroteaux et al. (1988) originally identified the synuclein sequence in the Pacific Torpedo electric organ (*Torpedo californica*) with the antibody to cholinergic vesicles. It was designated "synucleins" because the vesicles were localised at the presynaptic nerve terminals and nuclear envelope of neurones. The first human synuclein was identified biochemically as a fragment in the composition of amyloid or senile plaques in Alzheimer's disease patients and termed 'non-amyloid β component of Alzheimer's disease amyloid' (Uéda et al., 1993). The precursor protein of this peptide (NACP) was found to be analogous to rat SNCA (Uéda et al., 1993). Tobe et al. (1992) also identified the amino acid sequence of an abundant protein in rat brain, which they named 14-kD phosphoneuroprotein.

In 1994, the amino acid sequences of two homologous proteins from human brain which were identical to NACP and the human ortholog of the 14-kD phosphoneuroprotein were reported (Jakes et al., 1994). The authors noticed that both proteins were similar to synuclein from *Torpedo californica*, and therefore named them SNCA and β-synuclein, respectively. β-Synuclein may be neuroprotective against SNCA toxicity since it does not have the central non-amyloid β component of Alzheimer disease amyloid-associated region (Fan et al., 2006).

Three years later, the sequence of a novel protein was identified and named breast cancer specific gene1 (BCSG1 or γ-synuclein), due to its high expression in breast cancer tissues (Ji et al., 1997). A study of 6000 normal and cancerous breast tissues analysed by Northern blot and in situ hybridisation techniques found that BCSG1 was abnormally expressed in breast cancer tissues (Ji et al., 1997). Therefore, γ-synuclein over-expression was assumed to be involved in breast cancer progression from benign cancer or in-situ ductal carcinoma to a highly infiltrative malignant carcinoma (Ji et al., 1997).

Another study suggested that synucleins may be involved in the development of breast and ovarian cancers (Bruening et al., 2000). Variable expression of synucleins was found in breast and ovary carcinoma compared to control tissues by immunohistochemistry and Western blot analyses (Bruening et al., 2000). While 82% of stage III/IV ductal breast cancer expressed β-synuclein, γ-synuclein or both, at least one type of synuclein was present in 87% of ovarian cancers. Approximately 20% of pre-cancerous ovarian lesions such as epithelial inclusion cysts, hyperplastic papillary cells and epithelium showed γ-synuclein punctate expression, suggesting its involvement in the early development of ovarian cancer (Bruening et al., 2000).

1.16 The α-synuclein protein

1.16.1 Structure and location of α-synuclein

Research has now focused on SNCA as the primary precursor or aggressor found in some neurodegenerative disorders. Human SNCA is made up of 140 amino acids and is encoded by the *SNCA* gene on the long arm of chromosome 4q21.3-q22, which spans 111 kb in length (Venda et al., 2010) **(Fig 1.5)**. The *SNCA* gene is composed of seven exons, five of which correspond to a coding region that is highly conserved among vertebrates (Venda et al., 2010). Rodent SNCA is also 140 amino acids long, encoded by chromosome 6, and shows 95.3% similarity with the human protein (Lavedan, 1998).

SNCA is localised to the neuronal presynaptic terminals where interactions with phospholipids and proteins take place (Abeliovich et al., 2000). A fraction of SNCA was also found in axons of hippocampal neurones by immunofluorescence (Greten-Harrison et al., 2010) **(Fig 1.5 E)**. Although it is abundantly expressed in both central and peripheral nervous systems (Iwai et al., 1995), smaller amounts of SNCA can also be found in tissues such as heart, skeletal muscles, pancreas, skin, lungs, liver, spleen and kidney (Beyer et al., 2004; Beyer et al., 2008). Intracellularly, the highest concentration of the protein is localised to presynaptic terminals (Iwai et al., 1995).

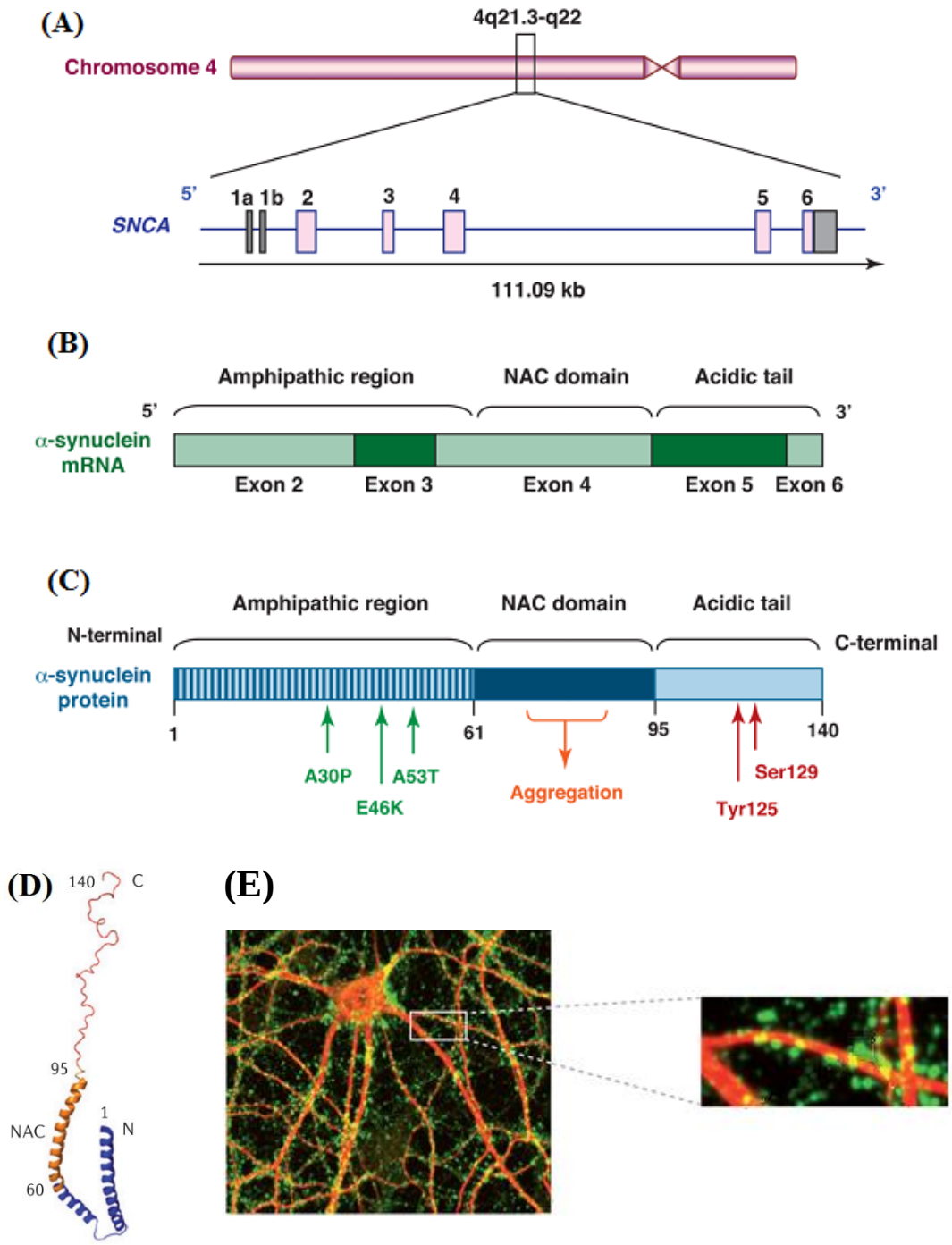

Figure 1.5: Schematic diagram of human SNCA: (A) *SNCA* gene structure on chromosome 4; (B) mRNA; (C) the three domains of the protein with common missense mutations (A30P, E46K, and A53T) and post-translational modifications; (D) representation of micelle-bound SNCA; and (E) location of SNCA: immunofluorescent staining of SNCA (green) and the neuronal dendritic marker MAP2 (red) in cultured cortical neurons from a wild-type mouse. NAC = non-amyloid β component of Alzheimer disease amyloid.

Sources: Venda et al., 2010; Lashuel et al., 2012

1.16.2 Structural components of α-synuclein

The primary structure of SNCA can be divided into three distinct domains (Clayton and George, 1998). Residues 1-60 are the amphipathic lipid-binding N-terminal portion dominated by seven repeats of 11 amino acid residues, including the consensus sequence KTKEGV (Bendor et al., 2013). The N-terminal domain is highly conserved among all synucleins, with approximately 80% sequence identity (Greten-Harrison et al., 2010). It is thought to interact with acidic phospholipid surfaces by adopting an α-helical structure upon lipid binding (Bendor et al., 2013). The three missense mutations (A30P, E46K, and A53T) responsible for familial Parkinson's disease are located in this region **(Fig 1.5 C)** (Venda et al., 2010).

Residues 61-95 form the central hydrophobic non-amyloid β component of Alzheimer's disease amyloid region, which is involved in protein aggregation and fibril formation (Bendor et al., 2013). Residues 96-140 comprise a highly acidic and proline-rich C-terminal region with the least-conserved sequence among synucleins (Bendor et al., 2013). Post-translational modifications such as nitration, oxidation, and phosphorylation at serine 129 and tyrosine 125 at the C-terminal region might also be essential for the regulation, localisation, and propensity of SNCA to aggregate (Venda et al., 2010) **(Fig 1.5 C)**. For example, phosphorylation at serine 129 increases the tendency of SNCA to deposit in Lewy bodies in the brains of patients with dementia with Lewy bodies (Anderson et al., 2006). Ubiquitination was also primarily found in Lewy bodies, possibly after serine 129 phosphorylation of SNCA (Anderson et al., 2006).

1.16.3 Physiological nature of α-synuclein

Although aggregation of misfolded SNCA is a pathognomonic feature of Parkinson's disease and other synucleinopathies, its normal physiological state in cells has not yet been confirmed. Indeed, studying its native structure in healthy cells and tissues is important in the context of therapeutic interventions to stabilise or maintain SNCA in its physiologically optimal concentration. SNCA has traditionally been identified as a natively unfolded monomer of about 14 kDa in size, which changes to a secondary structure upon binding to lipid membranes (Davidson et al., 1998).

Cell-derived native SNCA displays an α-helical structure without lipid insertion but has a higher lipid binding capability than the recombinant protein (Bartels et al., 2011). Several human cell lines and mouse brains also predominantly displayed folded tetramers (~58 kDa) and variable but lower amounts of monomers, dimers and trimers in native gel systems (Bartels et al., 2011). Native tetramers appear highly resistant to aggregation, whereas recombinant monomeric forms readily aggregate into amyloid-like fibrils *in vitro* (Bartels et al., 2011). Similarly, the non-pathogenic homologue, β-synuclein, showed oligomeric assemblies similar to SNCA conformers (Selkoe et al., 2014). Helical SNCA tetramers can dissociate rapidly to monomers and vice versa (Selkoe et al., 2014). Therefore, SNCA exists as both monomers and tetramers in dynamic equilibrium under normal physiological conditions.

1.16.4 Truncated isoforms of α-synuclein

In addition to the full-length *SNCA 140* isoform, at least three other natural isoforms of *SNCA* result from alternative splicing **(Fig 1.6)**: *SNCA* 112 results from an in-frame deletion that corresponds to the deletion of exon 5, leading to a total weight of about 11.4 kDa (Beyer et al., 2006); *SNCA* 126 is also an in-frame deletion that corresponds to the deletion of exon 3 and results in a total weight of about 13.1 kDa (Beyer et al., 2006); and *SNCA* 98, which lacks both exons 3 and 5 (Beyer et al., 2008).

Over-expression of *SNCA* 112 in a human neuroblastoma cell line (SH-SY5Y) resulted in proteasomal dysfunction and toxicity to the neurones, whereas full-length SNCA over-expression was innocuous (Kalivendi et al., 2010). Moreover, up-regulation of wild-type SNCA and *SNCA* 112 (nearly two-fold) in both substantia nigra and striatum was documented in Parkinson mice treated with the neurotoxin 1-methyl-4-phenyl-1,2,3,6-tetrahydropyridine (MPTP) (Kalivendi et al., 2010). Therefore, different isoforms resulting from alternative splicing of SNCA could be essential for the pathophysiology of Parkinson's disease.

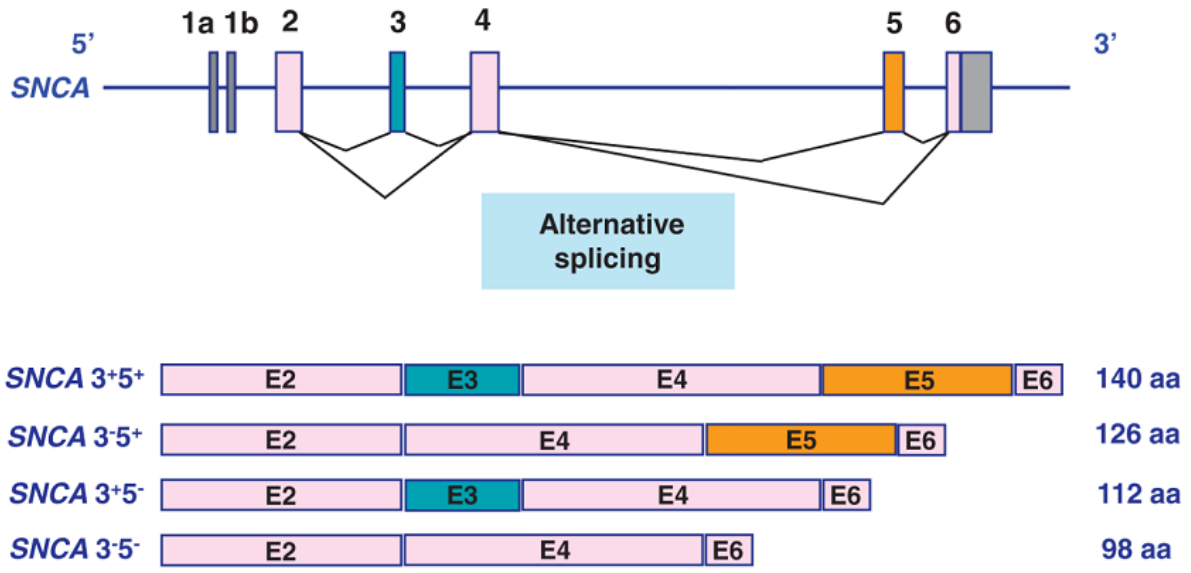

Figure 1.6: Alternative splicing of exons 3 and 5 generates four types of *SNCA* isoforms - *SNCA* 140, S *SNCA* 126, *SNCA* 112 and *SNCA* 98 (E= exon; aa = number of amino acids). Source: Venda et al., 2010

The composition of SNCA in the neuronal cytosol and Lewy bodies has also been shown to differ (Anderson et al., 2006). C-Terminally truncated forms such as Asp-115, Asp-119, Asn-122, Tyr-133, and Asp-135, with the molecular mass of 10-15 kDa, were detected in Lewy bodies of patients with dementia with Lewy bodies by liquid chromatography and mass spectrometry (Anderson et al., 2006), and phosphorylation at serine 129 was the most abundant post-translational modification in dementia with Lewy body brains (Anderson et al., 2006). Even though the role of these truncated forms is not known, they may be involved in aggregation processes as they were found to readily accumulate in Lewy bodies (Anderson et al., 2006).

1.16.5 Physiological functions of α-synuclein

The normal physiological function of SNCA remains poorly understood. Consistent with its localisation to pre-synaptic terminals, it may regulate vesicle trafficking and refilling, endocytosis and neurotransmitter release via interactions with the soluble N-ethylmaleimide-sensitive factor attachment protein receptor (SNARE) complex (both t-SNARE and v-SNARE) (Lashuel et al., 2012) **(Fig 1.7)**. Therefore, increased levels of SNCA may impair neurotransmitter release, vesicle recycling, trafficking and stability of SNARE complexes. Reduced levels of the protein may also cause problems in vesicle trafficking and refilling, and neurotransmitter uptake (Lashuel et al., 2012) **(Fig 1.7)**.

SNCA may also have a role in neurogenesis and synaptic plasticity by participating in actin polymerisation to rearrange the cytoskeleton (Cheng et al., 2010). Previous studies have shown SNCA involvement in the regulation of a variety of neurotransmission processes, and may be involved in monoamine transporter activities such as dopamine and serotonin neurotransmission. It was also shown to be important in mobilising glutamate from the reserve pool (Gureviciene et al., 2007), and in acetylcholine transmission in skeletal muscles (Pelkonen and Yavich, 2011).

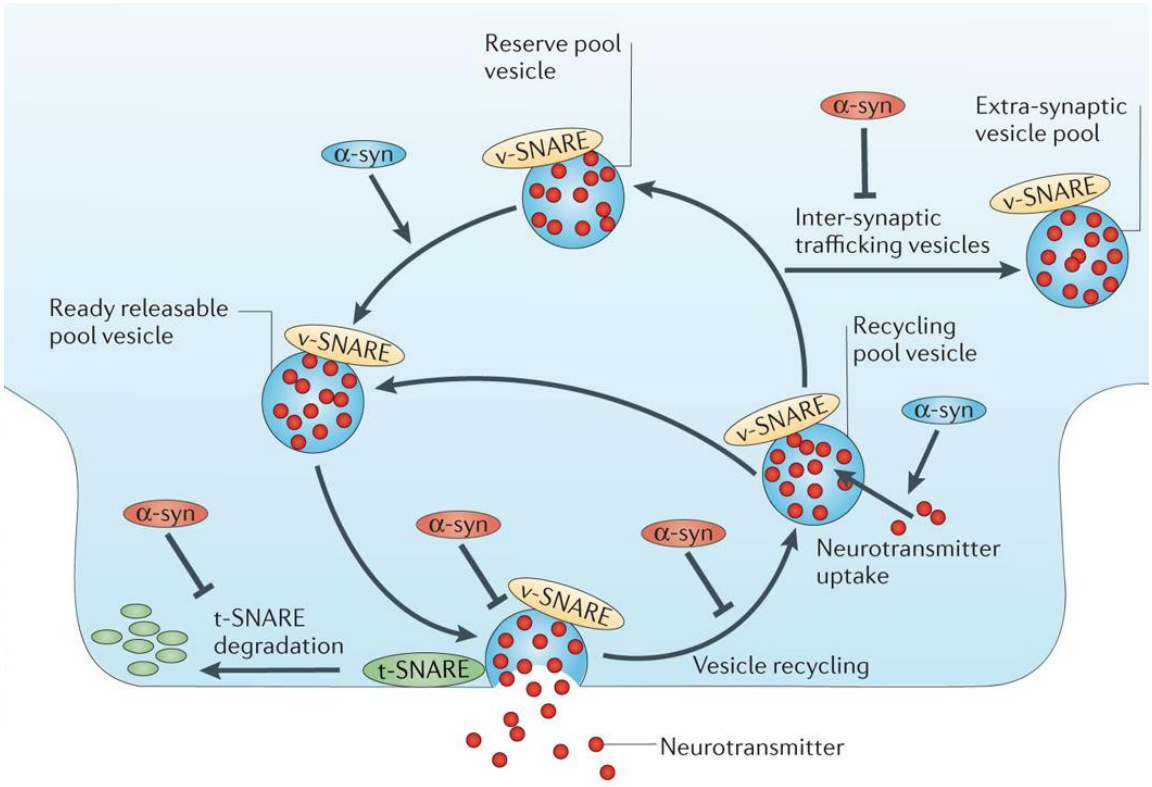

Figure 1.7: Schematic diagram showing the role of SNCA **in neurotransmission.**

SNCA regulates vesicle trafficking and vesicle refilling at the pre-synaptic terminal (α-syn blue). Accumulated SNCA (α-syn red) inhibits vesicle recycling, trafficking, SNARE complex interaction and neurotransmitter release.

Source: Lashuel et al., 2012

1.16.6 Importance of α-synuclein in normal central nervous system function

To understand the physiological functions of SNCA, targeted SNCA knockout mice (129X1/SvJ and C57BL/6 mixed strain) were created and studied by Abeliovich et al. (2000). The knockout mice were viable, fertile, and displayed normal brain architecture and dopamine regulation as measured by simple electrical stimulation (Abeliovich et al., 2000). The animals showed no up-regulation of β– and γ-synuclein, or a change in synphilin-1 (SNCA interacting protein) expression (Specht and Schoepfer, 2001). However, the mice exhibited an increase in dopamine release with paired stimuli, an 18% decrease in striatal dopamine, and reduced locomotor responses to amphetamine (Abeliovich et al., 2000). The study suggested that SNCA may play a role in presynaptic, activity-dependent negative regulation of dopamine neurotransmission.

The compensatory interaction between SNCA and other synaptic vesicle proteins has also been identified. Cysteine-string protein-α (CSPα) is a synaptic protein that inhibits SNARE complex assembly, and its deficiency leads to lethal, progressive neurodegeneration in affected animals (Chandra et al., 2005). Clinical features of CSPα knockout mice significantly improved with the transgenic expression of SNCA, but deletion of endogenous SNCA resulted in accelerated lethality (Chandra et al., 2005). Moreover, a recent case study demonstrated that a deficiency of endogenous SNCA in dopamine neurones reproduced the nigrostriatal degeneration in green monkeys (Collier et al., 2016). These findings raise the possibility of pathological "loss of function" of SNCA at the nerve terminals by its sequestration into Lewy bodies in Parkinson's disease and other synucleinopathies.

Kokhan et al. (2012) also stressed the importance of SNCA in normal cognition and behaviour. Using the SNCA-deficient mice from Abeliovich et al. (2000), the authors showed that 10- to 14-month-old knockout mice displayed reduced abilities in locomotion, and spatial and working memory in an array of behavioural tests (Kokhan et al., 2012). A decrease in total travel distance and speed of about 25% was found in transgenic mice compared to wild-type mice; a significantly reduced learning ability in both passive and active avoidance tests was also observed in the knockout animals. Moreover, the average time for knockout mice to find the hidden platform in the Morris water maze test significantly exceeded that of wild-type animals by Day 3 and onwards (Kokhan et al., 2012). All of these outcomes point to a significantly lower learning ability in aged SNCA knockout mice.

In contrast to those findings, Chen et al. (2002) did not find learning difficulties in six-month-old SNCA knockout mice in the Morris water maze (C57BL/6JOlaHsd strain). The use of younger mice and a slightly different testing protocol from Kokhan et al. (2012) may explain the difference. Moreover, Snca1Slab was also deleted in the C57BL/6JOlaHsd strain, which includes not only the *SNCA* gene but also the multimerin-1 gene (encoding multimerin 1), which is located close to the *SNCA* gene (Specht et al., 2004). Compared to targeted *SNCA* knockout, the potential neuronal side effects due to the absence of multimerin-1 in the C57BL/6JOlaHsd strain may potentially be translated (Ninkina et al., 2015). Therefore, when comparing these studies it is imperative to consider the types of SNCA knockout models that were used.

Increased expression of SNCA protects against paraquat-induced neurodegeneration, suggesting that it may play a protective role in toxin-induced neurodegeneration (Manning-Boğ et al., 2003). Interestingly, deletion of all three synucleins (α-, β-, and γ-synuclein) in mice results in no body weight difference or abnormality in brain architecture, neuronal cell loss, gliosis or apoptosis (Greten-Harrison et al., 2010). However, these triple α-, β-, γ-synuclein knockout mice displayed alterations in synaptic structures (decreased excitatory synapse size by 30%) and transmission, endocytosis abnormalities, age-dependent neuronal degeneration, retinal degeneration and decreased survival rate at 12-months of age (Greten-Harrison et al., 2010). Therefore, SNCA in normal physiological conditions is not essential for survival but may contribute to the long-term functioning of the central nervous system.

1.16.7 Improved functional outcomes in the absence of α-synuclein

Even though SNCA deficiency results in neurological deficits and alterations in synaptic transmission, especially in ageing animals, deletion of the protein may benefit some neurological disorders, as recently shown in studies modulating SNCA in Huntington's disease. Huntington's disease is a progressive, autosomal dominant neurodegenerative proteinopathy caused by a CAG triplet repeat expansion that encodes an expanded polyglutamine tract at the N-terminus of the huntingtin protein (Martin et al., 2015). Abundant SNCA deposits were observed as bead-like neuropil inclusions in the striatum and cerebral cortex in both Huntington human brain tissues and R6/1 Huntington mouse brains (Tomás-Zapico et al., 2012).

The deletion of SNCA resulted in a decreased number of mutant huntingtin inclusions in both huntingtin-transfected striatal neurones and in R6/1 mice (Tomás-Zapico et al., 2012); a reduction in inclusions was also seen in eight-month-old R6/1 mouse brains by immunostaining (Tomás-Zapico et al., 2012). Moreover, SNCA deficiency attenuated body weight loss and improved early motor impairment in the R6/1 mice (Tomás-Zapico et al., 2012). Corrochano et al. (2012) reinforced the protective role of SNCA deficiency in Huntington mice. In their study, deletion of SNCA in both R6/1 and N171-82Q Huntington mice resulted in increased numbers of LC3 II autophagosomes, and delayed tremor onset and weight loss (Corrochano et al., 2012). Therefore, SNCA deletion displayed a protective or beneficial effect in these mice.

Interestingly, SNCA null mice were resistant to MPTP neurotoxin-induced dopamine neurodegeneration, dopamine release and behavioural deficits (Dauer et al., 2002; Fornai et al., 2005). MPTP is an environmental risk factor for Parkinson's disease, which inhibits mitochondrial complex I and produces a pattern of dopamine neurodegeneration (Dauer et al., 2002). The resistance to MPTP in SNCA null mice appeared to result from the inability of the neurotoxin to inhibit complex I (Dauer et al., 2002). However, it is unknown whether this resistance is due to the absence of SNCA toxicity or changes in the presynaptic machinery. The study highlights the possibility that changes in normal SNCA expression may modify the vulnerability of dopaminergic neurones to an environmental toxin.

1.16.8 Over-expression of α-synuclein

At present, it remains largely unknown whether increased levels of SNCA cause neurodegeneration by gaining toxic function or by alterations in its physiological function. Interestingly, modest over-expression of human SNCA in mice resulted in reduced synaptic neurotransmission, similar to age-dependent neuronal dysfunction in triple α-, β-, γ-synuclein knockout mice (Greten-Harrison et al., 2010). It was demonstrated that over-expression of α-synuclein compromises endoplasmic reticulum to Golgi protein trafficking by inhibiting the formation of the SNARE complex (Thayanidhi et al., 2010).

Similarly, both wild-type and mutant human SNCA can increase the sensitivity of rat dopamine neurones to neurotoxicity (Zhou et al., 2000). Elevated levels of wild-type SNCA in the substantia nigra of rats caused dopaminergic neuronal degeneration and subsequent hormonal release (Gaugler et al., 2012). Nemani et al. (2010) confirmed that over-expression of SNCA

caused a decrease in synaptic vesicle exocytosis and neurotransmission, and a reduction in readily releasable and recycling synaptic vesicle pools in mouse hippocampus *in vitro*. Moreover, tremor onset and weight loss worsened with the increased expression of human wild type SNCA in Huntington mice (Corrochano et al., 2012). Increased levels of SNCA inhibited the intracellular trafficking of proteins, resulting in decreased activity of the lysosomal enzyme β-glucocerebrosidase *in vitro* (Mazzulli et al., 2011). These data highlight the importance of maintaining SNCA at its physiological level for optimal neurotransmission, and long-term operation and development of the central nervous system.

1.16.9 Degradation of α-synuclein

One of the most critical control steps in the aggregation process is the regular degradation and secretion of synthesised proteins. The ubiquitin-proteasome system has been shown to be responsible for degrading both wild-type and A53T mutant SNCA (Bennett et al., 1999). Selective inhibition of the ubiquitin-proteasome system by the proteasome inhibitor β-lactone blocked the normal degradation of SNCA (Bennett et al., 1999). Moreover, it has been demonstrated that phosphorylated-SNCA at Ser-129 (most common form in Lewy bodies) can be degraded in the proteasome pathway by an ubiquitin-independent pathway (Machiya et al., 2010).

A recent study showed that although the ubiquitin-proteasome system is the main degradation pathway for wild-type SNCA under physiological conditions *in vivo,* lysosomal autophagy is recruited when SNCA is pathologically elevated (Ebrahimi-Fakhari et al., 2011). Application of rapamycin, which stimulates autophagy, increased clearance of SNCA in a PC12 cell model (Webb et al., 2003). Both pathways were shown to be necessary for recombinant and wild-type SNCA turnover *in vitro* (Cuervo et al., 2004; Vogiatzi et al., 2008).

Clearance of over-expressed and transgenic SNCA by chaperone-mediated autophagy was shown *in vivo* by Mak et al. (2010). In addition to lysosomal chaperone-mediated autophagy that clears monomeric wild-type SNCA, autophagy is responsible for degrading wild-type, mutant and oligomeric species (Qiao et al., 2008; Vogiatzi et al., 2008; Alvarez-Erviti et al., 2010). Cathepsin D has been shown to be responsible for autophagy-dependent SNCA degradation, as its expression is linked to levels of the protein (Sevlever et al., 2008; Cullen et al., 2009). The lack of cathepsin D in mice has been shown to result in the accumulation of high

molecular weight SNCA in the brain (Qiao et al., 2008). Moreover, induction of cathepsin D reduced SNCA accumulation and neurotoxicity in dopaminergic cell lines (Qiao et al., 2008). Thus, small monomers and soluble oligomers of SNCA are degraded through the ubiquitin-proteasome system, while large oligomeric and mutant forms are cleared by the lysosomal pathway (Lee et al., 2004).

Other proteases, such as calpain-1, neurosin (kallikrein-6) and matrix metalloproteinases, have also been implicated in the cleavage of wild type or aggregated forms of SNCA *in vitro* (Dufty et al., 2007; Kasai et al., 2008; Choi et al., 2011). Such cleavage may generate truncated species of SNCA, as discussed above. While impaired degradation leads to the accumulation of SNCA, increased levels of SNCA can also generate abnormal species, which in turn may impair functioning of the ubiquitin-proteasome system or autophagy (Mazzulli et al., 2011). Therefore, abnormalities in proteolytic pathways may create a bidirectional positive loop causing neuronal cell death.

1.16.10 Pathological forms of α-synuclein

The unfolded monomeric forms of SNCA combine with each other to form unstable propagating dimers, which progressively give rise to oligomers of various morphologies such as ring-like oligomers (Lashuel et al., 2012). These oligomers eventually form small amyloid fibrils, which finally lead to the irreversible intracellular Lewy body **(Fig 1.8)**. Phospholipid membrane-bound monomers adopt an α-helical conformation, which undergoes transformation into β-sheet-rich structures and oligomers (including transmembrane amyloid pores) at high concentrations (Lashuel et al., 2012).

The intermediate species of SNCA such as prefibrillar oligomers have been shown to be toxic both *in vitro* and *in vivo*, causing increased cytotoxicity, mitochondrial dysfunction, endoplasmic reticulum trafficking, protein catabolism and synaptic transmission, and finally neurodegeneration (Conway et al., 2000a; Conway et al., 2000b; Outeiro et al., 2008; Winner et al., 2011). Neurones may isolate or convert toxic species to stable and less toxic fibrillar forms of SNCA, which is detected mostly as Lewy bodies (Winner et al., 2011). Interestingly, oligomers and fibrils can migrate between cells via proposed mechanisms such as direct penetration, endocytosis and membrane receptors (Lashuel et al., 2012).

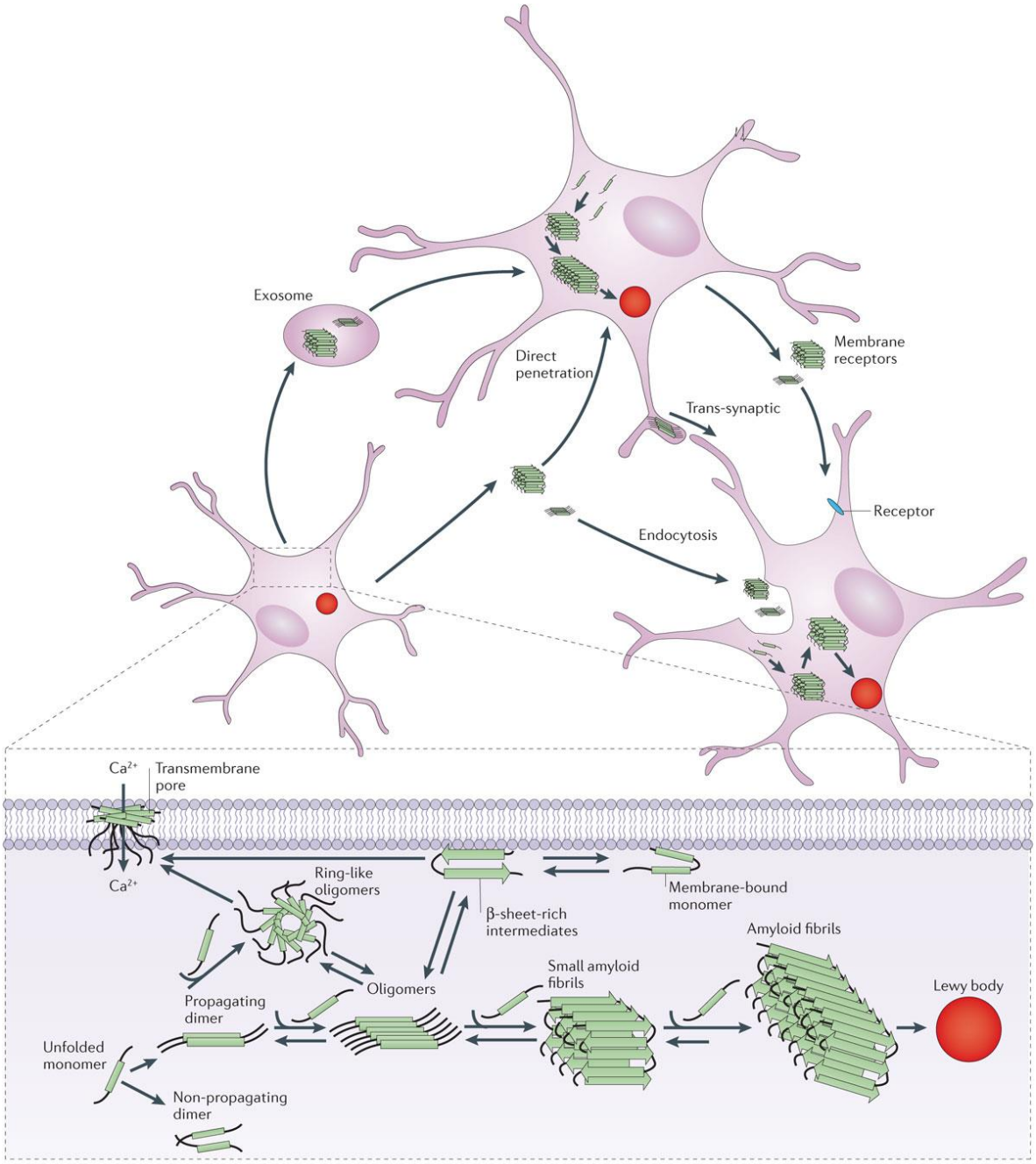

Figure 1.8: Schematic diagram of the SNCA pathological pathway.

Source: Lashuel et al., 2012

1.17 Clinical significance of α-synuclein in Parkinson's disease

Neurodegenerative disorders associated with the abnormal accumulation of SNCA aggregates in neurons, nerve fibres or glial cells in various brain regions are collectively known as 'α-synucleinopathies' (Wong et al., 2004), and include Parkinson's disease, dementia with Lewy bodies, Gaucher disease, and multiple system atrophy (Wong et al., 2004). It is postulated that these aggregates may physically distort the cellular compartments and subsequently disturb normal cellular function, or give rise to a toxic gain and/or loss of function, ultimately causing cell death.

Parkinson's disease is the most common movement disorder which affects approximately 8,000 people in Australia (Drury, 2014). The prevalence is highest amongst the elderly, with an incidence rate of 428 and 1903 (per 100,000) in over 60- and 80-years-old, respectively (Pringsheim et al., 2014). The disorder can be characterised by a triad of bradykinesia, rigidity, and resting tremor, along with other non-motor signs such as sleep disturbance, autonomic dysfunction, cognitive, psychiatric and sensory changes (Samii et al., 2004).

Mutations in the *SNCA* gene (A53T, A30P, E46K, G51D and H50Q), as well as wild-type genomic multiplications, are known to cause autosomal dominant familial forms of Parkinson's (Singleton et al., 2003; Chartier-Harlin et al., 2004; Appel-Cresswell et al., 2013; Lesage et al., 2013). They are responsible for 2–3% of late-onset sporadic cases, and about 50% of early-onset familial forms (Obeso et al., 2010). The most prominent feature in the Parkinson's brain is the progressive loss of dopaminergic neurones in the substantia nigra pars compacta and the locus coeruleus, resulting in a dopamine deficit and abnormal neural activity in basal ganglia (Sui et al., 2014). Moreover, degeneration of serotonergic neurones, noradrenergic neurones, and cholinergic neurones can also be identified in specific brain regions (Buddhala et al., 2015).

In addition to neurotransmitter loss, Spillantini et al. (1997) showed that Lewy bodies in neuronal perikarya and Lewy neurites in cellular processes were the pathological hallmarks in the brains of Parkinson's disease and dementia with Lewy bodies **(Fig 1.9)**. These intracellular microscopic inclusions are mainly composed of SNCA, which has also been found in extracellular biological fluids such as cerebrospinal fluid and blood plasma (Mollenhauer et al., 2011).

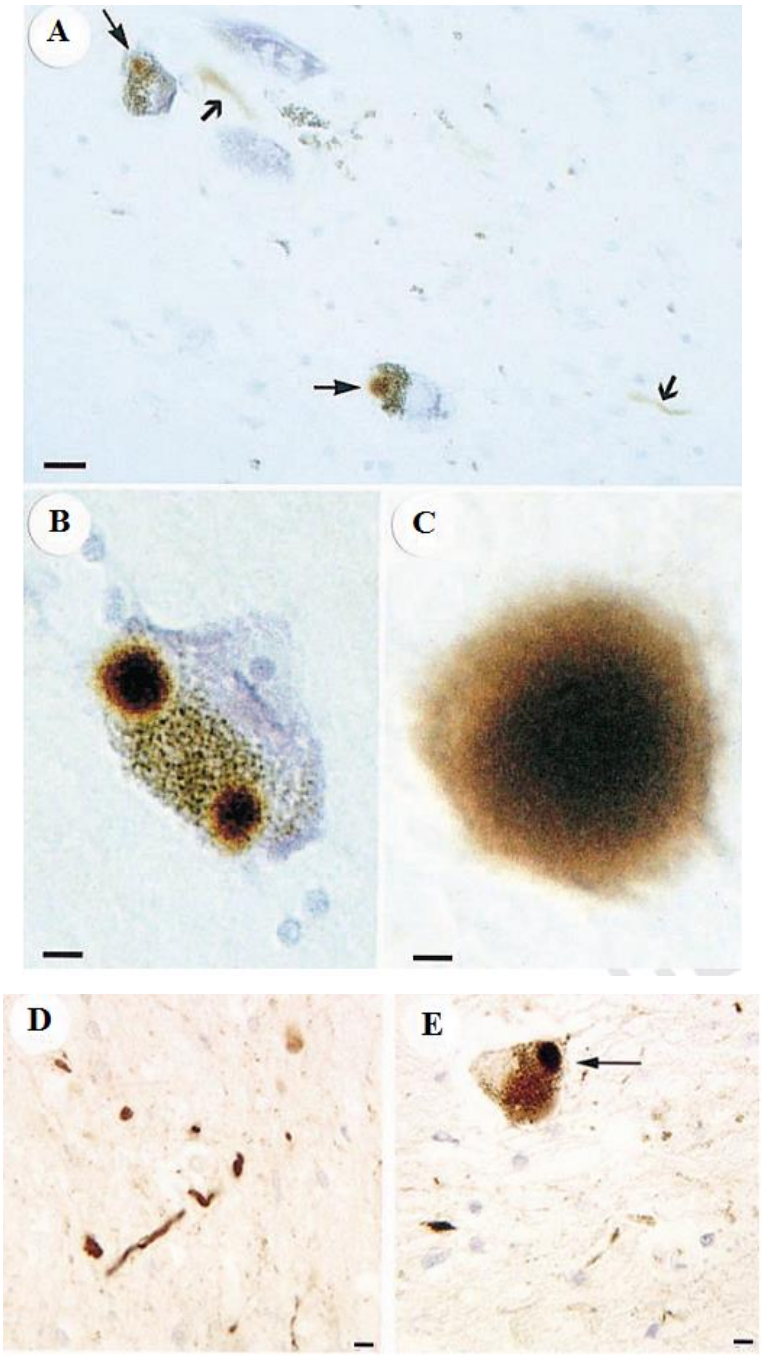

Figure 1.9: Histopathological features in Parkinson's disease. (A) Lewy bodies (thin arrows) and Lewy neurites (thick arrows) in substantia nigra of a Parkinson patient (scale bar 20 μm); (B) SNCA in pigmented nerve cell (scale bar 8 μm); (C) extracellular SNCA-positive Lewy body (scale bar, 4 μm); (D& E) SNCA-positive Lewy neurites and Lewy body, respectively, in the substantia nigra of a dementia with Lewy body patient (scale bar, 10 μm). Source: Spillantini et al., 1997

1.18 Link between lysosomal storage disorders and α-synuclein-related neurodegenerative disorders

Many studies have shown that Parkinson's disease is strongly linked to Gaucher disease, the most common of the LSDs (Mata et al., 2008; Sidransky et al., 2009). Gaucher disease is caused by a mutation in the *glucocerebrosidase1* gene, resulting in deficient lysosomal β-glucocerebrosidase and subsequent accumulation of glucocerebroside or glucosylceramide (Siebert et al., 2014). More specifically, genetic studies identified heterozygous *glucocerebrosidase1* mutations (β-glucocerebrosidase$^{+/-}$) as the most common risk factors for Parkinson's and Lewy body disorders (Lesage et al., 2011; Moraitou et al., 2011; Nishioka et al., 2011). Parkinson patients carrying the *glucocerebrosidase1* mutation are more likely to have an earlier onset and more pronounced cognitive dysfunction (Alcalay et al., 2012).

A common pathological feature in synucleinopathies, including Parkinson's and many LSDs, is the accumulation of SNCA caused by enhanced production, reduced degradation, or post-translational alterations of toxic species. Since SNCA is the primary component of Lewy bodies and its clearance is mediated by the autophagy-lysosomal pathway, there is a putative contention that lysosomal dysfunction in Gaucher disease results in SNCA accumulation that may lead to Parkinson's disease. Furthermore, increased levels of SNCA due to variations in the *SNCA* locus is the major genetic risk factor for sporadic Parkinson's (Devine et al., 2011). Abnormal accumulation of SNCA resulting in a toxic gain or loss of function may underlie the link between neurodegenerative LSDs and other neurodegenerative disorders.

Histopathological examination of brains from Gaucher patients with parkinsonism and Parkinson's disease patients with *glucocerebrosidase1* mutations revealed the presence of SNCA-containing Lewy bodies and Lewy neurites in the neocortical and hippocampal regions (Neumann et al., 2009). Furthermore, down-regulation of β-glucocerebrosidase activity led to impaired lysosomal degradation and subsequent SNCA deposition and neuronal toxicity in various cellular models (Mazzulli et al., 2011). Restoration of β-glucocerebrosidase activity by administration of adeno-associated viruses ameliorated SNCA and ubiquitin accumulation in the hippocampus, as well as the abnormal behavioural phenotype in Gaucher mice (Sardi et al., 2011).

Usenovic et al. (2012) reinforced the hypothesis of synucleinopathy in lysosomal dysfunction. The authors reported that depletion of ATP13A2 in skin fibroblasts from patients with Kufor-Rakeb syndrome and mouse primary neurones leads to lysosomal dysfunction, accumulation of autophagosomes and endogenous SNCA, and toxicity in primary cortical neurones (Usenovic et al., 2012). Kufor-Rakeb syndrome is a lysosomal disorder caused by mutations in lysosomal membrane protein ATP13A2 (or PARK9), manifesting early-onset parkinsonism, pyramidal degeneration and dementia (Park et al., 2011; Tan et al., 2011). These studies showed that either deficiency of β-glucocerebrosidase in Gaucher disease or the ATP13A2 membrane protein in Kufor-Rakeb syndrome caused lysosomal dysfunction and SNCA accumulation, highlighting the importance of intact lysosomal function for SNCA turnover.

However, Dermentzaki et al. (2013) did not observe either SNCA aggregation or lysosomal dysfunction after pharmacological inhibition of β-glucocerebrosidase in neuroblastoma SH-SY5Y cells and primary neuronal cells. A recent study in Gaucher disease zebrafish reported that affected fish showed intra-neuronal ubiquitin-positive inclusions and significantly reduced motor activity (Keatinge et al., 2015). SNCA is not present in the zebrafish genome, so it can, therefore, be reasonably conjectured that the neurodegeneration was not related to SNCA toxicity but rather to lysosomal pathology (Keatinge et al., 2015).

SNCA accumulation is a common feature of many neurodegenerative disorders, including LSDs, which suggest common cellular mechanisms and processes. Further studies to determine its role and function in the neurodegenerative process and its contribution to clinical phenotype are required. It is known that deficiency of lysosomal SGSH in MPS IIIA leads to the accumulation of its substrate, HS. However, much less understood are the downstream pathological events triggered by substrate storage or mutated enzymes in the lysosome. Determining whether SNCA is important to this process and to the resultant clinical phenotype is critical and is the basis for this study. The study utilises a well characterised and studied congenic MPS IIIA mouse model, and MPS IIIA mice in which SNCA has been either partially or fully knocked out.

1.19 Research significance and hypothesis

Defects in proteins that regulate protein sorting and degradation within the endocytic and lysosomal pathways cause an increased number of inherited early- or late-onset neurodegenerative disorders. These conditions are classified across the lifespan as disorders of lysosomal function, which feature extensive accumulation of misfolded proteins in the central nervous system and share the same traits of neurodegeneration observed in disorders such as Parkinson's, Alzheimer's and Huntington's diseases.

The clearance of aggregation-prone proteins is mainly achieved through the autophagy-lysosomal system. The main challenge is to identify fundamental mechanisms and targets involved in the removal of these proteins to develop specific therapeutics. To tackle this problem, a neurodegenerative LSD (MPS IIIA) has been chosen as the model for this study.

The recurrent observation of accumulation or aggregation of certain proteins such as SNCA, p-tau, ubiquitin and amyloid β in different neurodegenerative disorders, including MPS IIIA, indicates the possibility of a shared mechanism. The overall hypothesis is that removing or preventing the accumulation of proteins such as SNCA would alleviate the impaired lysosomal catabolism and hence improve both clinical and pathological manifestations.

In this study, an MPS IIIA mouse model deficient in SNCA was generated and characterised to study the clinical and neuropathological changes at different time points and determine whether SNCA deficiency mediates improvements in neurological sequelae.

The hypothesis of the project is that:
Deletion of SNCA in MPS IIIA mice will reduce the 'load' on protein catabolism mechanisms and thus delay or ameliorate the behavioural deficits and pathological features of the disorder.

1.20 Aims of the study

The overall aim of the study is to understand the contribution of SNCA-positive lesions to the expression of pathology and clinical disease in MPS IIIA mice. The specific objectives to achieve this are to:

(1) generate and establish an MPS IIIA mouse line deficient in SNCA and to characterise disease progression in these mice.

(2) evaluate the time-course of behavioural changes in SNCA-deficient MPS IIIA mice.

(3) determine the effect of SNCA knockout on pathological disease progression in MPS IIIA mice.

(4) distinguish the endogenous SNCA forms and quantify them in MPS IIIA brains

Understanding the contribution of SNCA to the development and progression of MPS IIIA brain pathology is anticipated to: (1) suggest alternate therapeutic strategies for MPS IIIA; and (2) provide new information about the pathological processes operating in more common neurological disorders such as Alzheimer's, Parkinson's and Huntington's diseases, and other synucleinopathies.

Chapter (2)
Materials and Methods

2.1 Materials

2.1.1 Electrophoresis

Agarose DNA grade 3.0-3.5%	AppliChem, Germany
Bromophenol blue	Bio-Rad Laboratories, USA
DNA ladder 100bp	Bio-Rad Laboratories, USA
Genomic DNA purification kit	ThermoFisher Scientific, USA
PUC 19 HpaII size marker	Geneworks, Australia
Vectastain elite ABC kit	Vector Laboratories
Xylene cyanol	Sigma-Aldrich, USA

2.1.2 Genotyping

10x HotStar taq polymerase buffer	Qiagen, Germany
α-Synuclein primers	Geneworks, Australia
AciI (10U/μl)	New England Biolabs, USA
Deoxynucleotide mix (dNTP)	Qiagen, Germany
HotStar taq DNA polymerase	Qiagen, Germany
MPS IIIA primers	Geneworks, Australia
Restriction enzyme	New England Biolabs, USA
SnapStrip 8 strip dome cap PCR tubes	Interpath Services, Australia
Ultraflux dome cap PCR tubes	Scientific Specialities, USA
Water for injection	Becton Dickinson, USA

2.1.3 Buffers and Substrates

6x loading buffer	Mixture of 1x TAE 5 ml, glycerol 5 ml, bromophenol blue 10 mg, xylene cyanol 10 mg

10x PBS stock solution	NaCl 80 g, KCL 2 g, Na2HPO4 11.5 g, KH2PO4 2 g made up to 1 L with Milli-Q water, pH 7.4
1x PBS working solution	100 ml 10x PBS, 900 ml Milli-Q water made up to 1 L, pH 7.4
50x TAE (Tris base, acetic acid and EDTA)	Tris base 242 g, 57.1 ml glacial acetic acid, 100 ml 0.5M EDTA (pH 8.0) made up to 1 L with Milli-Q water
6x gel loading buffer	5ml 1x TAE, 5 ml glycerol, 10 mg bromophenol blue, 10 mg xylene cyanol
Citrate buffer	2.5 ml 5M NaOH, 0.96 g citric acid (anhydrous), 0.25 ml Tween 20 (pH 6) made up to 500 ml with distilled water
	20 mM Tris, 0.5M NaCl in Milli-Q water, pH 7.0-7.5
Ethylenediaminetetraacetic acid (EDTA)	Sigma-Aldrich, USA
GelRed nucleic acid gel stain (10,000x in water)	Biotium, USA
Target retrieval solution	Dako, Denmark
TE buffer	10 mM Tris, 1mM EDTA (pH 8.0)
Tissue homogenisation buffer (Tris-NaCl)	10 mM Tris-HCl, 1 mM EDTA, 2 μg/ml DNase-inactivated RNase

2.1.4 Histological Reagents

100% Ethanol	ChemSupply, Australia
Bovine serum albumin	Sigma-Aldrich, USA
Haematoxylin and eosin	ThermoFisher Scientific, USA
Horse-radish peroxidase	Bio-Rad Laboratories, USA
Hydrogen peroxide	ChemSupply, Australia
Microscope slides (Superfrost plus)	Menzel-Glaser, Germany
PapPen	DakoCytomation, Denmark
Paraformaldehyde	Sigma-Aldrich, USA
Superfrost plus coverslips (22x 40mm)	Menzel-Glaser, Germany
Xylenes (sulphur free)	ChemSupply, Australia

2.1.5 Antibodies, Enzymes and Serum

Biotinylated donkey anti-goat/rabbit/mouse IgG antibody (secondary antibodies)	Jackson Immunoresearch Lab, USA
Diaminobenzidine substrate (DAB)	Dako, Germany
Immun-Star HRP Chemiluminescent Substrate kit	Bio-Rad (1705040)
Normal Donkey Serum (NDS)	Jackson Immunoresearch Lab, USA
Proteinase K	ThermoFisher Scientific, USA
Mouse anti-LIMP-II monoclonal antibody against a synthetic peptide (Mimotopes, Australia), mapping to the C-terminal region of human LIMP-II	In-house, Australia
Mouse anti-α-synuclein monoclonal antibody	BD Biosciences (610786)
Rabbit anti-α-synuclein polyclonal antibody	Abcam, USA (ab52168)
Rabbit anti-α-synuclein polyclonal antibody	Sigma-Aldrich, USA (SAB21022)
Rabbit anti-β-actin monoclonal HRP antibody	Abcam, USA (ab49900)
Rabbit anti-GFAP polyclonal antibody	Dako, Germany (Z334)
Rabbit anti-paired helical filament-tau (PHF-tau) antibody	Jackson Immunoresearch Lab, USA
Rabbit anti-tyrosine hydroxylase polyclonal antibody	Millipore, Germany (AB152)
Rabbit anti-ubiquitin polyclonal antibody	Dako, Germany (z0458)

2.1.6 Animal handling and tissue harvesting

70% Ethanol	ChemSupply, Australia
1 ml syringes	Becton Dickinson, USA
50 ml syringes	Terumo, Japan
23 G and 25 G needles	Becton Dickinson, USA
Anodised aluminium brain slicer	Braintree Scientific, Inc
Butterfly needles, 23G	Becton Dickinson, USA

2.1.7 Mass Spectrometry reagents

2,2-Dimethoxypropane	Sigma-Aldrich, USA (D136808)
Ammonium acetate	Sigma-Aldrich, USA
Acetonitrile (Optima LCMS grade)	Fisher Scientific, Victoria, Australia
Ammonium formate, 10 mM	Sigma-Aldrich, USA
Butanolic hydrochloride	Sigma-Aldrich, USA (87472)
Dopamine-D_4 internal standard	Sigma-Aldrich, USA
d9-Butanol from CDN isotopes	Pointe-Claire, Quebec, Canada
Formic acid	Sigma-Aldrich, USA
Heparan sulphate sodium salt	Celsus Laboratories, Cincinnati, OH, USA

2.1.8 Cell culture

Dulbecco's Modified Eagle's Media (DEME)	ThermoFisher Scientific, USA
Glutamine	ThermoFisher Scientific, USA
Ham's nutrient F12 media	ThermoFisher Scientific, USA
Normal bovine serum	ThermoFisher Scientific, USA
Penicillin G (5000 U/ml), Streptomycin sulphate (5000 mg/ml)	ThermoFisher Scientific, USA
Skin fibroblast cell medium	50% DMEM, 50% F12, 20% normal bovine serum, 1% glutamine, 1% penicillin G/ streptomycin sulphate
Sucrosome skin fibroblast cell medium	50% DMEM, 50% F12, 20% normal bovine serum, 1% glutamine, 1% penicillin G/ streptomycin sulphate, 100 mM sucrose
Sucrose	Sigma-Aldrich, USA

2.1.9 Miscellaneous

BCA protein kit	ThermoFisher Scientific, USA
96-well polystyrene microplates (F- and V-bottom plates)	Greiner Bio-One, Germany
Non-toxic food colouring	Queens Fine Foods, Australia
Paint (BreatheEasy low sheen acrylic in white)	Berger Paints, Australia
Skim milk powder	Diploma, Australia

2.2 Methods

2.2.1 Mouse colony breeding and maintenance

Three female and three male SNCA knockout mice (B6; 129X1-Snca^{tm1Rosl}/J; stock #03692) were purchased from the Jackson Laboratory, Bar Harbor, Maine, USA. Dr. Arnon Rosenthal and team (Rinat Neuroscience Corporation) created the knockout mice. Three male and six female congenic MPS IIIA mice (B6; Cg-Sgsh^{mps3a}) were obtained from the in-house colony established and maintained at the Women's and Children's Hospital Health Network, North Adelaide, South Australia, Australia. All procedures and experiments were undertaken in the Animal Care Facility at the Women's and Children's Hospital Health Network, with the approval of the University of Adelaide (M-2014-039, M-2014-040, M-2014-041), Women's and Children's Hospital Health Network (AE-978-4-2017, AE-974-4-2016, AE-975-4-2017) and the South Australian Health and Medical Research Institute (SAM/8) Animal Ethics Committees. Gene technology approval (B141-PC1 Notifiable Low Risk Dealings, NLRD) was obtained from the Biosafety Committees of the Women's and Children's Hospital Health Network, University of Adelaide and the South Australian Health and Medical Research Institute.

Mice were housed in a constant temperature/humidity controlled facility with a 14 hr light:10 hr dark cycle, and were given food and water *ad libitum*; mice were provided with plastic houses, cardboard and tissue paper for environmental enrichment. The birth date of mouse pups was taken as being the date on which the pups were first observed. Pups were toe-tagged on Days five to seven of life and weaned at three-weeks of age. Whenever possible, female and male mice were separated and housed in same-sex groups. The mice were monitored daily (including weekends by the Animal Facility staff), and body weight was measured weekly. The morphological phenotypes of both newborn pups and adult animals were assessed and the pattern of any abnormalities or changes was noted.

"Normal" or wild type mice (ie not heterozygotes) were used in the behavioural and subsequent biochemical and histological assessments. While we were unable to backcross the mice into the C57B/6 strain due to time limitation, anecdotally, there was no significant difference between black coatings and brown coatings in several behavioural testings such as open field test, elevated plus maze test and the water maze test.

2.2.2 Genotyping of mice

2.2.2.1 Toe tagging

A sample of toe tissue corresponding to identification number was collected from mice at five- to seven-days of age using sharp iris scissors sterilised with 70% ethanol prior to each use **(Fig 2.1)**. The pups in the cage were removed from the dam simultaneously and placed on soft towels on a bench-coat. Following toe excision, the tissue was placed into a 1.5 ml sterile Eppendorf tube and kept cold on ice. After the procedure, all the pups were placed on bedding material and returned to the dam. The number of pups were counted and monitored on the following day to record maternal rejection or scavenging.

2.2.2.2 Genomic DNA extraction

Toe tissue was utilised to extract clean DNA for PCR genotyping, using a commercial DNA extraction kit according to the manufacturer's instructions (ThermoFisher Scientific). In brief, 200 µl of resuspended salt lysis buffer (composed of 180 µl digestion solution + 20 µl proteinase K solution provided with the kit) was added to each toe to digest proteins and inhibit nucleases. Samples were vortexed briefly and pulsed in a bench centrifuge to ensure that the toe was fully immersed in the buffer. The buffer was then left to completely lyse the toe tissue by overnight incubation at 56°C.

The next day, 20 µl RNase solution was added to the tube to remove RNA, and incubated for 10 min at room temperature; 200 µl of lysis solution was then added and mixed thoroughly for 15 sec until a homogeneous mixture was obtained. Four hundred µl of 50% ethanol was then added, followed by thorough mixing. The prepared lysate was transferred onto a purification column (contained with the kit), which was inserted in a collection tube. The column was centrifuged for 1 min at 6000 g and the flow-through solution was discarded. The DNA retained in the silica membrane of the column was washed twice with alcohol wash solution from the kit. Finally, 100 µl elution buffer was added to the column to elute the highly purified genomic DNA under low ionic strength conditions.

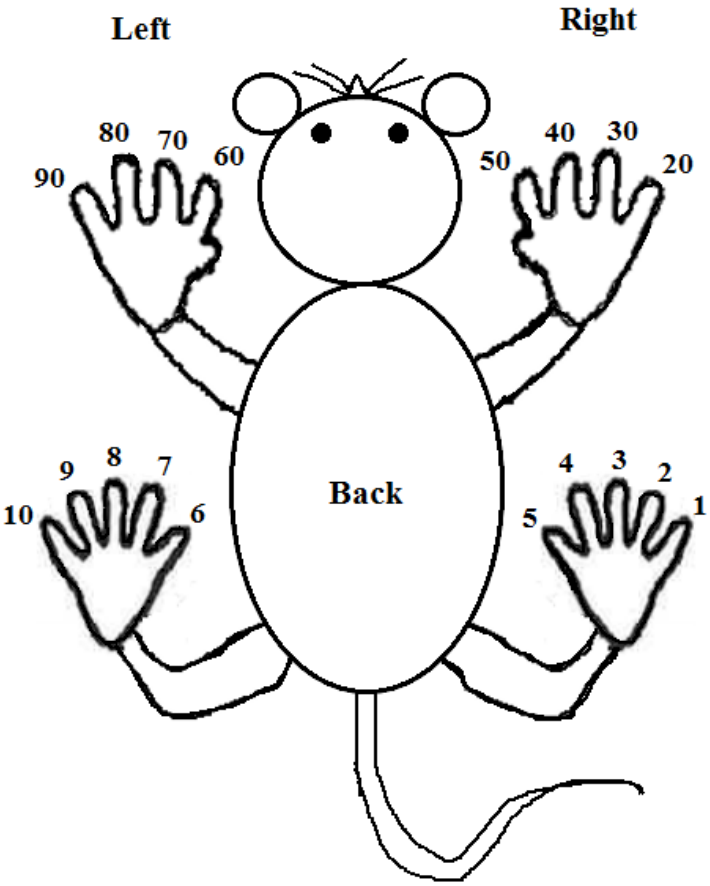

Figure 2.1: Mouse toe-tagging system seen from above.

2.2.2.3 PCR and restriction digest analysis of the sulphamidase (*SGSH*) gene

Five μl of purified genomic DNA was added to 5 μl 10x PCR buffer and mixed with 100 ng of oligonucleotides 5' MS12 (5' NNT CTG TCT TCC TCA GCG 3') and 3' MS4 (5' GAT AAG GCT GTG GCG GGA CAG GG 3'), 5mM dNTP mix and 0.25 units Taq polymerase. Water for injection was added to bring the reaction to a final volume of 50 μl. The mutation region was amplified following 3 min at 94°C, 35 cycles of 45 sec at 94°C, 45 sec at 57°C, 40 sec at 72°C, and 4 min final extension at 72°C.

The *SGSH* gene fragment of 105 bp, spanning the point mutation in exon 2 and a portion of intron sequence, was amplified. The PCR products were then subjected to AciI digestive enzyme at 37°C overnight. AciI cuts the GG in the sequence CAGCGG in which the site is abolished in point mutation (G to A) at nucleotide position 91. Moreover, a second AciI site was present in the 3' primer. Therefore, the final products were seen at 94 bp and 11 bp in mutant mice, and 78 bp, 16 bp and 11 bp in wild-type mice, and all the products in heterozygous mice on a 4.5% agarose gel **(Fig 2.2)**.

2.2.2.4 PCR analysis of the α-synuclein (*SNCA*) gene

PCR analysis to determine the presence or absence of the *SNCA* gene in all mice was undertaken using a previously published method (Abeliovich et al., 2000). Five μl of purified DNA was added to 5 μl 10x PCR buffer (Qiagen) and mixed with primers specific to exon 2 of the *SNCA* gene (5' ATG GAT GTG TTC ATG AAA GGA CTT TCA A 3'), (5' TAC ATA GAG GAC TCC CTC TTT TGT CT 3'), and the neomycin resistance gene (NRG) (5' AGG CGA TAG AAG GCG ATG CG 3'), (5' CAA GAC CGA CCT GTC CGG TG 3'). Five mM dNTP mix, 0.25 units Taq polymerase (Qiagen) and water for injection were then added to the reaction to make a final volume of 20 μl. The targeted DNAs were amplified following 3 min at 94°C, 32 cycles of 45 sec at 94°C, 45 sec at 60°C, 45 sec at 72°C, and 4 min final extension at 72°C. PCR products subsequently underwent electrophoresis on a 3.5% agarose gel. The product at 120 bp in normal wild-type SNCA, 630 bp in SNCA knockout, and both products in SNCA heterozygous mice were seen on a gel **(Fig 2.3)**.

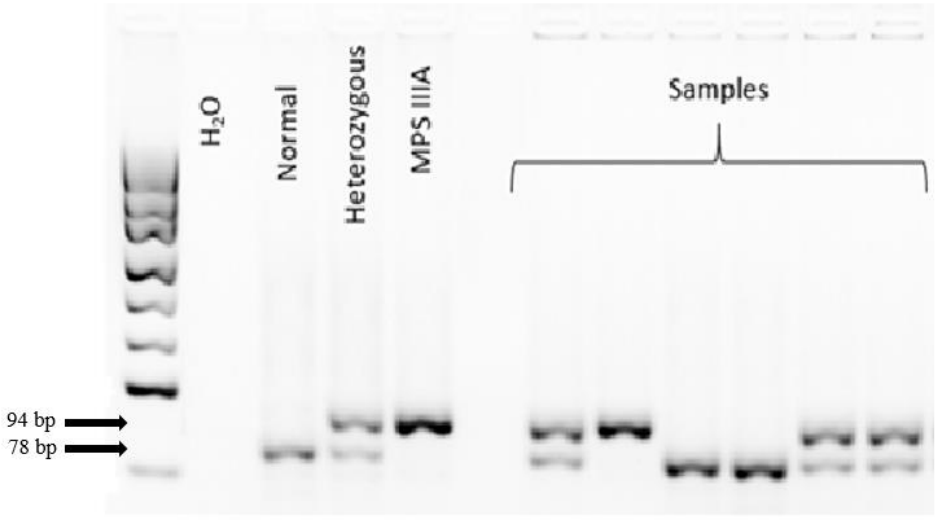

Figure 2.2. Electrophoresis gel separation of genomic DNA from wild-type normal, heterozygote and MPS IIIA mice. Molecular product 94 bp for MPS IIIA, 78 bp product in normal, and both 94 bp and 78 bp products in heterozygotes can be observed. The molecular sizes are indicated by arrows and compared with pUC19/HpaII markers. The 11 bp and 16 bp are too small to be observed on the gel.

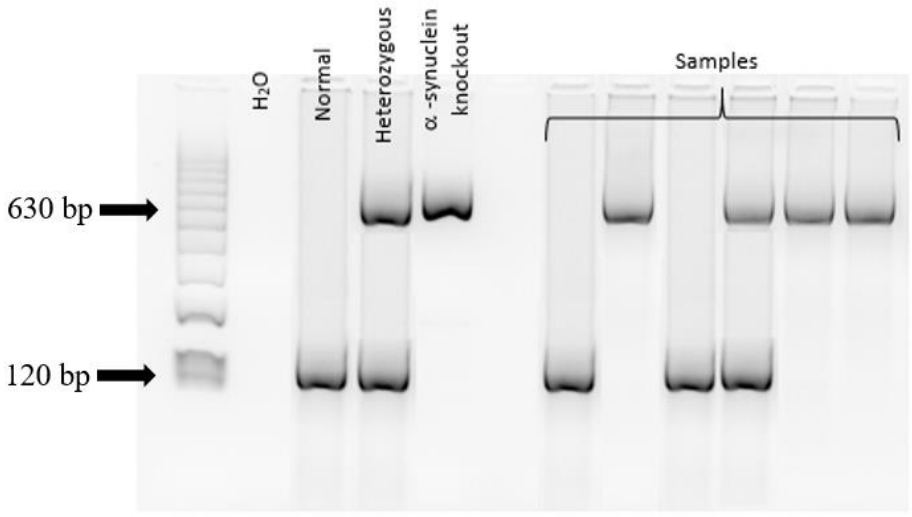

Figure 2.3. Electrophoresis gel separation of genomic DNA from wild-type normal, heterozygotes and SNCA knockout mice. Molecular product 120 bp for normal SNCA, 630 bp product for SNCA knockout, and both products for SNCA heterozygotes can be observed. The molecular sizes are indicated by arrows and compared with pUC19/HpaII markers.

2.2.3 Monitoring food and water intake

Mice designated for behavioural testing were single-housed from 10-weeks of age. The average intake of food and water was monitored in this cohort of mice. Genotype status and identification numbers of animals were blinded to the experimenter. All mice had equal access to standard chow and water *ad libitum* during the analysis period. The environment was maintained at constant humidity and temperature. The cages, lids and water bottles were checked daily to determine whether there was any leakage or spillage of water or food.

The weight of each lid containing food, and that of the respective water bottle, was measured separately when the mice were 12- and 22-weeks of age. Individual water bottles and lids containing food were measured again when mice were 13- and 23-weeks of age. The difference between the measurements was regarded as the amount of food and water consumed within one-week by each animal.

2.2.4 Assessing the level of cage soiling

Along with food and water intake, the amount of faecal and urinary excretion was also monitored for comparative purposes. The level of cage soiling by 12-week old mice was measured qualitatively and graded mild (+), medium (++), heavy (+++). Genotype status and identification number of mice were blinded to the experimenter. The assessments were made independently by Kyaw Kyaw Soe and Sarah Tamang (Lysosomal Diseases Research Unit, South Australian Health and Medical Research Institute). The weight of individual cages (with new bedding present) was recorded when mice were 21- and 22-weeks of age. The difference between measurements was regarded as the amount of soiling by each animal.

2.2.5 Behavioural testing

Behavioural analyses were performed on cohorts of naïve male mice to avoid any influence of female hormone acting on behavioural performance. Prior to performing the behavioural testing, all mice were single-housed. This occurred at 10-weeks of age and ensured each mouse was exposed to the same environment during testing. Mice underwent testing in the Open Field test at 12-weeks of age, the Elevated Plus maze test at 15-weeks of age, the Morris water maze test at 20-weeks of age, and foot print gait test at 21-weeks of age.

All testing was conducted between 7:00 AM and 4:00 PM under normal lighting conditions. The animals were single-housed from 10-weeks of age and were transferred into the test room one-week prior to each behavioural test to acclimatise to the environment. Mice were always tested in random order, with the experimenter blinded to their genotype status.

2.2.5.1 Open Field test

This test involved placing the mouse onto the bottom of an open cage in which the floor was divided into 15 squares measuring 9 cm x 10 cm each and 15 cm high **(Fig 2.4)** (Hemsley and Hopwood, 2005). The frequency of rearing up on hind-limbs and grooming behaviour during 5 min of free running was counted manually. The mouse was also simultaneously monitored with a video camera attached to a computer fitted with HVS OpenField Image Software (www.hvsimage.com). The number of line crosses and the path length of the mice in the 5 min test were documented. The number of faecal boli and urinary spots in the open field were also recorded after each test. The cage was cleaned with 70% ethanol-soaked tissues and dried thoroughly after each mouse.

2.2.5.2 Elevated Plus maze test

The Elevated Plus maze test involved placing the mouse on a plus-shaped maze containing two open arms and two closed arms measuring 50 cm x 7 cm **(Fig 2.5)** (Lau et al., 2008). The test allowed for 5 min of free running, during which time the movements of the mouse were video-recorded. The camera was mounted to the ceiling above the maze, and connected to a computer fitted with HVS PlusMaze Image Software (www.hvsimage.com). The frequency of visits to each arm, path length and time spent in each individual arm were recorded for each mouse within the 5 min period. After each trial, the maze was thoroughly cleaned with 70% ethanol to remove odour and waste.

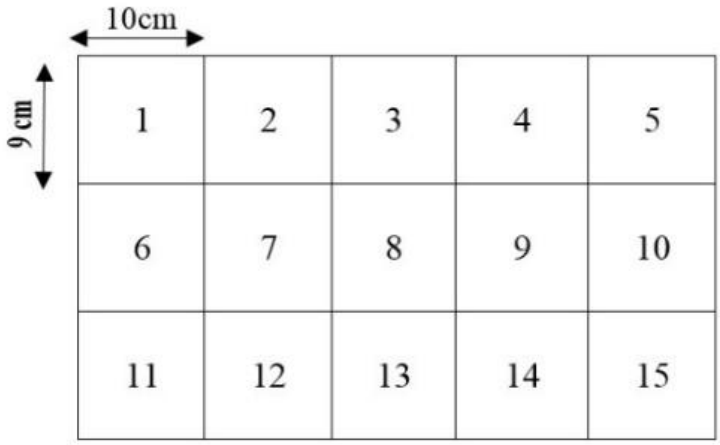

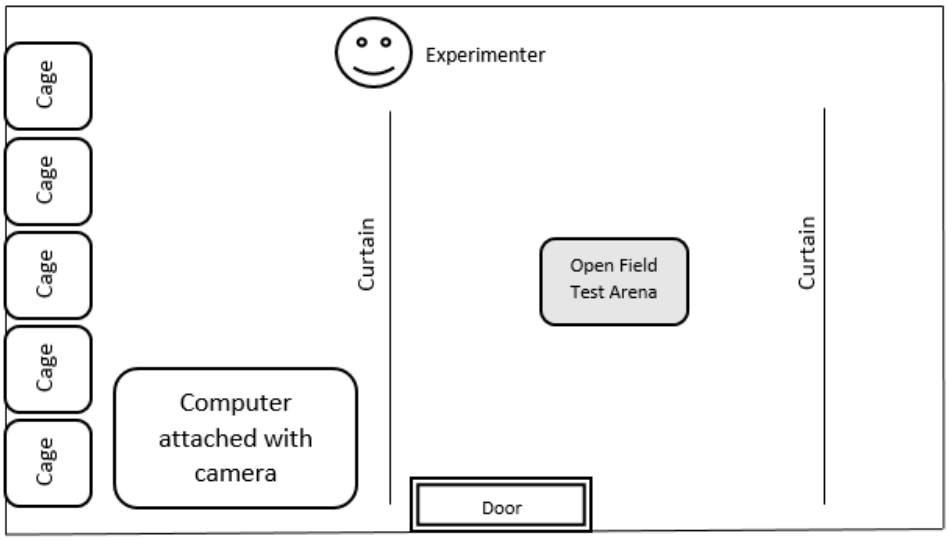

Figure 2.4. Open Field cage and test arena diagram.

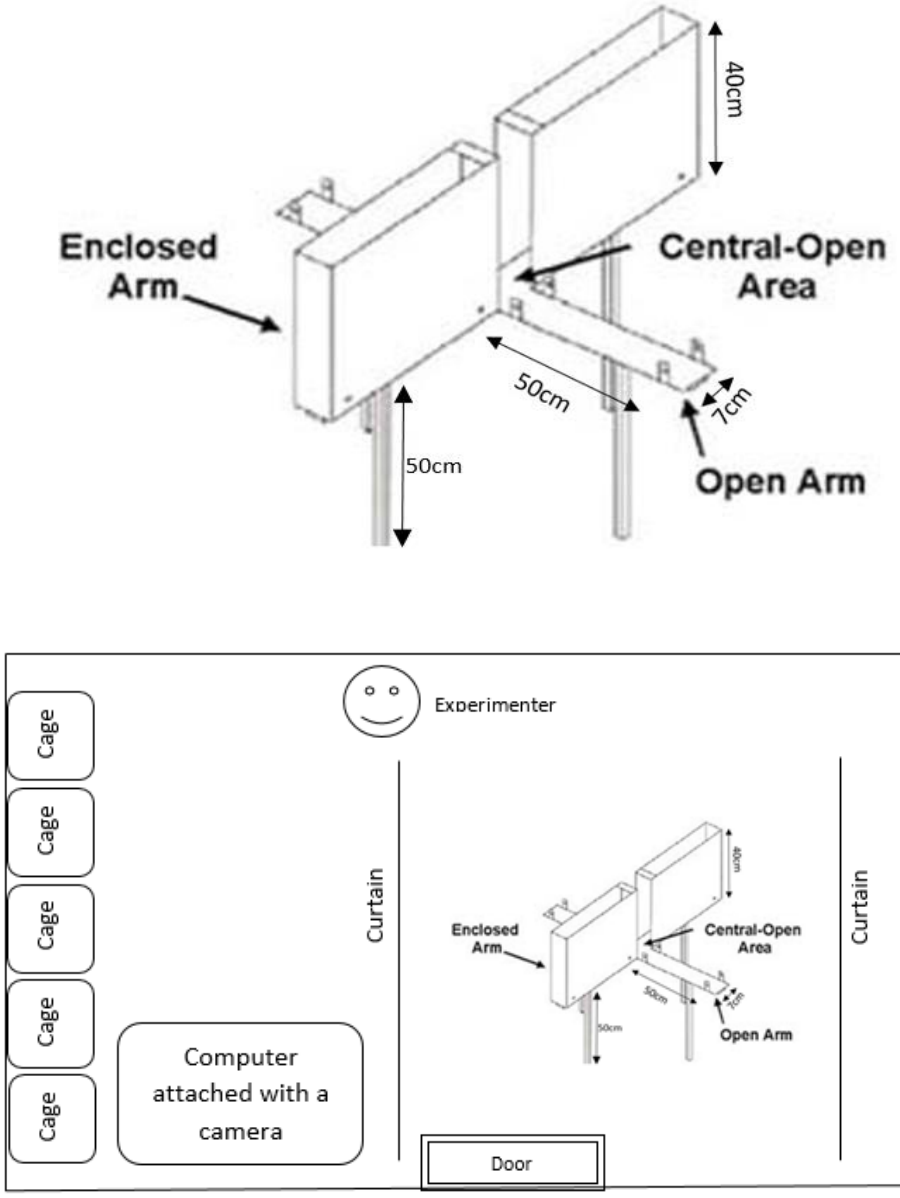

Figure 2.5. Elevated Plus maze set-up and test arena diagram.

2.2.5.3 Morris water maze test

The same groups of single-housed mice underwent the Morris water maze, as per Hemsley et al. (2009). The metallic pool was 120 cm in diameter and 40 cm in height and was filled 30 cm deep with water (21 ± 1°C). The water was made opaque by adding non-toxic white-coloured paint (Berger Paints, Australia). The mice were allowed to learn and locate a hidden platform in the *Acquisition phase* for five consecutive days. This was followed by the *Probe phase* in which the swimming pattern and spatial memory of the animals were recorded for 90 sec with the platform removed. The final *Visual phase* tested the vision and ability of the animals to swim to locate a visible platform.

The *Acquisition phase* involved four 90 sec swims on each of five successive days (Days 1-5). The time taken to find a hidden circular platform (10 cm in diameter) situated in the north-eastern quadrant from the four starting points (north, east, south and west) was measured for a maximum of 90 sec in each swim **(Fig 2.6 A)**. All animals were given 15 sec to rest on the platform; they were offered a paintbrush on which to sit before being taken back to their respective cage. The cages were placed on electronic heat mats to prevent hypothermia between swims. Tissue paper was provided to the animals to dry their bodies quickly.

There were two visual cues and a curtain placed around the testing room as swimming navigation tools for the mice. An inter-trial interval of at least 10 min was maintained across all four trials each day (Days 1 to 5) to minimise the development of hypothermia. Between each swim and at the end of the swimming protocol, mice were returned to their cages, which were placed on heat pads. Tissue paper (in addition to normal bedding) was placed in each cage to absorb water rapidly from the skin.

On Day 6 (*Probe phase*), the swim pattern was monitored in a single swim for 90 sec with no platform in the pool **(Fig 2.6 B)**. On the final day (*Visual phase*), a butterfly flag was placed on the platform which was also moved to an opposite quadrant of the pool, i.e. south-western quadrant **(Fig 2.6 C)**. The visual cues were removed from the room. The time taken for each mouse to find the platform was recorded over the course of four swims up to 90 sec per swim. The mouse did not have to swim again if it found the platform in under 10 sec as it fulfilled the criterion of the visual test. Mice taking longer than 10 seconds were required to swim from another starting point for up to 90 sec.

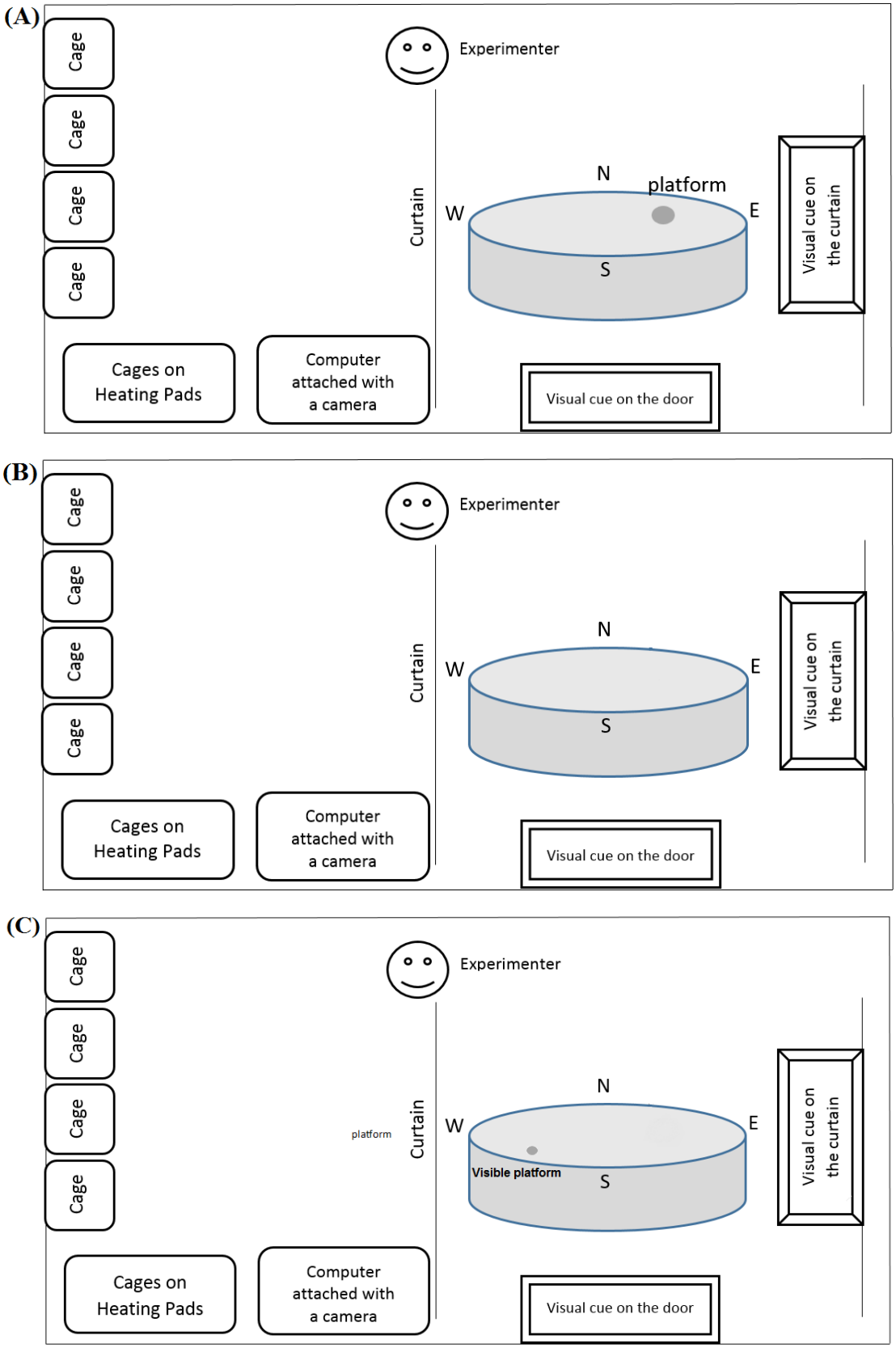

Figure 2.6. Morris water maze schematic diagram. (A) "*Acquisition Phase*" test arena with platform located in north-eastern quadrant; (B) "*Probe Phase*" test arena with no platform'; and (C) "*Visual Phase*" test arena with platform located in the south-western quadrant.

2.2.5.4 Foot print gait test

Gait testing was performed on the same groups of animals. The mice were allowed to practice walking down the walkway a few times to acclimatise them to the testing equipment. Afterwards, the hind-paws of each mouse were dipped in non-toxic food colouring (Queens Fine Foods, Australia) and the mouse was placed on the paper-lined walkway (50 cm length x 12 cm width x 15 cm height) so that the foot prints were recorded (Hemsley and Hopwood, 2005). Mice moved towards a darkened goal box at the end of the walkway for two trials.

Once the paint had dried on the paper, the distance between footprints for both right and left hind-limbs was measured **(Fig 2.7)**. The mean of these measurements was taken as the average gait length for each mouse for both right and left hind-limbs. Moreover, a perpendicular line was drawn from each footprint to measure gait width in the correct walking direction. The average of three lengths or widths was taken for at least two runs per mouse.

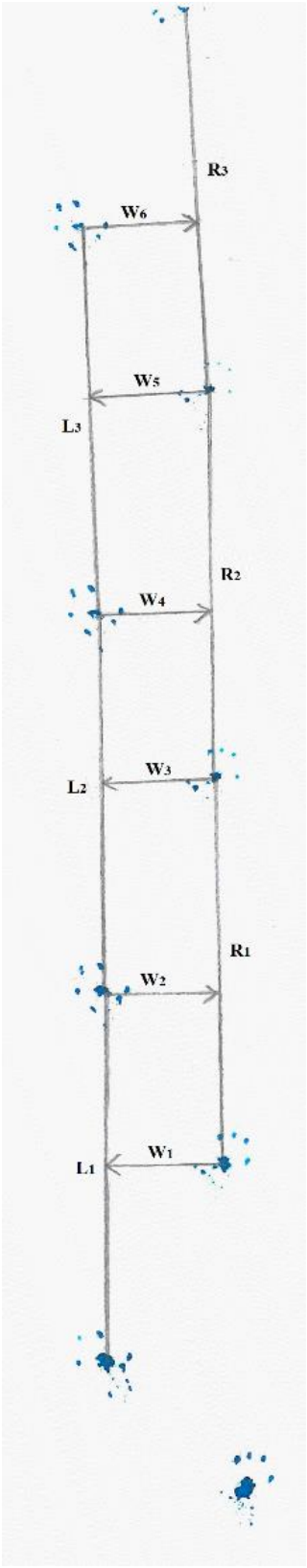

Figure 2.7. Sample foot print diagram.

2.2.6 Perfusion fixation

Reagents were prepared fresh on the morning of the day of tissue collection: 1x PBS working solution was obtained by mixing 100 ml 10x PBS and 900 ml distilled water. Reagent grade 4% PFA (w/v) in PBS (pH 7.4) was also prepared fresh. Mice were humanely euthanised via 0.5-1% CO_2 overdose in a small gas chamber. Once confirmed dead by the absence of a corneal reflex and the pain reflex on pinching toes.

Each mouse limb was pinned to a styrofoam board in the fume hood. The abdominal cavity was opened along the mid-line to reach the diaphragm, which was then gently cut to expose the heart. A 23G butterfly needle was connected to the perfusion apparatus and inserted into the left ventricle. After stabilising the butterfly needle with two pins, the right auricle was snipped with scissors and about 20 ml of ice-cold 1x PBS was administered before switching to 4% PFA. A well-perfused body can be observed by a pale liver, muscle stiffening and tail/limb twitching.

After approximately 20 ml of 4% PFA perfusion, the brains were quickly removed, placed into a brain blocker, and sectioned down the mid-line to provide two hemispheres. Both hemispheres were immediately immersed in 4% PFA for seven-days at 4°C before replacing the PFA with PBS to permit examination of tissues by light microscopy. In addition to the brain, organs such as heart, lungs, liver, spleen and kidney were also collected.

2.2.7 Histology

2.2.7.1 Embedding and processing of brain tissues

Brain hemispheres were treated with a series of buffered formalin, 70% ethanol, 85% ethanol, 95% ethanol, 100% ethanol, and chloroform in an automatic tissue processor. Processed samples were embedded in paraffin wax with the sagittal alignment towards the plane of cut sectioning. Medial sagittal sections of paraffin-embedded brain tissue were cut on a rotary microtome (Leica, Wetzlar, Germany) until the target brain regions were exposed (approximately 0.96 mm and 1.2 mm from the mid-line) using a mouse brain atlas for guidance (Paxinos and Franklin, 2004).

2.2.7.2 Immunohistochemical staining

2.2.7.2.1 Haematoxylin and eosin immunostaining

Medial sagittal sections were stained with haematoxylin and eosin. The anatomical landmarks of brain sections were determined with the use of the mouse brain atlas (Paxinos and Franklin, 2004). Sections were de-paraffinised by sequential treatment with 100% ethanol three-times (5 min each) and xylene solution twice (5 min each). The slides were then stained with hematoxylin and eosin for one min each before coverslips were applied.

2.2.7.2.2 Tyrosine hydroxylase

To enable localisation of the substantia nigra in tissue sections, tyrosine hydroxylase staining was undertaken. Sections adjacent to tyrosine hydroxylase-stained sections were used in the immunostaining analyses described in subsequent sections of Chapter 2. Sections were de-paraffinised as above, and epitope retrieval was achieved by boiling in citrate buffer (pH 6.2), with subsequent heating on 'low medium' mode in a standard kitchen microwave for 10 min. The slides were then cooled to 50°C and blocked with 10% normal donkey serum for 2 hr at room temperature. Overnight incubation with an anti-tyrosine hydroxylase polyclonal primary antibody raised in rabbit (Millipore, Germany) was performed at room temperature (1: 2,500 dilution in 2% NDS).

The next day, endogenous peroxidases were quenched with 0.3% hydrogen peroxidase in PBS for 30 min after washing the slides with PBS. Biotinylated donkey anti-rabbit IgG antibody (1:1000 dilution in PBS) was applied for 2 hr before incubation with Vectastain ABC reagent for 1 hr at room temperature. The tissue sections were then visualised using the diaminobenzidine (DAB) liquid chromogen system (DAKO, Glostrup, Denmark). The slides were dehydrated with sequential 100% ethanol three-times and xylene twice for 1 min each before coverslips were applied.

2.2.7.2.3 Glial fibrillary acidic protein

The staining procedure for glial fibrillary acidic protein (GFAP) was performed according to the method Hemsley et al. (2009). In brief, sections were de-paraffinised as above and epitope retrieval achieved by boiling in citrate buffer (pH 6.2) and subsequent heating on 'low medium' mode in a standard kitchen microwave for 10 min. The slides were then cooled to 50°C and blocked with 10% normal donkey serum for 2 hr at room temperature. Overnight incubation

with an anti-GFAP polyclonal primary antibody raised in rabbit (Dako, Germany) was performed at room temperature (1: 13,000 dilution in 2% NDS).
The next day, endogenous peroxidases were quenched with 0.3% hydrogen peroxidase in PBS for 30 min after washing the slides with PBS. Biotinylated donkey anti-rabbit IgG antibody (1:1,000 dilution in PBS) was applied for 2 hr before incubation with Vectastain ABC reagent for 1 hr at room temperature. The tissue sections were then visualised using the DAB liquid chromogen system. The slides were dehydrated with sequential 100% ethanol three-times and xylene twice for 1 min each before coverslips were applied.

2.2.7.2.4 Lysosomal integral membrane protein II

The staining procedure for lysosomal integral membrane protein II (LIMP-II) was performed according to the method of Hemsley et al. (2009). Sections were de-paraffinised as above and epitope retrieval achieved by boiling in target retrieval solution (pH 6.0) and subsequent heating on 'low medium' mode in a standard kitchen microwave for 10 min. The slides were then cooled to 50°C and blocked with 10% normal donkey serum for 2 hr at room temperature. Overnight incubation with an anti-LIMP-II monoclonal primary antibody raised in mouse (in-house) was performed at room temperature (1:800 dilution in 2% NDS).

The next day, endogenous peroxidases were quenched with 0.3% hydrogen peroxidase in PBS for 30 min after washing the slides with PBS. Biotinylated donkey anti-mouse IgG antibody (1:1,000 dilution in PBS) was applied for 2 hr before incubation with Vectastain ABC reagent for 1 hr at room temperature. The tissue sections were then visualised using the DAB liquid chromogen system. The slides were dehydrated with sequential 100% ethanol three-times and xylene twice for 1 min each before coverslips were applied.

2.2.7.2.5 Ubiquitin

The staining procedure was performed according to the method of Hemsley et al. (2009). Sections were de-paraffinised as above and blocked with 10% normal donkey serum for 2 hr at room temperature. Overnight incubation with an anti-ubiquitin polyclonal primary antibody raised in rabbit (Dako, Germany) was performed at room temperature (1: 8,000 dilution in 2% NDS).

The next day, endogenous peroxidases were quenched with 0.3% hydrogen peroxidase in PBS for 30 min after washing the slides with PBS. Biotinylated donkey anti-rabbit IgG antibody (1:1,000 dilution in PBS) was applied for 2 hr before incubation with Vectastain ABC reagent for 1 hr at room temperature. The tissue sections were then visualised using the DAB liquid chromogen system with haematoxylin counterstaining (as described in 2.2.7.2.1). The slides were dried with sequential 100% ethanol three-times and xylene twice for 1 min each before coverslips were applied.

2.2.7.2.6 Phospho-PHF-tau

The staining procedure was performed according to the method of Beard et al. (manuscript in preparation). Sections were de-paraffinised as above and blocked with 10% normal donkey serum for 2 hr at room temperature. Overnight incubation with an anti-paired helical filament tau polyclonal primary antibody raised in rabbit (Jackson Laboratory, USA) was performed at room temperature (1:250 dilution in 2% NDS).

The next day, endogenous peroxidases were quenched with 0.3% hydrogen peroxidase in PBS for 30 min after washing the slides with PBS. Biotinylated donkey anti-rabbit IgG antibody (1:1,000 dilution in PBS) was applied for 2 hr before incubation with Vectastain ABC reagent for 1 hr at room temperature. The tissue sections were then visualised using the DAB liquid chromogen system with haematoxylin counterstaining. The slides were dehydrated with sequential 100% ethanol three-times and xylene twice for 1 min each before coverslips were applied.

2.2.8 Image analysis

Mounted and cover-slipped sagittal brain sections were scanned on a NanoZoomer Digital slide scanner (Hamamatsu Photonics K.K, Japan) and obtained as high-resolution digital images. Using a mouse brain atlas (Paxinos and Franklin, 2004), six brain regions related to voluntary motor activity (such as primary motor cortex, striatum and brainstem), learning and memory (dentate gyrus of hippocampus), energy intake and endocrine centre (hypothalamus), and the dopaminergic neuronal region (substantia nigra)) were chosen for analysis. Mouse genotype status and identification number were blinded to the experimenter during all staining procedures, slide scanning and post-scanning image analysis.

Using high-resolution scanned digital images, p-tau and ubiquitin-stained inclusions (≥ 5 μm) in five specific brain regions were manually counted by using NanoZoomer Digital Pathology version 2.5.14 software (Hamamatsu Photonics K.K). Lesions with a diameter of ≥ 5 μm were counted and the data was log-transformed; results were expressed as the number of aggregates per mm^2. Background staining of ubiquitin and p-tau did not affect the counting of spheroidal lesions

Thresholding based on the optical density of positive immunostaining was applied to the images stained with glial fibrillary acidic protein and lysosomal integral membrane protein II in a consistent manner using AnalySIS Lifescience software (Version 2.8, Build 1235; Olympus Soft Imaging Solutions, Munster, Germany). Data were summarised as the percentage of immunoreactivity of the respective stained region.

2.2.9 Fresh tissue collection

Mice were humanely euthanised via 0.5-1% CO_2 overdose in a small gas chamber. Once confirmed dead, ~20 ml of ice-cold 1x PBS was administered via the left ventricle of the heart until the liver became pale (as per 2.2.6). The brain was quickly removed, placed into a brain blocker and dissected. Samples were taken from the following regions: olfactory lobes, striata, cerebral cortices, hippocampi and brainstem. The samples were snap-frozen in liquid nitrogen and kept at -80°C until analysis.

2.2.10 Homogenisation and sonication of brain tissues

Brain tissues were mixed with 500 μl of Tris-NaCl buffer (20 mM Tris-HCl (pH 7.2) and 500 mM NaCl in Milli-Q water), and homogenised using an UltraTurrax T10 IKA-Labortechnik homogeniser (Janke and Kunkel, Germany) on ice at 8000 RPM for 30 sec. The homogenates were then sonicated twice on ice for 30 sec using the Misonix Sonicator (Microson XL 2000, Ultra Cell Disruptor, USA). Both homogeniser and sonicator probes were thoroughly rinsed with Milli-Q water after each use. The products were immediately assayed for protein content or stored in -80°C until analysis.

2.2.11 Biochemical analysis

2.2.11.1 Bicinchoninic acid protein assay

The total protein content of brain homogenates was determined using a micro-bicinchoninic acid (BCA) protein assay method (Smith et al., 1985), and performed according to the manufacturer's instructions (ThermoFisher Scientific). In brief, a standard curve ranging from 1 mg to 20 mg of bovine serum albumin was added in duplicate to wells of non-protein-binding 96-well plates. Brain homogenates (2-10 µl volume) were then added in duplicate to respective wells. Moreover, QC samples (MPS IIIA mouse brain homogenates) were added in duplicate to every assay plate. The total volume of the wells was made up to 100 µl with Milli-Q water.

Finally, 100 µl of micro-BCA working reagent was added to each well, covered, and incubated at 37°C for 2 hr. The protein concentration was determined by measuring the absorbance wavelength of 562 nm on a Multilabel Counter Victor3 (Perkin Elmer 1420, USA). Samples were repeated if one or both duplicates had greater than 10% of the coefficient of variation (% CV) or if the protein concentration fell outside the 2 µg and 16 µg range of the standard curve.

2.2.11.2 Cell culturing

All the mouse skin fibroblast cell lysates were kindly provided by Leanne Winner (Lysosomal Diseases Research Unit, South Australian Health and Medical Research Institute). In brief, cultured skin fibroblasts derived from normal and MPS IIIA mice were placed in six-well plates with "skin fibroblast cell medium" (Section 2.1.8) and allowed to reach confluence in a 5% CO_2 atmosphere incubator. Once confluent, cells were grown in a fresh aliquot of "skin fibroblast cell medium" containing 100 mM sucrose that was changed every 4 days for 14-days to induce sucrosome formation; control cell lines were grown in the same cell medium without sucrose. Cells were harvested, resuspended into 200 µl of 10 mM Tris/HCl, pH 7, 0.15 M NaCl with 10% SDS buffer solution; protein content was either determined immediately, or the sample was stored at -80°C until analysis.

2.2.11.3 Immunoblotting

Brain tissues were homogenised in 500 µl of cold extraction buffer (20 mM Tris-HCl (pH 7.2), 500 mM NaCl and 1% Triton X-100, containing protease inhibitor mixture), sonicated for 10 sec and heated at 95°C for 5 min. The extracts were then centrifuged at 16,000 g for 10 min to separate Triton-soluble (supernatant) and Triton-insoluble (pellet) fractions. Skin fibroblast

lysates were also reconstituted in extraction buffer. Total protein was determined using the micro-BCA protein assay kit as above (Section 2.2.11.1).

Equivalent protein amounts of each sample were electrophoresed through a 4-12% acrylamide SDS-PAGE gel employing the NuPage system (Invitrogen), and then transferred to a polyvinylidene difluoride (PVDF) membrane. The membrane was then exposed to 0.4% PFA in PBS for 30 min at room temperature before blocking for 1 hr at room temperature in PBS + 0.1% Tween 20 + 10% skim milk powder, and was then incubated overnight in primary antibody against α-synuclein (1:1000) in conditioned medium at 4°C. Next morning, the membrane was washed three-times for 5 min at room temperature in PBS + 0.1% Tween 20, and incubated at room temperature for 1 hr in PBS + 0.1% Tween 20 + 2.5% skim milk powder + 1/5000 horse-radish peroxidase-linked sheep anti-mouse IgG (GE Healthcare). Finally, the membrane was washed three-times for 5 min at room temperature in PBS + 0.1% Tween 20, drained, treated with the Immune-star horse-radish peroxidase substrate kit (Bio-Rad), and exposed to film.

2.2.11.4 Heparan sulphate quantification

The method of Trim et al. (2015) was used to measure HS in mouse tissues. Briefly, the striatum from one mouse brain hemisphere was homogenised in 500 µl of 0.02 M Tris/0.5 M NaCl, pH 7.4. Homogenates were subjected to two cycles of sonication (30 sec each) and stored at -80°C until analysis. The total protein concentration was determined using the micro-BCA assay (2.2.11.1). One hundred µg total homogenate protein was freeze-dried overnight in a SpeedVac Concentrator (Thermo Fisher Scientific, Waltham, MA, USA) in a 12 ml glass tube.

The dried homogenate was then resuspended in 50 µl 2,2-dimethoxypropane, followed by the addition of 1000 µl butanolic hydrochloride. After heating at 100°C for 2 hr, the samples were completely dried by nitrogen gas at 45°C for 1 hr. Each sample was then reconstituted in 200 µl 10 mM ammonium acetate containing *ca.*1 µg/ml deuterated HS internal standard, and mixed for 30 min at room temperature on an orbital shaker (Ratek Instruments, Boronia, Vic, Australia.). The samples were centrifuged at 13,000 RPM for 15 min on a Biofuge Pico (Heraeus, Germany). Supernatants of 180 µl were carefully collected, and placed into a 96-well microtitre plate at 6°C held in the Agilent 1290 infinity II sample holder until analysis.

2.2.11.4.1 Liquid chromatography/mass spectrometry of heparan sulphate

The analysis was performed by Dr. Paul Trim (Mass Spectrometry Core Facility, Lysosomal Diseases Research Unit, South Australian Health and Medical Research Institute). Samples were analysed by electrospray ionisation-tandem mass spectrometry on a PE Sciex API 4000 QTrap triple-quadrupole mass spectrometer (AB/Sciex, Concord, Ontario, Canada). Liquid chromatographic (LC) separation prior to mass spectrometry (MS) analysis was performed on a 1290 Infinity II LC system (Agilent) equipped with a 2.1 mm ID x 5 mm Zorbax Eclipse Plus C18 guard column and a 2.1 mm x 50 mm Zorbax Eclipse Plus C18 Rapid Resolution reversed phase analytical column, both with 1.8 µm particle size (P/N. 821725-901, S/N. USEDP01821 and P/N. 959757-902, S/N. USDAY21298, respectively).

A binary solvent gradient was utilised to elute the samples. Mobile phase (A) solvent contained water/formic acid (999:1 v/v), and mobile phase (B) solvent was composed of acetonitrile/formic acid (999:1 v/v). A 7.5 µl injection of a sample was loaded on the column at a flow rate of 350 µl per min using 99% mobile phase (A) solvent. Chromatographic separation was performed using the gradient shown in **Table 2.1**. The gradient used ran from 99% to 90% mobile phase (A) over 4.5 min at the same flow rate. The column was then washed for 1.1 min with 99% mobile phase (B), followed by column equilibration over 2.3 min with 99% mobile phase (A).

Data were acquired in multiple reaction monitoring mode. In this mode, three transitions were monitored for 50 ms each, *m/z* 468.245 to 162.077, *m/z* 486.384 to 162.077, and *m/z* 510.255 to 278.160 for the measurement of HS disaccharides (HS transition), deuterated HS disaccharides (internal standard transition) from spiked internal standard and chondroitin sulphate/dermatan sulphate disaccharides (CS/DS transition), respectively. The peak areas were calculated using Analyst 1.6.2 software (AB/Sciex). Final HS values were calculated by the peak area ratios for HS and internal standard for all samples individually. All samples were analysed in a random order interspersed every three injections with a blank injection of Milli-Q water. The dominant peak out of multiple peaks was integrated for the analysis.

Table 2.1. The chromatographic gradient used for the analysis of butanolic products of heparan sulphate.

Time	%A	%B	Flow (ml/min)
0.01	99	1	0.350
2.00	95	5	0.350
2.01	80	20	0.350
5.0	75	25	0.350
5.01	1	99	0.350
7.5	99	1	0.350
8.5	99	1	0.350

2.2.11.5 Ganglioside quantification

Gangliosides were extracted from the homogenised and sonicated striata based on the method of Folch et al. (1957). Five hundred µg of each sample homogenate was transferred to a 10 ml glass tube and made up to equal volumes by adding Milli-Q water. A 'reagent blank' (Milli-Q water), a 'reagent blank + internal standard', a 'matrix blank' (Tris-NaCl buffer), a 'matrix blank + internal standard', a 'sample QC blank' (MPS IIIA brain homogenate) and a 'sample QC blank + internal standard' were also included.

Twenty-two µl of the $d_{35}G_{M1}$ internal standard was added to each sample except for the appropriate blanks by using a positive displacement pipette. The internal standard was made up of a 50:50 mixture of two $d_{35}G_{M1}$ species (18:1/18:0 and 20:1/18:0). To all tubes, 2 ml of $CHCl_3$/MeOH (2:1) was then added. The tubes were shaken on a platform shaker/tube rotator at 40 RPM for 10 min and allowed to stand on the bench for 50 min. Samples were mixed with 200 µl of Milli-Q water for partition, shaken on a platform shaker at 40 RPM for 10 min, and then centrifuged at 3500 RPM for 5 min to separate two layers.

C18 extraction columns were primed with 3x 1 ml methanol followed by 3x 1ml Milli-Q water. The upper aqueous layers from centrifugation were loaded onto their respective columns and transferred with glass Pasteur pipettes. The solution was allowed to enter the solid phase of the column completely, after which the columns were washed with 1x 1 ml Milli-Q water. Gangliosides were then eluted with 3x 1 ml methanol into clean 10 ml glass tubes. The eluted samples were dried under N_2 at 40°C. The dried samples were resuspended in 100 µl of 100% methanol (MeOH)/10 mM ammonium formate (NH_4COOH). The resuspended samples were then centrifuged at 3500 RPM for 5 min; approximately 80 µl of supernatant from each tube was then carefully pipetted into a 96-well microtitre plate before LC/MS analysis.

2.2.11.5.1 Liquid chromatography/mass spectrometry of gangliosides

The analysis was performed by Stephen Duplock (Mass Spectrometry Core Facility, Lysosomal Diseases Research Unit, South Australian Health and Medical Research Institute). Reverse-phased liquid chromatographic separation before MS analysis was performed using a 3 µm Alltima C18 column (50 × 2.1 mm) (Alltech Associates, Deerfield, IL), strictly maintained at 21°C. A binary solvent gradient was utilised to elute the samples. Mobile phase (A) solvent contained 30% tetrahydrofuran/20% CH_3OH/50% H_2O in 5 mM NH_4COOH, and mobile phase

(B) solvent was composed of 70% tetrahydrofuran/20% CH_3OH/10% H_2O in 5 mM NH_4COOH. Twenty µl of the resuspended sample was injected first into 70% mobile phase (A), followed by a linear ramp (0.01–3.0 min) 100% mobile phase (B) for 3 min. It was then transferred to 70% mobile phase (A) (6.01–9.0 min) for equilibration prior to the next injection.

The column flow was diverted to the waste collection from 0-1.6 min by a valco 10-port post-column valve. G_{M2} molecular species were identified by ion scanning for *m/z* 290, depending on the free sialic acid in negative ion mode.

Samples were analysed by electrospray ionisation-tandem MS on a PE Sciex API 4000 QTrap triple-quadrupole mass spectrometer. Gangliosides GM_2 16:1/18:0, 18:1/18:0, 20:1/18:0, and GM_3 C16:1/18:0, C18:1/18:0, C18:1/24:1 species were quantified by negative ion multiple reaction monitoring mode with a turbo-ion spray source at 200 °C and -4500 voltage. Concentrations of gangliosides were measured by relating the peak area of each species to the peak area of the internal standard. The internal standard $d_{35}G_{M1}$ 18:1/18:0 species was used for quantification.

2.2.11.6 Dopamine quantification

The level of the neurotransmitter dopamine in the striatum in one brain hemisphere was measured using the method of Kim et al. (2014). The weight of half of the striatum from each mouse was measured; acetonitrile was then added to the tissue according to its weight (10 µl/1 mg). The solution was mixed with 20 µl dopamine-D_4 internal standard (1,000 ng/ml) before sonication for 60 sec. The sample was then cooled at -20°C for 30 min before centrifugation at 12,000 RPM for 10 min at 4°C. The resultant supernatants were transferred to 96-well plates and injected into the LC-MS/MS system autosampler.

The analysis was performed by Stephen Duplock (Mass Spectrometry Core Facility, Lysosomal Diseases Research Unit, South Australian Health and Medical Research Institute). Liquid chromatographic separation prior to MS analysis was by means of a Waters Acquity UPLC system equipped with a 2.1 mm ID x 150 mm BEH C18 1.7 µm analytical column. A binary solvent system was used, with mobile phase (A) consisting of aqueous 10 mM ammonium formate and 0.15% formic acid, and mobile phase (B) consisting of acetonitrile. Sample injection was 5 µl with a flow rate of 300 µl/min, and column temperature of 50°C. Initial

conditions were 99.9% mobile phase A and 0.1% mobile phase B for 0.5 min. Chromatographic separation was performed using a gradient from 99.9% (A) to 10% (B) over 2 min and held at 10% (B) for 1 min. Mobile phase (B) was increased to 99% over 0.1 min and held for 0.9 min before returning to initial conditions over 0.1 min. These conditions were equilibrated over the next 3 min prior to the next injection. Total run time per sample was 7 min.

MS was performed on an API 4000 QTrap triple quadrupole mass spectrometer. Data were acquired in multiple reaction monitoring (MRM) mode using the above acquisition method and quantitation method 'dopamine + D exchange MRMs'. The peak area ratios for dopamine were calculated and quantified against D_4 dopamine internal standard using Microsoft Excel Software. Final results were expressed in ng per mg tissue.

2.2.12 Statistical analysis

Statistical analysis of Morris water maze data was performed in consultation with Dr. Stuart Howell, Data Management and Analysis Centre, University of Adelaide.

Morris water maze data were analysed using SAS 9.3 software (SAS Institute Inc, Cary, NC, USA). The data were summarised as means with standard deviations and 95% confidence intervals and median with range. Linear mixed effects models were applied, with "animal" treated as a random factor. Swim latency, path length, speed, thigmotaxis time and thigmotaxis path were log transformed prior to analysis due to violations of the distributional assumptions of a linear mixed effect model. The data were transformed back to the original scale prior to reporting. Thus, the reported differences in least square means represent the ratio of two geometric means. Circling was dichotomised to represent 1 versus the remainder (<1 and ≥ 2) and summarised using proportions. A linear mixed effects model was applied using a binomial distribution and logit link function. "Animal" was treated as the random factor. The results were transformed to odds ratios prior to reporting. The data were plotted using GraphPad Prism V_6 software (GraphPad Prism Software Inc., San Diego, CA, USA).

The remaining data were assessed using GraphPad Prism V_6 software. Statistical analysis was performed using one-way analysis of variance (ANOVA) followed by a *post-hoc* Bonferroni correction to adjust for multiple group comparisons. Data are presented as mean ± SEM with P

< 0.05 considered be statistically significant. Due to normality violations, histological data were log-transformed $Y = (\text{Log } Y + 1)$ and then examined in the same manner.

Chapter (3)

Generation and characterisation of MPS IIIA mice deficient in α-synuclein

3.1 Introduction

Congenic MPS IIIA mice display similar disease characteristics to those described for the human disorder. At birth, they are indistinguishable from normal, and start to exhibit unique phenotypes such as facial dysmorphism, skin thickening, dishevelled fur, and hepatosplenomegaly by seven- to eight-weeks of age (Crawley et al., 2006). Moreover, progressive features, such as a distinct hunched posture and mild skeletal deformity are present as mice age.

SNCA null mice (B6; 129X1-*Snca*^{tm1Rosl}/J; SNCA$^{-/-}$; Jackson Laboratory, USA) are viable, fertile, normal in size and do not display any gross phenotypic abnormalities. A wild-type complement of dopamine neurons, fibres and synaptic terminals is present, and the overall brain architecture appears to be intact (Abeliovich et al., 2000).

This study aimed to create MPS IIIA mice deficient in *SNCA* (MPS IIIA-SNCA$^{-/-}$) and examine the effects on disease phenotype. MPS IIIA mice heterozygous for SNCA (MPS IIIA-SNCA$^{+/-}$) and those with wild-type SNCA levels (MPS IIIA-SNCA$^{+/+}$) were also included in this study, along with wild-type-SNCA$^{+/+}$ mice (Normal). Wild-type mice with an SNCA knockout background (SGSH$^{+/+}$ SNCA$^{-/-}$) were not included in this study as previous studies reported that these transgenic mice show little or no significant phenotypic and pathological changes compared to wild-type mice (Abeliovich et al., 2000; Cabin et al., 2002; Chen et al., 2002; Chandra et al., 2004; Robertson et al., 2004).

MPS IIIA mice were crossed with SNCA$^{-/-}$ mice to create carrier/heterozygous animals (first generation); these were inter-crossed to create the second generation. Both genotypes were characterised regarding breeding/husbandry characteristics. The crossing of second generation mice created sufficient animals for phenotypic and pathological evaluation. The experimental design for characterising the third generation mice is shown in **Table 3.1**.

Table 3.1. Experimental design: number of animals from each of the four genotypes in the behavioural and pathological studies.

Number of animals required				
Purpose/ Genotype	**$SGSH^{+/+}$ $SNCA^{+/+}$ (Normal)**	**$SGSH^{-/-}$ $SNCA^{+/+}$ (MPS IIIA-$SNCA^{+/+}$)**	**$SGSH^{-/-}$ $SNCA^{+/-}$ (MPS IIIA-$SNCA^{+/-}$)**	**$SGSH^{-/-}$ $SNCA^{-/-}$ (MPS IIIA-$SNCA^{+/-}$)**
Biochemical evaluation @ 3-weeks	5	5	5	5
Histological evaluation @ 3-weeks	5	5	5	5
Biochemical evaluation @ 12-weeks	5	5	5	5
Histological evaluation @ 12-weeks	5	5	5	5
Behavioural studies @ 12-, 15-, 20- and 21-weeks	16	16	16	16
Subsequent Biochemical evaluation @ 22-weeks	5	5	5	5
Histological evaluation @ 22-weeks	5	5	5	5
Total	36	36	36	36

Only male mice were utilised in the behavioural analyses because MPS IIIA female mice have shown delayed or no phenotypic change in other studies, possibly due to female hormonal effects (Hemsley and Hopwood, 2005; Crawley et al., 2006).

The Morris water maze test has the greatest standard deviation compared to other behavioural assays, so previously obtained data were used to conduct a power calculation (Gliddon and Hopwood, 2004; Crawley et al., 2006). The standard deviation in the Morris water maze test was 30 and 16 for normal and MPS IIIA mice, respectively; means were 43 sec and 69 sec for control normal and MPS IIIA mice, respectively. There would be 95% power to detect a difference with an alpha of 0.05, with a group size of 16.

Previous data regarding the quantification of HS in unaffected and MPS IIIA mouse brain using a mass spectrometry-based method showed that normal tissue had 17.4 (relative intensity per mg tissue), and MPS IIIA tissue had 42.6 (relative intensity per mg tissue) with a standard deviation of 15. If an alpha = 0.05 and a power of 95% were used to obtain a difference between groups, n=5 mice would be required per group for biochemical assays (Hemsley et al., 2007). Quantification of glial fibrillary acidic protein immunostaining in the rostral cerebral cortex of 30-week-old MPS IIIA and unaffected animals in a previous study indicated that the mean of the thresholded area was 0.37% in MPS IIIA mice, and 0.9% in normal mice with a standard deviation of 0.3 (Savas et al., 2004). If an alpha of 0.05 and a power of 95% were used to detect a difference between groups, n=5 mice would be required per group for histological investigations.

3.2 Results

3.2.1 Genotyping of animals

Identification of the D31N mutation in the *SGSH* gene and deficiency of the *SNCA* gene was performed by PCR, as outlined in Chapter 2 (sections 2.2.2.3 and 2.2.2.4). A toe tagging system was used between five- to seven-days of age to individually identify mice; tissue lysates were used for genotyping.

3.2.2 Breeding for the first generation

Three male and female adult breeding pairs of *SNCA* knockout mice ($SNCA^{-/-}$) were obtained from the Jackson Laboratory. To generate MPS IIIA SNCA-deficient mice, congenic MPS IIIA mice (B6.Cg-$Sgsh^{mps3a}$; $SGSH^{-/-}$) were paired with $SNCA^{-/-}$ mice. As outlined in Table 3.2, nine congenic MPS IIIA mice (three males and six females) were crossed with six *SNCA* knockout mice (three males and three females). There were two unsuccessful harem matings out of nine.

The first generation mice were healthy, showed no physical abnormality and increased their body weight in a manner comparable to their wild-type counterparts. There were 75 progenies, heterozygous for both *SGSH* and *SNCA* genes ($SGSH^{+/-}$ $SNCA^{+/-}$). The mean litter size was 4.1, with 42 males (56%) and 33 females (44%) obtained. The average body weight of both sexes from three- to seven-weeks of age is shown in **Fig 3.1**. Male mice were significantly heavier than females by four-weeks of age ($P = 0.0001$) until seven-weeks of age ($P < 0.0001$). There was no incidence of cannibalism or ill health in resultant heterozygous pups.

Table 3.2. The outcome of the cross between MPS IIIA and SNCA knockuout ($SNCA^{-/-}$) males (M) and females (F).

Pairing type	No. pairs	Successful pairings	1st litter			2nd litter			Average litter size = 4.1	
			Total	Male	Female	Total	Male	Female	Total	Cannibalism
$SNCA^{-/-}$ (F) X MPS IIIA (M)	3	3	19	10	9	29	18	11	48	0
MPS IIIA (F) X $SNCA^{-/-}$ (M)	6	4	18	11	7	9	3	6	27	0
Total	9	7	37	21 (57%)	16 (43%)	38	21 (55%)	17 (45%)	75	0

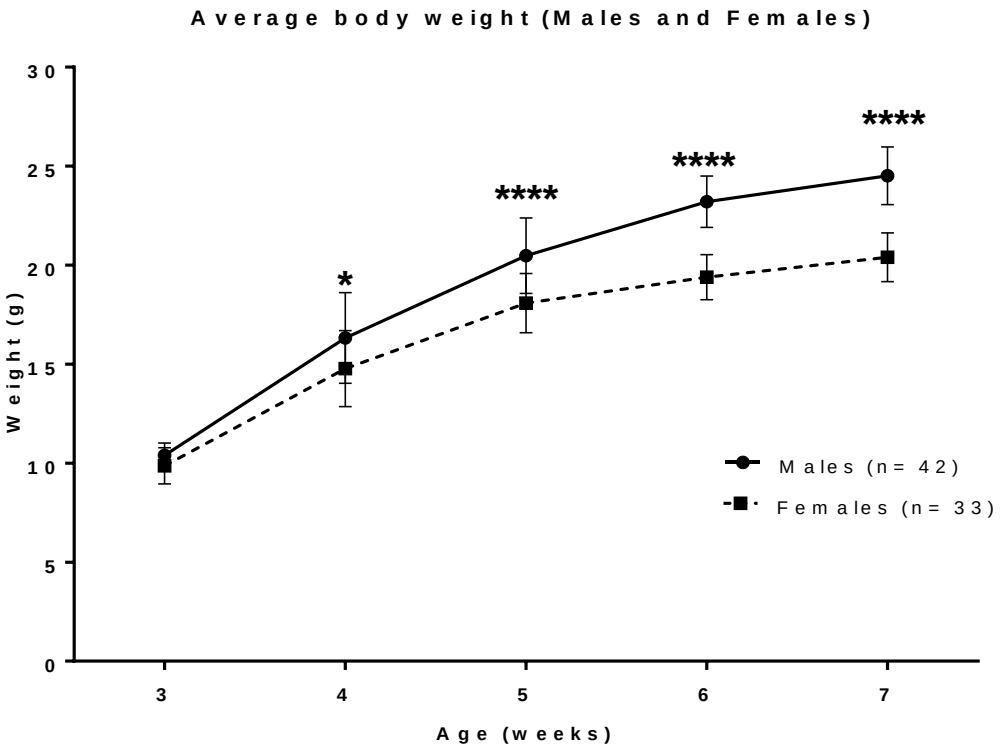

Figure 3.1. Mean body weight for first generation male and heterozygous female mice ($SGSH^{+/-}$ $SNCA^{+/-}$) from three- to seven-weeks of age. Data are presented as the mean ± SEM (n=42 males, 33 females). Statistical analysis was performed using two-way ANOVA for all the groups followed by Bonferroni's multiple comparison tests between the groups. * $P < 0.05$; ****$P < 0.0001$ male versus female body weight. The number of animals in each group is shown in brackets.

3.2.3 Breeding for the second generation

The first generation heterozygotes ($SGSH^{+/-}$ $SNCA^{+/-}$) were crossed using strict brother x sister mating. There were 39 pairings in total, 36 of which were successful; 299 mice were obtained across two rounds of breeding, and progeny exhibited nine different genotypes at the predicted ratio of ~11% in each genotype (Table 3.3). Of the offspring, there were 161 males (53.8%) and 138 females (46.2%), with an average litter size of ~4.2. The incidence of cannibalism was 1.7% (n= 5) across both litters.

Body weights were recorded on a weekly basis and are shown in **Fig 3.2 A** (males) and **Fig 3.2 B** (females). Body weight was similar in all groups at weaning. By four-weeks of age, both male and female MPS IIIA-$SNCA^{-/-}$ mice were significantly heavier than their Normal counterparts with P = 0.0282 and P = 0.0048, respectively. Thereafter, male MPS IIIA mice with all different *SNCA* genotypes were heavier than their Normal counterparts until eight-weeks of age even though the difference was not statistically significant **(Fig 3.2 A)**. On the other hand, all female MPS IIIA groups of mice gained weight similar to their age-matched Normal counterparts **(Fig 3.2 B)**.

Table 3.3. Breeding outcomes of the second generation by pairing MPS IIIA and SNCA knockout mice.

Genotype outcome	$SGSH^{+/+}$ $SNCA^{+/+}$	$SGSH^{+/+}$ $SNCA^{+/-}$	$SGSH^{+/+}$ $SNCA^{-/-}$	$SGSH^{+/-}$ $SNCA^{+/+}$	$SGSH^{+/-}$ $SNCA^{+/-}$	$SGSH^{+/-}$ $SNCA^{-/-}$	$SGSH^{-/-}$ $SNCA^{+/+}$	$SGSH^{-/-}$ $SNCA^{+/-}$	$SGSH^{-/-}$ $SNCA^{-/-}$	Cannibalism
Outcome (%)	28 (9.4%)	35 (11.7%)	29 (9.7%)	27 (9%)	68 (22.7%)	34 (11.4%)	22 (7.4%)	32 (10.7%)	24 (8%)	
Males (%)	15 (53.5%)	20 (57%)	16 (55%)	16 (59%)	32 (47%)	16 (47%)	14 (63%)	18 (56%)	14 (58%)	5 (1.7%)
Females (%)	13 (46.5%)	15 (43%)	13 (45%)	11 (41%)	36 (53%)	18 (53%)	8 (37%)	14 (44%)	10 (42%)	

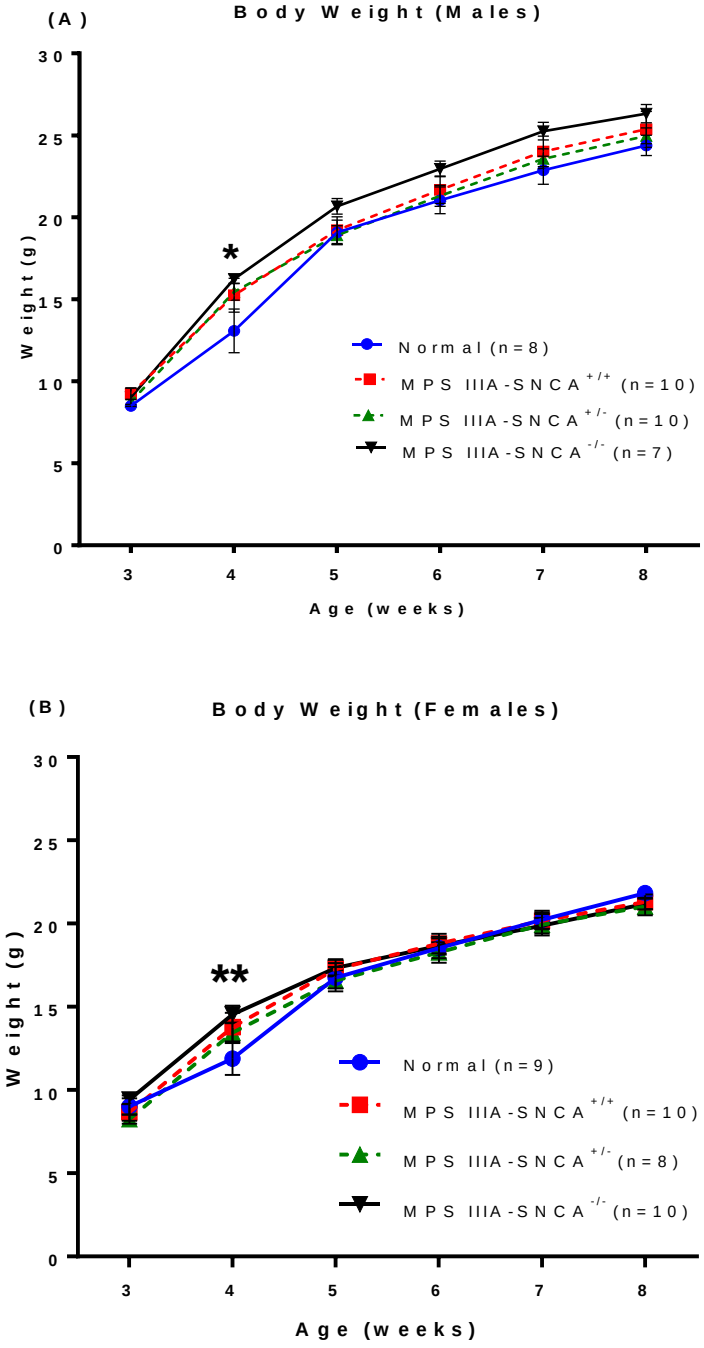

Figure 3.2. Mean body weights of the second generation male (A) and female mice (B) between four genotypes. Mean ± SEM shown (n=7-10 males per group, 8-10 per females per group). Data are presented as the mean ± SEM (n= 42 males, 33 females). Statistical analysis was performed using repeated measures two-way ANOVA for all the groups followed by Bonferroni's multiple comparison tests between the groups. * $P < 0.05$; ** $P < 0.01$ normal versus MPS IIIA. The number of animals in each group is shown in brackets.

3.2.4 Breeding for the third generation

To create sufficient mice for phenotyping and subsequent pathological investigations, 40 pairings of mice with five different genotypes were carried out (Table 3.4). All nine pairings of mice with a normal genotype were successful, with 49 males and 38 female offspring obtained. In contrast, pregnancy was not always successful from MPS IIIA pairings, with infertility observed. Furthermore, a high cannibalism rate was also noted in some females. The total number of pups generated was greater in the first litter than the second, in all types of pairings **(Fig 3.3)**.

The average overall litter size of the third generation was 4.5, with a total number of 273 mice from 32 successful pairings out of 40. The litter size was highest in Normal x Normal pairings with 4.8, MPS IIIA-SNCA$^{+/-}$ x MPS IIIA-SNCA$^{+/-}$ (4.6), MPS IIIA-SNCA$^{-/-}$ x MPS IIIA-SNCA$^{+/-}$ (4.4), MPS IIIA-SNCA$^{+/-}$ x MPS IIIA-SNCA$^{-/-}$ (3.9), and MPS IIIA-SNCA$^{+/+}$ x MPS IIIA-SNCA$^{+/+}$ (3.4). The overall cannibalism rate was 6%. The percentage of male and female offspring from the first litter was 47.5% and 52.5%, respectively. From the second litter, it was 70% and 30%, respectively **(Table 3.4)**.

The MPS IIIA-SNCA$^{+/+}$ pairings produced 48 offspring in total with two unsuccessful pairings out of nine. Both sexes of MPS IIIA-SNCA$^{+/-}$ and MPS IIIA-SNCA$^{-/-}$ mice were fertile and produced 101 pups in total. However, not all of the pairings were successful, indicating individual fertility issues. At the same time, there were 37 pups from MPS IIIA-SNCA$^{+/-}$ inter-pairings. Notably, there were 15 total incidences of cannibalism from MPS IIIA pairings, while there were only two such incidences in normal x normal pairings.

Table 3.4. Breeding outcomes for the third generation

Pairing Type	No. pairs	Successful pairings	1st litter			2nd litter			Overall litter size = 4.5		
			Total	Male	Female	**Total**	Male	Female	**Total alive**	Litter size	Cannibalism/ Found dead
Normal X Normal	9	9	**53**	27	26	**34**	22	12	**87**	4.8	2
MPS IIIA- SNCA$^{+/+}$ X MPS IIIA- SNCA$^{+/+}$	9	7	**39**	23	16	**9**	5	4	**48**	3.4	1
MPS IIIA-SNCA$^{+/-}$ (F) X MPS IIIA- SNCA$^{-/-}$ (M)	8	5	**37**	14	23	**2**	2	0	**39**	3.9	3
MPS IIIA- SNCA$^{-/-}$ (F) X MPS IIIA- SNCA$^{+/-}$ (M)	8	7	**36**	17	19	**26**	18	8	**62**	4.4	6
MPS IIIA- SNCA$^{+/-}$ X MPS IIIA- SNCA$^{+/-}$	6	4	**18**	6	12	**19**	16	3	**37**	4.6	5
Total	40	32	**183**	87 (47.5%)	96 (52.5%)	**90**	63 (70%)	27 (30%)	**273**	4.5	17 (6%)

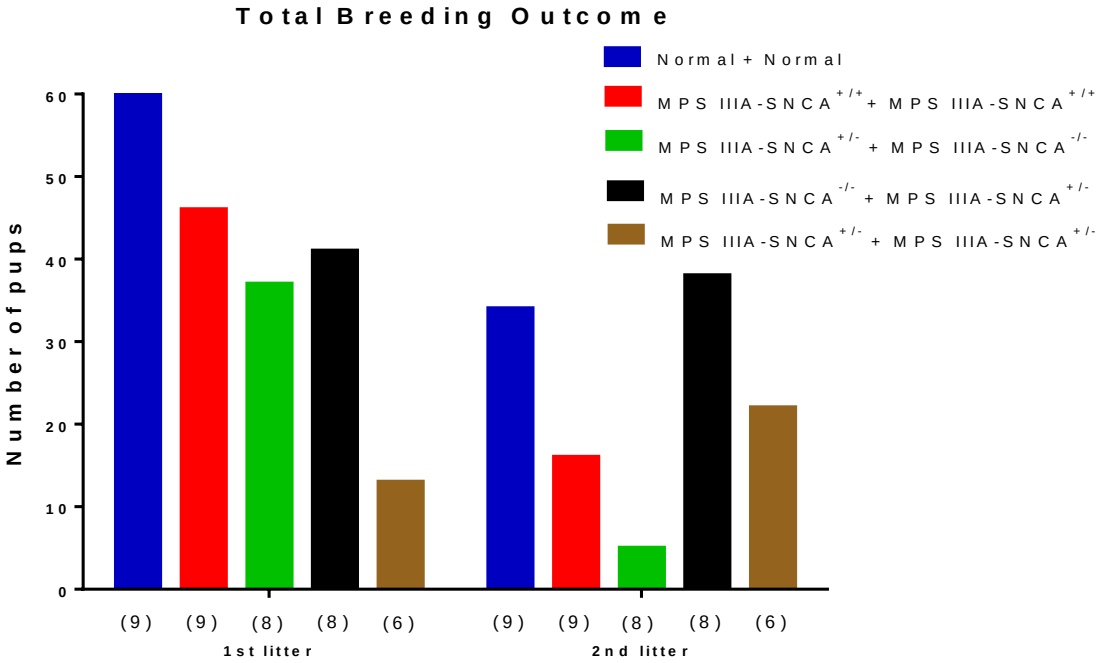

Figure 3.3. The total number of pups from the first and second litters, from five different pairings. The number of pairings is shown in brackets. The number of pairings in each group is shown in brackets.

Body weights were recorded weekly up to 21-weeks in males and only 12-weeks in females (because more female mice were not required for behavioural experiments). The body weights of the four experimental genotypes (males and females) were plotted and analysed separately **(Fig 3.4)**. Normal male mice were initially heavier than sex-matched MPS IIIA mice (especially $SNCA^{+/+}$ and $SNCA^{-/-}$) from three-weeks until five-weeks of age. Thereafter, MPS IIIA-$SNCA^{+/-}$ males became significantly heavier than their Normal counterparts at 10-, 11-, 12- and 17-weeks of age **(Fig 3.4 A)**. MPS IIIA-$SNCA^{+/+}$ and MPS IIIA-$SNCA^{-/-}$ mice tended to be heavier than Normal mice. There was no statistically significant difference in body weight between female Normal and MPS IIIA mice at any age **(Fig 3.4 B)**. Similar to male mice, Normal female mice were initially heavier than female MPS IIIA mice until about six-weeks of age. Thereafter, female MPS IIIA mice with different *SNCA* backgrounds gained more weight than their Normal littermates until 12-weeks of age.

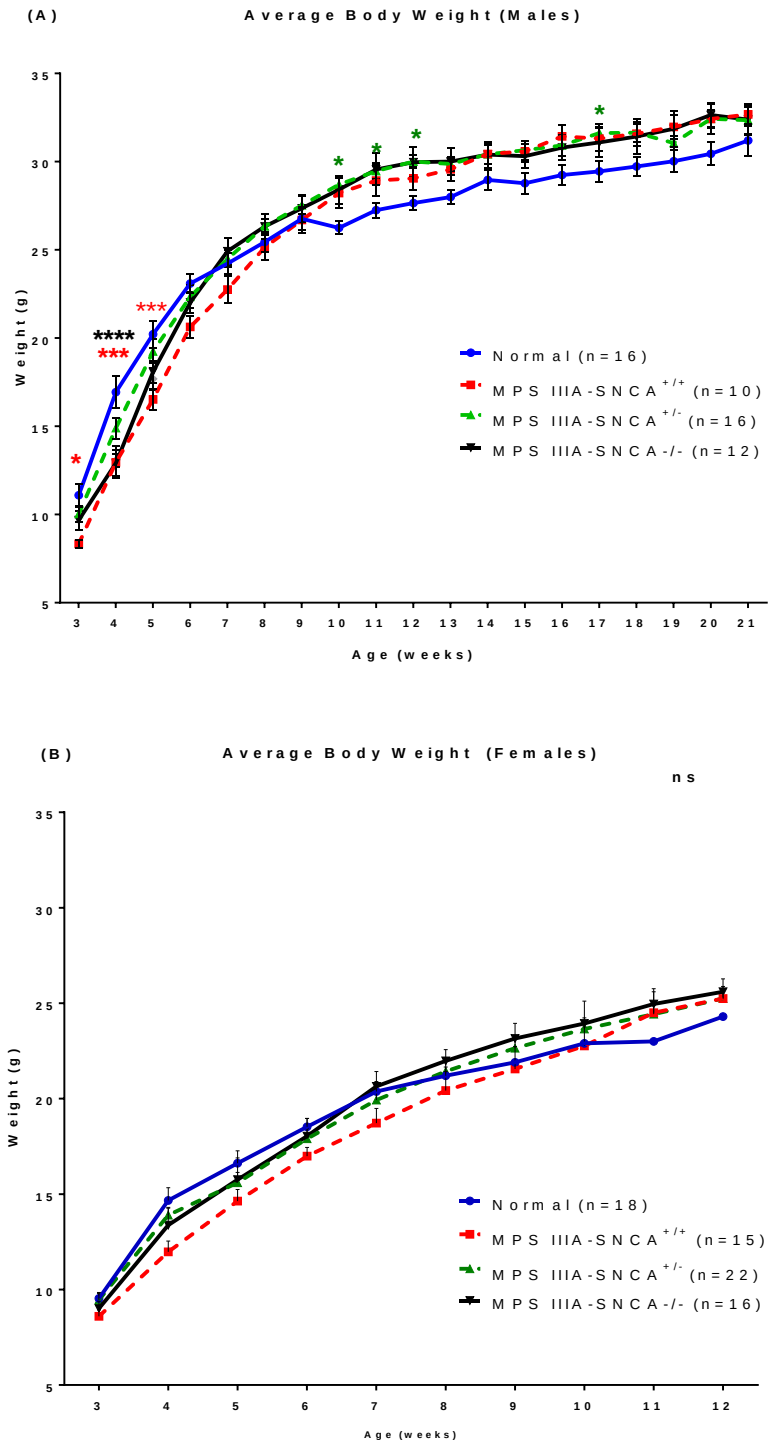

Figure 3.4. Mean body weights of the third generation (A) Males and (B) Females. Data are presented as the mean ± SEM. Statistical analysis was performed by using repeated measures two-way ANOVA for all the groups followed by Bonferroni's multiple comparison tests between the groups. * $P < 0.05$; ** $P < 0.01$; *** $P < 0.001$ normal versus MPS IIIA body weight. The number of animals in each group is shown in brackets.

3.2.5 Characteristics of the third generation mice

3.2.5.1 General appearance

Similar to congenic MPS IIIA-SNCA$^{+/+}$ mice, SNCA-deficient mice (MPS IIIA-SNCA$^{+/-}$ and MPS IIIA-SNCA$^{-/-}$) were phenotypically indistinguishable from Normal mice at birth and were healthy while young. At the weaning age of 19- to 21-days, MPS IIIA-SNCA$^{-/-}$ mice appeared hypoactive (cf. normal mice), with MPS IIIA-SNCA$^{-/-}$ mice being easier to catch and weigh, while wild type animals were jumpy and difficult to catch. At 10-weeks of age, male mice with all three types of MPS IIIA genotypes began to display aggressiveness towards other cage mates. Fight wounds were occasionally observed, necessitating separation into single cages.

All MPS IIIA mice began to exhibit a characteristic facial appearance, indifference to the environment and less interaction with other mice from 10-weeks of age. By 20-weeks, MPS IIIA-SNCA$^{+/-}$ and MPS IIIA-SNCA$^{-/-}$ mice displayed a scruffy coat, hunched posture, blunted facial features, and more limited movement, similar to the phenotype observed in MPS IIIA-SNCA$^{+/+}$ mice **(Fig 3.5)**.

3.2.5.2 Food and water intake in the experimental male mice

Food and water intake in the experimental mouse colonies was anecdotally observed to be much higher compared to other unrelated groups of mice housed in the same facility (as noted by staff in the Women's and Children's Hospital Animal Facility). Therefore, the average intake of food and water by the experimental male mice (16 Normal, 10 MPS IIIA-SNCA$^{+/+}$, 16 MPS IIIA-SNCA$^{+/-}$ and 12 MPS IIIA-SNCA$^{-/-}$) was monitored over the course of one-week at each of 12- and 22-weeks of age. The method described in **Chapter 2 (Section 2.2.3)** was used.

A significantly higher than average food intake was observed in in all three MPS IIIA genotypes **(Fig 3.6)**. At 12-weeks of age, MPS IIIA-SNCA$^{-/-}$ mice consumed an average of 32 g food per week, similar to that recorded in MPS IIIA- SNCA$^{+/+}$ and MPS IIIA-SNCA$^{+/-}$ mice. Normal mice, however, only ingested 28 g of food per week, on average **(Fig 3.6 A)**. At 22-weeks of age, the weekly food consumption of each of the three MPS IIIA genotypes had increased to nearly 40 g, while the food intake of Normal mice was only 33 g per week **(Fig 3.6 B)**. There was a significantly higher energy requirement in all four groups of mice at 22-weeks of age compared to that in the same mice at 12-weeks of age **(Fig 3.6 C)**.

(A) **(B)**

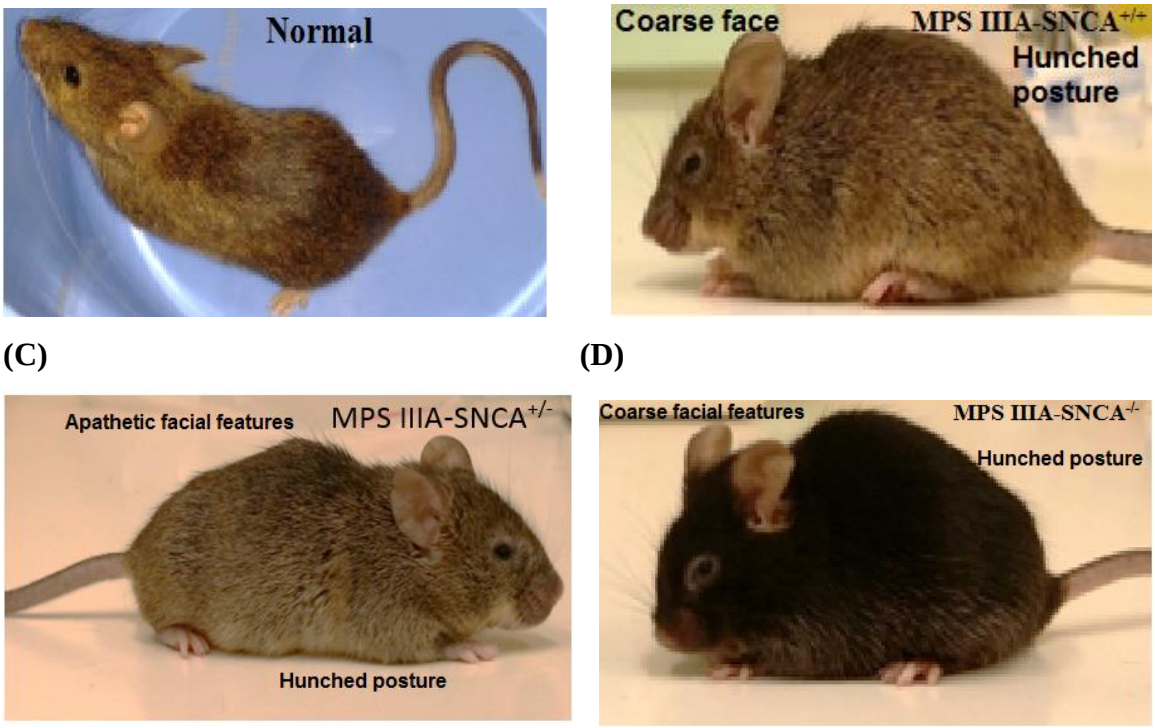

(C) **(D)**

Figure 3.5. Photographs of 20-week-old Normal (A), MPS IIIA-SNCA$^{+/+}$ (B), MPS IIIA-SNCA$^{+/-}$ (C); and MPS IIIA-SNCA$^{-/-}$ (D) mice. Note active features observed in a Normal mouse but hunched posture, blunted and apathetic facial features exhibited in MPS IIIA mice with or without *SNCA* gene.

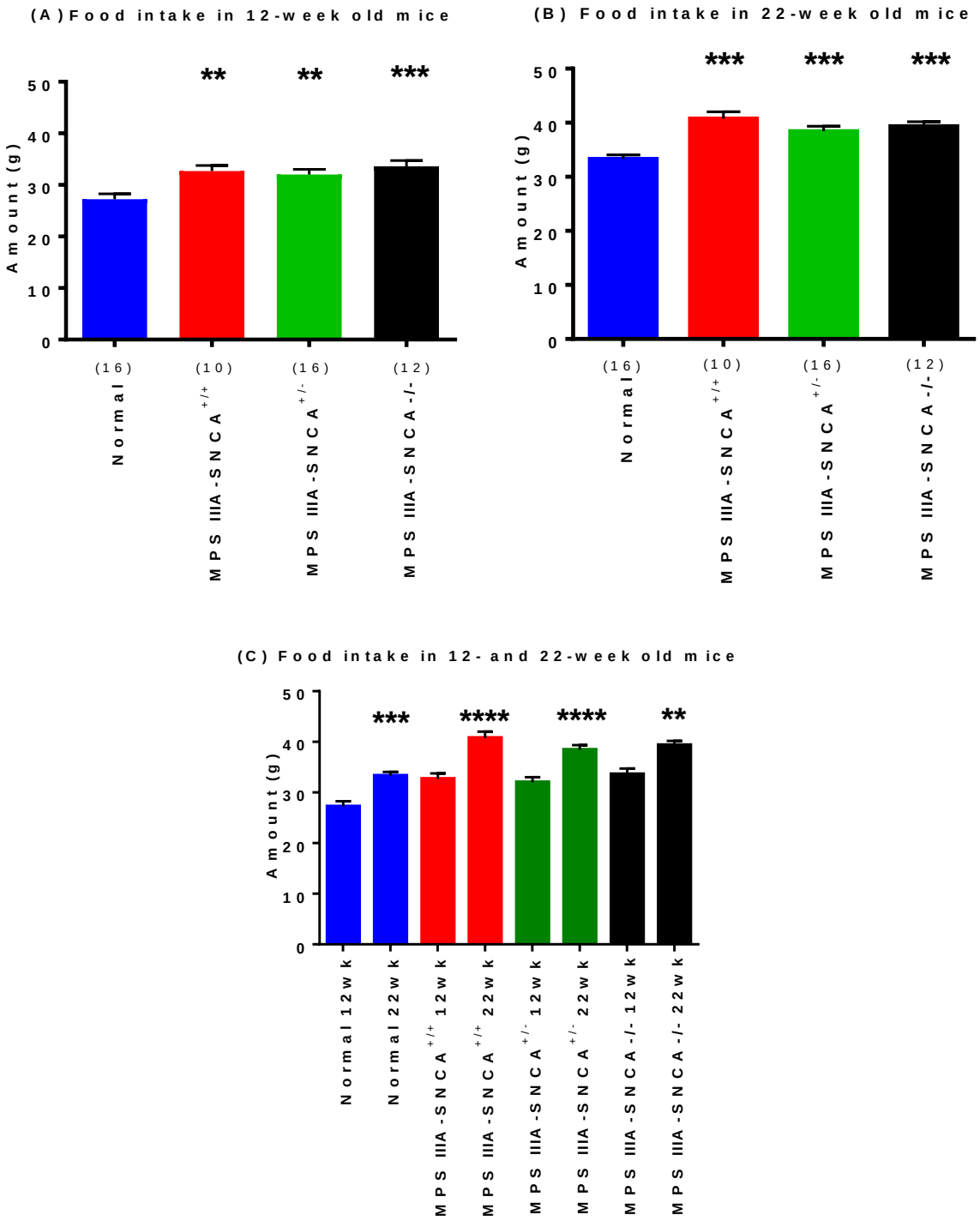

Figure 3.6. One-week food intake in (A) 12-week, and (B) 22-week old mice. The graph in (C) shows the age comparison within the same group. Statistical analysis was performed using one-way ANOVA for all the groups followed by Bonferroni's multiple comparison tests between the groups. Data are presented as the mean ± SEM. ** $P < 0.01$; *** $P < 0.001$ and **** $P < 0.0001$ compared to normal control. The number of animals in each group is shown in brackets.

On the other hand, the weekly water intake at 12- and 22-weeks of age did not differ significantly between the four groups of mice **(Fig 3.7)**. The average water consumption was 38 ml in Normal and MPS IIIA-SNCA$^{-/-}$ mice, while MPS-SNCA$^{+/+}$ and MPS IIIA-SNCA$^{+/-}$ mice drank 42 ml per week at 12-weeks of age **(Fig 3.7 A)**. By 22-weeks of age, the Normal group maintained an intake of 38 ml per week, while MPS IIIA mice (with SNCA$^{+/+}$, SNCA$^{+/-}$ and SNCA$^{-/-}$) had slightly increased their intake, with 46 ml, 43 ml and 40 ml, respectively **(Fig 3.7 B)**.

The level of cage dirtiness, including faecal boli and urinary spots, was qualitatively assessed in the same groups of mice at 12-weeks of age. Quantitative assessments of soiling were made at 22-weeks of age **(Fig 3.8)**. Genotype status of the animals was blinded to the experimenter in both measurements. There were no significant changes in cage dirtiness at either age. At 12-weeks of age, the majority of mouse cages were moderately soiled after one-week regardless of genotype **(Fig 3.8 A)**. By 22-weeks of age, all mice produced ~ 12 g of waste in their cages, albeit slightly higher in the MPS IIIA groups (SNCA$^{+/+}$, SNCA$^{+/-}$ and SNCA$^{-/-}$) **(Fig 3.8 B)**.

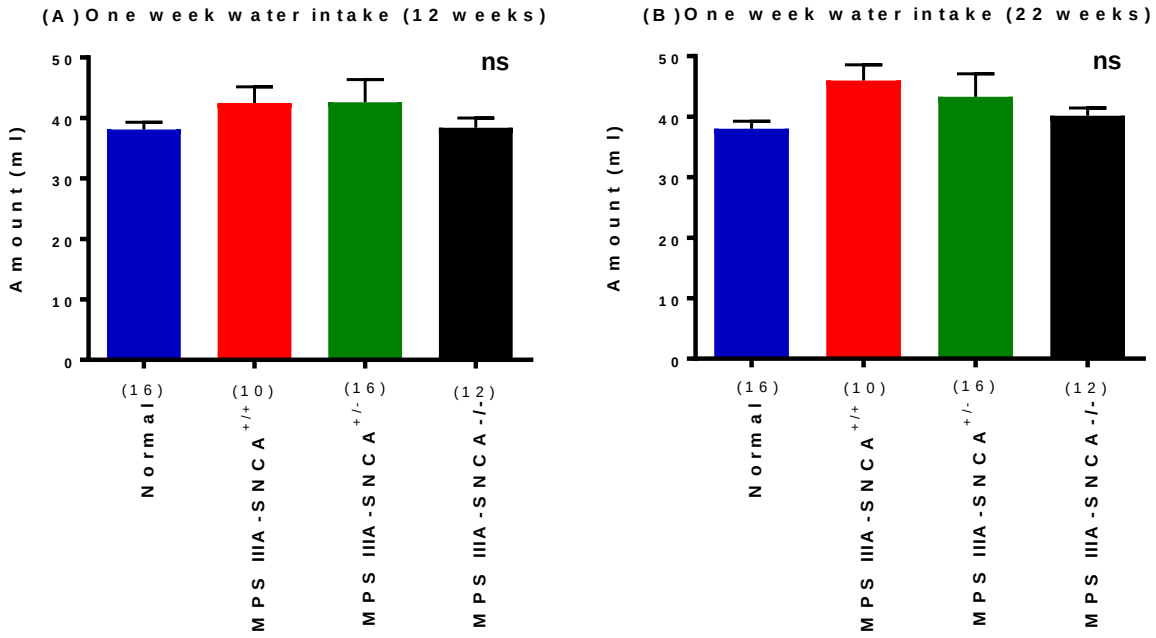

Figure 3.7. One-week water intake in mice at (A) 12-weeks, and (B) 22-weeks of age. Statistical analysis was performed using one-way ANOVA for all the groups followed by Bonferroni's multiple comparison tests between the groups; ns = non-significant. The number of animals in each group is shown in brackets.

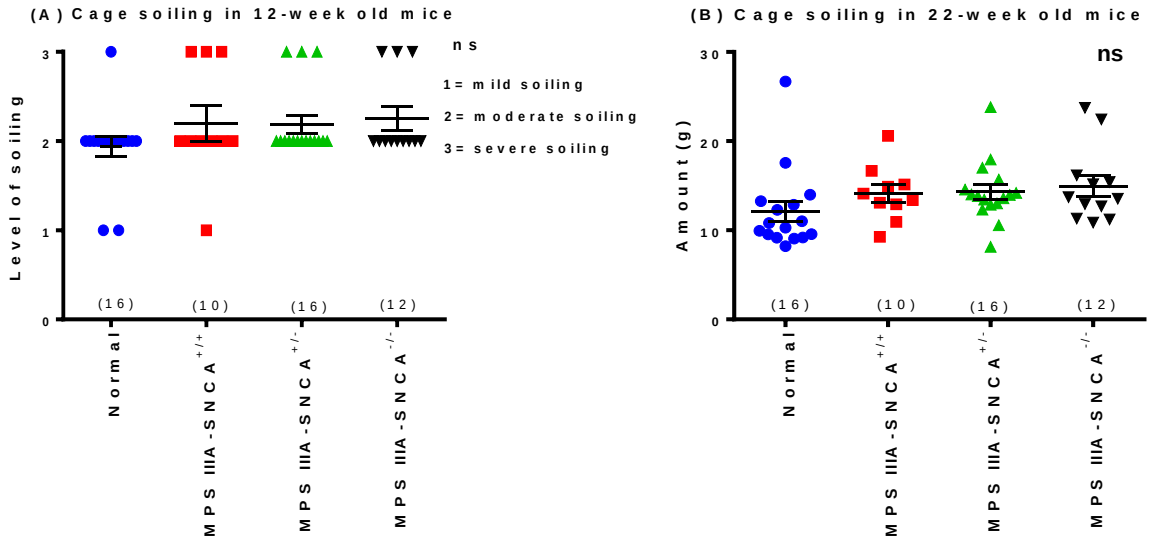

Figure 3.8. One-week cage soiling in mice at (A) 12-weeks, and (B) 22-weeks of age. Statistical analysis was performed using one-way ANOVA followed by Bonferroni's multiple comparison tests between the groups; ns = non-significant. The number of animals in each group is shown in brackets.

3.3 Discussion

This study's first aim was to create MPS IIIA mice which lacked the *SNCA* gene (MPS IIIA-SNCA$^{-/-}$) and to subsequently characterise their general features compared to Normal, MPS IIIA-SNCA$^{+/+}$ and MPS IIIA-SNCA$^{+/-}$ mice. Congenic MPS IIIA (B6.Cg-Sgsh^{mps3a}) and *SNCA* knockout mice (B6; 129X1-*Snca*^{tm1Rosl}/J) of both genders were fertile and able to reproduce normally. Synucleins do not play essential roles in fertility, nor does knocking them out affect overall viability, cause any apparent morbidity, mortality or alterations in gross somatic features (Abeliovich et al., 2000; Greten-Harrison et al., 2010).

3.3.1 Fertility outcomes

SNCA knockout (SNCA$^{-/-}$) mice did not show scavenger behaviour such as cannibalism of their pups. The average litter size of *SNCA* knockout x MPS IIIA mouse breeding in both genders was 4.1, which is comparable to Normal breeding. Their MPS IIIA progeny mice (with SNCA$^{+/+}$, SNCA$^{+/-}$ or SNCA$^{-/-}$ backgrounds), however, displayed aggressive behaviour, and there were 15 incidents of cannibalism in MPS IIIA inter-pairings compared to only two occasions in Normal x Normal pairings in the third generation. The aggressive behaviour observed in both human and mouse MPS IIIA may result from neurodegeneration in the hypothalamus and periaqueductal gray (Nidiffer and Kelly, 1983; Gregg and Siegel, 2001). Therefore, it appears that the D31N mutation in mice rather than *SNCA* gene modification had an adverse effect on mouse breeding behaviour.

Both males and females across all of the experimental groups were fertile by eight-weeks of age. However, all three groups of MPS IIIA mice showed a higher pregnancy failure rate with increased cannibalistic behaviour, similar to congenic MPS IIIA mice. While breeding the Normal mice was 100% successful, only 80% of pairings were successful in MPS IIIA mice, suggesting individual fertility issues in these animals. As a result, the total number of pups was higher in Normal pairings than in the affected animals in both litters in the third generation. Similar observations were made in both MPS IIIA-SNCA$^{+/-}$ and MPS IIIA-SNCA$^{-/-}$ mice, suggesting that the effects were due to the D31N mutation rather than *SNCA* knockout. As expected, the sex ratio of pups in all pairings was approximately 1:1.

3.3.2 Body weight and general characteristics

The average body weight of MPS IIIA-SNCA$^{-/-}$ mice was noticeably heavier than the age-matched controls by 10-weeks of age, but was similar to that of MPS IIIA-SNCA$^{+/+}$ and MPS IIIA-SNCA$^{+/-}$ mice. This highlights similar disease progression in MPS IIIA-SNCA$^{-/-}$ mice compared to MPS IIIA mice with different *SNCA* backgrounds. The mean body weight, onset of tremor and overall health improved with the deletion of the *SNCA* gene in adult male Huntington disease mice (Corrochano et al., 2012; Tomás-Zapico et al., 2012). *SNCA* deletion alone in MPS IIIA mice did not correct the increase in average body weight.

The increased body weight in MPS IIIA mice was mainly due to abnormal enlargement of organs such as the liver, spleen and a distended urinary bladder, all common features in congenic MPS IIIA mice and other LSD animal models (Bhaumik et al., 1999; Gliddon and Hopwood, 2004; Roberts et al., 2006). Moreover, it was documented that MPS IIIA male mice were 129% heavier, and MPS IIIA female mice were 117% heavier than normal control mice by 16-weeks of age (Roberts et al., 2006). A reduction in body weight gain in both sexes and clinical improvements were observed in MPS IIIA littermates treated with the glycosaminoglycan synthesis inhibitor 'rhodamine B' from four-weeks of age (Roberts et al., 2006). Gastrointestinal pathology showed increased nutrient absorption due to thickened submucosa and a slower gastric emptying rate, which was proposed to increase body weight in MPS IIIA mice (Roberts et al., 2009).

MPS IIIA mice with SNCA$^{+/+}$, SNCA$^{+/-}$ and SNCA$^{-/-}$ backgrounds showed similar clinical features to congenic MPS IIIA mice. They were also all phenotypically indistinguishable from Normal mice at birth. However, MPS IIIA-SNCA$^{-/-}$ mice were less active than the three other genotypes at three-weeks of age (personal observation). Moreover, they displayed more aggressive behaviour towards their cage mates, especially the males (personal observation), by 10-weeks of age. With increasing age, characteristic features such as hunched posture, scruffy coat, and typical facial features became pronounced across all three MPS IIIA genotypes, reflecting a similar pattern of MPS IIIA disease progression.

3.3.3 Feeding and energy intake

Apart from the apparent physical features, there are few reports on gastrointestinal pathology in LSD models. All of the male MPS IIIA mice (regardless of $SNCA^{+/+}$, $SNCA^{+/-}$ or $SNCA^{-/-}$ genotype) displayed significantly higher energy consumption compared to the age-matched Normal mice at both young (12-week) and adult (22-week) ages, indicating the effect of the D31N *SGSH* mutation on feeding behaviours. Moreover, a slightly, but not statistically significant increase in water intake was also seen in the three MPS IIIA groups compared to Normal mice at both ages.

Increased food ingestion has previously been reported in several murine models of LSD, including MPS I, MPS VII, Niemann-Pick type B, and infantile neuronal ceroid lipofuscinosis (Woloszynek et al., 2007). Due to impaired lysosomal recycling these cells become "energy hungry", increasing the energy requirement for the synthesis of raw materials. Additional energy may also be utilised for the management of stored substrates such as HS within lysosomes in MPS IIIA (Woloszynek et al., 2007). Dietary intervention with a high fat and simple sugar diet lowered protein catabolism and improved body weight in MPS VII mice (Woloszynek et al., 2009).

3.3.4 Role of heparan sulphate in energy intake

Abnormal gastrointestinal pathology, such as enlarged intestinal organs, increased submucosal thickness, and increased sucrose activity has been observed in MPS IIIA mice, which has the potential for increased food intake (Roberts et al., 2009). In addition to intestinal pathology in MPS IIIA, accumulated HS can influence appetite and satiety by regulating the anti-satiety hormones in the hypothalamus. Increased HS proteoglycan (syndecan) was shown to result in obesity (Reizes et al., 2001) while its removal led to decreased food intake and body weight (Zcharia et al., 2004). Thus, abnormal proteoglycan metabolism in MPS IIIA can have an impact on body weight via feeding behaviour and energy balance.

Deficiencies in adipose tissue and leptins, important for thermoregulation, were observed in MPS I, MPS IIIB, MPS VII, Niemann-Pick types A/B, and infantile neuronal ceroid lipofuscinosis mice (Woloszynek et al., 2007). Lysosomal dysfunction has been shown to cause widespread adipose tissue deficits and insulin resistance in several LSD (Woloszynek et al., 2007). Therefore, accumulating lysosomal substrates may represent an inaccessible energy

store with resultant high-energy intake. Enzyme replacement therapy in MPS I reduced liver size, normalised the caloric density, and reduced both glycosaminoglycan storage and re-accumulation of lipid in the liver (Woloszynek et al., 2007).

3.4 Conclusion

SNCA null mice were fertile and were successfully able to produce MPS IIIA progeny with different *SNCA* genotypes when paired with congenic MPS IIIA mice. MPS IIIA-SNCA$^{-/-}$ knockout mice were viable, fertile and phenotypically indistinguishable from Normal mice at birth. However, distinct characteristics of MPS IIIA such as reduced fertility, cannibalism, coarse facies, hunched posture, unkempt coat, increased body weight and limited locomotion were present in all of the MPS IIIA groups in this study. Moreover, MPS IIIA mice ate more than their Normal littermates at both 12- and 22-weeks of age, indicating a possible increase in energy requirement for the synthesis of raw materials, or possible dysregulation of the brain's appetite and satiety centre. In conclusion, the reduction or abrogation absence of *SNCA* did not improve the general characteristics and pathological features associated with MPS IIIA mice. In the next chapter, the behaviour of these mice was evaluated using different standardised tests.

Chapter (4)

Behavioural assessment of MPS IIIA mice deficient in α-synuclein

4.1 Introduction

A series of standardised and well-accepted behavioural tests have been established and used to assess the emotional and intelligence profiles in mice, and to measure and compare their general activity, anxiety levels, gait, and learning and memory. The Open Field test provides qualitative and quantitative information about exploratory activity, anxiety and locomotion of a mouse in a small defined place (Hall and Ballachey, 1932). The Elevated Plus maze test examines the emotional and anxiety-related behaviours in rodents by measuring the frequency of arm entries and risk-taking behaviour (Rodgers and Dalvi, 1997). Spatial learning and memory abilities in rodents can be examined using the Morris water maze test (Morris, 1984). The gait test has been formulated to analyse patterns of hind-limb gait to detect defects in movement (Steinberg et al., 1989).

Behavioural changes resulting from the progressive neuropathology in MPS IIIA have been previously studied in mixed strain mice (129SvJ and CD1, with some C57BL/6 and SJL strain contributions) (Hemsley and Hopwood, 2005) and congenic mice (Lau et al., 2008). Neither strain displays any distinguishable phenotypic changes at birth, but their activity starts to change in the Open Field test by three-weeks of age. Both mixed strain MPS IIIA males and females showed significantly increased line crossing, rearing frequency, path length and percentage of time moving in an open field, compared with unaffected three-week old mice (Hemsley and Hopwood, 2005). This short period of hyperactivity was followed by hypoactivity in male mice between six- and 15-weeks of age. After three-weeks of age, the level of activity in mixed strain female mice did not differ from their normal counterparts. Congenic C57BL/6 MPS IIIA males were significantly less active than unaffected mice by 10- to 12-weeks of age in an Open Field test (Lau et al., 2008; Hemsley et al., 2009).

A further developmental abnormality in MPS IIIA mice is measurable in the Elevated Plus maze test. This test was developed by Pellow et al. (1985) to assess anxiety responses in rodents. The test is a maze with two open and two closed arms, which form a plus-shape. Naïve congenic

MPS IIIA mice showed reduced anxiety in the plus maze test, with increases in risk-taking behaviour recorded by ~18-weeks of age (Lau et al., 2008). MPS IIIA mice spent more time in the (riskier/less-safe) open arms and visited those arms more often compared to normal littermates.

MPS IIIA mice displayed significant impairments in learning and memory in the Morris water maze by ~20-weeks of age in the absence of physical disability such as skeletal abnormalities or visual compromise (Crawley et al., 2006; Fraldi et al., 2007). MPS IIIA mice took a significantly longer time to locate the hidden platform on successive training days.

By 18-weeks of age, MPS IIIA mice showed significant impairment in motor performance in the hind-limb gait test (Fraldi et al., 2007), with significantly reduced gait length and width compared to normal controls. Impaired gait has also been recorded in mice with Parkinson's disease (Wang et al., 2012). A summary of the progressive behavioural changes detected in congenic MPS IIIA mice in previous studies is presented in **Fig 4.1 A**.

To clarify the role of SNCA in MPS IIIA disease progression, the clinical milestones found in previous studies were incorporated into the design of the behavioural study of MPS IIIA SCNA-deficient mice (MPS IIIA-SNCA$^{+/-}$ and MPS IIIA-SNCA$^{-/-}$), along with MPS IIIA-SNCA$^{+/+}$ and Normal controls. Due to fertility issues and increased cannibalism in MPS IIIA mice, the required number of 16 male mice was not achieved for two of the four genotypes (MPS IIIA-SNCA$^{+/+}$ (n=10); MPS IIIA-SNCA$^{-/-}$ (n=12); MPS IIIA-SNCA$^{+/-}$ (n=16); Normal (n=16)). All four genotypes underwent Open Field activity testing at 12-weeks of age, Elevated Plus maze testing at 15-weeks of age, and Morris water maze testing and motor gait analysis at 20- and 21-weeks of age, respectively **(Fig 4.1 B)**. At 10-weeks of age, mice were individually housed, and moved into the testing room at least 24 hr prior to clinical phenotyping to enable habituation.

(A)

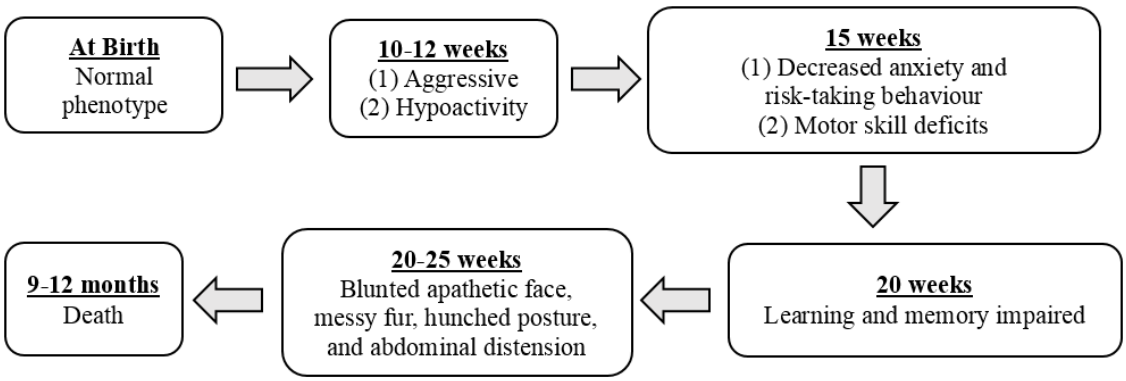

(B)

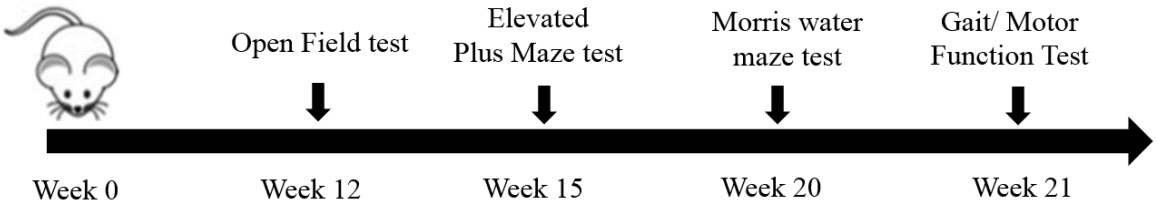

Figure 4.1. (A) Progressive disease manifestations in naive congenic MPS IIIA mice. (B) Overall clinical phenotyping timeline.

4.2 Results

4.2.1 Open Field activity test

The Open Field test of exploratory activity was performed in 12-week old naive male mice. As shown in **Fig 4.2**, all MPS IIIA mice, regardless of *SNCA* status ($SNCA^{+/+}$, $SNCA^{+/-}$, and $SNCA^{-/-}$) showed significantly reduced total activity (lines crossing + rears) in the Open Field test compared to Normal mice **(Fig 4.2 A)**. There were no significant differences in activity between the three different MPS IIIA genotypes. No significant difference in grooming activity was noted between Normal mice and the three MPS IIIA genotypes, although a trend towards reduced grooming was observed in the MPS IIIA cohorts **(Fig 4.2 D)**.

The testing revealed a marked reduction in total path length and speed in all three MPS IIIA cohorts, compared to the Normal group **(Fig 4.3 A, B)**. Moreover, there was also a significant decrease in the percentage time that MPS IIIA-$SNCA^{-/-}$ animals spent moving in the 5 min test period **(Fig 4.3 C)**. However, none of the four genotypes exhibited any significant difference in time spent in the potentially aversive open central region **(Fig 4.3 D)**. Likewise, the total number of faecal boli and urinary spots was comparable between the four genotypes **(Fig 4.4E)**.

Figure 4.2. Open Field activity in naive Normal, MPS IIIA-SNCA$^{+/+}$, MPS IIIA-SNCA$^{+/-}$, and MPS IIIA-SNCA$^{-/-}$ male mice at 12-weeks of age. The number of lines crossed was recorded on an automated tracking device, while the number of rears up on hind-limbs, and the number of bouts of grooming were measured manually. The assessed parameters were: (A) total activity (line crossing + rearing); (B) the number of lines crossed; (C) hind-limb rears; and (D) frequency of grooming in the 5 min recording period. Data are shown as mean ± SEM and * indicates a significant difference compared to the Normal group. A one-way ANOVA followed by post-hoc Bonferroni's multiple comparison test was used and *P < 0.05, **P < 0.01 and ***P < 0.001, ns = not significant. The number of animals involved is shown in brackets.

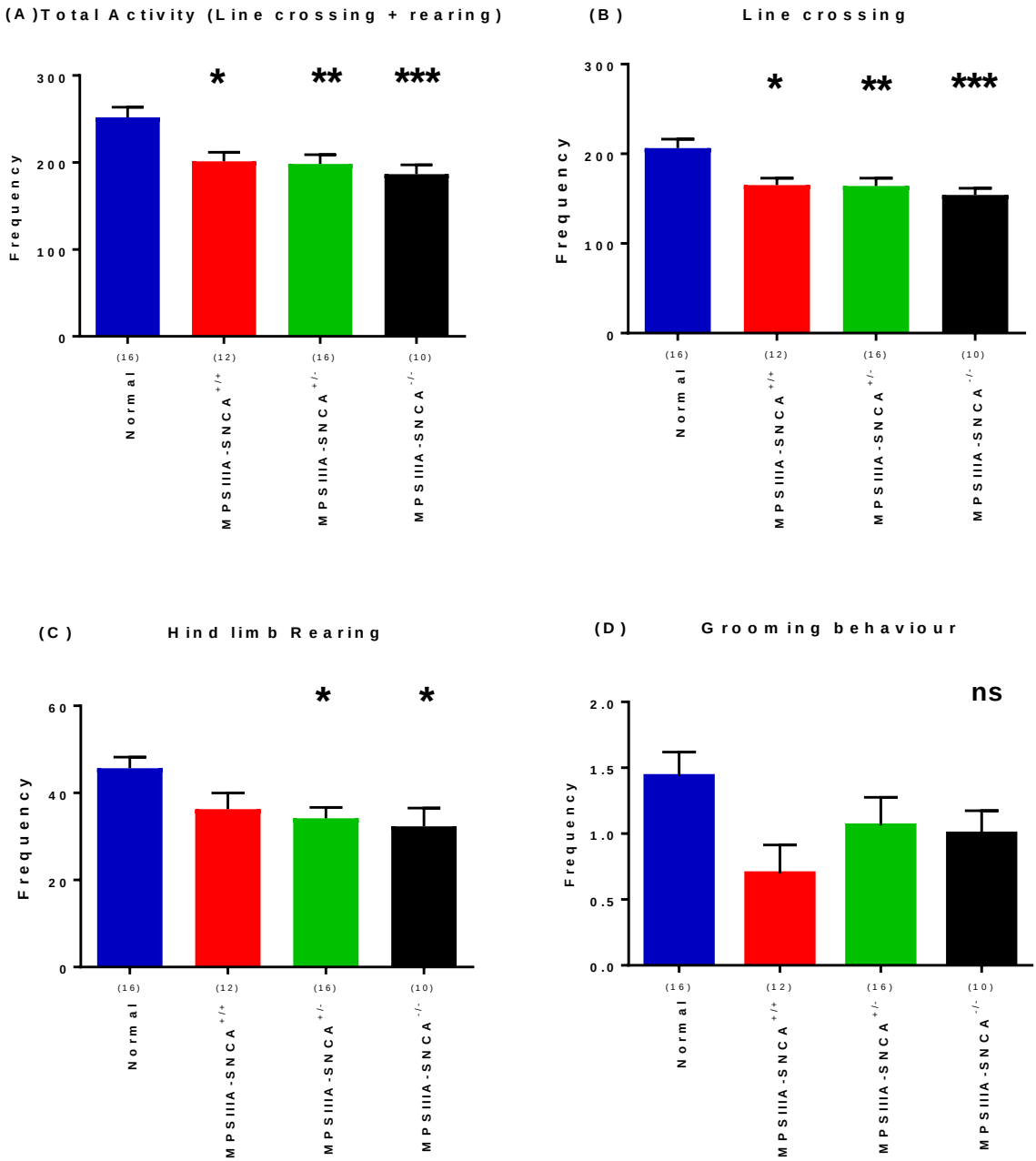
(A)Total Activity (Line crossing + rearing)
Frequency
300
200
100
0
*
**
***
(16)
(12)
(16)
(10)
Normal
MPSIIIA-SNCA+/+
MPSIIIA-SNCA+/-
MPSIIIA-SNCA-/-
(B) Line crossing
Frequency
300
200
100
0
*
**
***
(16)
(12)
(16)
(10)
Normal
MPSIIIA-SNCA+/+
MPSIIIA-SNCA+/-
MPSIIIA-SNCA-/-
(C) Hind limb Rearing
Frequency
60
40
20
0
*
*
(16)
(12)
(16)
(10)
Normal
MPSIIIA-SNCA+/+
MPSIIIA-SNCA+/-
MPSIIIA-SNCA-/-
(D) Grooming behaviour
Frequency
2.0
1.5
1.0
0.5
0.0
ns
(16)
(12)
(16)
(10)
Normal
MPSIIIA-SNCA+/+
MPSIIIA-SNCA+/-
MPSIIIA-SNCA-/-

Figure 4.3. Open Field activity test in Normal, MPS IIIA-SNCA$^{+/+}$, MPS IIIA-SNCA$^{+/-}$, and MPS IIIA-SNCA$^{-/-}$ naive male mice at 12-weeks of age. The activity of each animal was recorded on an automated tracking device, while the number of faecal boli and urinary frequency was noted manually after each test. The assessed parameters were: (A) path length; (B) the speed at which the animals travelled; (C) % time moving in the field; (D) central region activity (three central squares shown in diagram) and; (E) frequency of bowel and bladder activity in the 5 min recording period. Data are shown as mean ± SEM and * indicates a significant difference compared to the Normal group. A one-way ANOVA followed by post-hoc Bonferroni's multiple comparison test was used and *P < 0.05, **P < 0.01 and ***P < 0.001, ns = not significant. The number of animals involved is shown in brackets.

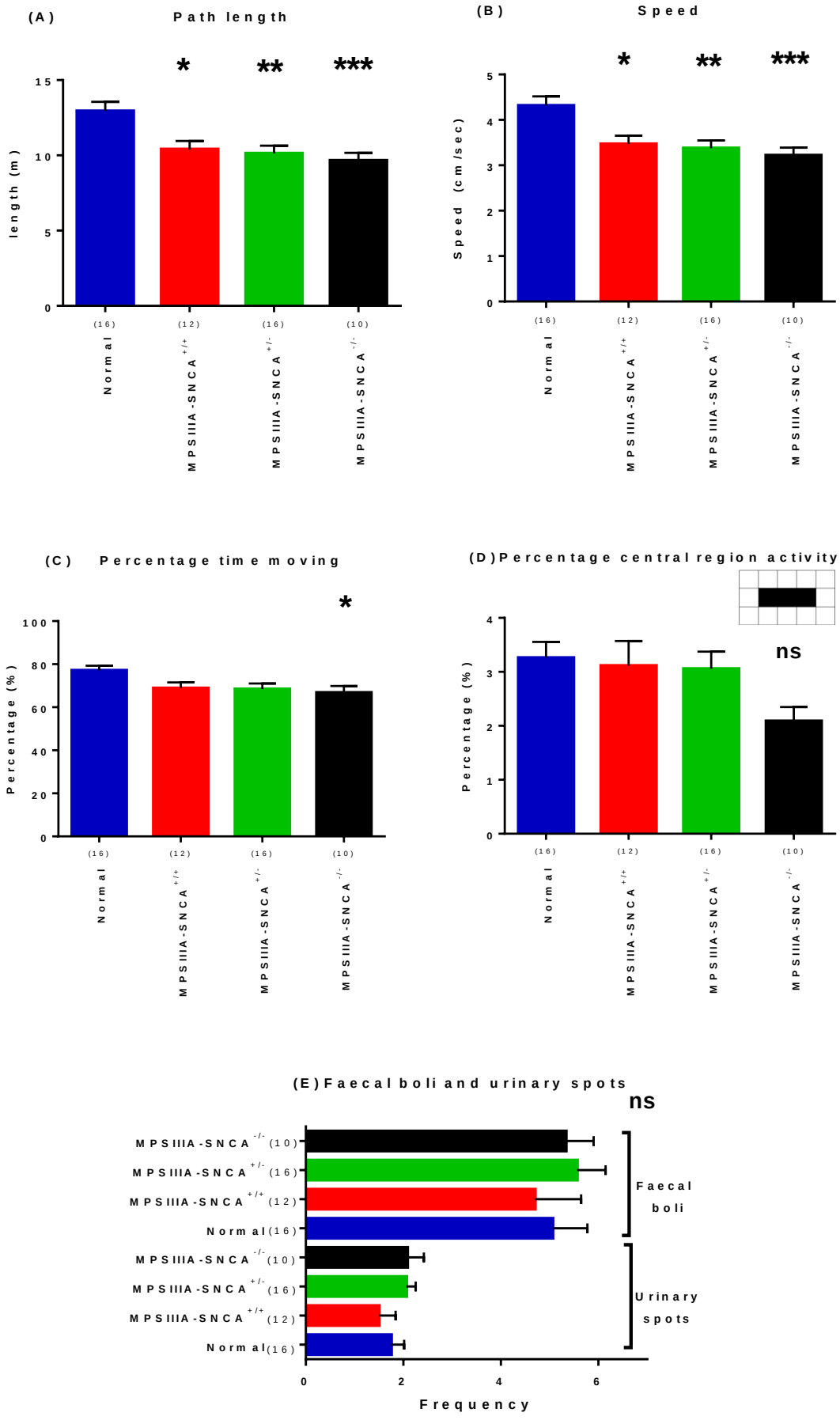
(A) Path length
length (m)
15
10
5
0
*
**
***
(16)
(12)
(16)
(10)
Normal
MPSIIIA-SNCA +/+
MPSIIIA-SNCA +/-
MPSIIIA-SNCA -/-
(B) Speed
Speed (cm/sec)
5
4
3
2
1
0
*
**
***
(16)
(12)
(16)
(10)
Normal
MPSIIIA-SNCA +/+
MPSIIIA-SNCA +/-
MPSIIIA-SNCA -/-
(C) Percentage time moving
Percentage (%)
100
80
60
40
20
0
*
(16)
(12)
(16)
(10)
Normal
MPSIIIA-SNCA +/+
MPSIIIA-SNCA +/-
MPSIIIA-SNCA -/-
(D) Percentage central region activity
Percentage (%)
4
3
2
1
0
ns
(16)
(12)
(16)
(10)
Normal
MPSIIIA-SNCA +/+
MPSIIIA-SNCA +/-
MPSIIIA-SNCA -/-
(E) Faecal boli and urinary spots
ns
MPSIIIA-SNCA -/- (10)
MPSIIIA-SNCA +/- (16)
MPSIIIA-SNCA +/+ (12)
Normal (16)
MPSIIIA-SNCA -/- (10)
MPSIIIA-SNCA +/- (16)
MPSIIIA-SNCA +/+ (12)
Normal (16)
Faecal boli
Urinary spots
0
2
4
6
Frequency

4.2.2 Elevated Plus maze test

At 15-weeks of age, the same four groups of male mice were subjected to the Elevated Plus maze test for a single 5 minute session. There was a significant reduction in total path length and speed in the MPS IIIA-SNCA$^{+/-}$ and MPS IIIA-SNCA$^{-/-}$ mice compared to the Normal cohort **(Fig 4.4 A, B)**, consistent with results from the Open Field activity test. MPS IIIA-SNCA$^{+/+}$ mice, however, did not show a significantly decreased path length or speed compared to their Normal counterparts, although a downward trend was observed in MPS IIIA-SNCA$^{+/+}$ mice in both assays.

The MPS IIIA-SNCA$^{-/-}$ animals made significantly less total arm entries compared to their Normal counterparts, particularly into the centre square and closed arms **(Fig 4.4 C, D, E)**. All four genotypes made a similar number of entries into the open arms over the 5 min test period **(Fig 4.4 F)**. Although no significant difference was observed in the percentage of time spent in the closed arms or the central square between the genotypes, MPS IIIA-SNCA$^{-/-}$ mice notably spent only 1% of the entire recording period in the open arms compared to the other groups, which spent more than 2% **(Fig 4.5 A, B, C)**. The total number of faecal boli and urinary spots after each test was largely comparable between each genotype **(Fig 4.5 D)**.

Figure 4.4. Elevated Plus maze test in naive Normal, MPS IIIA-SNCA$^{+/+}$, MPS IIIA-SNCA$^{+/-}$, and MPS IIIA-SNCA$^{-/-}$ male mice at 15-weeks of age. The four groups of mice were tested for 5 min and the motion of each animal was recorded on an automated tracking device. The parameters assessed were: (A) path length; (B) speed; (C) total arm entries; (D) central square entries; (E) closed arms entries; and (F) open arms entries. Data are shown as mean ± SEM and * indicates a significant difference compared to the Normal group. A one-way ANOVA followed by post-hoc Bonferroni's multiple comparison test was used and **P < 0.01 and ***P < 0.001, ****P < 0.0001, ns = not significant. The number of animals involved is shown in brackets.

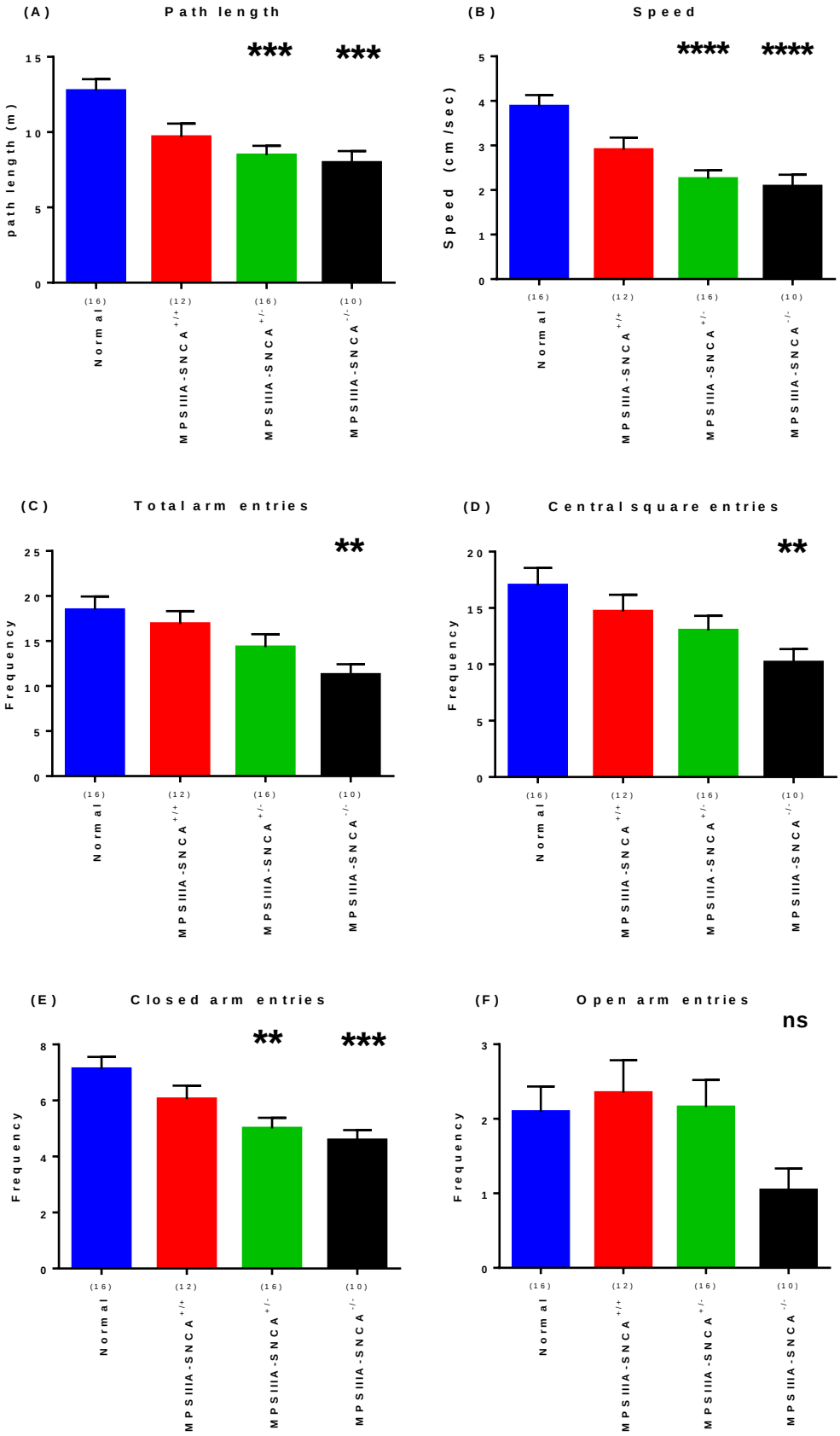
(A)
Path length
path length (m)
***
***
(B)
Speed
Speed (cm/sec)
****
****
(C)
Total arm entries
Frequency
**
(D)
Central square entries
Frequency
**
(E)
Closed arm entries
Frequency
**
***
(F)
Open arm entries
Frequency
ns
(16)
(12)
(16)
(10)
Normal
MPSIIIA-SNCA+/+
MPSIIIA-SNCA+/-
MPSIIIA-SNCA-/-

Figure 4.5. Elevated Plus maze test in naive Normal, MPS IIIA-SNCA$^{+/+}$, MPS IIIA-SNCA$^{+/-}$, and MPS IIIA-SNCA$^{-/-}$ male mice at 15-weeks of age. The four groups were tested for 5 min and the motion of each animal was recorded on an automated tracking device. The parameters assessed were: (A) % time spent in closed arms; (B) % time spent in the central square; (C) % time spent in open arms; and (D) bladder and bowel movements. Data are shown as mean ± SEM and * indicates a significant difference compared to the Normal group. A one-way ANOVA followed by post-hoc Bonferroni's multiple comparison test was used and *P < 0.05, ns = not significant. The number of animals involved is shown in brackets.

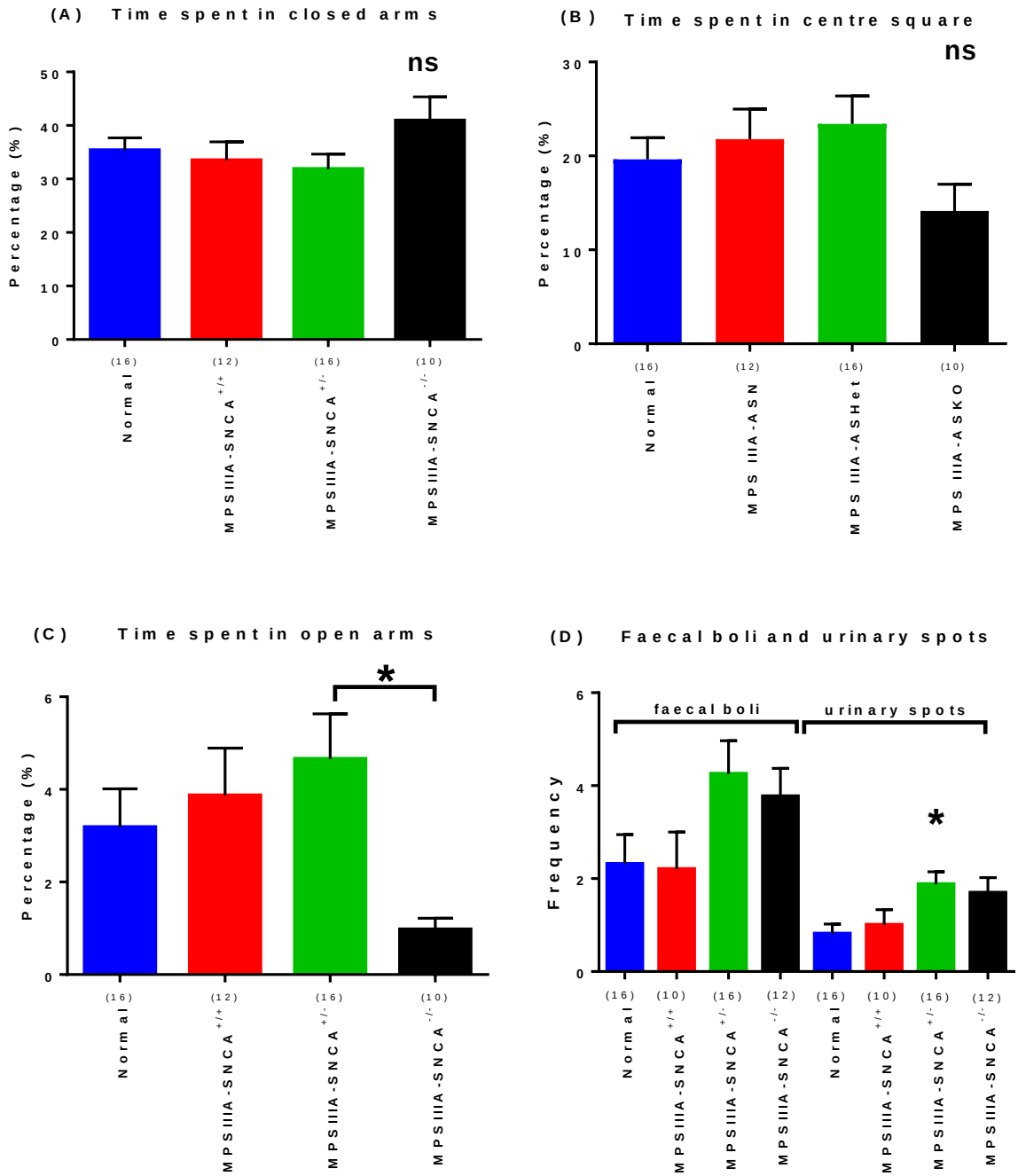
(A) Time spent in closed arms
ns
Percentage (%)
50
40
30
20
10
0
(16)
(12)
(16)
(10)
Normal
MPSIIIA-SNCA+/+
MPSIIIA-SNCA+/-
MPSIIIA-SNCA-/-
(B) Time spent in centre square
ns
Percentage (%)
30
20
10
0
(16)
(12)
(16)
(10)
Normal
MPS IIIA-ASN
MPS IIIA-ASHet
MPS IIIA-ASKO
(C) Time spent in open arms
*
Percentage (%)
6
4
2
0
(16)
(12)
(16)
(10)
Normal
MPSIIIA-SNCA+/+
MPSIIIA-SNCA+/-
MPSIIIA-SNCA-/-
(D) Faecal boli and urinary spots
faecal boli
urinary spots
*
Frequency
6
4
2
0
(16)
(10)
(16)
(12)
(16)
(10)
(16)
(12)
Normal
MPSIIIA-SNCA+/+
MPSIIIA-SNCA+/-
MPSIIIA-SNCA-/-
Normal
MPSIIIA-SNCA+/+
MPSIIIA-SNCA+/-
MPSIIIA-SNCA-/-

4.2.3 Morris water maze test

4.2.3.1 Latency

At 20-weeks of age, the same four groups of male mice were subjected to the Morris water maze to examine their memory and spatial navigation abilities (Morris, 1984). The mice were allowed to learn and locate the hidden platform from four cardinal points in the *Acquisition phase* for five consecutive days. This phase was followed by *Probe phase* in which a single 90 s swim with the platform removed was recorded. The final *Visual phase* tested vision and ability of the animals to locate an easily-seen platform.

The average time for each swim on the five days of testing in the *Acquisition phase* is shown in **Fig 4.6 A**. The daily average latency (search time to locate the hidden platform) is also plotted **(Fig 4.6 B)**. The overall time taken to find the platform in the *Acquisition phase* significantly decreased over the test period in all test groups, indicating that the training over the five-day course was successful.

The effect of Group and Day on search time was significant ($p = 0.0002$), indicating that the effects of Day on latency differed across Groups. The mean search time for the Normal mice on Day 1 was 59.83 sec, while that of all the MPS IIIA groups was more than 67 sec on average **(Fig 4.6 A, B)**. A significant difference between the Normal and MPS IIIA animals was first observed on Day 2: the Normal mice took 14.22 sec on average to find the platform, whereas MPS IIIA-SNCA$^{+/+}$, MPS IIIA-SNCA$^{+/-}$, MPS IIIA-SNCA$^{-/-}$ mice took 34.58 sec (P= 0.0002), 34.55 sec (P= 0.0003) and 29.63 sec (P= 0.0009), respectively. On Day 3, the Normal mice found the platform within 10.52 sec on average, and the MPS IIIA-SNCA$^{+/+}$ and MPS IIIA-SNCA$^{-/-}$ mice took 26.35 sec (P= 0.0004) and 27.52 sec (P= <0.0001), respectively.

A similar trend was observed on Days 4 and 5. The Normal mice reached the hidden platform within 9.69 sec (Day 4) and 8.52 sec (Day 5) on average; MPS IIIA-SNCA$^{+/+}$ mice took 19.63 sec (P= 0.0383) on Day 4 and 15.15 sec (P= 0.0448s) on Day 5, and MPS IIIA-SNCA$^{+/-}$ mice took 21.05 sec (P= 0.0012) and 14.77 sec (P= 0.0080) on the successive days. MPS IIIA-SNCA$^{-/-}$ mice took longer than the Normal cohort to reach the platform on these Days, with latencies of 25.38 sec (< 0.0001) recorded on Day 4 and 18 sec (P= 0.0005) on Day 5. However, there was no significant difference between the three MPS IIIA groups on any testing day.

Figure 4.6. Acquisition Phase in the Morris water maze: naive male Normal, MPS IIIA-SNCA$^{+/+}$, MPS IIIA-SNCA$^{+/-}$, and MPS IIIA-SNCA$^{-/-}$ mice were tested at 20-weeks of age. The parameters assessed were: (A) average search time in each of the four tests per day for the four different genotypes; and (B) daily average search time for the four genotypes over the five-day test. Data are shown as mean ± SEM and * indicates a significant difference compared to the Normal group. A one-way ANOVA followed by post-hoc Bonferroni's multiple comparison test was used and **P < 0.01 and ***P < 0.001. The number of animals involved is shown in brackets.

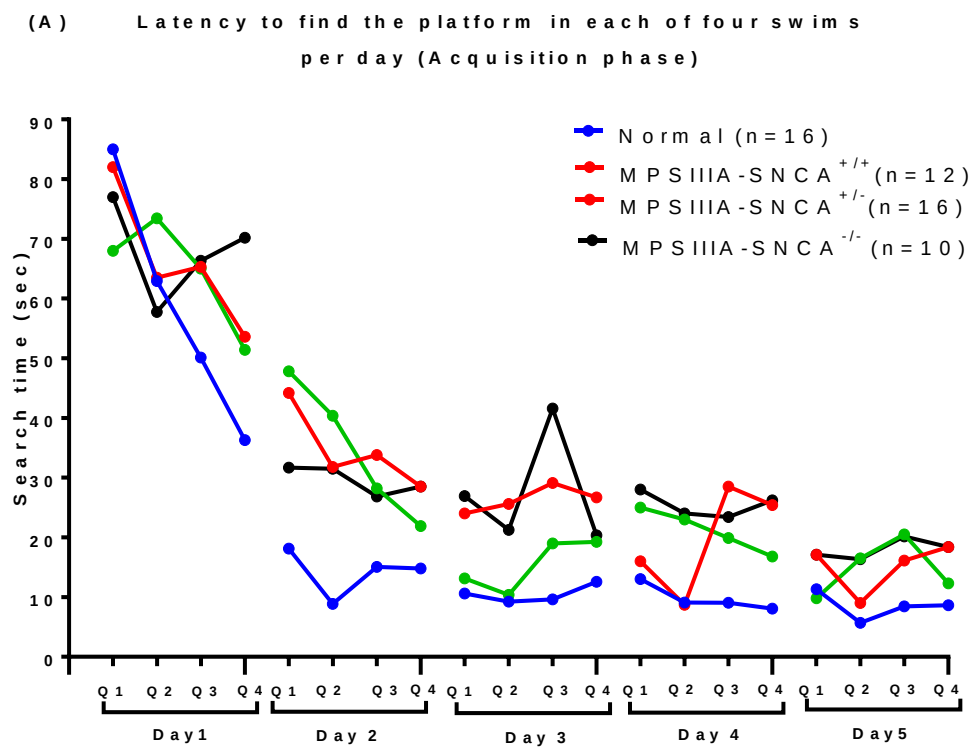
(A) Latency to find the platform in each of four swims per day (Acquisition phase)
Search time (sec)
0
10
20
30
40
50
60
70
80
90
Normal (n=16)
MPSIIIA-SNCA +/+ (n=12)
MPSIIIA-SNCA +/- (n=16)
MPSIIIA-SNCA -/- (n=10)
Q1 Q2 Q3 Q4
Day1
Day 2
Day 3
Day 4
Day5

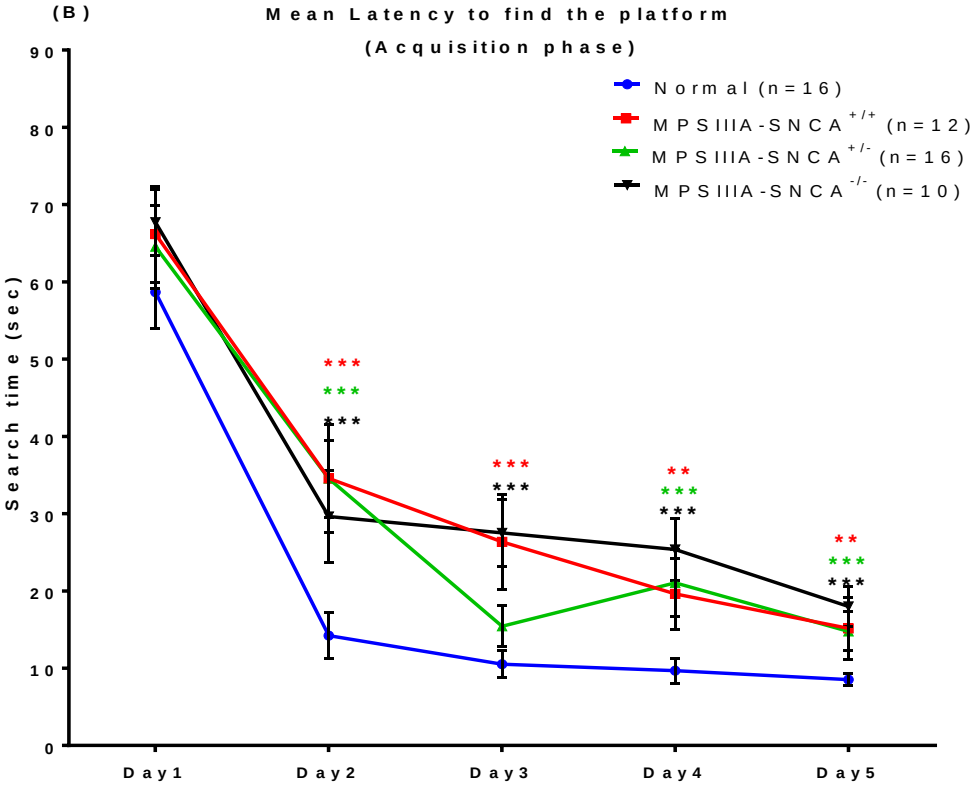
(B) Mean Latency to find the platform (Acquisition phase)
Search time (sec)
0
10
20
30
40
50
60
70
80
90
Normal (n=16)
MPSIIIA-SNCA +/+ (n=12)
MPSIIIA-SNCA +/- (n=16)
MPSIIIA-SNCA -/- (n=10)
***
***
***
***
***
***
**
***
***
**
***
***
Day1
Day2
Day3
Day4
Day5

4.2.3.2 Path length and speed

The interaction of Group and Day on path length was significant (P = 0.002), indicating that the effects of Day on path length differed across the Groups. The path length to the platform became progressively shorter in all four genotypes over the five-day *Acquisition Phase*, indicating that navigation ability had improved during training **(Fig 4.7 A)**. The mean path length was significantly greater in MPS IIIA-SNCA$^{+/+}$, MPS IIIA-SNCA$^{+/-}$, and MPS IIIA-SNCA$^{-/-}$ animals *cf* their Normal counterparts (path length = 3.29 m) on Day 2, with path lengths of 5.13 m (P = 0.0088), 5.58 m (P = 0.0011) and 4.67 m (P = 0.0357), respectively. The path length was significantly greater on Days 3, 4 and 5 in all MPS IIIA groups compared with the Normal group: Normal mice travelled 2.0 m on average for these three-days of the test; MPS IIIA-SNCA$^{+/+}$, MPS IIIA-SNCA$^{+/-}$ and MPS IIIA-SNCA$^{-/-}$ travelled an average of 3.2 m (P = 0.0153), 2.9 m (P = 0.0169) and 3.9 m (P = 0.0011), respectively.

The interaction of Group and Day on swimming speed was not significant (P = 0.338). The main effect of Day was not significant (P= 0.809), however, speed varied significantly by Group (P < 0.0001). Post-hoc comparisons indicate that the mean speed of the Normal mice was 25% (or 1.25-times) higher than that for MPS IIIA-SNCA$^{+/+}$ mice (P < 0.0001), 13% higher than that for MPS IIIA-SNCA$^{+/-}$ mice (P = 0.003), and 21% higher than that for MPS IIIA-SNCA$^{-/-}$ mice (P < 0.0001). Mean speed for MPS IIIA-SNCA$^{+/+}$ mice was 0.91-times that of MPS IIIA-SNCA$^{+/-}$ mice (P = 0.029) **(Fig 4.7 B)**. Normal mice located the platform in less than 15 sec on each of Days 2 to 5, while the other three genotypes took more than 30 sec for the same task. Therefore, Normal mice learned quicker and reduced the search time with a faster swim speed.

4.2.3.3 Time spent in the target and non-target quadrants

The interaction between Group and Day on the percentage of time spent in the target quadrant was not significant (p= 0.303). There was a significant main effect for Group (P < 0.0001) and Day (P < 0.0001). Following adjustment for Group, time in the target quadrant was significantly lower on Day 1 when compared to Day 2 (P < 0.0001), Day 3 (P < 0.0001), Day 4 (P < 0.0001) and Day 5 (P < 0.0001). Time in the target quadrant was significantly lower on Day 2 when compared to Day 3 (P = 0.011), Day 4 (P = 0.003) and Day 5 (P = 0.002) **(Fig 4.7 C)**.

Following adjustment for Day, mean time in the target quadrant was significantly higher in Normal mice compared to MPS IIIA-SNCA$^{+/+}$ (P = 0.009), MPS IIIA-SNCA$^{+/-}$ (P = 0.002) and MPS IIIA-SNCA$^{-/-}$ (P < 0.0001) mice. Moreover, mean time to the target quadrant was significantly higher in MPS IIIA-SNCA$^{+/+}$ mice compared to MPS IIIA-SNCA$^{-/-}$ mice (P = 0.006), and in MPS IIIA-SNCA$^{+/-}$ mice compared to MPS IIIA-SNCA$^{-/-}$ mice (P = 0.004) (**Fig 4.7 C**).

The interaction between Group and Day on the percentage of time in the non-target quadrants was not significant (P = 0.209). There was a significant main effect for both Group (P = 0.0001) and Day (P < 0.0001). Following adjustment for Group, the percentage of time in the non-target quadrants was significantly higher on Day 1 compared to Day 2 (P < 0.0001), Day 3 (P < 0.0001), Day 4 (P < 0.0001) and Day 5 (P < 0.0001) across all groups. In addition, all four genotypes spent significantly more time in the non-target area on Day 2 than Day 3 (P = 0.009), Day 4 (P = 0.0027) and Day 5 (P = 0.002) (**Fig 4.7 D**).

Following adjustment for Day, the mean percentage of time in the non-target area was significantly lower in the Normal group compared to the MPS IIIA-SNCA$^{+/+}$ (P = 0.0082), MPS IIIA-SNCA$^{+/-}$ (P = 0.0007) and MPS IIIA-SNCA$^{-/-}$ (P < 0.0001) groups. Moreover, mean time to the non-target area was significantly higher in MPS IIIA-SNCA$^{-/-}$ imce compared to MPS IIIA-SNCA$^{+/+}$ (P = 0.0315) and MPS IIIA-SNCA$^{+/-}$ mice (P = 0.0495) (**Fig 4.7 D**).

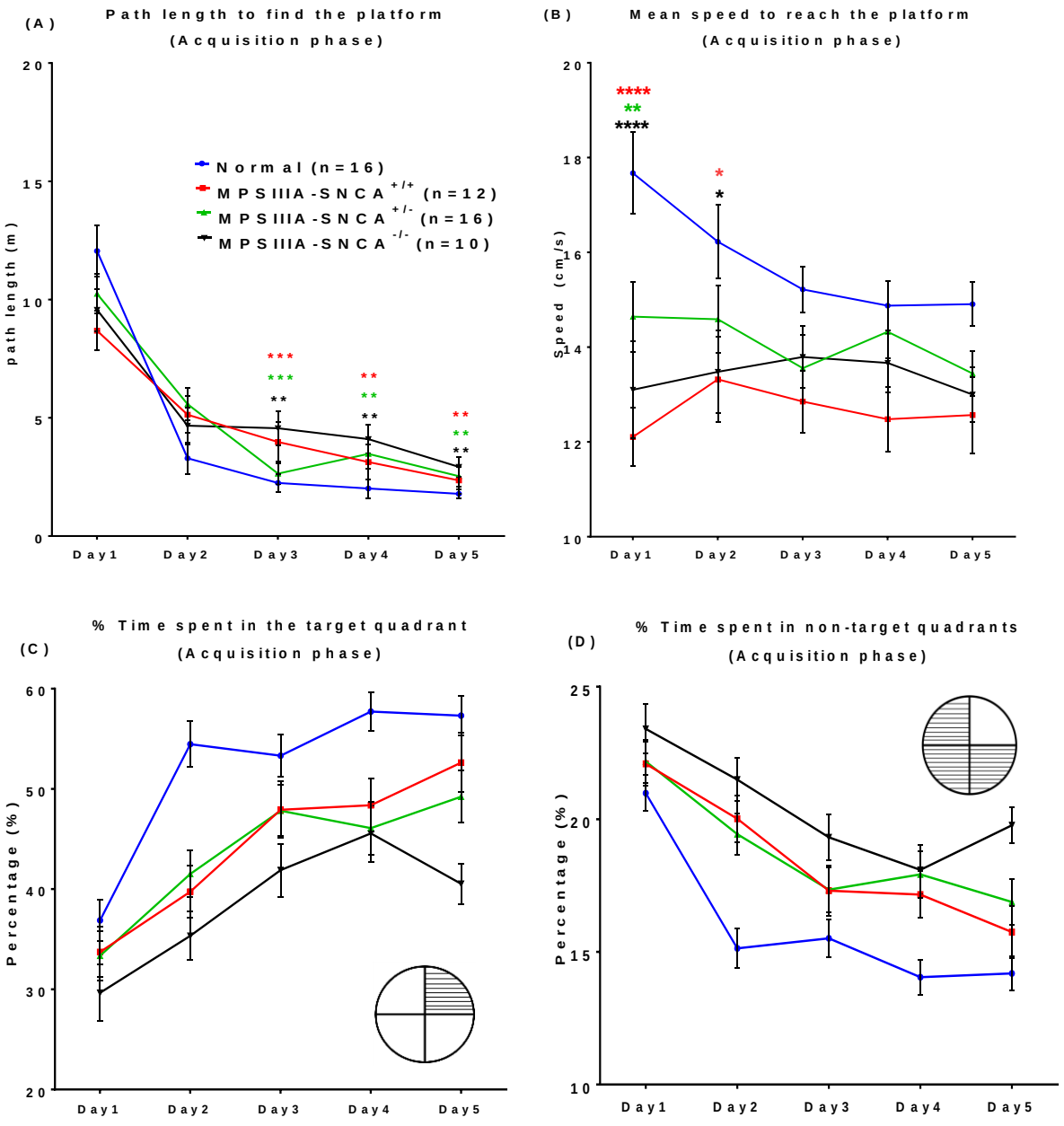

Figure 4.7. Acquisition Phase of the Morris water maze: naive male Normal, MPS IIIA-SNCA$^{+/+}$, MPS IIIA-SNCA$^{+/-}$, and MPS IIIA-SNCA$^{-/-}$ mice were tested at 20-weeks of age. The parameters assessed were: (A) daily mean path length; (B) average swim speed; (C) percentage of time spent in the target quadrant (shaded quadrant); and (D) percentage of time spent in the non-target quadrants (shaded quadrants). Data are shown as mean ± SEM and * indicates a significant difference compared to the Normal group. A one-way ANOVA followed by post-hoc Bonferroni's multiple comparison test was used and **P < 0.01 and ***P < 0.001. The number of animals involved is shown in brackets.

4.2.3.4 Probe phase and visual test

In the *Probe Phase*, all mice undertook one 90 sec swim session with the platform removed from the pool. There was no significant difference between the four genotypes, with mice spending most of their time (40% on average) swimming in the north-eastern quadrant, where the hidden platform had been located in the *Acquisition Phase* **(Fig 4.8 A)**. Moreover, all mice across all four genotypes showed a preference towards the two quadrants closest to the north-eastern quadrant (22%, 22.6%, 20% and 21.8% for the Normal, MPS IIIA-SNCA$^{+/+}$, MPS IIIA-SNCA$^{+/-}$ and MPS IIIA-SNCA$^{-/-}$ groups, respectively), spending the least amount of swimming time in the opposite south-western quadrant (14.8%, 13.9%, 17.1% and 13.5% for the Normal, MPS IIIA-SNCA$^{+/+}$, MPS IIIA-SNCA$^{+/-}$ and MPS IIIA-SNCA$^{-/-}$ groups, respectively). Importantly, the accuracy with which the mice reached the 10 cm diameter platform in the north-eastern quadrant was significantly lower in all three MPS IIIA groups (P = 0.03, 0.04, 0.04) compared to the Normal group **(Fig 4.8 B)**, and calculated using the following formula:

$$\%\ \text{Accuracy to reach the platform} = \frac{\text{No. of visit to the platform}}{\%\ \text{path length spent in the target quadrant}} \quad \text{X } 100$$

Moreover, the path length and speed of swimming was significantly higher in the Normal genotype than MPS IIIA SNCA$^{+/+}$ ($P < 0.0001$), MPS IIIA SNCA$^{+/-}$ ($P < 0.005$) or MPS IIIA SNCA$^{-/-}$ ($P < 0.0001$) **(Fig 4.8 C, D)**. However, there was no significant difference in either path length or swim speed between the MPS IIIA-SNCA$^{+/+}$, MPS IIIA-SNCA$^{+/-}$ and MPS IIIA-SNCA$^{-/-}$ mice. The frequency of thigmotaxis (circling to find the platform) in the pool was significantly lower in MPS IIIA mice in the *Probe phase* **(Fig 4.8 E)**. The percentage of time that mice swam slowly (swimming less than 0.05 m per second) was marginally higher in MPS IIIA-SNCA$^{+/+}$ and MPS IIIA-SNCA$^{+/-}$ mice, but significantly greater in MPS IIIA-SNCA$^{-/-}$ mice than their Normal counterparts **(Fig 4.8 F)**.

To rule out whether compromised visual function or capability contributed to swimming times, all mice underwent visual testing at the completion of the *Probe Phase* testing protocol: all mice in all four genotypes found the visible platform located in the south-western quadrant in less than 10 sec (data not shown) without the aid of external cues.

Figure 4.8. Probe Phase test in the Morris water maze: naive male Normal, MPS IIIA-SNCA$^{+/+}$, MPS IIIA-SNCA$^{+/-}$, and MPS IIIA-SNCA$^{-/-}$ mice were tested at 20-weeks of age. The parameters assessed were: (A) percentage of average time spent in the target (T) and non-target quadrants (NT); (B) accuracy finding the platform square area (shaded square in the diagram); (C) path length; (D) swim speed; (E) frequency of circling in the pool (thigmotaxis); and (F) percentage of time spent swimming slowly. Data are shown as mean ± SEM and * indicates a significant difference compared to the Normal group. A one-way ANOVA followed by post-hoc Bonferroni's multiple comparison test was used and *P < 0.05, **P < 0.01, ****P < 0.0001. The number of animals involved is shown in brackets.

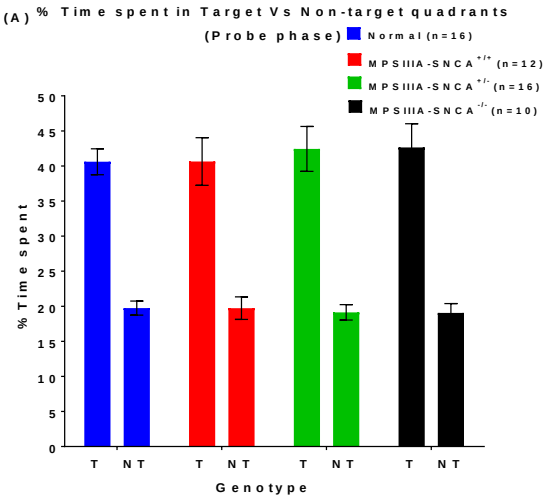
(A) % Time spent in Target Vs Non-target quadrants
(Probe phase)
Normal (n=16)
MPSIIIA-SNCA+/+ (n=12)
MPSIIIA-SNCA+/- (n=16)
MPSIIIA-SNCA-/- (n=10)
% Time spent
T NT T NT T NT T NT
Genotype

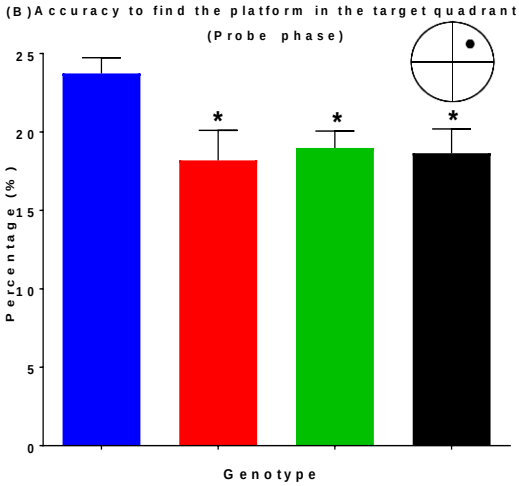
(B) Accuracy to find the platform in the target quadrant
(Probe phase)
Percentage (%)
Genotype

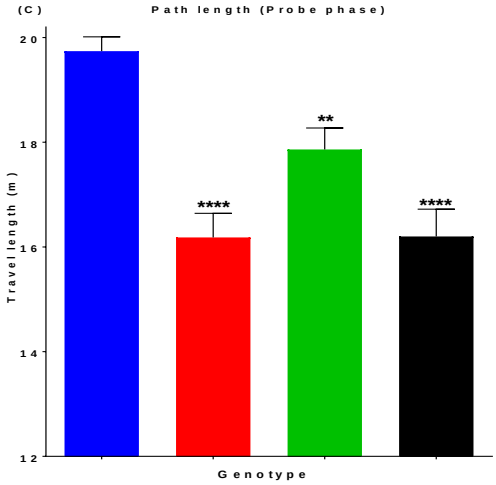
(C) Path length (Probe phase)
Travel length (m)
Genotype

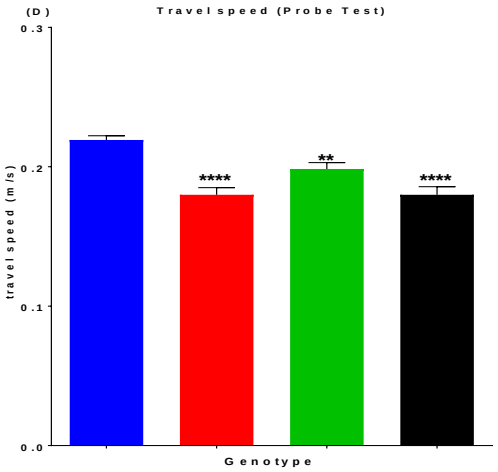
(D) Travel speed (Probe Test)
travel speed (m/s)
Genotype

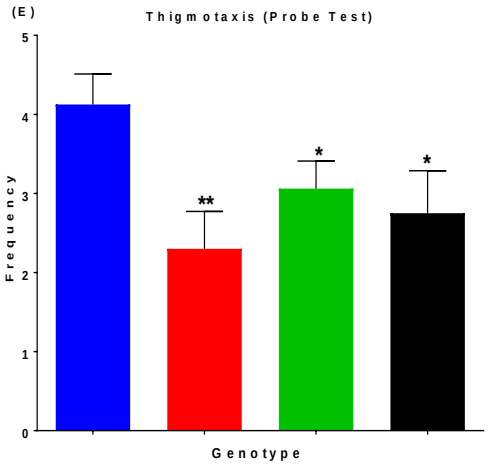
(E) Thigmotaxis (Probe Test)
Frequency
Genotype

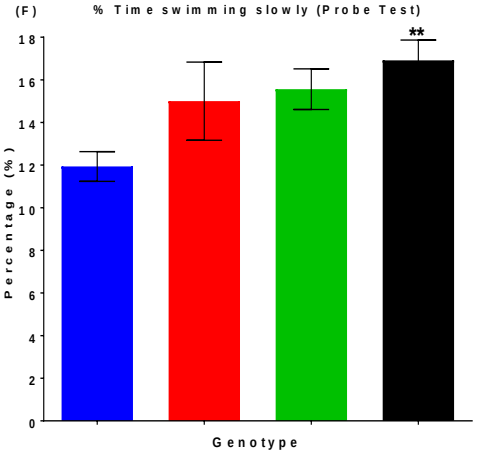
(F) % Time swimming slowly (Probe Test)
Percentage (%)
Genotype

4.2.4 Motor gait test

Gait parameters were assessed in the same groups of mice using the standard motor gait test at 21-weeks of age. All animals were acclimatised to the testing environment by allowing them to explore in the test arena for two times, before the actual performance was done. The gait test detects gait movement deficits, which can be observed in several neurological disorders and lesions such as Parkinson's disease or motor dysfunction due to injury to dopamine-mediated pathways in rodents (Meredith and Kang, 2006). The results of gait length and width testing are shown in **Fig. 4.9**. All MPS IIIA groups exhibited marked differences in gait performance compared to Normal littermates. There was a marginally significant age-by-disease group interaction in mean gait length for males (P = 0.062). However, staggering gait or hind-limb tremor when walking were not observed in any of the MPS IIIA mice regardless of genotype.

Significant reductions in gait length (both right and left legs) were observed in all MPS IIIA mice compared to Normal mice (P = 0.0002) **(Fig 4.9 A)**. Gait length in the Normal group was 71 mm on average on both sides, and 60 mm, 65 mm and 61 mm (on average) in MPS IIIA-SNCA$^{+/+}$, MPS IIIA-SNCA$^{+/-}$ and MPS IIIA-SNCA$^{-/-}$ mice, respectively. However, mean gait length was similar in all cohorts of MPS IIIA mice.

In addition, there was a significant difference in gait width between some MPS IIIA and Normal mice **(Fig 4.9 B)**. Although the gait width of MPS IIIA-SNCA$^{+/+}$ and MPS IIIA-SNCA$^{+/-}$ mice was significantly narrower (P = 0.0001), gait width in MPS IIIA-SNCA$^{-/-}$ mice was only marginally narrower than the Normal group **(Fig 4.9 B)**.

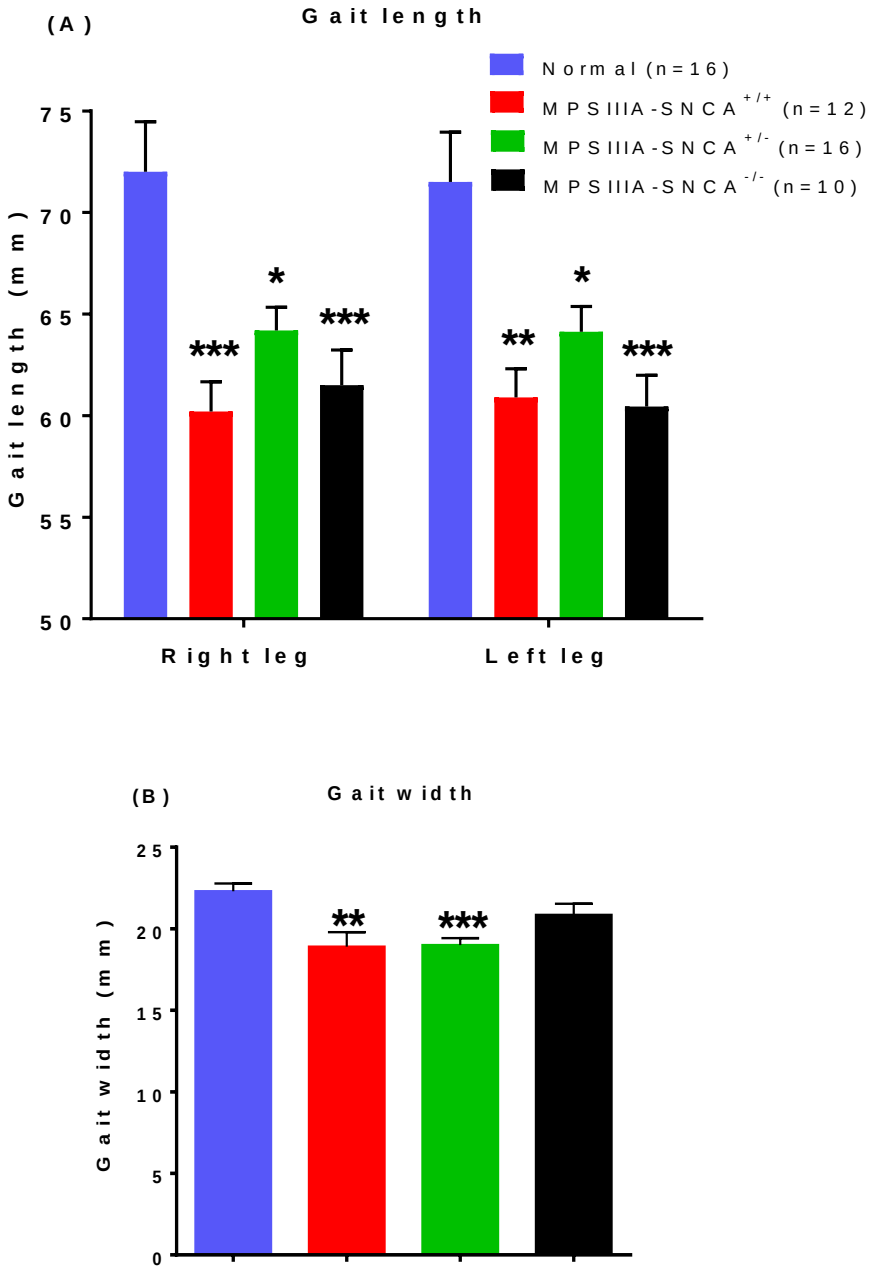

Figure 4.9. Hind-limb gait length and width were assessed in naïve Normal, MPS IIIA-SNCA$^{+/+}$, MPS IIIA-SNCA$^{+/-}$ and MPS IIIA-SNCA$^{-/-}$ male mice at 21-weeks of age. The assessed parameters were: (A) gait length for both hind-limbs; and (B) gait width. Data are shown as mean ± SEM and * indicates a significant difference compared to the Normal group. A one-way ANOVA followed by post-hoc Bonferroni's multiple comparison test was used and *P < 0.05, **P < 0.01 and ***P < 0.001, ns = not significant. The number of animals involved is shown in brackets.

4.3 Discussion

4.3.1 Reduced locomotor activity in mice with the MPS IIIA genotype

Only male mice of same genetic background (129X1/SvJ and C57BL/6 strain contributions) were utilised in the behavioural analyses because MPS IIIA female mice have shown delayed or no phenotypic change in other studies, possibly due to female hormonal effects (Hemsley and Hopwood, 2005; Crawley et al., 2006). We do note, however, that female MPS IIIA mice were found to be hyperactive and impulsive (less sense of danger) than wild type counterparts at 16, 24 and 32 weeks in the open field and elevated plus maze tests by Langford-Smith et al. (2011). The authors also reported that there was no significant differences in activity, anxiety and neuromuscular strength found between male wild type and MPS IIIA mice (Langford-Smith et al., 2011). These differences between two groups may be attributable to differences in housing, genetic background, or handling in each group's animal facility.

Whilst difficulties were experienced in produincg sufficient mice of some genotypes (ie., < 16 per each group), all MPS IIIA mice were observed to display significantly reduced activity, travel length and speed than their Normal counterparts in the Open Field test by 12-weeks of age. MPS IIIA-SNCA$^{-/-}$ mice were also significantly hypoactive. These outcomes are similar to those reported previously in both mixed strain and congenic C57BL/6 MPS IIIA mice (Hemsley and Hopwood, 2005; Crawley et al., 2006). The outcomes also indicate that deficiency of *SNCA* does not improve the MPS IIIA behavioural phenotype.

These findings replicate those of Abeliovich et al. (2000) where both sexes of seven- to 12-week-old *SNCA* knockout mice exhibited normal locomotor activity in the Open Field test. An amphetamine challenge test by Abeliovich et al was performed in order to elicit activity changes in animals with a-synuclein knockout. Our primary aim was to investigate MPS IIIA mice in the absence of α-synuclein.

The lack of *SNCA* involvement in locomotor activity and anxiety-related behaviour has also been reported (George et al., 2008; Senior et al., 2008; Peña-Oliver et al., 2010; Keatinge et al., 2015). Keatinge et al. (2015) reported that homozygous (β-glucocerebroside$^{-/-}$) and heterozygous (β-glucocerebroside$^{+/-}$) Gaucher disease zebrafish exhibited 50% and 25% decreases in total movement in water than normal fish, respectively. The *SNCA* gene is not expressed in the zebrafish genome, suggesting that disease phenotype and neurodegeneration

are not mediated by *SNCA* toxicity but rather by the lysosomal storage pathology. Therefore, reduced activity in the MPS IIIA-SNCA$^{-/-}$ mice may be due to the pathology associated with MPS IIIA rather than *SNCA* status.

On the other hand, it is important to recognise that another synuclein member may compensate for the functional gap caused by the deletion or reduced activity/ expression of one synuclein. For example, α–β–synuclein double knockout mice showed significant changes in neurotransmitter release although single *SNCA* deletion did not change any brain function (Chandra et al., 2004). Slower motor learning skills and neuromuscular pathology were observed in SNCA$^{-/-}$ mice (Pelkonen and Yavich, 2011), and they performed poorly in the Rotarod test, a test of balance, grip strength and motor coordination in animals. In addition, acetylcholine release was excessive, and there was prolonged duration of the end-plate potential at the muscular end-plate after repetitive electrical stimulation (Pelkonen and Yavich, 2011). That study suggests impaired motor control caused by abnormal signalling at the neuromuscular junction, indicating that *SNCA* may be important in regulating acetylcholine at the neuromuscular junction and fine skeletal motor control.

Another study reported a significant decrease in path length and speed but not total activity or numbers or rears in aging (10-month old) SNCA$^{-/-}$ animals in the Open Field test (Kokhan et al., 2012). Moreover, striatal dopamine was significantly reduced in aging SNCA$^{-/-}$ mice (Al-Wandi et al., 2010), while only a small decrease in dopamine neurons was observed in young SNCA$^{-/-}$ mice (Robertson et al., 2004). According to the above data, SNCA may play a role in locomotion and motor learning skills, especially in aging mice, possibly because of its regulatory function in acetylcholine and dopaminergic neurotransmission.

4.3.2 Increased anxiety in MPS IIIA-SNCA$^{-/-}$ mice

It is recognised that the amygdala is responsible for the development and expression of anxiety and conditioned fear in animals (Davis, 1992). Further, increased entry of rodents into the open arms of the Elevated Plus maze is also observed following anxiolytic drugs, while more time is spent in closed arms with anxiogenic drugs (Macúchová et al., 2016). Lau et al. (2008) has shown that congenic naive MPS IIIA male mice were significantly less active in the Elevated Plus maze at 18- and 20-weeks of age, and also observed the risk-taking and anti-anxiety behaviour of these mice, which readily explored the open arms compared to wild-type animals

at 18- and 20-weeks of age. The change in the anxiety state that is observed in several LSD mouse models (including MPS IIIA) may be caused by the presence of pathological depositions of HS, G_{M2} and G_{M3} gangliosides, or free cholesterol in the amygdala (McGlynn et al., 2004).

In this study, MPS IIIA-SNCA$^{-/-}$ mice showed increased anxiety by spending only 2% time exposed in the central aversive region in the Open Field test. In the Elevated Plus maze test, MPS IIIA-SNCA$^{+/+}$ mice were comparable to congenic MPS IIIA mice, and showed a trend towards hypoactivity and risk-taking behaviour by exploring more in the open arms, even though the data are not significant. The slight difference in anxiety expression between MPS IIIA-SNCA$^{+/+}$ mice in this study compared to the congenic MPS IIIA strain may be a strain-dependent effect and the age of the experimental animals (Bouwknecht and Paylor, 2002). MPS IIIA-SNCA$^{+/-}$ and MPS IIIA-SNCA$^{-/-}$ mice were also significantly less active (path length and speed) and exhibited reduced entries into the closed arms and the central area, indicating a high level of anxiety in these animals compared to Normal animals.

Although SNCA A53T transgenic mice showed reduced anxiety by visiting the open arms more often (George et al., 2008), a study conducted in eight- to 12–week-old SNCA knockout mice reported that SNCA was not involved in unconditioned anxiety (Peña-Oliver et al., 2010). According to the present data, significant hypoactivity and high anxiety levels are present in all groups of MPS IIIA mice, indicating it is due to the effects of MPS IIIA disease progression itself rather than SNCA pathology.

4.3.3 Spatial learning and memory impaired in MPS IIIA-SNCA$^{-/-}$ mice

Mice were tested for spatial reference memory and learning ability in a standard Morris water maze, with a hidden platform and external visual cues. All three groups of MPS IIIA performed significantly more poorly than their Normal counterparts in both phases of the test. Indeed, all three MPS IIIA mice groups quickly learned the location of the hidden platform by spending much of the time in the target quadrant, as shown in the *Probe phase*. The mice also demonstrated intact vision in the visual test, suggesting no extraneous visual or sensorimotor impairment.

Although there was no significant difference in performance among MPS IIIA groups with or without *SNCA* deficiency, their learning speed during the *Acquisition phase* was higher than

mixed strain or congenic MPS IIIA mice in earlier studies. All three groups of MPS IIIA mice in this experiment spent 35 sec on average searching for the hidden platform on Day 2, while congenic and mixed strains took 60 sec and 80 sec, respectively, to do the same task (Gliddon and Hopwood, 2004; Crawley et al., 2006). These different findings may be due to the use of different mouse strains and experimental conditions, e.g. water temperature was 21 ± 1°C in this study, while congenic mice and mixed strains were exposed to warmer temperature such as 27 ± 1°C and 21-25°C, respectively. It has also been shown that male rodents can learn faster in cold water than warm water during the *Acquisition phase* due to stress-related corticosterone actions (Sandi et al., 1997).

The poor locomotor performance (decreased path length and speed) displayed by all three groups of MPS IIIA mice in the *Acquisition phase* may not specifically reflect cognitive and memory problems, although their swim times were much slower than the Normal mice. Central motor defects or neuromuscular pathology may be the cause of the poor performance, since poor motor functioning was demonstrated in the Open Field, Elevated Plus maze and motor gait tests. Moreover, the three groups of MPS IIIA mice showed a significant increase in tendency to swim slowly (< 0.05 m/sec) compared to their Normal counterparts, indicating impaired motor functioning, as seen in the Open Field, Elevated Plus maze, Morris water maze and gait tests. On the other hand, *Probe phase* data reveal a cognitive deficit in MPS IIIA mice as they showed much less accuracy in locating the platform area. Therefore, assessing performance in the Morris water maze in mice at an earlier age - before motor symptoms start to overwhelm cognitive ability - may better highlight differences.

Interestingly, the importance of *SNCA* in aging mice has been demonstrated: Morris water maze testing showed that 40-week-old *SNCA* knockout mice were significantly less able to learn by Days 4 and 5 compared to their normal counterparts (Kokhan et al., 2012), and this did not improve during the study period. On average, the knockout animals spent 50 sec locating the hidden platform on Days 4 and 5, while the wild-type animals took only 25 sec. The use of older mice and different test conditions in that study may explain the difference in outcome in this study, as it has been shown that long-term memory and learning acquired by the cerebral cortex and subsequent neurogenesis and synaptogenesis are age-dependent (Blumenfeld-Katzir et al., 2011). *SNCA* has also been found to have important roles in learning and cognition by modulating serotonin and dopamine transporters (Oaks and Sidhu, 2011), glutamate (Gureviciene et al., 2007), and acetylcholine (Pelkonen and Yavich, 2011) neurotransmission.

However, a Morris water maze study on 24-week-old *SNCA* knockout mice showed no significant impairment in performance compared to wild-type littermates (Chen et al., 2002).

4.3.4 Impaired motor gait in MPS IIIA-SNCA$^{-/-}$ mice

Although gait length was significantly reduced by 18-weeks of age in congenic MPS IIIA males (Crawley et al., 2006), it was comparable to normal in mixed strain MPS IIIA mice (Hemsley and Hopwood, 2005). Reduced gait width was not evident until 32-weeks of age in congenic MPS IIIA mice but was noted at 15-weeks of age in the mixed strain. Therefore, there may be strain-dependent changes in gait in MPS IIIA mice. In the present study, both gait width and length were significantly shorter in MPS IIIA mice (all three *SNCA* genotypes) compared to their Normal counterparts. *SNCA* status did not affect gait performance in any of the three MPS IIIA groups. The motor dysfunction in MPS IIIA mice may severely impair locomotor activity and swim speed in behavioural tests such as the Open Field, Elevated Plus maze and Morris water maze tests.

The impaired gait in the MPS IIIA mice may indicate pathological involvement of the extrapyramidal system; it may also indicate pathological bone involvement as MPS IIIA mice exhibit a severe hunched posture by ~20-weeks of age. Moreover, reduced amplitude of walking strides and asymmetric gait kinetics were observed in Gaucher disease type 1 (Sorrentino et al., 2016); Gaucher disease zebrafish also developed curvature of the spine at 12-weeks of age and showed slow and abnormal swimming patterns (Keatinge et al., 2015). Motor impairment such as hind-limb tremor, staggering gait and outward extension of fore-limbs when walking has also been observed in Niemann-Pick disease type C mice (Võikar et al., 2002).

4.4 Conclusion

In summary, the present study utilised a battery of standard behavioural tests to determine whether the absence of *SNCA* contributed to behavioural changes in MPS IIIA mice. Significant hypoactivity, altered motor phenotypes and reduced spatial learning skills were observed in MPS IIIA-SNCA$^{-/-}$ mice, which replicate those in MPS IIIA-SNCA$^{+/+}$, MPS IIIA-SNCA$^{+/-}$ and congenic MPS IIIA mice in previous studies, indicating that neurological outcomes are SNCA-independent. The difference in SNCA genotype may explain the increased anxiety and reduced risk-taking behaviour in MPS IIIA-SNCA$^{-/-}$ mice, which exhibited fewer entries to the central region and the open arms of the Elevated Plus maze. In the next chapter, histopathological

markers associated with MPS IIIA were quantified to determine the contribution of *SNCA* to disease pathology.

Chapter (5)

Histopathological evaluation in MPS IIIA mice deficient in α-synuclein

5.1 Introduction

The *SNCA* gene was knocked out in MPS IIIA mice and the effects on clinical disease parameters were evaluated using several behavioural tests, as discussed in Chapter 4. This chapter outlines the biochemical and neuropathological features of these mice and assesses whether *SNCA* knockout alleviated or delayed pathological disease progression. The study timeline and the specific brain areas examined are shown (**Fig 5.1 A, B)**. Both sexes of mice aged 3- and 12-weeks were used in the biochemical and histological analyses. All 22-week-old were males as they were the cohort that underwent behavioural testing. All sample preparation was undertaken by the candidate. Liquid chromatographic separation and mass spectrometry analysis was performed by Dr. Paul Trim (Heparan sulphate) and Stephen Dupluck (gangliosides and dopamine). All data was analysed and interpreted by the candidate.

As reviewed in Chapter 1, MPS IIIA results from a deficiency of SGSH and the subsequent lysosomal accumulation of HS as well secondary accumulation of acidic glycosphingolipids, specifically G_{M2} and G_{M3} gangliosides, in the brain (McGlynn et al., 2004). Histologically, the MPS IIIA mouse brain has been shown to exhibit elevated punctate cytoplasmic staining with lysosomal integral membrane protein-II, which is indicative of endo/lysosomal expansion (Hemsley et al., 2008). Ubiquitin-positive axonal spheroids have also been observed in the cuneate nucleus and brainstem by seven-weeks of age (Savas et al., 2004), and widespread ubiquitin-inclusions are seen by 20-weeks of age (Savas et al., 2004).

Moreover, staining with the glial cell marker (glial fibrillary acidic protein) and microgliosis was significantly elevated from four–weeks of age (Hassiotis et al., 2014). Intracellular filamentous inclusions or hyperphosphorylated-tau with paired helical filaments are also evident in the medial entorhinal cortex and dentate gyrus in MPS IIIB mice (Ohmi et al., 2009; Ohmi et al., 2011); β-amyloid, cholesterol, and ubiquitin are also deposited in those neuronal cells (Ohmi et al., 2011). This study investigated whether reducing *SNCA* expression mediated a reduction in any of these cardinal neuropathological features in the MPS IIIA mouse.

(A)

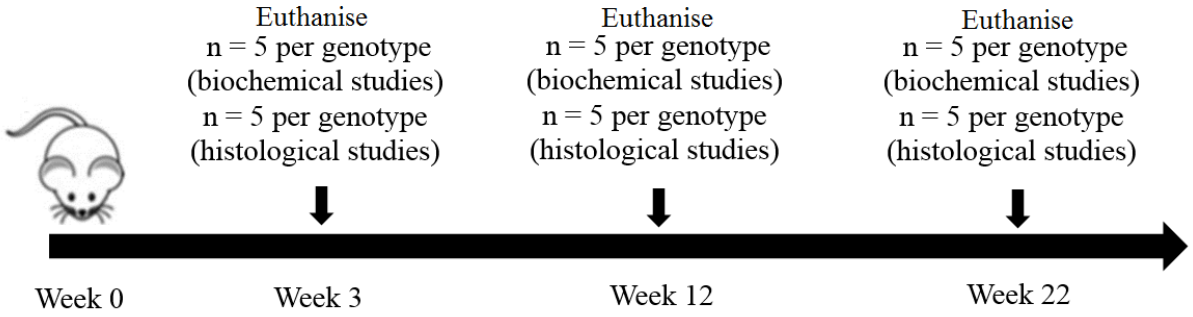

(B)

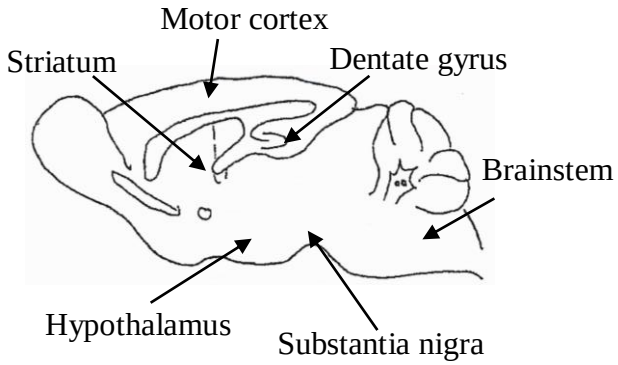

Figure 5.1. (A) Overall study design; and (B) brain areas examined in sagittal plane for histological investigations.

5.2 Results

5.2.1 Spleen weight

Organomegaly, in particular, splenomegaly due to substrate deposition, is a prominent clinical feature in MPS IIIA. To examine the effects of *SNCA* gene deletion in MPS IIIA mice, the weight of the whole spleen was determined in each of the four groups of mice at three different time points **(Fig 5.2)**. Only whole spleens and parts of liver were taken out from animals at the time of organ collection. Therefore, spleens weights were only reliably measured for the group comparison.

Spleen weights from 12- and 22-week old MPS IIIA mice with each of the different *SNCA* genotypes (MPS IIIA-SNCA$^{+/+}$, MPS IIIA-SNCA$^{+/-}$ and MPS IIIA-SNCA$^{-/-}$) trended higher than that of their Normal counterparts, although this did not achieve statistical significance. There was no difference in spleen weight between the cohorts of MPS IIIA mice with the three different *SNCA* genotypes.

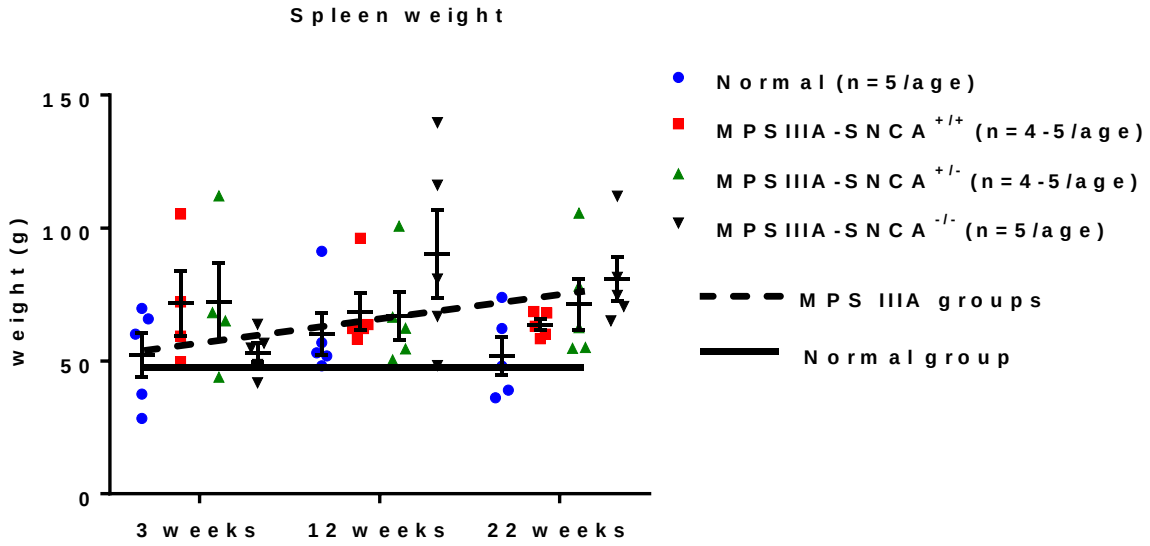

Figure 5.2. Spleen weight for three-, 12- and 22-week old mice with four different genotypes. Data are shown as mean ± SEM. Straight lines indicate the line of best fit for the Normal mice and all three groups of MPS IIIA mice. The number of animals involved is shown in brackets.

5.2.2 Quantification of heparan sulphate

HS levels in the striata of Normal, MPS IIIA-SNCA$^{+/+}$, MPS IIIA-SNCA$^{+/-}$ and MPS IIIA-SNCA$^{-/-}$ mice were assessed at three-, 12- and 22-weeks of age by tandem mass spectrometry. Peak areas of the deuterated internal standard from 72 injections are shown in **Fig 5.3 A**. Measurement reproducibility can be gauged from the internal standard counts, as this was spiked into each sample. The reproducibility gauge ensures that the measurement of HS is consistent between samples and controls. Two internal standard injections from quality control samples were out of the acceptable range and were not included in the calculation.

As shown in **Fig 5.3 B**, HS levels were significantly higher in all three groups of MPS IIIA mice at all three ages compared to their Normal counterparts ($P < 0.0001$). HS levels in Normal mice were consistently low, at approximately one a.u (arbitrary unit). On the other hand, HS levels increased significantly between three- and 22-weeks of age in MPS IIIA-SNCA$^{+/+}$ mice ($P= 0.0070$) and MPS IIIA-SNCA$^{-/-}$ mice ($P = 0.0003$) but not in MPS IIIA-SNCA$^{+/-}$ mice ($P > 0.9$). Post-hoc testing using Bonferroni's multiple comparison test revealed no difference in HS levels between age-matched MPS IIIA-SNCA$^{+/+}$, MPS IIIA-SNCA$^{+/-}$ and MPS IIIA-SNCA$^{-/-}$ mice.

5.2.3 Quantification of gangliosides G_{M2} and G_{M3} in brain

Previous reports show that two types of gangliosides (G_{M2} and G_{M3}) are deposited in the MPS IIIA mouse brain (McGlynn et al., 2004). To determine whether the absence of the *SNCA* gene in MPS IIIA mice effected a change in ganglioside accumulation, six of the most abundant gangliosides in the striata were measured by liquid chromatography-MS/MS (LC-MS/MS) in all four groups of mice at three-, 12- and 22-weeks of age.

Statistically significant elevations in almost all G_{M2} and G_{M3} species were observed in MPS IIIA mice compared to age-matched Normal mice **(Fig 5.4, 5.5)**. While ganglioside levels in Normal mice were relatively stable across the three ages tested, ganglioside accumulation in MPS IIIA mice was significantly higher at the same time points. There were no statistically significant differences between MPS IIIA mice with or without the *SNCA* gene.

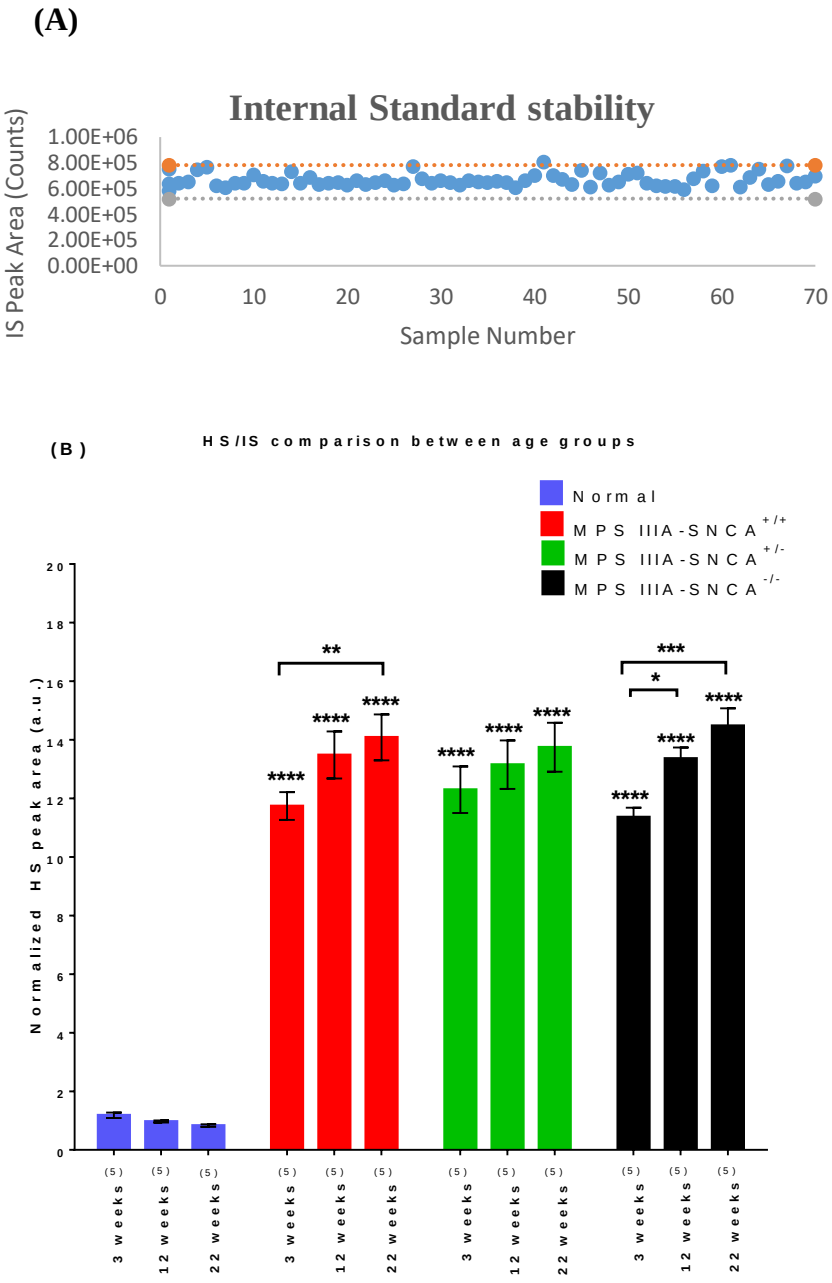

Figure 5.3. The plot of normalised HS peak areas in Normal, MPS IIIA-SNCA$^{+/+}$, MPS IIIA-SNCA$^{+/-}$, and MPS IIIA-SNCA$^{-/-}$ mice. (A) Internal standard (IS) stability for all 72 samples with 7.5 µl injections; dotted lines represent ± 20% from the median IS peak area. (B) Normalised HS level. Data are shown as mean ± SEM and * indicates a significant difference compared to the Normal group. *P < 0.05, **P < 0.01, ***P < 0.001, ****P < 0.0001, a.u = arbitrary unit. A two-way ANOVA followed by post-hoc Bonferroni's multiple comparison test is used. The number of animals involved is shown in brackets.

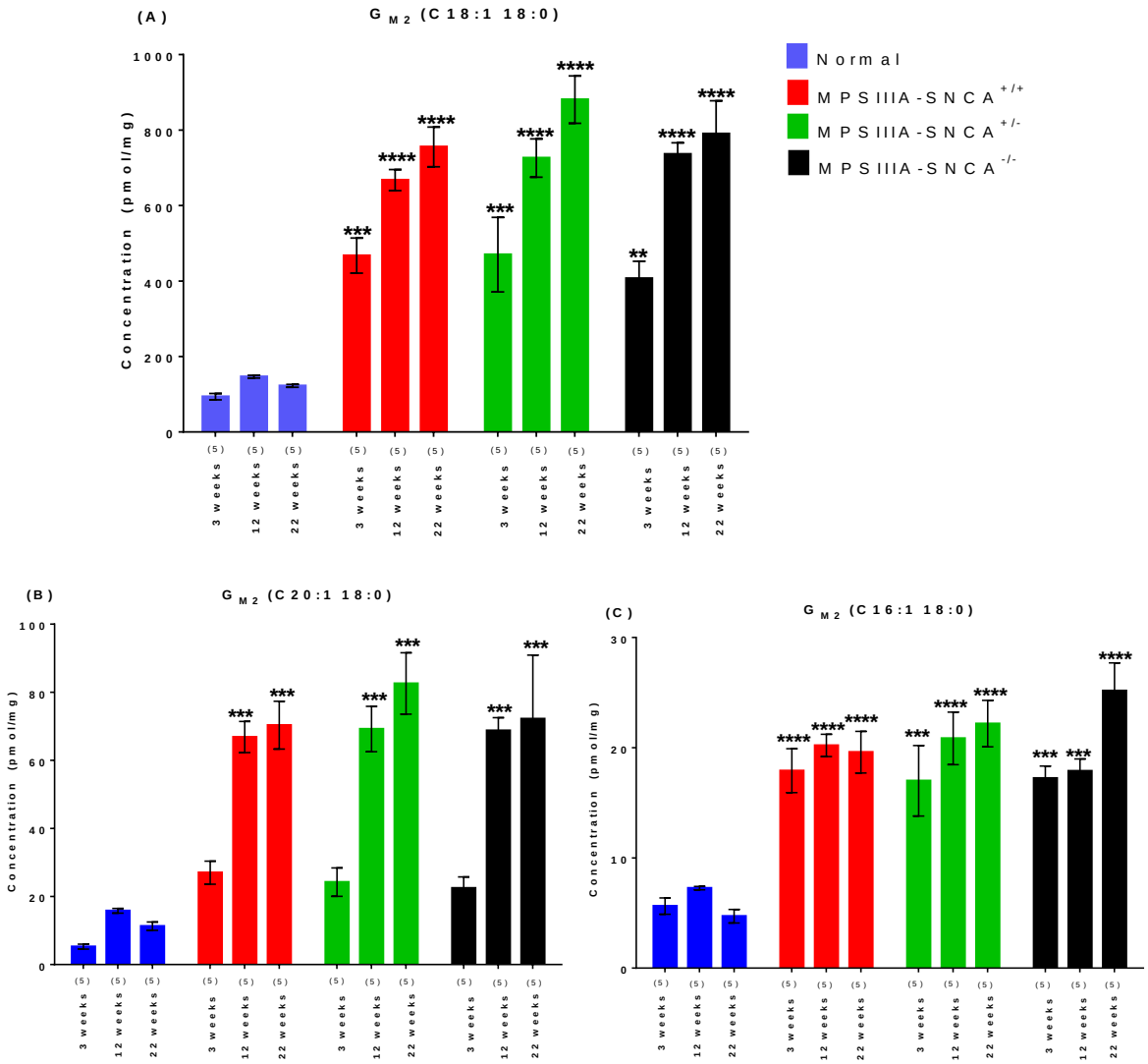

Figure 5.4. Comparison of striatal G_{M2} ganglioside levels in Normal, MPS IIIA-SNCA$^{+/+}$, MPS IIIA-SNCA$^{+/-}$, and MPS IIIA-SNCA$^{-/-}$ mice. Ganglioside species measured were: (A) G_{M2} C18:1 18:0; (B) G_{M2} C20:1 18:0; and (C) G_{M2} C16:1 18:0. Data are shown as mean ± SEM and * indicates a significant difference compared to the Normal group: **P < 0.01, ***P < 0.001, ****P < 0.0001, ns = not significant. A two-way ANOVA followed by post-hoc Bonferroni's multiple comparison test was used. The number of animals involved is shown in brackets.

Figure 5.5. Comparison of striatal G_{M3} ganglioside levels in Normal, MPS IIIA-SNCA$^{+/+}$, MPS IIIA-SNCA$^{+/-}$, and MPS IIIA-SNCA$^{-/-}$ mice. Ganglioside species measured were: (A) G_{M3} C18:1 18:0; (B) G_{M3} C20:1 18:0; (C) G_{M3} C16:1 18:0; (D) G_{M3} C18:1 22:0; and (E) G_{M3} C18:1 24:1. Data are shown as mean ± SEM and * indicates a significant difference compared to the Normal group. A two-way ANOVA followed by post-hoc Bonferroni's multiple comparison test was used and *P < 0.05, **P < 0.01, ***P < 0.001, ****P < 0.0001, ns = not significant. The number of animals involved is shown in brackets.

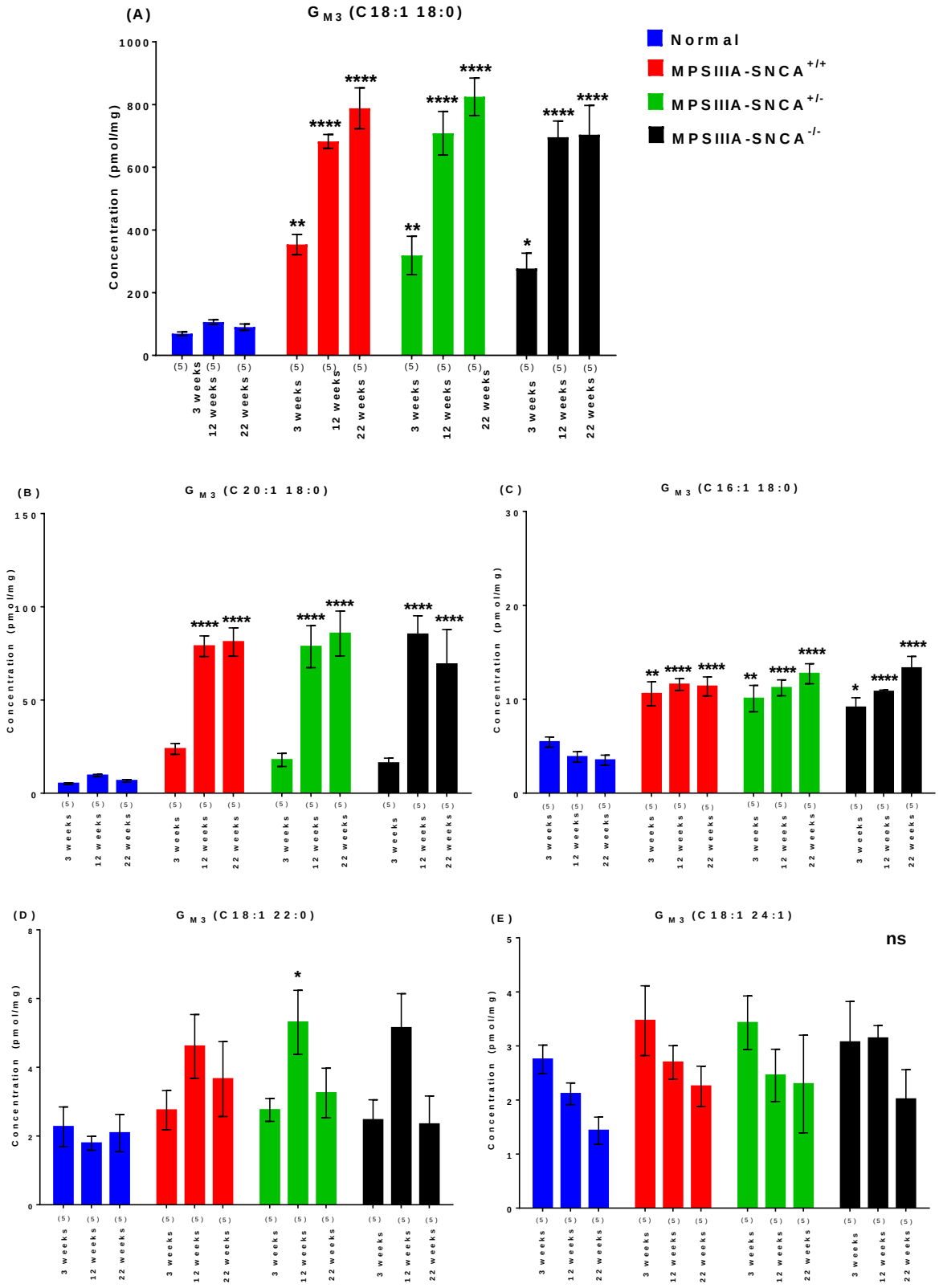
(A)
GM3 (C18:1 18:0)
Concentration (pmol/mg)
Normal
MPSIIIA-SNCA+/+
MPSIIIA-SNCA+/-
MPSIIIA-SNCA-/-
3 weeks
12 weeks
22 weeks
(B)
GM3 (C20:1 18:0)
(C)
GM3 (C16:1 18:0)
(D)
GM3 (C18:1 22:0)
(E)
GM3 (C18:1 24:1)
ns

5.2.4 Levels of striatal dopamine

Striatal dopamine content was significantly reduced in *SNCA* knockout mice compared to wild-type mice (18% reduction) (Abeliovich et al., 2000). However, to date, neurotransmitter levels in the MPS IIIA mouse brain have not been evaluated. To explore impaired motor behaviour in MPS IIIA mice, striatal dopamine was measured in the experimental cohorts of mice at three-, 12- and 22-weeks of age by LC-MS/MS.

The interaction between Group and Age on striatal dopamine content was not significant ($P = 0.9338$) **(Fig 5.6A)**. Striatal dopamine levels showed a downward trend in all three groups of MPS IIIA mice compared to Normal mice.

However, there was a significant main effect for Group ($p < 0.001$). All three groups of MPS IIIA mice exhibited significantly decreased dopamine levels in the striatum than Normal mice **(Fig 5.6B)**. There was a 28-34% striatal dopamine loss in MPS IIIA mice compared to Normal mice at all three ages combined. There was no significant difference between the three groups of MPS IIIA mice.

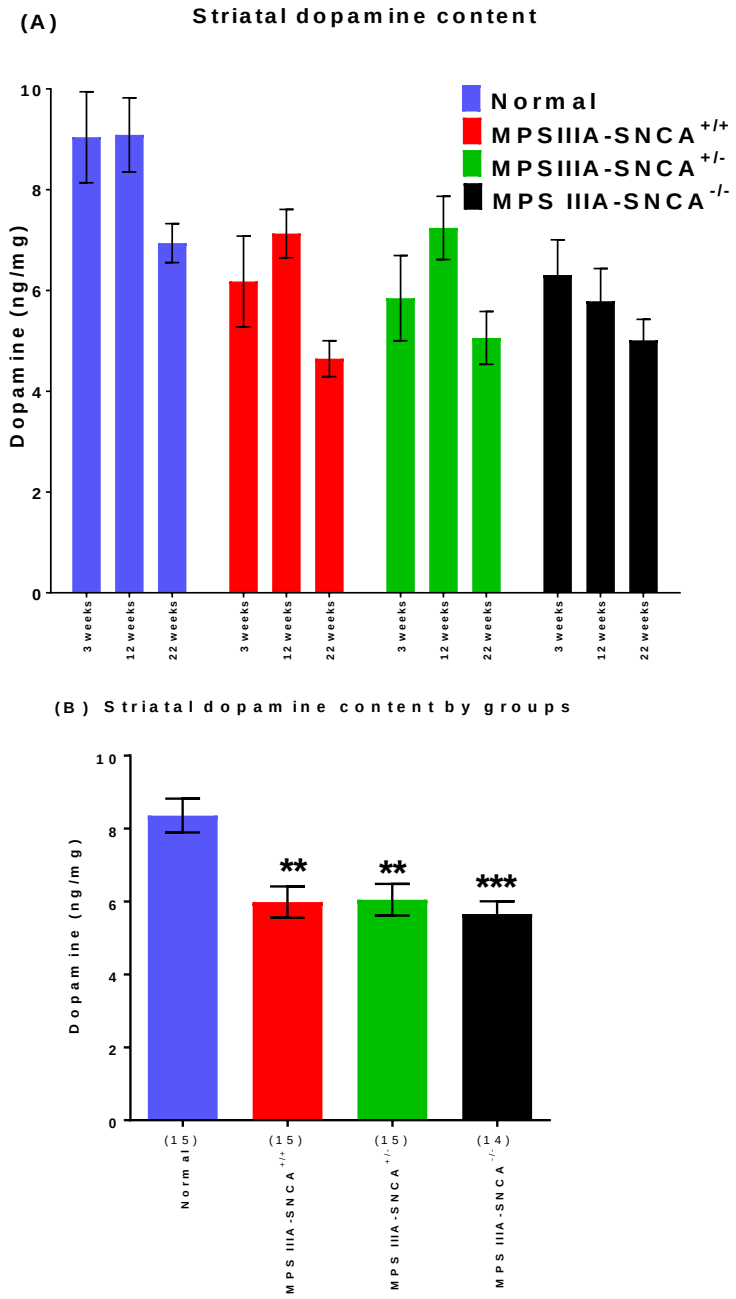

Figure 5.6. (A) Striatal dopamine content in Normal, MPS IIIA-SNCA$^{+/+}$, MPS IIIA-SNCA$^{+/-}$, and MPS IIIA-SNCA$^{-/-}$ mice at three-, 12- and 22-weeks of age. (B) Striatal dopamine content comparison of the four genotype groups with all the three different ages combined. Data are shown as mean ± SEM and * indicates a significant difference compared to the Normal group. A two-way ANOVA followed by post-hoc Bonferroni's multiple comparison tests is used: ** and *** represent $P < 0.01$ and $P < 0.001$, respectively. The number of animals involved is shown in brackets.

5.2.5 Immunohistological analysis

Six different brain regions (motor cortex, striatum, dentate gyrus, hypothalamus, substantia nigra and brainstem) were examined using immunohistochemical/histochemical techniques to detect pathological lesions containing ubiquitin and phosphorylated-tau. Furthermore, glial fibrillary acidic protein and lysosomal integral membrane protein II were examined as they have been found to increase with disease progression in the MPS IIIA mouse brain (Hemsley et al., 2008; Hassiotis et al., 2014).

5.2.5.1 Proteinaceous inclusions: ubiquitin

Representative images of ubiquitin staining are shown in **Fig 5.7**. Dot-like structures consistent with axonal spheroids have been reported in both mixed strain and congenic MPS IIIA mice (Savas et al., 2004; Crawley et al., 2006). Ubiquitin-positive lesions start to accumulate in the superior colliculus, periaqueductal grey and pontine nucleus at four-weeks of age and rapidly spread to other brain areas between six- and nine-weeks of age in MPS IIIA mice (Hassiotis et al., 2014).

In the present study, ubiquitin-positive inclusions were not detected in the regions examined in either Normal or MPS IIIA mice at three-weeks of age **(Fig 5.8)**. However, a large number of inclusions were present in all three MPS IIIA mice genotypes by 12-weeks of age, particularly in the brainstem (consistent with previous reports). By 22-weeks of age, all the examined regions (except motor cortex and striatum) displayed significantly increased numbers of inclusions. Ubiquitin immunoreactivity was not significantly different between MPS IIIA-SNCA$^{+/+}$, MPS IIIA-SNCA$^{+/-}$ and MPS IIIA-SNCA$^{-/-}$ mice.

5.2.5.2 Proteinaceous inclusions: hyperphosphorylated-tau

Representative images of hyperphosphorylated-tau staining are shown in **Fig 5.9**. Dot-like structures consistent with phosphorylated-tau proteins were documented in the medial entorhinal cortex and dentate gyrus of MPS IIIB mice (Ohmi et al., 2009). Similar phosphorylated-tau-positive inclusions were observed in congenic MPS IIIA mouse brain (Beard *et al.*, unpublished).

In this study, phosphorylated-tau-positive inclusions were not detected in Normal mice at any age, nor were they detected in the three MPS IIIA groups at three-weeks of age. However, the number of phosphorylated-tau lesions increased modestly with age in all three MPS IIIA genotypes in all of the brain regions examined, particularly in the brainstem region, by 12- and 22-weeks of age **(Fig 5.10)**. Tau immunoreactivity was not significantly reduced in any area of the brain in MPS IIIA mice lacking *SNCA*.

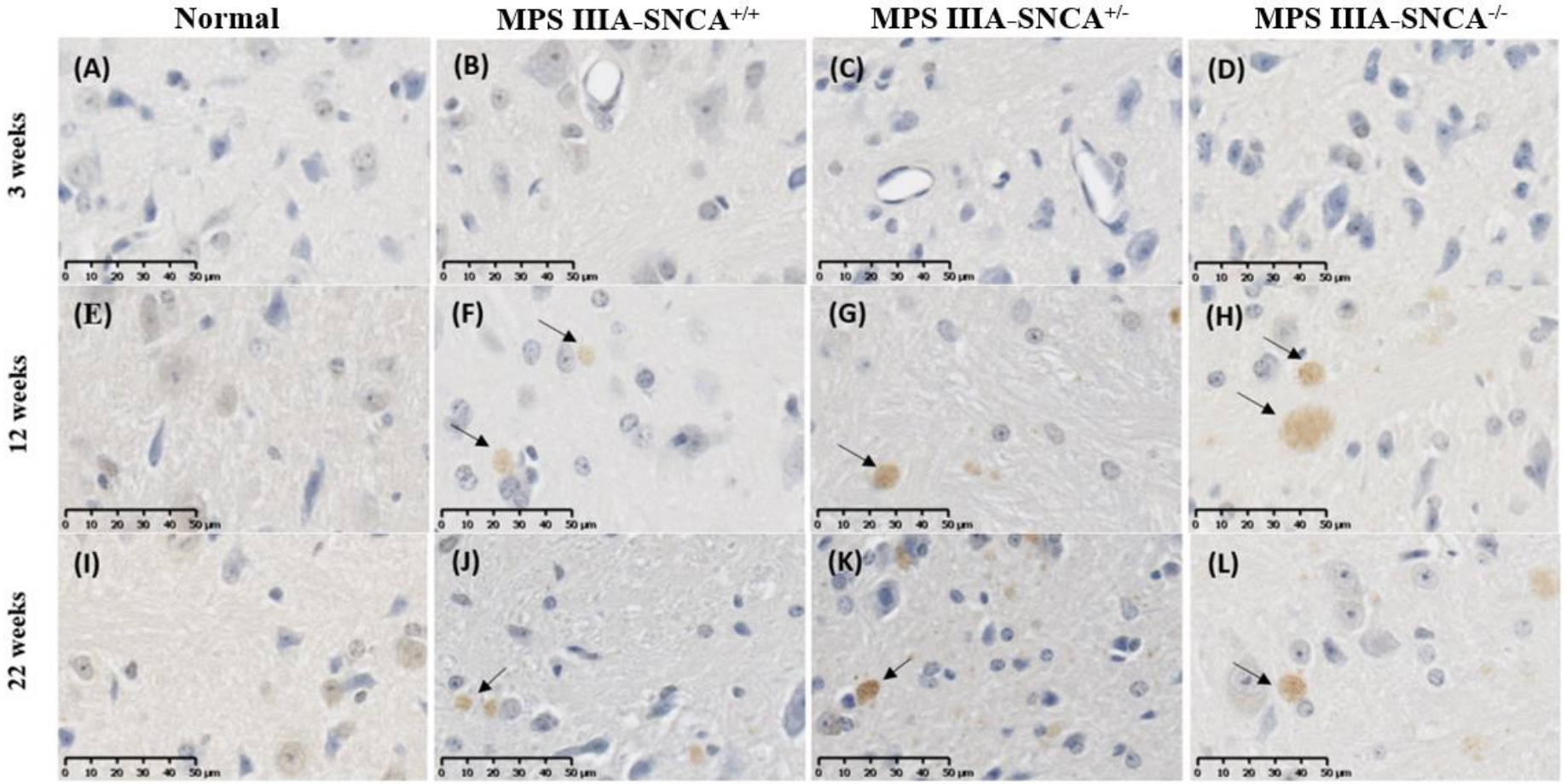

Figure 5.7: Representative images of ubiquitin staining in the brainstem from Normal (A, E, I); MPS IIIA-αsyn$^{+/+}$ (B, F, J); MPS IIIA-αsyn$^{+/-}$ (C, G, K); and MPS IIIA-αsyn$^{-/-}$ (D, H, L) mice at 3-weeks of age. Arrows indicate ubiquitin-positive inclusions. Scale bar = 50 µm.

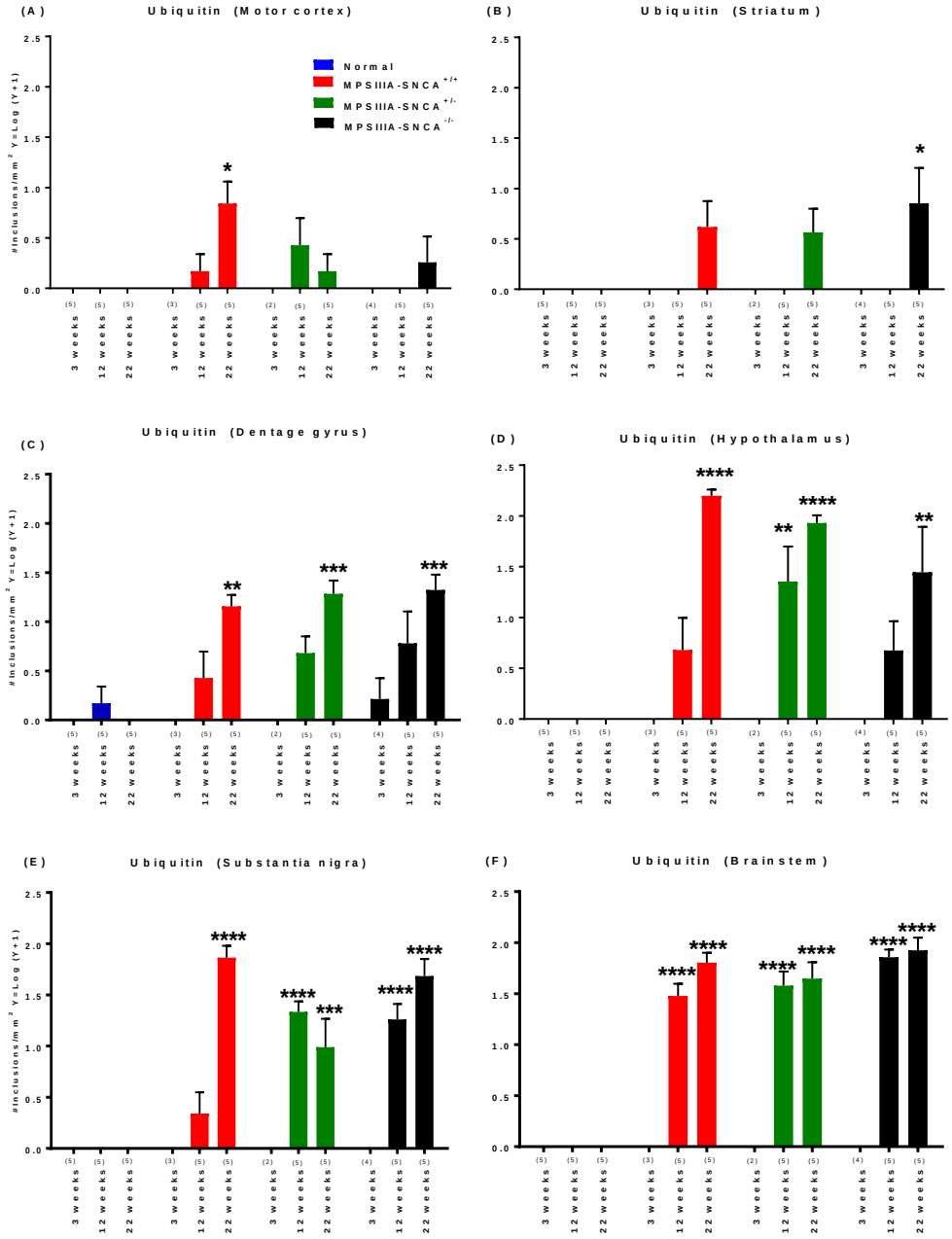

Figure 5.8. Ubiquitin-positive inclusions in Normal, MPS IIIA-SNCA$^{+/+}$, MPS IIIA-SNCA$^{+/-}$, and MPS IIIA-SNCA$^{-/-}$ mice at three-, 12- and 22-weeks of age. Brain regions examined were: (A) motor cortex (M1); (B) striatum; (C) dentate gyrus; (D) hypothalamus; (E) substantia nigra; and (F) brainstem. Data are shown as mean ± SEM and * indicates a significant difference compared to the age-matched Normal group. A two-way ANOVA followed by post-hoc Bonferroni's multiple comparison test is used and *P < 0.05, **P < 0.01, ***P < 0.001, ****P < 0.0001. The number of animals involved is shown in brackets.

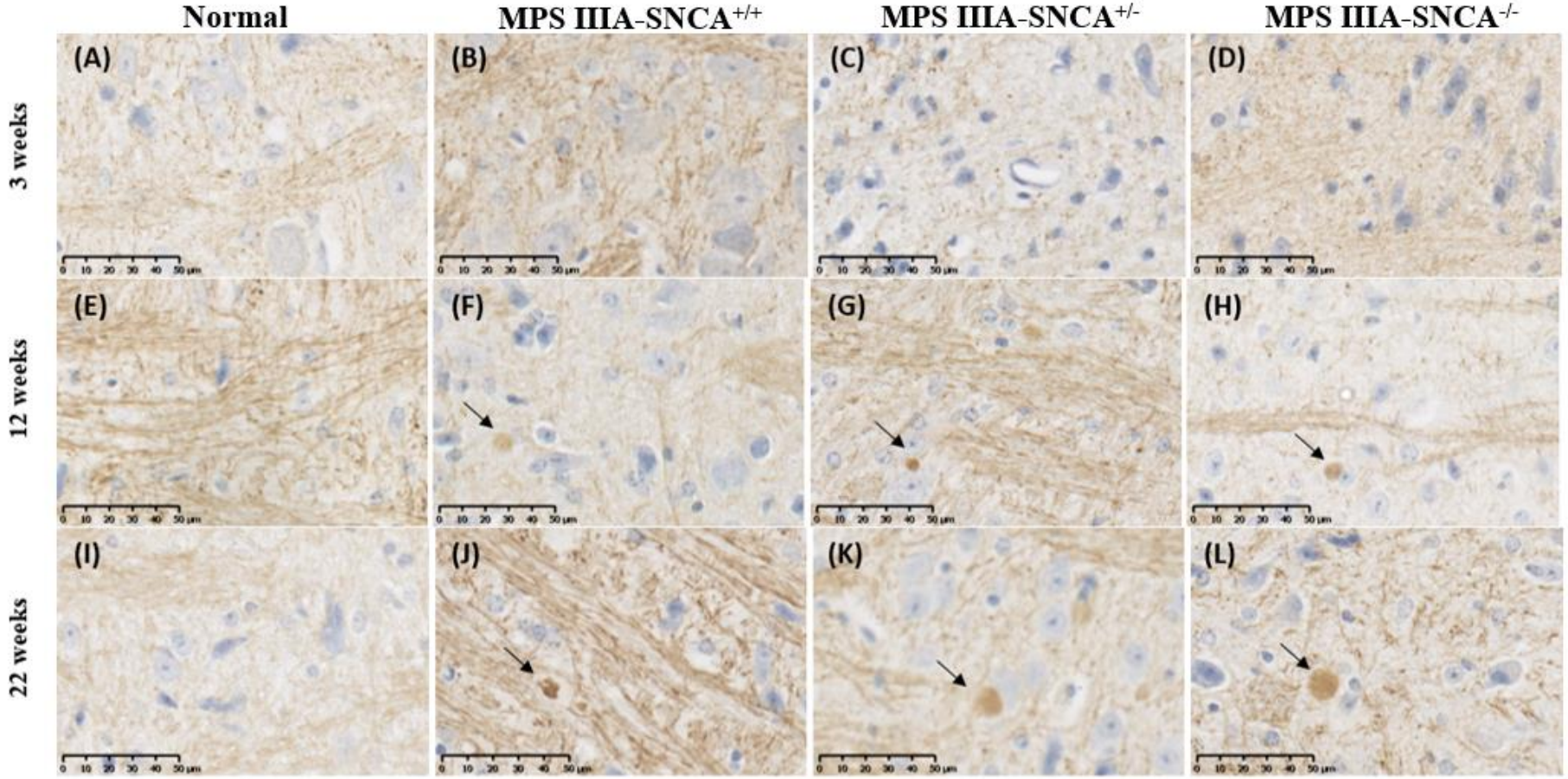

Figure 5.9: Representative images of phosphorylated-tau in the brainstem from Normal (A, E, I); MPS IIIA-SNCA$^{+/+}$ (B, F, J); MPS IIIA-SNCA$^{+/-}$ (C, G, K); and MPS IIIA-SNCA$^{-/-}$ (D, H, L) mice at 3-weeks of age. Arrows indicate ubiquitin-positive inclusions. Scale bar = 50 µm.

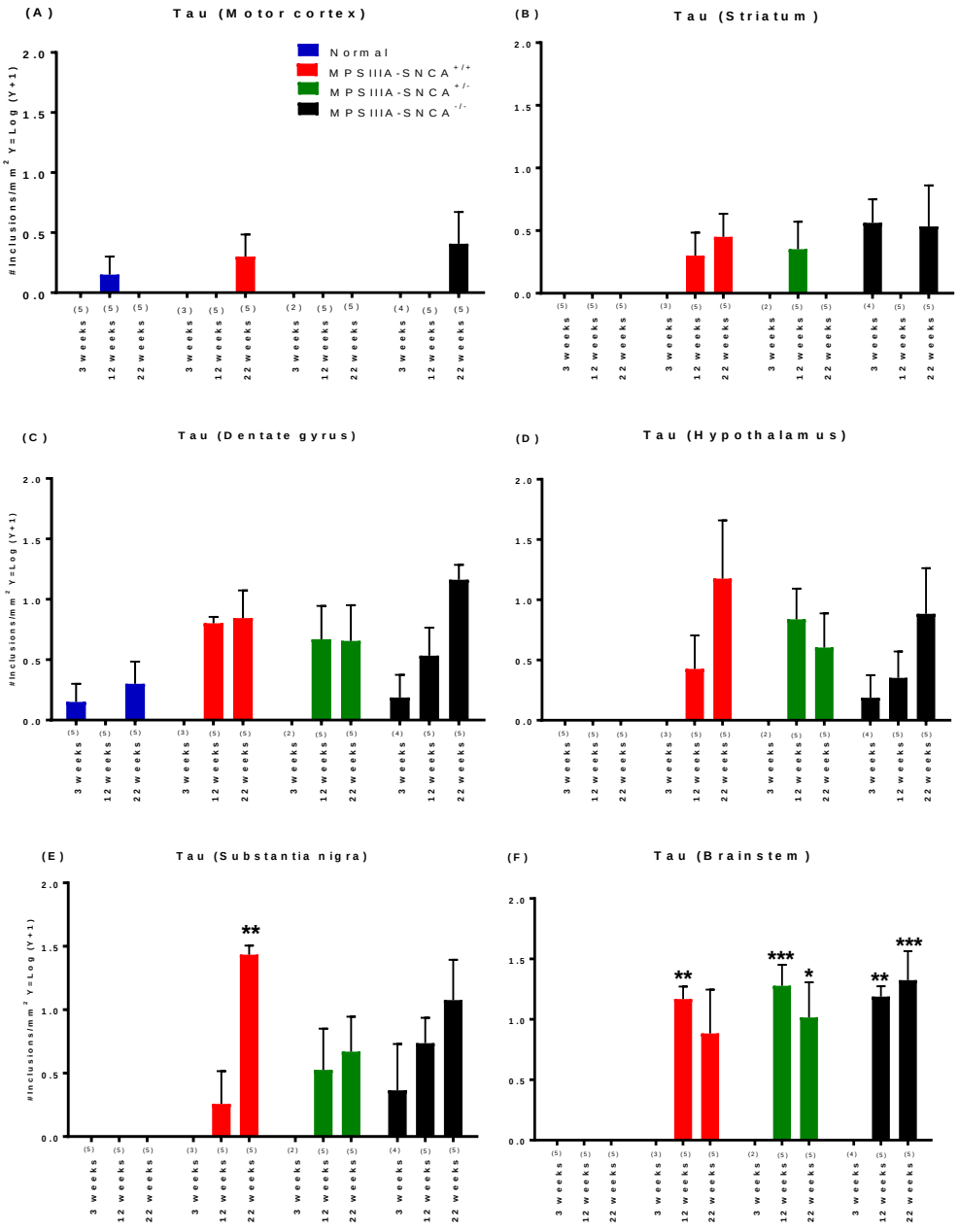

Figure 5.10. Phosphorylated-tau inclusions in Normal, MPS IIIA-SNCA$^{+/+}$, MPS IIIA-SNCA$^{+/-}$, and MPS IIIA-SNCA$^{-/-}$ mice at three-, 12- and 22-weeks of age. Brain regions examined were: (A) motor cortex (M1); (B) striatum; (C) dentate gyrus; (D) hypothalamus; (E) substantia nigra; and (F) brainstem. Data are shown as mean ± SEM and * indicates a significant difference compared to the age-matched Normal group. A two-way ANOVA followed by post-hoc Bonferroni's multiple comparison test is used and *P < 0.05, **P < 0.01, ***P < 0.001, ****P < 0.0001. The number of animals involved is shown in brackets.

5.2.5.3 Glial fibrillary acidic protein expression

Neuroinflammatory changes, as determined via increased glial fibrillary acidic protein expression, indicative of astrocyte activation, were seen in both mixed strain and congenic MPS IIIA mice compared to age-matched normal counterparts (Savas et al., 2004; Hemsley et al., 2009). To identify whether *SNCA* had an effect on neuroinflammation in MPS IIIA, glial fibrillary acid protein staining was quantified in all four groups of mice.

Representative images of staining are shown in **Fig 5.11**. The extent of astrogliosis was significantly high in all three MPS IIIA groups in all of the brain areas examined, except in substantia nigra and dentate gyrus ($P < 0.0001$ *cf*. Normal) **(Fig 5.12)**. Staining was significantly more intense in the motor cortex of all three MPS IIIA genotypes at three-weeks of age, and subsequently increased with age compared to Normal mice. Widespread increases in glial cell activity were observed in all of the other brain areas examined in all three MPS IIIA groups, particularly in the striatum and brainstem at 12- and 22-weeks of age. The statistically significant increase in staining over the course of time (especially from 3-weeks old to 12-weeks old) was seen in all three groups of MPS IIIA mice compared to the wild type group, but there was no significant difference between MPS IIIA mice ($SNCA^{+/+}$, $SNCA^{+/-}$ and $SNCA^{-/-}$).

5.2.5.4 Lysosomal integral membrane protein II expression

Elevations in the endosomal/lysosomal integral membrane protein II (LIMP-II) marker have been observed in MPS IIIA mouse brain, indicating endosomal/lysosomal enlargement due to accumulation of both primary and secondarily stored substrates (Hemsley et al., 2008; Hemsley et al., 2009). To assess whether *SNCA* had an effect on lysosomal pathology in MPS IIIA mice, LIMP-II immunoreactivity was quantified across the four groups of experimental mice.

Representative images of LIMP-II staining in the brainstem are shown in **Fig 5.13**. Intense staining of intra-cytoplasmic vesicular structures is apparent throughout all of the brain regions examined in all MPS IIIA mice regardless of genotype. Cytoplasmic expression of this marker was significantly elevated in all but motor cortex and striatal regions in all MPS IIIA groups at three-weeks of age ($P < 0.0001$) **(Fig 5.14)**. An age-dependent increase in staining was observed across the six brain regions examined in all groups of MPS IIIA mice by 12-weeks of age. The highly significant increases in immunoreactivity over the course of time was noted in all three

groups of MPS IIIA mice compared to the Normal group, but there was no significant difference between $SNCA^{+/+}$, $SNCA^{+/-}$ and $SNCA^{-/-}$ mice.

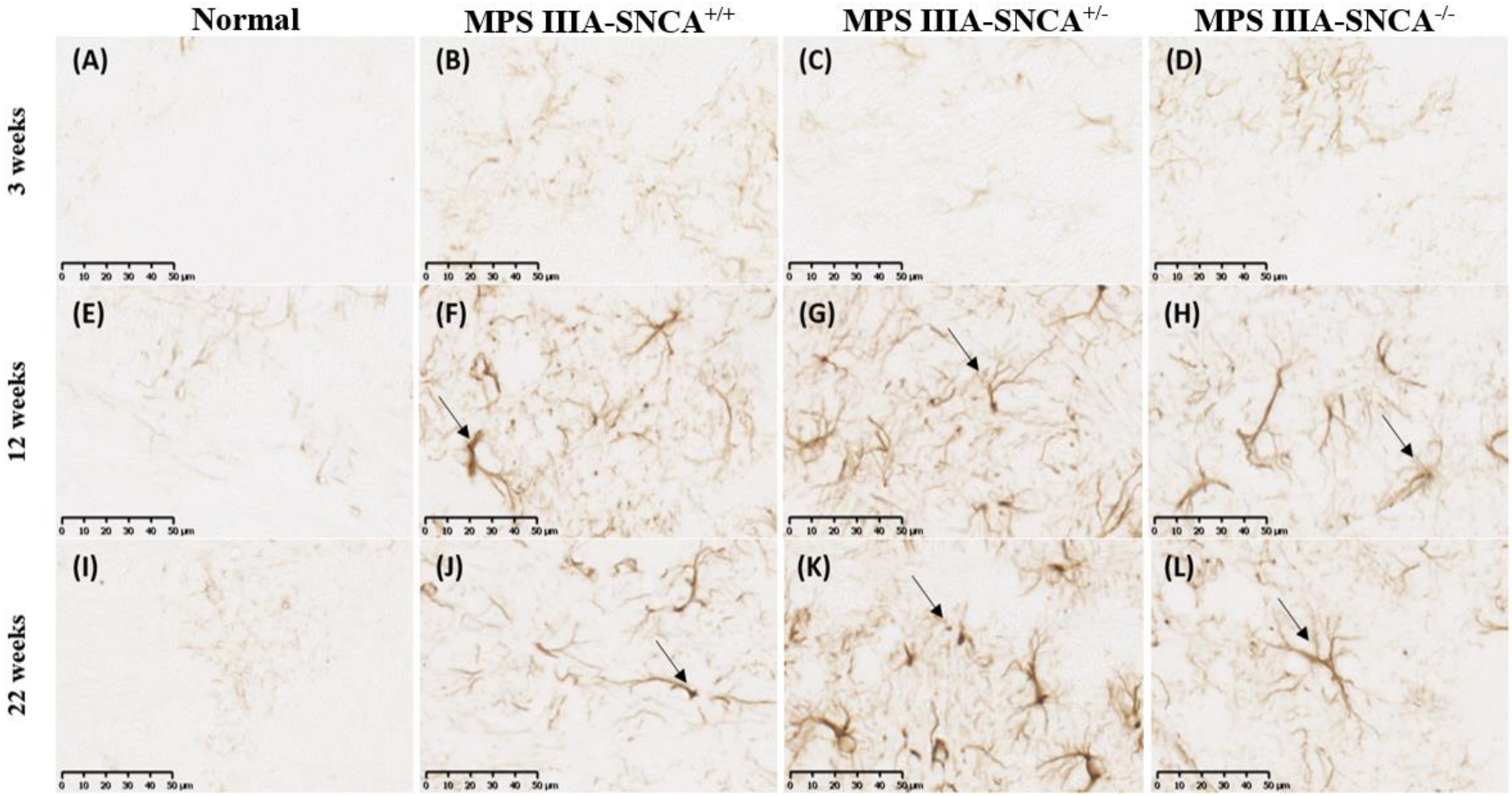

Figure 5.13: Representative images of GFAP staining in the brainstem from Normal (A, E, I); MPS IIIA-SNCA$^{+/+}$ (B, F, J); MPS IIIA-SNCA$^{+/-}$ (C, G, K); and MPS IIIA-SNCA$^{-/-}$ (D, H, L) mice at 3-weeks of age. Arrows indicate LIMP-II immunoreactive cells. Scale bar = 50 µm.

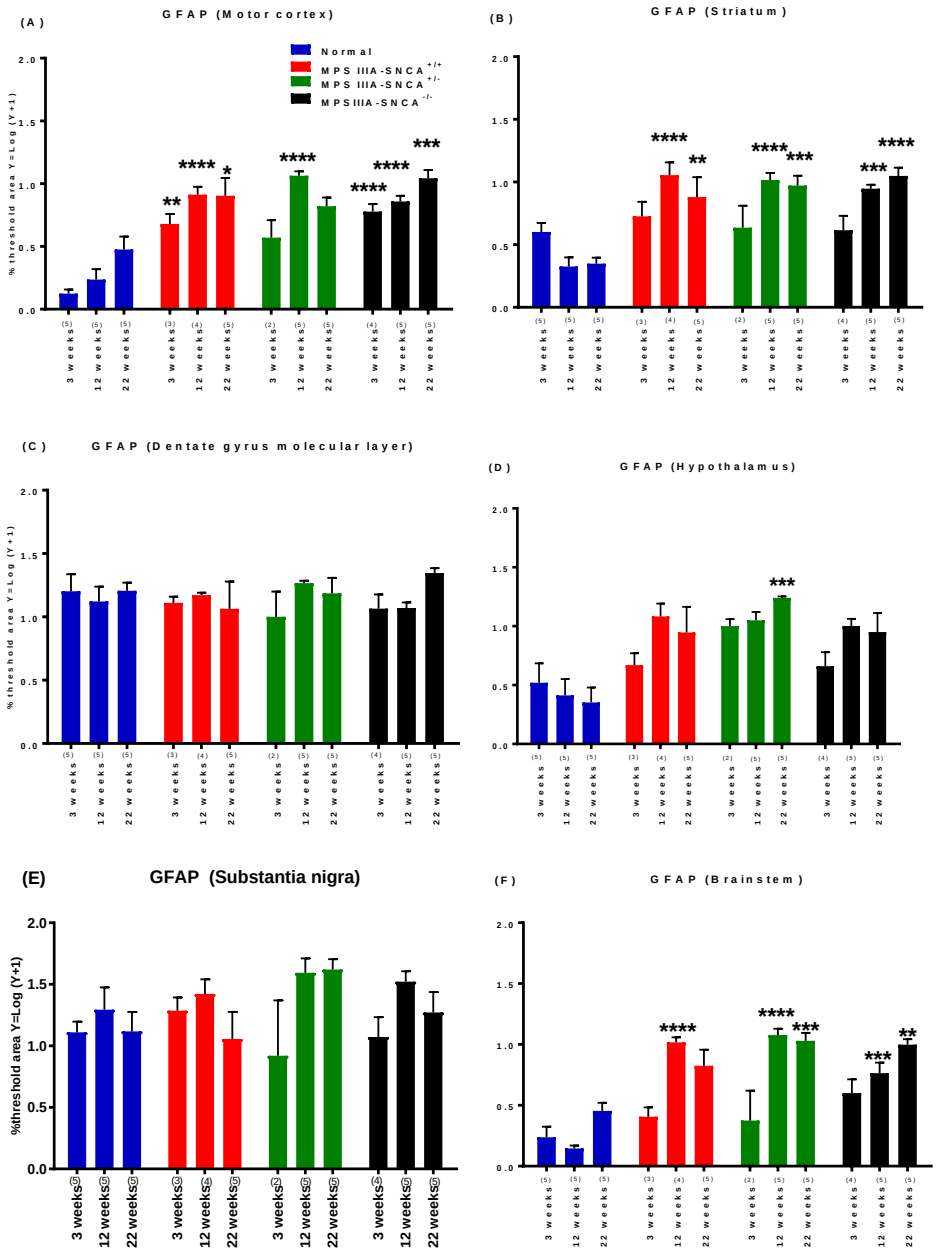

Figure 5.12. Brain tissue was stained using an antibody to glial fibrillary acidic protein in Normal, MPS IIIA-SNCA$^{+/+}$, MPS IIIA-SNCA$^{+/-}$, and MPS IIIA-SNCA$^{-/-}$ mice at three-, 12- and 22-weeks of age. Brain regions examined were: (A) motor cortex (M1); (B) striatum; (C) dentate gyrus; (D) hypothalamus; (E) substantia nigra; and (F) brainstem. Data are shown as mean ± SEM and * indicates a significant difference compared to the age-matched Normal group. A two-way ANOVA followed by post-hoc Bonferroni's multiple comparison test is used and *P < 0.05, **P < 0.01, ***P < 0.001, ****P < 0.0001. The number of animals involved is shown in brackets.

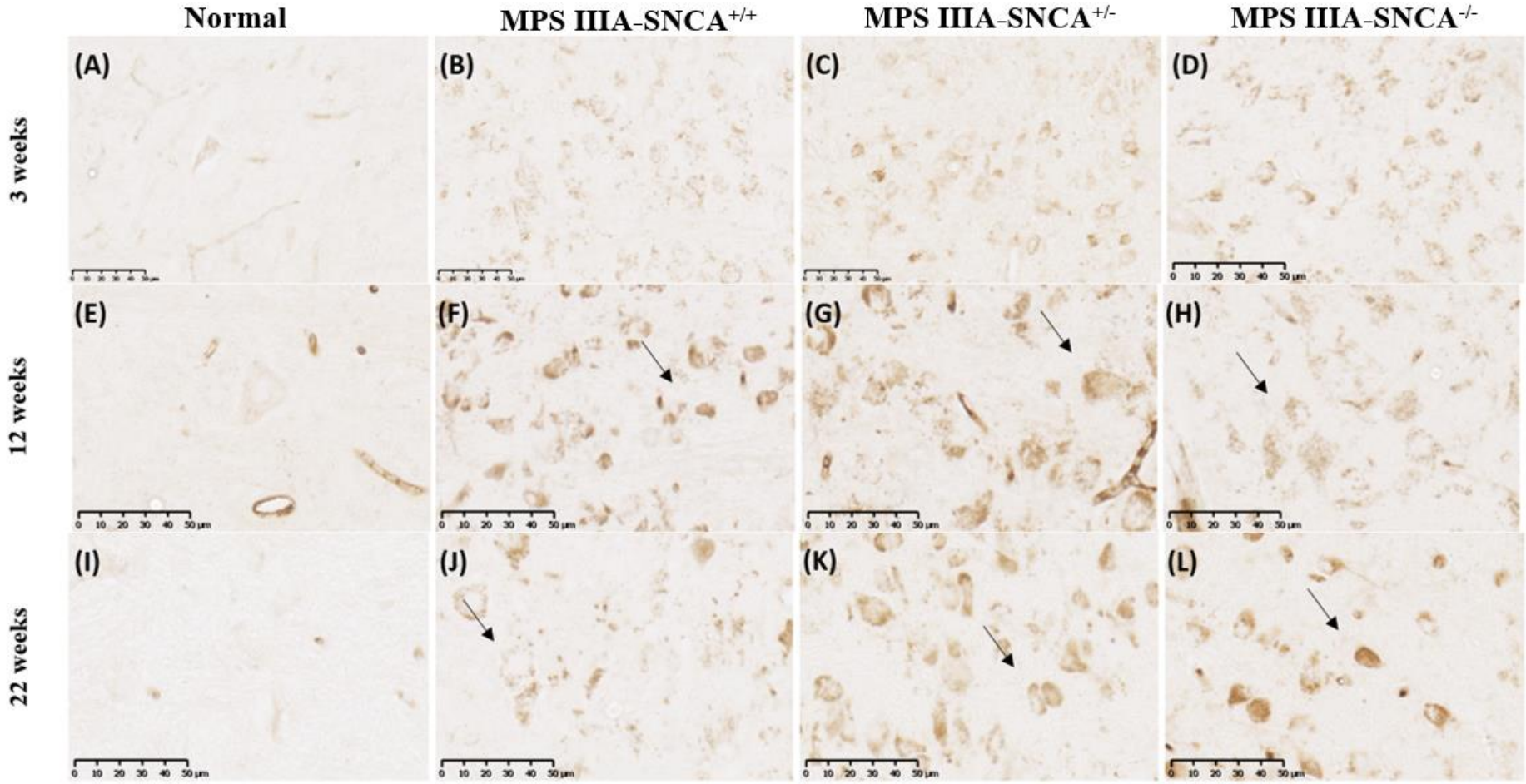

Figure 5.13: Representative images of LIMP-II staining in the brainstem from Normal (A, E, I); MPS IIIA-SNCA$^{+/+}$ (B, F, J); MPS IIIA-SNCA$^{+/-}$ (C, G, K); and MPS IIIA-SNCA$^{-/-}$ (D, H, L) mice at 3-weeks of age. Arrows indicate LIMP-II immunoreactive cells. Scale bar = 50 µm.

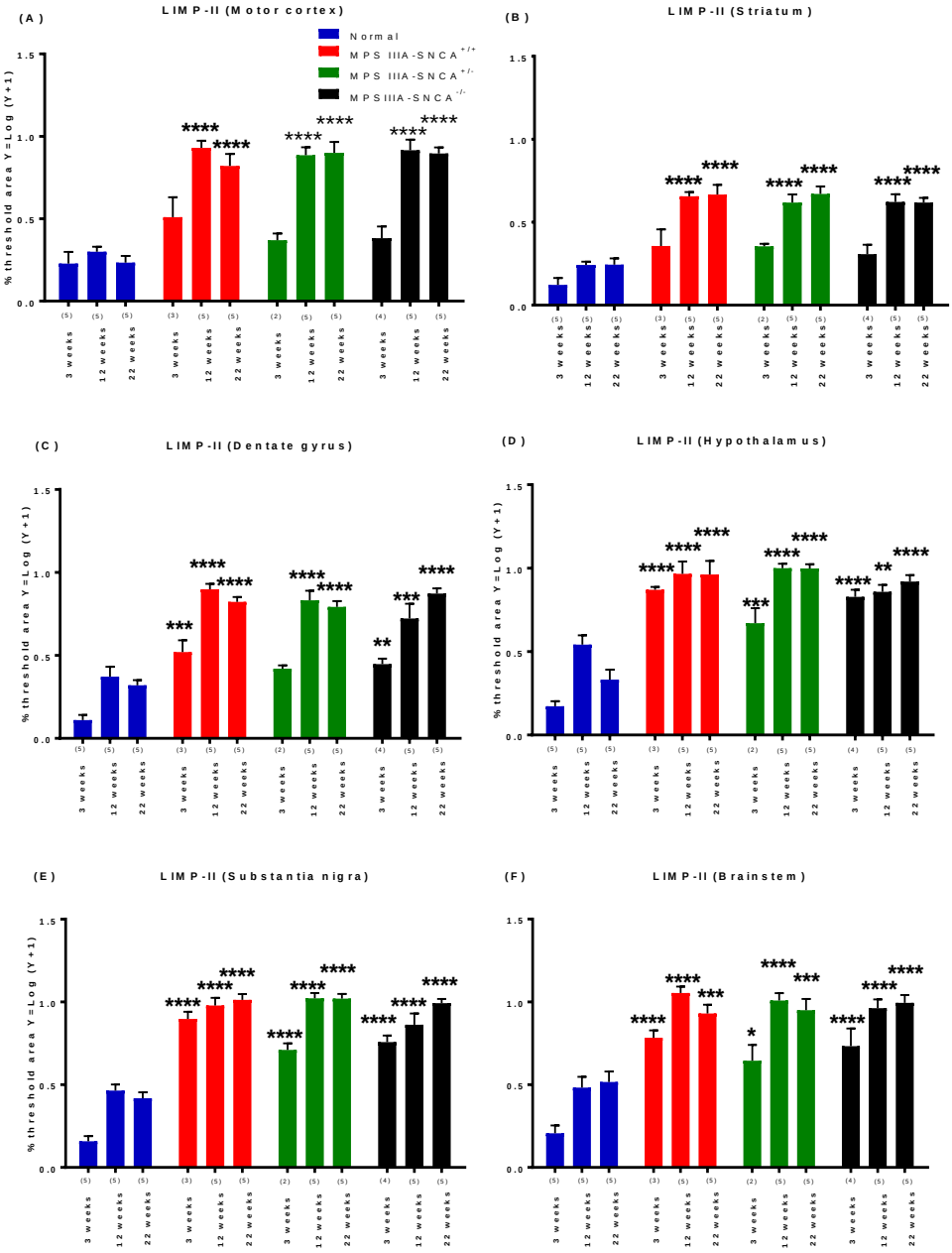

Figure 5.14. Quantification of the extent of lysosomal integral membrane protein II immunostaining in Normal, MPS IIIA-SNCA$^{+/+}$, MPS IIIA-SNCA$^{+/-}$, and MPS IIIA-SNCA$^{-/-}$ mice at three-, 12- and 22-weeks of age. Brain regions examined were: (A) motor cortex (M1); (B) striatum; (C) dentate gyrus; (D) hypothalamus; (E) substantia nigra; and (F) brainstem. Data are shown as mean ± SEM and * indicates a significant difference compared to the age-matched Normal group. A two-way ANOVA followed by post-hoc Bonferroni's multiple comparison test is used and *P < 0.05, **P < 0.01, ***P < 0.001, ****P < 0.0001. The number of animals involved is shown in brackets.

5.3 Discussion

The therapeutic potential of targeting *SNCA* to reduce its pathological burden in several synucleinopathies has been suggested. Previous studies show that knocking out the *SNCA* gene in Huntington's disease mice improved pathological features, such as decreased numbers of autophagosomes and amelioration of huntingtin inclusions (Corrochano et al., 2012; Tomás-Zapico et al., 2012).

Organomegaly, such as hepatosplenomegaly and bladder distension, is a primary clinical feature of many LSDs, and is an indicator the severity and stage of the disorder. Gastrointestinal pathology, such as increased weight of the stomach and duodenum was found in MPS IIIA mice (Roberts et al., 2009). MPS IIIA mice have also been reported to be significantly heavier than normal littermates, primarily due to organomegaly (Crawley et al., 2006). Similarly, the data presented here indicate that MPS IIIA mice were significantly heavier than Normal mice regardless of *SNCA* status; visceral organs and urinary bladder were also larger and distended in the MPS IIIA cohorts (personal observation).

To test the contribution of SNCA to the development and propagation of neuropathological lesions in MPS IIIA, brains from MPS IIIA mice with two copies ($SNCA^{+/+}$), one copy ($SNCA^{+/-}$) and complete absence ($SNCA^{-/-}$) of the *SNCA* gene were analysed. Normal littermates were used as controls, and tissues were evaluated biochemically and histologically at different stages of the disease. MPS IIIA-$SNCA^{+/-}$ and MPS IIIA-$SNCA^{-/-}$ mice showed comparable age-dependent accumulation of primary and secondary substrates, similar to MPS IIIA-$SNCA^{+/+}$ mice. In addition, disease progression in all three MPS IIIA cohorts was similar, as evidenced by elevations in protein markers or intense staining of several other pathological markers. Moreover, disruption of the *SNCA* gene did not affect dopamine content in MPS IIIA mice. Therefore, taken together, the results suggest that deficiency or absence of *SNCA* has not had an effect on MPS IIIA disease progression, at least with respect to the disease lesions evaluated here.

5.3.1 α-Synuclein has no effect on biochemical changes in MPS IIIA

Elevations in the levels of HS-derived disaccharides have been detected in the brain and other organs in both mixed strain and congenic MPS IIIA mice (Crawley et al., 2006; King et al., 2006). HS levels in MPS IIIA mouse brains were 40x normal at birth and plateaued at 100x

normal by 20-weeks of age (King et al., 2006; Trim et al., 2014). Granular, lipid-like substrates such as gangliosides (G_{M2} and G_{M3}) accumulate in storage vacuoles of MPS IIIA neuronal cells between eight- and 14-weeks of age (Bhaumik et al., 1999). Ganglioside deposition is believed to result from inhibition of ganglioside degradative enzymes by accumulated HS (McGlynn et al., 2004).

Here, progressive elevations in both HS and gangliosides was evident in all MPS IIIA mice from three- to 22-weeks of age regardless of *SNCA* status. Neurobehavioral signs and neuropathological changes in affected animals coincided with the increase in HS accumulation. Deletion or deficiency of *SNCA* did not have any impact on the primary and secondary substrate burden in both MPS IIIA-SNCA$^{+/-}$ and MPS IIIA-SNCA$^{-/-}$ mice.

Ganglioside accumulation is associated with disease severity, and inhibition of ganglioside synthesis has improved both pathological and clinical features even after neurological features are evident (Kaidonis et al., 2016). Moreover, lower ganglioside levels mediated a suppression of glial fibrillary acidic protein, interleukin-1β and other inflammatory gene expression (Kaidonis et al., 2016).

5.3.2 Absence of α-synuclein does not correct the lysosomal pathology and proteinaceous accumulation

Knockout of the *SNCA* gene in Huntington disease mice abrogated the pathological disease cascade ((Corrochano et al., 2012; Tomás-Zapico et al., 2012). To determine whether knockout of *SNCA* in MPS IIIA mice had the same effect, this study examined several disease lesion markers in fixed tissue. Histological markers such as ubiquitin and phosphorylated-tau (neurodegeneration markers), glial fibrillary acidic protein (astroglial marker) and lysosomal integral marker protein II (endo/lysosomal marker) were utilised for evaluation. The data showed no reduction in the expression of any of these histological markers in MPS IIIA mice (SNCA$^{+/+}$, SNCA$^{+/-}$ and SNCA$^{-/-}$) compared to Normal mice.

The increased number of ubiquitin inclusions indicates possible ubiquitin-proteasome system dysfunction or changes in the cellular ubiquitination structure in MPS IIIA mice (Ebrahimi-Fakhari et al., 2011). Abnormal number of ubiquitin inclusions have been recorded in the brains of multiple sulphatase deficiency and MPS IIIA mice (Settembre et al., 2008), MPS VI rats

(Higashi et al., 1993), MPS VII mice (Heuer et al., 2002), Niemann–Pick disease type C mice (Higashi et al., 1993), and Huntington's disease mice (Bennett et al., 2007), and human brain tissues from Alzheimer's and Parkinson's diseases, as well as other neurodegenerative disorders (Lowe et al., 1988). Each of these disorders exhibit protein accumulation and subsequent neurodegeneration due to defects in the ubiquitin-proteasome system as well as autophagy (Dennissen et al., 2012).

Impaired lysosomal autophagy can disrupt the continuous clearance of cytosolic proteins by the ubiquitin-proteasome system. Since the ubiquitin-proteasome system and lysosomal autophagy interact with each other, defects in lysosomal autophagy can also lead to the accumulation of polyubiquitinated proteins and neurodegeneration (Komatsu et al., 2006). Inhibition of autophagy by deleting autophagic genes Atg5 or Atg7 results in the accumulation of ubiquitinated proteins in mice (Hara et al., 2006; Komatsu et al., 2006).

The pathological presence of phosphorylated-tau inclusions, particularly in the brainstem, suggests neurodegeneration in MPS IIIA mice. Tau-positive inclusions and neurofibrillary tangles are detected not just in Alzheimer's disease but also in MPS IIIB mice (Ohmi et al., 2009) and Niemann-Pick type C mice (Walkley and Suzuki, 2004), further supporting lysosomal dysfunction as being a contributory factor in neurodegeneration. As tau accumulation has been shown as a result of inhibition of lysosomal autophagy (Hamano et al., 2008b), lysosomal dysfunction in MPS IIIA mice may be largely responsible for the deposition of tau.

5.3.3 Decreased levels of dopamine in MPS IIIA mice

The present data revealed a significant effect for Group in striatal dopamine content between MPS IIIA and Normal mice. All three groups of MPS IIIA mice showed 32%-34% (on average) loss in dopamine levels compared to Normal mice. *SNCA* gene deletion had little effect on dopamine content in MPS IIIA mice regardless of genotype status. These findings are consistent with a previous study in α-β-synuclein double knockout mice, which showed an 18% decrease in dopamine content in the brain, while single synuclein knockout mice did not show any abnormality (Chandra et al., 2004). It suggests a possible compensatory mechanism for the loss of one synuclein by another due to their similar molecular structures.

Since 20%-30% loss of striatal dopamine can produce a profound change in motor phenotypes in rodents (Gaugler et al., 2012), the hypoactivity and decreased path speed in MPS IIIA mice may be due to a deficiency in dopamine. Moreover, cognitive behaviour may be affected in dopamine-deficient MPS IIIA mice since dopamine is also important for complex task performance by frontal brain regions (Volkow et al., 1998). Therefore, reduced dopamine levels in the MPS IIIA mice in this study may be a cause of the significantly impaired motor function, hypoactivity and cognitive changes observed in the Open Field, Elevated Plus maze, Morris water maze, and gait tests.

Emerging evidence describes a possible link between LSDs and Parkinson's disease because heterozygous mutations in some LSD genes are risk factors for Parkinson's disease (Deng et al., 2015). G_{M1} and G_{M2} gangliosidosis, Gaucher disease, the neuronal ceroid lipofuscinoses and Fabry disease develop clinical and pathological features similar to Parkinson's disease, such as dopaminergic neuron death in the substantia nigra, striatal dopamine loss, and accumulation of *SNCA*, which lead to motor impairment, rigidity, bradykinesia, and rest tremor (Inzelberg and Korczyn, 1994; Nijssen et al., 2002; Buechner et al., 2006; Wu et al., 2011; Alcalay et al., 2014). Some of these parkinsonian signs can be relieved with levodopa, the standard treatment for Parkinson's disease (Nijssen et al., 2002; Buechner et al., 2006). Moreover, autophagosome numbers are increased in MPS IIIA, and there is reduced clearance of proteins and damaged organelles (Settembre et al., 2008). It is therefore likely that common cellular mechanisms exist between some LSD genes and Parkinson's disease that lead to similar disease pathology such as autophagy defects, down-regulation of the ubiquitin-proteasome system, altered calcium homeostasis and lipid metabolism, oxidative stress and mitochondrial dysfunction (Deng et al., 2015)

5.3.4 Conclusion

This study has shown that deletion of one or two copies of *SNCA* did not improve or worsen the existing MPS IIIA pathology or affect the disease course, suggesting that SNCA does not have a role in MPS IIIA pathology. Time-dependent primary and secondary substrate deposition due to SGSH deficiency was evident in MPS IIIA mice that lacked or reduced *SNCA*, along with lysosomal enlargement and astrogliosis. The pathological markers for protein inclusions and neuropathological changes were also present in MPS IIIA-*SNCA*$^{-/-}$ mice. A defect in autophagy may largely account for the accumulation of undegraded ubiquitin, phosphorylated-tau and other proteinaceous inclusions in the MPS IIIA mouse brain. Interestingly, striatal dopamine in all three MPS IIIA-SNCA groups studied in this study was lower than the Normal group, suggesting a possible link between lysosomal dysfunction and neurotransmitter abnormalities. Given that the data suggest a lack of *SNCA* involvement in MPS IIIA pathology, the nature and quantity of SNCA in congenic MPS IIIA brain was then investigated in Chapter (6).

Chapter (6)

Immunodetection of endogenous α-synuclein in MPS IIIA mice

6.1 Introduction

SNCA accumulation is evident in LSDs such as Gaucher disease, GM2 gangliosidosis, the MPS disorders, cathepsin D deficiency and multiple sulphatase deficiency (Shachar et al., 2011). Oligomeric/ aggregated forms of plasma SNCA were detected in Gaucher disease and several other LSDs by enzyme-linked immunosorbent assay (Pchelina et al., 2014). While healthy human brain contains monomeric SNCA only, the monomeric and larger oligomeric species (110–140 kDa globular proteins) are significantly increased in homozygous (β-glucocerebroside$^{-/-}$) and heterozygous (β-glucocerebroside$^{+/-}$) human Gaucher disease brains, as measured by SDS-PAGE/Western blot of primary cultures or induced pluripotent stem cell neurons (Mazzulli et al., 2011). *In vivo,* SNCA oligomers formed by mutant E57K and E35K are more toxic to dopaminergic neurones than fibrils (Winner et al., 2011; Rockenstein et al., 2014). Thus, lysosomal β-glucocerebrosidase deficiency may promote the formation of toxic oligomeric SNCA, which may play a role in Gaucher disease pathogenesis.

Immunohistological data suggest that wild-type SNCA starts to accumulate in MPS IIIA mouse brain as early as three-weeks of age and becomes widespread in all brain regions (Beard et al., unpublished). Deposition of phosphorylated SNCA, cell death and oxidative damage in human MPS IIIB and MPS II brains has also been documented in post mortem examination (Hamano et al., 2008a). Settembre et al. (2008) demonstrated a defect in autophagy in MPS IIIA, due to the failure of autophagosome-lysosome fusion, is seen in MPS IIIA and multiple sulphatase deficiency mouse brains and hypothesised that this leads to SNCA accumulation in affected embryonic fibroblast cells. However, it remains unknown as to whether the total amount of wild-type SNCA protein is elevated or whether the accumulated species of SNCA are oligomers in MPS IIIA mouse brain.

The aim of this preliminary study was to measure the total amount of SNCA and to distinguish its different forms in MPS IIIA and age-matched Normal and Heterozygous (SGSH$^{+/-}$) mouse brains. The level of endogenous wild-type SNCA in Normal, Heterozygous and MPS IIIA

mouse brains was quantified by immunoblotting, as described in **Chapter 2 (Section 2.2.11.3)**. Mouse brain homogenates from 17-week-old Normal, Heterozygous and MPS IIIA mice were analysed using two different SNCA antibodies that target different antigenic epitopes **(Fig 6.1)**. In addition, skin fibroblasts from Normal and MPS IIIA mice were grown in bovine cell culture medium with or without sucrose, and used to quantify SNCA **(Fig 6.1)**. The transferred polyvinylidene difluoride membranes were treated with 4% PFA mild fixation to avoid poor detection of SNCA species before being blocked by the addition of 5% skim milk powder, as described by Lee and Kamitani (2011).

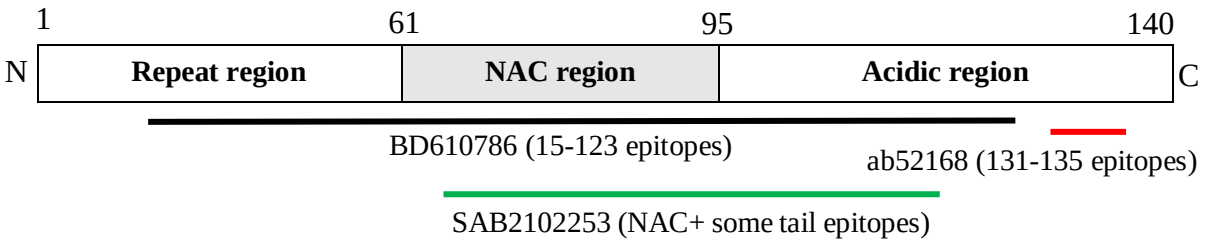

Figure 6.1. Diagram of components of SNCA and three different antibodies targeting specific antigenic epitopes within the protein. The BD610786 antibody targets the immunogenic location at 15-123 amino acids; the ab52168 antibody targets the α-synuclein C-terminal tail at 131-135 amino acids; and the SAB2102253 antibody targets the non-amyloid β component of Alzheimer's disease amyloid (NAC) region + some tail epitopes.

6.2 Results

6.2.1 α-Synuclein in mouse brain homogenates

To determine the total amount and structure of SNCA in brain homogenates of 17-week old MPS IIIA and Normal mice, brain homogenates were subjected to Western blotting using an anti-SNCA antibody that captures the C-terminal tail at 131-135 epitopes (ab52168). Increased levels of monomeric and tetrameric forms of SNCA were present in MPS IIIA compared to Normal mouse brain. An almost two-fold increase in both monomers (~14 kDa) and tetramers (~ 65 kDa) was detected in the MPS IIIA brain homogenate compared to Normal (**Fig 6.2 A, B)**.

In a subsequent experiment, supernatant (Triton-soluble, TS) and sediment (Triton-insoluble, TI) fractions of Normal, Heterozygous and MPS IIIA brains were obtained after high centrifugation at 16,000 g. The fractions were then exposed to an anti-SNCA antibody (SAB21022) that recognises the 'non-amyloid β component of Alzheimer's disease amyloid' and some parts of the C-terminal region of SNCA: almost two-times more SNCA was detected in TS.MPS IIIA than TS.Normal and TS.Heterozygous brains. Moreover, SNCA in the TI.MPS IIIA fraction was ~2.5- and ~1.5-times higher than in the TI.Normal and TI.Heterozygous fractions, respectively **(Fig 6.2 C, D)**. High molecular oligomeric or aggregated structures were not identified in MPS IIIA brain homogenates using either anti-SNCA antibody.

6.2.2 α-Synuclein in mouse skin fibroblasts

All the mouse skin fibroblast cell lysates in this experiment were kindly provided by Leanne Winner (Lysosomal Diseases Research Unit, South Australian Health and Medical Research Unit). Normal and MPS IIIA mouse skin fibroblasts were grown in the presence or absence of 100 mM sucrose (Section 2.2.11.2 for the details of the medium used) and the total amount of SNCA was quantified by immunoblot. Hence, four different types of skin fibroblasts were examined: (1) Normal cells grown in the non-sucrose cell medium; (2) MPS IIIA cells grown in the non-sucrose cell medium; (3) sucrose-treated Normal cells; and (4) sucrose-treated MPS IIIA cells. Skin fibroblasts were exposed to an anti-SNCA antibody (BD610786) that recognises immunogens spanning nearly the entire length of the protein.

SNCA monomeric protein was nearly five-fold higher in sucrose-treated Normal fibroblasts and MPS IIIA fibroblasts in the non-sucrose medium than Normal fibroblasts in the non-sucrose medium (**Fig 6.3 A, B)**. Therefore, sucrose-treated Normal fibroblasts showed a similar increase in SNCA to MPS IIIA cells in the non-sucrose medium. Interestingly, sucrose-treated MPS IIIA fibroblasts showed ~16-times more SNCA than Normal cells in the non-sucrose medium. Moreover, there was ~three-times more SNCA in sucrose-treated MPS IIIA fibroblasts than sucrose-treated Normal and MPS IIIA cells in the non-sucrose medium. To rule out detection of non-specific bands in the gels, only secondary donkey anti-mouse biotinylated antibody was used. Bands at ~55 kDa and 70 kDa were formed by the secondary antibody unrelated to SNCA species **(Fig 6.3 C)**.

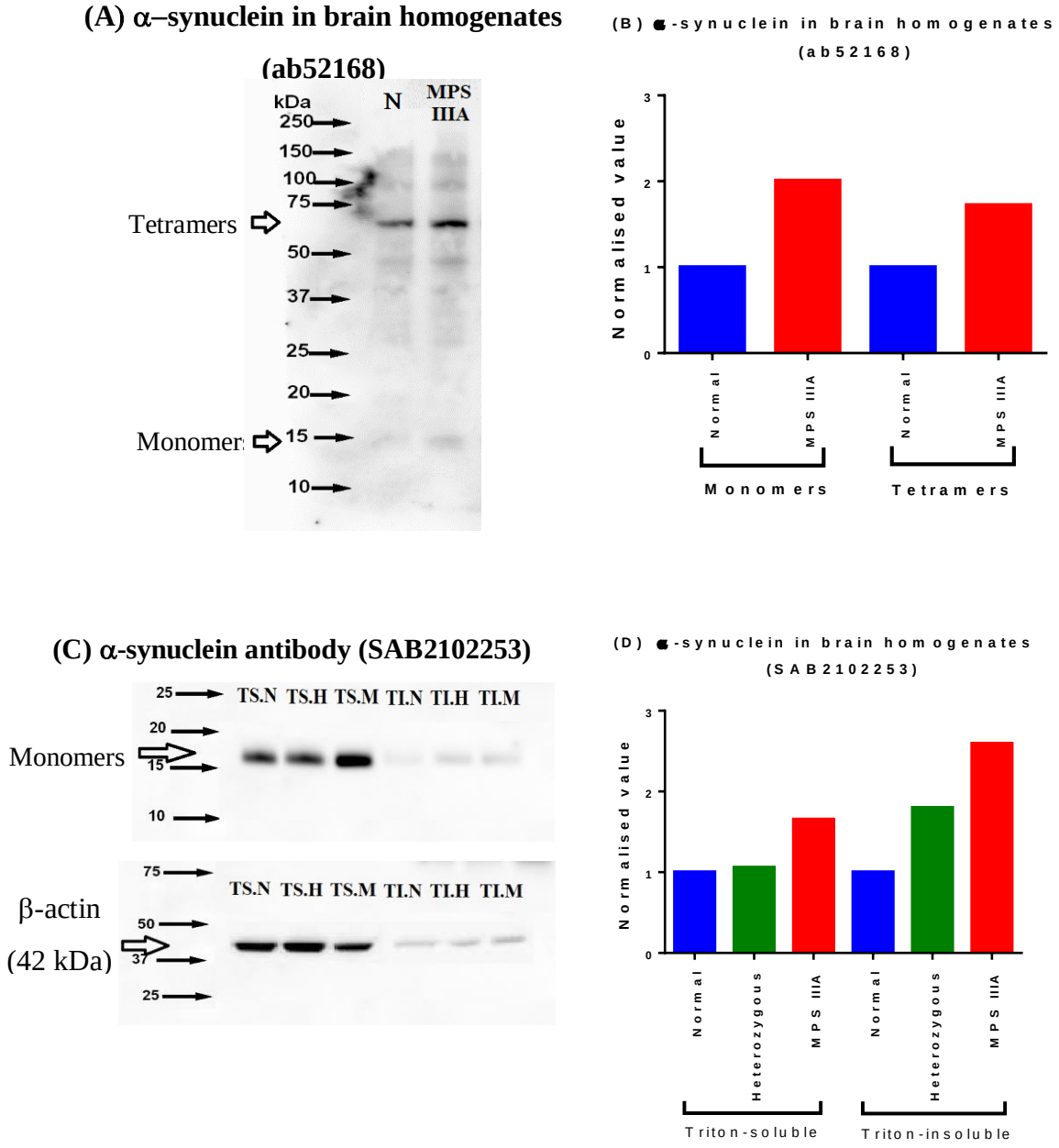

Figure 6.2. Immunoblot analysis of endogenous SNCA in mouse brain homogenates at 17-weeks of age: (A) monomeric and tetrameric forms in Normal (N) and MPS IIIA mice (with antibody ab52168); (B) the normalised ratio of the monomer and tetramer signal; (C) monomeric forms in Normal (N), Heterozygous (H) and MPS IIIA (M) mice (with antibody SAB2102253). β-Actin is a loading control, and (D) the normalised ratio of the monomer signal to β-actin. TS = Triton-soluble, TI = Triton-insoluble. Normalised ratio to β-actin.

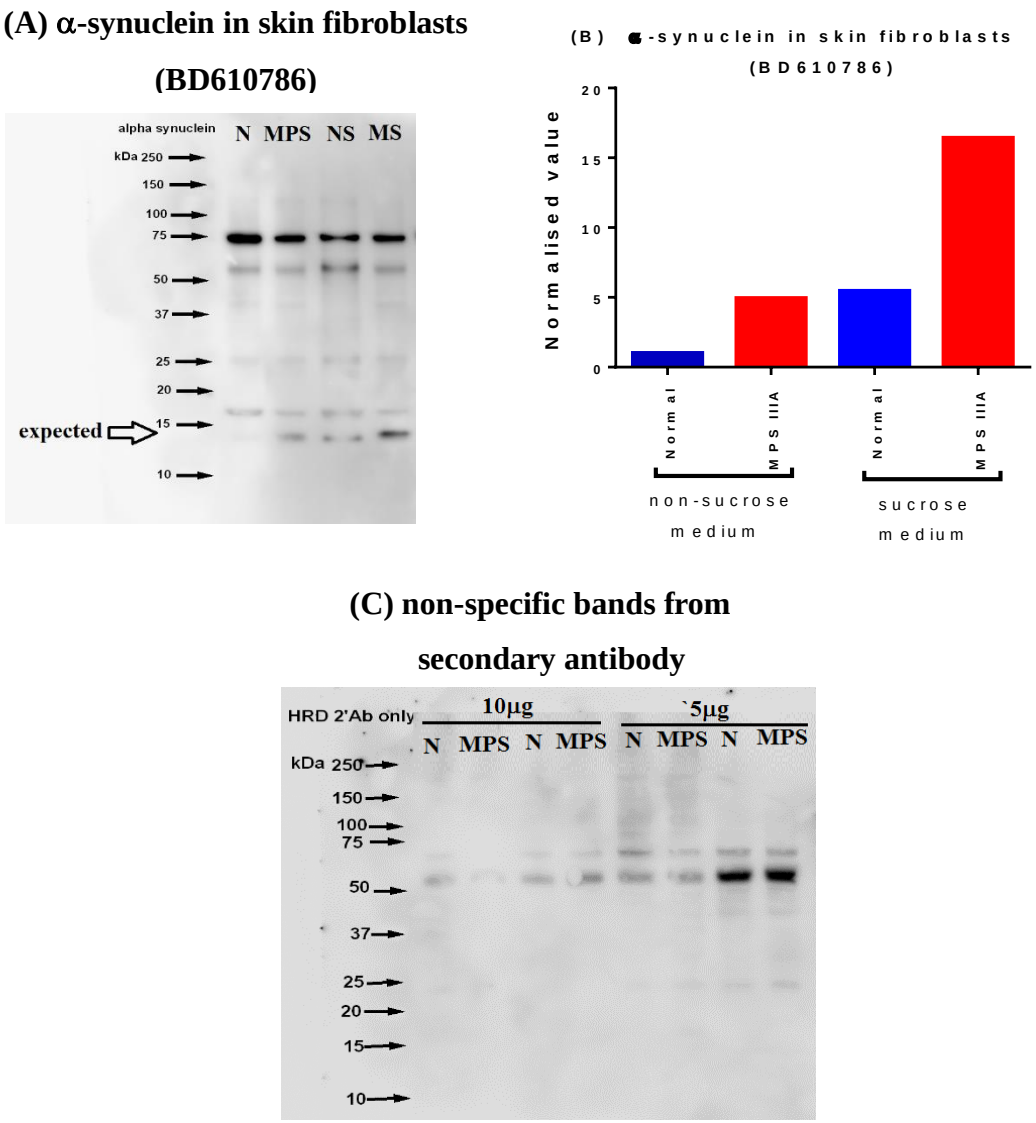

Figure 6.3. Immunoblot analysis of SNCA in mouse skin fibroblast lysates: (A) 14 kDa monomeric forms in Normal fibroblasts grown in the non-sucrose medium (N); MPS IIIA fibroblasts grown in the non-sucrose medium (MPS); sucrose-treated Normal fibroblasts (NS); and sucrose-treated MPS IIIA fibroblasts (MS) (with antibody BD610786); (B) the normalised ratio of the monomeric signal. (C) Non-specific background bands (~55 kDa and 70 kDa) seen in mouse brain homogenates (N= Normal, MPS= MPS IIIA) with secondary antibody only (biotinylated donkey anti-mouse).

6.3 Discussion

6.3.1 Increased level of α-synuclein in MPS IIIA brain

These data demonstrated that SGSH deficiency in MPS IIIA leads to increased accumulation of SNCA in its native monomer and tetramer forms. SNCA is primarily a tetramer with less propensity to aggregate in physiological conditions (Bartels et al., 2011). A state of dynamic equilibrium exists between SNCA's helical tetramers and unfolded monomers, and aberrations in this balance cause insoluble fibril formation from monomers (Selkoe et al., 2014). Mutations in Parkinson's disease (A30P, E46K, and A53T) can significantly change the equilibrium by shifting stable tetramers towards aggregate-prone toxic monomers (Wang et al., 2011).

Studies have shown that both the ubiquitin-proteasome system and lysosomal autophagy are responsible for degradation of wild-type SNCA in neural cells (Webb et al., 2003; Vogiatzi et al., 2008). Therefore, abnormal accumulation of SNCA and other aggregate-prone proteins in MPS IIIA might be associated with alterations in these pathways. Moreover, failure of autophagosome-lysosome fusion is the primary cause of accumulation of aggregate-prone autophagy substrates such as SNCA in MPS IIIA skin fibroblasts and macrophage cells (Settembre et al., 2008). Induction of autophagy by beclin 1 and rapamycin reduces SNCA accumulation, and neuritic and synaptic pathology in transgenic mice (Spencer et al., 2009).

6.3.2 Increased level of α-synuclein in MPS IIIA cells

Normal fibroblasts can replicate the nature of LSDs when exposed to sucrose culture medium (Isaac et al., 2000). Lysosomal storage occurs when skin fibroblasts rapidly absorb and store sucrose from the medium but fail to degrade the sugar due to the absence of invertase (Isaac et al., 2000). Loss of β-glucocerebrosidase activity in cell culture has been shown to compromise lysosomal protein degradation and result in the accumulation of SNCA, leading to neurotoxicity in an aggregation-dependent manner (Mazzulli et al., 2011). In the present study, lysosomal dysfunction in sucrose-treated Normal fibroblasts and MPS IIIA fibroblasts with or without sucrose medium led to an increase in the total amount of SNCA. Therefore, there is a direct correlation between lysosomal dysfunction and SNCA accumulation.

Cell lines containing sucrose medium show increases in storage vacuoles, lysosomal proteins and mRNA expression such as lysosome-associated membrane proteins-1 and -2, and mannose-6-phosphate receptors (Karageorgos et al., 1997). The addition of invertase to correct the cell storage pathology returned lysosomal proteins and mRNA to basal levels (Karageorgos et al., 1997). The increased amount of SNCA protein in sucrose-treated Normal and MPS IIIA fibroblasts with or without sucrose medium may partially be regulated at the mRNA level. Indeed, SNCA mRNA expression in the MPS IIIA mouse brain was almost two-times higher than in Normal mice (Arfi et al., 2011). Therefore, lysosomal proteinopathy may also be a complex, integrated process controlled at, or after, the level of transcription. However, mechanisms behind SNCA mRNA over-expression remain poorly understood.

Interestingly, sucrose-treated MPS IIIA fibroblasts accumulated nearly three-times more SNCA than sucrose-treated Normal cells or MPS IIIA cells in the non-sucrose medium. The additional overload of sucrose may have worsened any existing lysosomal-impaired autophagy and led to the subsequent accumulation of excessive protein in MPS IIIA fibroblasts. This indicates that the protein-degrading function in the latter two cell lines (sucrose-treated Normal cells and MPS IIIA cells in the non-sucrose medium) may be less impaired than in sucrose-treated MPS IIIA cells. The MPS IIIA cells used here were derived from congenic MPS IIIA mice (Bhattacharyya et al., 2001), which have 3% residual SGSH activity, so this finding may possibly reflect the activity of SGSH.

6.4 Conclusion

The present data suggest that normal/ native SNCA, rather than aggregated forms, accumulates in MPS IIIA tissues and cells, due possibly to inefficient autophagy and/or an impaired ubiquitin-proteasome system. Only one animal per genotype was used in this pilot study, and the limitation of samples prohibited statistical analysis. Further investigation is required to investigate the pathological basis of changes in MPS IIIA gene expression, including SNCA.

Chapter (7)
Conclusions and Future Work

7.1 Introduction

Mucopolysaccharidosis type IIIA (MPS IIIA or Sanfilippo syndrome type A) is a severe and debilitating neurodegenerative LSD resulting from mutations in the *SGSH* gene encoding the lysosomal enzyme SGSH, which is involved in the degradation of HS (Muenzer, 2011). As a result of low or absent SGSH activity, HS accumulates within cells and compromises cellular function. MPS IIIA patients exhibit progressive mental decline and die in their mid-late teens as there is no safe and effective treatment available for this condition (Neufeld and Muenzer, 2001). We are hampered by the lack of knowledge about the biological basis of neurodegeneration in this disorder.

A well-characterised and studied MPS IIIA murine model that has a D31N mutation in the *SGSH* gene was used in this study because it replicates the pathological and clinical features seen in the human disorder. It is unknown whether HS or secondary deposition of gangliosides or accumulation of neuronal proteins, neuroinflammation, or oxidative stress underlie the disease pathology and symptoms. Our laboratory has recently demonstrated early-localised accumulation of SNCA followed closely by ubiquitin, phosphorylated tau and amyloid precursor protein in the brains of MPS IIIA mice. Post-mortem examination of human MPS III brains confirmed SNCA accumulation (Hamano et al., 2008a).

The physiological function of SNCA in neuronal and other cell types and its pathological involvement in neurodegenerative disorders remains poorly understood. SNCA aggregates or inclusions in neurons have long been recognised as pathognomonic signs in Parkinson's disease, dementia with Lewy bodies and other synucleinopathies (Spillantini et al., 1997; Devine et al., 2011). It has also been shown that toxic oligomers of SNCA can accumulate in non-neuronal cells when the lysosomal degradation pathway is blocked (Lee et al., 2004).

The hypothesis for this study was that deletion of the *SNCA* gene in MPS IIIA mice would reduce the 'load' on protein catabolism mechanisms and thus delay or ameliorate the behavioural deficits and pathological features of the disorder. More importantly, understanding the pathological pathways operating in this single gene disorder may help explain cellular mechanisms that underpin more complex neurodegenerative disorders such as Parkinson's, Alzheimer's and Huntington's diseases, as lysosomal dysfunction has also been implicated in their pathogenesis (Zhang et al., 2009). Therefore, this study aimed to evaluate the ramification of *SNCA* knockout in MPS IIIA mice compared to MPS IIIA mice with one to two copies of the *SNCA* gene and normal control mice.

7.2 Summary

SNCA knockout ($SNCA^{-/-}$) mice were successfully paired with MPS IIIA mice to produce a colony with four different genotypes required for experiments. There are no difference in fertility, overall viability, morbidity, premature mortality or particular facial phenotypes in the $SNCA^{-/-}$ mice. The knockout mice were crossed with MPS IIIA mice to produce Normal control, MPS IIIA-$SNCA^{+/+}$, MPS IIIA-$SNCA^{+/-}$ or MPS IIIA-$SNCA^{-/-}$ mice. The three MPS IIIA-SNCA genotypes showed a significant number of unsuccessful pregnancies, aggressiveness towards cage mates and characteristic facial features as seen in congenic MPS IIIA mice.

In addition to the characterisation of mice, parameters studied included standard behavioural testing, and histopathological and biochemical testing to differentiate the role of *SNCA* in disease pathology. MPS IIIA mice, regardless of *SNCA* genotype, showed significantly increased food intake when compared with Normal littermates, suggesting either an increased energy requirement for the synthesis of raw materials or dysregulation of the brain's appetite and satiety centre. MPS IIIA-$SNCA^{-/-}$ mice were significantly hypoactive in several tests of performance, but were comparable to MPS IIIA-$SNCA^{+/+}$ mice, as shown by reduced square entries, travel length, and speed in behavioural testing. Interestingly, MPS IIIA-$SNCA^{-/-}$ spent a significantly lower percentage of time moving in the Open Field test, and entry to both the closed arms and central area in the Elevated Plus maze was considerably less than the other groups of mice. The MPS IIIA-$SNCA^{-/-}$ mice were slow swimmers and unable to learn as quickly as Normal littermates in the Morris water maze, however these findings were similar to the other MPS IIIA groups in this study. This may relate to striatal dopamine levels, which showed a downward trend in all three MPS IIIA groups, compared to Normal mice.

As anticipated, HS concentration increased with age in all three MPS IIIA groups irrespective of *SNCA* gene status. This increase coincided with apparent neurobehavioral and neuropathological changes in these animals. Moreover, increased levels of gangliosides (G_{M2} and G_{M3}) were present in all three MPS IIIA groups as early as three-weeks of age. There is a strong evidence of the pathological role of gangliosides in MPS IIIA (Walkley, 2004; Kaidonis et al., 2016), however changes in *SNCA* genotype did not affect ganglioside storage.

Histologically, the level of markers of proteinaceous inclusions containing ubiquitin or phosphorylated tau remained unchanged indicating that deficiency or deletion of *SNCA* did not alleviate the MPS IIIA proteinopathy. Intense staining of lysosomal integral membrane protein II and expression of glial fibrillary acidic protein was not different between the three groups of MPS IIIA mice as expected, suggesting that accumulation of SNCA is uncoupled from lysosomal expansion and neuroinflammation, respectively. Finally, preliminary immunoblot data demonstrated increased SNCA monomers and tetramers in MPS IIIA brain homogenates and skin fibroblasts compared to age-matched healthy counterparts. However, pathological oligomeric forms of SNCA were not detected at any time, despite use of antibodies targeting different immunogens. A schema showing the cascade of changes is described in **Fig 7.1**.

These findings contradict those obtained in Huntington's disease mice where deletion of *SNCA* ameliorated the pathological features and improved the functional outcomes, including the overall survival rate, the onset of tremor and weight loss in Huntington's disease mice (Corrochano et al., 2012; Tomás-Zapico et al., 2012). Murine models of Huntington's disease exhibit mutant aggregated SNCA compared to wild-type forms in MPS IIIA mice. Thus, Huntington disease-SNCA$^{-/-}$ mice benefited from the removal of SNCA by reducing the 'load' on mutant protein degradation systems. However, MPS IIIA mice did not appear to benefit from deletion of *SNCA*, potentially because of the nature or state of SNCA that accumulates but does not initiate the accumulation of other proteins in cells.

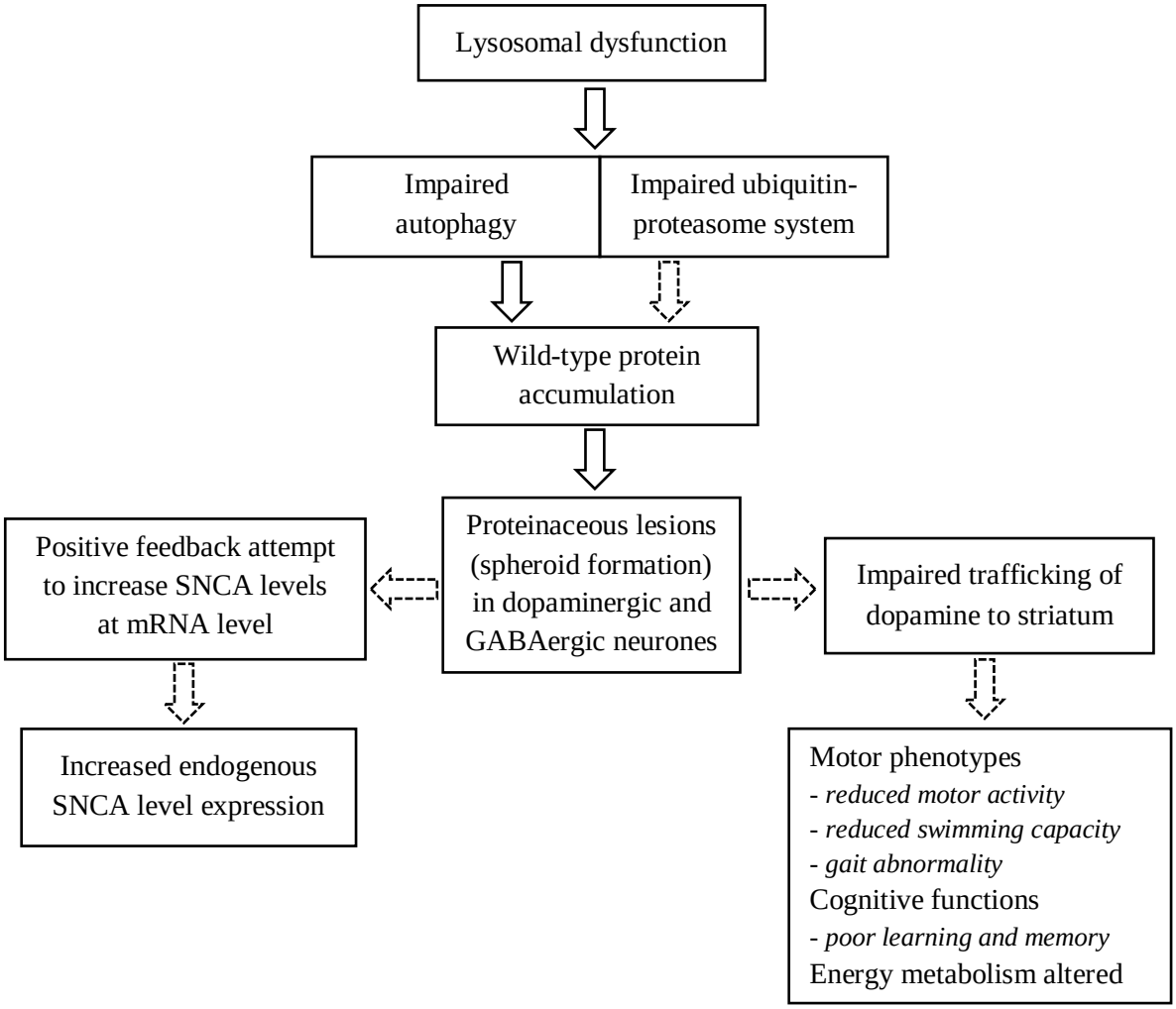

Figure 7.1. Schema depicting the cascade of (possible) changes in MPS IIIA murine model. The lysosomal storage in MPS IIIA impairs the autophagy and possibly the ubiquitin-proteasome system, resulting in an accumulation of undegraded wild-type proteins (eg., SNCA). The proteinaceous lesions can be observed as spheroid formation in neurones, especially in dopaminergic and GABAergic neurones in the MPS IIIA brain (Hassiotis et al.,unpublished). Potential disruption of dopamine trafficking may affect motor phenotypes (hypoactivity, reduced path length, swimming speed, and gait abnormality in a series of behavioural tests), cognitive dysfunction (spatial learning and memory in Morris water maze test) and altered energy metabolism in MPS IIIA mice. Moreover, a positive feedback may exist to attempt to increase endogenous SNCA expression in striatum and elsewhere in the MPS IIIA brain.

7.3 Conclusions and Implications

This is the first study investigating the pathological role of SNCA deposition in the brains of MPS IIIA mice. Disruption of the *SNCA* gene did not ameliorate the behavioural changes that have been reported to occur in previous studies in MPS IIIA mice. We observed a similar level of substrate deposition and subsequent pathological and clinical disease progression in MPS IIIA-SNCA$^{-/-}$ mice and the other groups of MPS IIIA mice in this study. Therefore, there appears to be no correlation between SNCA accumulation and clinical disease progression in MPS IIIA. However, a possible functional link may exist between the accumulation of proteinaceous lesions in MPS IIIA and motor phenotypes, and decreased axonal transport of dopamine and subsequent reduction in striatal dopamine levels may underline the motor phenotype **(Fig 7.1)**.

Moreover, undegraded SNCA in its physiological forms, rather than its pathogenic oligomeric structures, was elevated in congenic MPS IIIA mouse tissues. Studies have also shown that impaired autophagy compromises the ubiquitin-proteasome system pathway by obstructing and delaying the transfer of ubiquitinated substrates to the proteasomes (Korolchuk et al., 2009; Qiao and Zhang, 2009). Therefore, autophagy impairment may be responsible for the accumulation of both autophagy- and proteasome-dependent proteins. This may explain why SNCA accumulation in MPS IIIA mouse brain is not a primary pathological feature but rather a downstream secondary event, possibly due to disruption of both autophagic and ubiquitin-proteasome system pathways.

This finding may have implications for future therapeutic strategies to target and enhance the cellular degradation pathways to counteract accumulated proteinaceous inclusions. MPS IIIA-SNCA$^{-/-}$ mice exhibited SNCA-independent proteinopathy and neurodegeneration, and it is an excellent model for the study of novel therapeutics and pathological mechanisms for not only MPS IIIA but other LSDs and other neurodegenerative disorders.

7.4 Future directions

The cellular mechanism for protein clearance relies on two systems: autophagy and the ubiquitin-proteasome system. Autophagy and potentially, the ubiquitin-proteasome system are dysfunctional in MPS IIIA, which results in the accumulation of many undegraded proteins in affected brains. The present study shows that the absence of a single protein (SNCA) does not change disease progression in MPS IIIA. The basis for autophagy dysfunction has been proposed (Settembre et al., 2008), however impairments in the ubiquitin-proteasome system in MPS IIIA deserve further attention.

Soluble N-ethyl-maleimide-sensitive factor attachment protein (SNAP) receptors (SNAREs) mediate the trafficking of lysosomal proteins and fusion of cellular membranes (Settembre et al., 2013). The defect in autophagosome-lysosome fusion results in autophagy dysfunction in many LSDs (Settembre et al., 2008). It has also been shown that abnormal cholesterol deposition in LSDs impairs the lysosomal membrane fusion machinery by perturbing SNAREs, which eventually leads to an endocytic traffic jam and lysosomal dysfunction (Fraldi et al., 2010). Therefore, maintaining low levels of cholesterol or restoring the normal function of SNARE complexes may improve lysosomal trafficking, fusion machinery, and overall lysosomal function.

It has been shown that autophagy and the ubiquitin-proteasome system are compensatory interacting systems, and a 'rescue role' of autophagy in protein degradation in the presence of proteasome impairment has been demonstrated (Ebrahimi-Fakhari et al., 2011). The finding that the ubiquitin-proteasome system may remain functional in autophagy-impaired multiple sulphatase deficiency raises the possibility of pharmacological induction of the ubiquitin-proteasome system pathway to compensate for autophagy deficiency as a new therapeutic approach for LSDs.

Both ubiquitin-proteasome system and lysosomal autophagy are responsible for the degradation of SNCA (Ebrahimi-Fakhari et al., 2011). Exogenous recombinant preformed α-syn fibrils could act as a seed and recruit endogenous soluble SNCA, forming insoluble inclusions in cells overexpressing SNCA, leading to synaptic dysfunction and neuronal death (Volpicelli-Daley et al., 2011). Whether increased levels of SNCA cause additional lysosomal damage by compromising one or both protein degradation systems is an interesting question. Therefore,

over-expression of SNCA may give more information and understanding about the pathological role of α-synuclein and lysosomal dysfunction in the MPS IIIA mouse model.

MPS IIIA mice were found to be in an "energy hungry" state with increased food intake observed, possibly due to impaired lysosomal recycling of raw materials such as glycosaminoglycans. Woloszynek et al. (2009) showed that a simple sugar and high fat diet to maintain glycosaminoglycan synthesis modestly improved body weight and lysosomal autophagy in MPS I and MPS VII mice. Therefore, a targeted nutrient diet scheme as an adjunct therapy may be beneficial for better cell energy utilisation. Increased food intake by MPS IIIA mice may also indicate abnormal HS deposition in the central anti-satiety centre or gastrointestinal pathology (Reizes et al., 2001; Roberts et al., 2009). Inhibition of glycosaminoglycan synthesis with rhodamine B treatment improved body weight gain and substrate storage in MPS VI and MPS IIIA mice (Roberts et al., 2006). Therefore, a combination of substrate reduction therapy and diet modification may be beneficial for LSDs. Moreover, the role of aberrant neurotransmission as a basis for satiety dysfunction also deserves further study.

Finally, the amount of striatal dopamine was significantly decreased in MPS IIIA mice, compared to control mice, regardless of the *SNCA* genotype. Motor neurological symptoms in MPS IIIA mice may result from abnormal levels of dopamine. In future studies, it will be important to examine dopaminergic systems when evaluating a therapeutic approach, in order to determine the importance of this observation and its potential contribution to the motor symptoms.

In conclusion, this study found that deletion of the *SNCA* gene in MPS IIIA mice did not significantly influence the clinical and pathological progression associated with MPS IIIA. Accumulation of SNCA is presumably one of the secondary manifestations of a defect in autophagy or ubiquitin-proteasome system dysfunction. The data presented in this thesis have expanded our understanding of the murine MPS IIIA phenotype and its pathological mechanisms. Given these observations, stimulating autophagy and/or the ubiquitin-proteasome system may be a potential therapeutic target for MPS IIIA, other LSD, and lysosome-dependent neurodegenerative disorders. Finally, lysosomes have more complex functions and roles in cells than simply being garbage disposers, and the growing understanding of the lysosomal

degradation system may help explain the pathogenesis of many neurological conditions in the future.

Bibliography

Abeliovich, A., Schmitz, Y., Farinas, I., Choi-Lundberg, D., Ho, W. H., Castillo, P. E., Shinsky, N., Verdugo, J. M., Armanini, M., Ryan, A., Hynes, M., Phillips, H., Sulzer, D. & Rosenthal, A. 2000. Mice lacking alpha-synuclein display functional deficits in the nigrostriatal dopamine system. *Neuron,* 25**,** 239-52.

Al-Wandi, A., Ninkina, N., Millership, S., Williamson, S. J., Jones, P. A. & Buchman, V. L. 2010. Absence of α-synuclein affects dopamine metabolism and synaptic markers in the striatum of aging mice. *Neurobiology of Aging,* 31**,** 796-804.

Albano, L. M., Sugayama, S. S., Bertola, D. R., Andrade, C. E., Utagawa, C. Y., Puppi, F., Nader, H. B., Toma, L., Coelho, J. & Leistner, S. 2000. Clinical and laboratorial study of 19 cases of mucopolysaccharidoses. *Revista do Hospital das clínicas,* 55**,** 213-218.

Alcalay, R., Caccappolo, E., Mejia-Santana, H., Tang, M.-X., Rosado, L., Reilly, M. O., Ruiz, D., Ross, B., Verbitsky, M. & Kisselev, S. 2012. Cognitive performance of GBA mutation carriers with early-onset PD The CORE-PD study. *Neurology,* 78**,** 1434-1440.

Alcalay, R. N., Dinur, T., Quinn, T., Sakanaka, K., Levy, O., Waters, C., Fahn, S., Dorovski, T., Chung, W. K. & Pauciulo, M. 2014. Comparison of Parkinson risk in Ashkenazi Jewish patients with Gaucher disease and GBA heterozygotes. *JAMA neurology,* 71**,** 752-757.

Alvarez-Erviti, L., Rodriguez-Oroz, M. C., Cooper, J. M., Caballero, C., Ferrer, I., Obeso, J. A. & Schapira, A. H. 2010. Chaperone-mediated autophagy markers in Parkinson disease brains. *Archives of Neurology,* 67**,** 1464-1472.

Anderson, J. P., Walker, D. E., Goldstein, J. M., De Laat, R., Banducci, K., Caccavello, R. J., Barbour, R., Huang, J., Kling, K. & Lee, M. 2006. Phosphorylation of Ser-129 is the dominant pathological modification of α-synuclein in familial and sporadic Lewy body disease. *Journal of Biological Chemistry,* 281**,** 29739-29752.

Appel‐Cresswell, S., Vilarino‐Guell, C., Encarnacion, M., Sherman, H., Yu, I., Shah, B., Weir, D., Thompson, C., Szu‐Tu, C. & Trinh, J. 2013. Alpha‐synuclein p. H50Q, a novel pathogenic mutation for Parkinson's disease. *Movement Disorders,* 28**,** 811-813.

Appelqvist, H., Wäster, P., Kågedal, K. & Öllinger, K. 2013. The lysosome: from waste bag to potential therapeutic target. *Journal of Molecular Cell Biology,* 5**,** 214-226.

Arfi, A., Richard, M., Gandolphe, C., Bonnefont-Rousselot, D., Thérond, P. & Scherman, D. 2011. Neuroinflammatory and oxidative stress phenomena in MPS IIIA mouse model: the positive effect of long-term aspirin treatment. *Molecular Genetics and Metabolism,* 103**,** 18-25.

Ausseil, J., Desmaris, N., Bigou, S., Attali, R., Corbineau, S., Vitry, S., Parent, M., Cheillan, D., Fuller, M. & Maire, I. 2008. Early neurodegeneration progresses independently of microglial activation by heparan sulfate in the brain of mucopolysaccharidosis IIIB mice. *PloS One,* 3**,** e2296.

Baehner, F., Schmiedeskamp, C., Krummenauer, F., Miebach, E., Bajbouj, M., Whybra, C., Kohlschütter, A., Kampmann, C. & Beck, M. 2005. Cumulative incidence rates of the mucopolysaccharidoses in Germany. *Journal of Inherited Metabolic Disease,* 28**,** 1011-1017.

Bartels, T., Choi, J. G. & Selkoe, D. J. 2011. [agr]-Synuclein occurs physiologically as a helically folded tetramer that resists aggregation. *Nature,* 477**,** 107-110.

Bendor, J. T., Logan, T. P. & Edwards, R. H. 2013. The function of α-synuclein. *Neuron,* 79**,** 1044-1066.

Bennett, E. J., Shaler, T. A., Woodman, B., Ryu, K.-Y., Zaitseva, T. S., Becker, C. H., Bates, G. P., Schulman, H. & Kopito, R. R. 2007. Global changes to the ubiquitin system in Huntington's disease. *Nature,* 448**,** 704-708.

Bennett, M. C., Bishop, J. F., Leng, Y., Chock, P. B., Chase, T. N. & Mouradian, M. M. 1999. Degradation of α-synuclein by proteasome. *Journal of Biological Chemistry,* 274**,** 33855-33858.

Beyer, K., Domingo-Sàbat, M., Humbert, J., Carrato, C., Ferrer, I. & Ariza, A. 2008. Differential expression of alpha-synuclein, parkin, and synphilin-1 isoforms in Lewy body disease. *Neurogenetics,* 9**,** 163-172.

Beyer, K., Humbert, J., Ferrer, A., Lao, J. I., Carrato, C., López, D., Ferrer, I. & Ariza, A. 2006. Low alpha-synuclein 126 mRNA levels in dementia with Lewy bodies and Alzheimer disease. *Neuroreport,* 17**,** 1327-1330.

Beyer, K., Lao, J., Carrato, C., Mate, J., Lopez, D., Ferrer, I. & Ariza, A. 2004. Differential expression of α - synuclein isoforms in dementia with Lewy bodies. *Neuropathology and Applied Neurobiology,* 30**,** 601-607.

Bhattacharyya, R., Gliddon, B., Beccari, T., Hopwood, J. J. & Stanley, P. 2001. A novel missense mutation in lysosomal sulfamidase is the basis of MPS III A in a spontaneous mouse mutant. *Glycobiology,* 11**,** 99-103.

Bhaumik, M., Muller, V. J., Rozaklis, T., Johnson, L., Dobrenis, K., Bhattacharyya, R., Wurzelmann, S., Finamore, P., Hopwood, J. J., Walkley, S. U. & Stanley, P. 1999. A mouse model for mucopolysaccharidosis type III A (Sanfilippo syndrome). *Glycobiology,* 9**,** 1389-96.

Blumenfeld-Katzir, T., Pasternak, O., Dagan, M. & Assaf, Y. 2011. Diffusion MRI of structural brain plasticity induced by a learning and memory task. *PloS One,* 6**,** e20678.

Boelens, J. J., Prasad, V. K., Tolar, J., Wynn, R. F. & Peters, C. 2010. Current international perspectives on hematopoietic stem cell transplantation for inherited metabolic disorders. *Pediatric Clinics of North America,* 57**,** 123-145.

Bouwknecht, J. A. & Paylor, R. 2002. Behavioral and physiological mouse assays for anxiety: a survey in nine mouse strains. *Behavioural Brain Research,* 136**,** 489-501.

Brailsford, J. F. 1929. Chondro-osteo-dystrophy: Roentgenographic & clinical features of a child with dislocation of vertebrae. *The American Journal of Surgery,* 7**,** 404-410.

Brion, J. P., Couck, A., Passareiro, E. & Flament-Durand, J. 1985. Neurofibrillary tangles of Alzheimer's disease: an immunohistochemical study. *Journal of Submicroscopic Cytology,* 17**,** 89-96.

Bruening, W., Giasson, B. I., Klein‐Szanto, A. J., Lee, V. M. Y., Trojanowski, J. Q. & Godwin, A. K. 2000. Synucleins are expressed in the majority of breast and ovarian carcinomas and in preneoplastic lesions of the ovary. *Cancer,* 88**,** 2154-2163.

Buddhala, C., Loftin, S. K., Kuley, B. M., Cairns, N. J., Campbell, M. C., Perlmutter, J. S. & Kotzbauer, P. T. 2015. Dopaminergic, serotonergic, and noradrenergic deficits in Parkinson disease. *Annals of clinical and translational neurology,* 2**,** 949-959.

Buechner, S., De Cristofaro, M. T. R., Ramat, S. & Borsini, W. 2006. Parkinsonism and Anderson Fabry's disease: a case report. *Movement Disorders,* 21**,** 103-107.

Burkholder, T., Foltz, C., Karlsson, E., Linton, C. G. & Smith, J. M. 2012. Health evaluation of experimental laboratory mice. *Current Protocols in Mouse Biology***,** 145-165.

Burman, C. & Ktistakis, N. T. Autophagosome formation in mammalian cells. Seminars in Immunopathology, 2010. Springer, 397-413.

Cabin, D. E., Shimazu, K., Murphy, D., Cole, N. B., Gottschalk, W., Mcilwain, K. L., Orrison, B., Chen, A., Ellis, C. E. & Paylor, R. 2002. Synaptic vesicle depletion correlates with attenuated synaptic responses to prolonged repetitive stimulation in mice lacking α-synuclein. *The Journal of neuroscience,* 22**,** 8797-8807.

Chandra, S., Fornai, F., Kwon, H.-B., Yazdani, U., Atasoy, D., Liu, X., Hammer, R. E., Battaglia, G., German, D. C. & Castillo, P. E. 2004. Double-knockout mice for α-and β-synucleins: effect on synaptic functions. *Proceedings of the National Academy of Sciences of the United States of America,* 101**,** 14966-14971.

Chandra, S., Gallardo, G., Fernández-Chacón, R., Schlüter, O. M. & Südhof, T. C. 2005. α-Synuclein cooperates with CSPα in preventing neurodegeneration. *Cell,* 123**,** 383-396.

Chartier-Harlin, M.-C., Kachergus, J., Roumier, C., Mouroux, V., Douay, X., Lincoln, S., Levecque, C., Larvor, L., Andrieux, J. & Hulihan, M. 2004. α-Synuclein locus duplication as a cause of familial Parkinson's disease. *The Lancet,* 364**,** 1167-1169.

Chen, P. E., Specht, C. G., Morris, R. G. & Schoepfer, R. 2002. Spatial learning is unimpaired in mice containing a deletion of the alpha‐synuclein locus. *European Journal of Neuroscience,* 16**,** 154-158.

Chinen, Y., Higa, T., Tomatsu, S., Suzuki, Y., Orii, T. & Hyakuna, N. 2014. Long-term therapeutic efficacy of allogenic bone marrow transplantation in a patient with mucopolysaccharidosis IVA. *Molecular genetics and metabolism reports,* 1**,** 31-41.

Choi, D.-H., Kim, Y.-J., Kim, Y.-G., Joh, T. H., Beal, M. F. & Kim, Y.-S. 2011. Role of matrix metalloproteinase 3-mediated α-synuclein cleavage in dopaminergic cell death. *Journal of Biological Chemistry,* 286**,** 14168-14177.

Clarke, L. A., Randall, D. R. & Sinclair, G. 2012. Mucopolysaccharidosis (MPS) diagnostic methods, systems, kits and assays associated therewith. Patent No. 8,105,788. 31 Jan. 2012.

Clayton, D. F. & George, J. M. 1998. The synucleins: a family of proteins involved in synaptic function, plasticity, neurodegeneration and disease. *Trends in Neurosciences,* 21**,** 249-254.

Cleary, M. & Wraith, J. 1993. Management of mucopolysaccharidosis type III. *Archives of Disease in Childhood,* 69**,** 403-406.

Collier, T. J., Redmond, D. E., Steece-Collier, K., Lipton, J. W. & Manfredsson, F. P. 2016. Is Alpha-Synuclein Loss-of-Function a Contributor to Parkinsonian Pathology? Evidence from Non-human Primates. *Frontiers in Neuroscience,* 10**,** 12.

Constantopoulos, G. & Dekaban, A. S. 1978. Neurochemistry of the mucopolysaccharidoses: brain lipids and lysosomal enzymes in patients with four types of mucopolysaccharidosis and in normal controls. *Journal of Neurochemistry,* 30**,** 965-973.

Constantopoulos, G., Iqbal, K. & Dekaban, A. S. 1980. Mucopolysaccharidosis types IH, IS, II and IIIA: glycosaminoglycans and lipids of isolated brain cells and other fractions from autopsied tissues. *Journal of Neurochemistry,* 34**,** 1399-1411.

Conway, K., Lee, S. J., Rochet, J. C., Ding, T., Harper, J., Williamson, R. & Lansbury, P. 2000a. Accelerated Oligomerization by Parkinson's Disease Linked α - Synuclein Mutants. *Annals of the New York Academy of Sciences,* 920**,** 42-45.

Conway, K. A., Lee, S.-J., Rochet, J.-C., Ding, T. T., Williamson, R. E. & Lansbury, P. T. 2000b. Acceleration of oligomerization, not fibrillization, is a shared property of both α-synuclein mutations linked to early-onset Parkinson's disease: implications for pathogenesis and therapy. *Proceedings of the National Academy of Sciences,* 97**,** 571-576.

Corrochano, S., Renna, M., Carter, S., Chrobot, N., Kent, R., Stewart, M., Cooper, J., Brown, S. D., Rubinsztein, D. C. & Acevedo-Arozena, A. 2012. alpha-Synuclein levels modulate Huntington's disease in mice. *Human Molecular Genetics,* 21**,** 485-94.

Coutinho, M. F., Prata, M. J. & Alves, S. 2012. Mannose-6-phosphate pathway: a review on its role in lysosomal function and dysfunction. *Molecular Genetics and Metabolism,* 105**,** 542-550.

Crawley, A. C., Gliddon, B. L., Auclair, D., Brodie, S. L., Hirte, C., King, B. M., Fuller, M., Hemsley, K. M. & Hopwood, J. J. 2006. Characterization of a C57BL/6 congenic mouse strain of mucopolysaccharidosis type IIIA. *Brain Research,* 1104**,** 1-17.

Crowther, R., Olesen, O., Jakes, R. & Goedert, M. 1992. The microtubule binding repeats of tau protein assemble into filaments like those found in Alzheimer's disease. *FEBS Letters,* 309**,** 199-202.

Cuervo, A. M., Stefanis, L., Fredenburg, R., Lansbury, P. T. & Sulzer, D. 2004. Impaired degradation of mutant α-synuclein by chaperone-mediated autophagy. *Science,* 305**,** 1292-1295.

Cullen, V., Lindfors, M., Ng, J., Paetau, A., Swinton, E., Kolodziej, P., Boston, H., Saftig, P., Woulfe, J. & Feany, M. B. 2009. Cathepsin D expression level affects alpha-synuclein processing, aggregation, and toxicity in vivo. *Molecular Brain,* 2**,** 1.

Dauer, W., Kholodilov, N., Vila, M., Trillat, A.-C., Goodchild, R., Larsen, K. E., Staal, R., Tieu, K., Schmitz, Y. & Yuan, C. A. 2002. Resistance of α-synuclein null mice to the parkinsonian neurotoxin MPTP. *Proceedings of the National Academy of Sciences,* 99**,** 14524-14529.

Davidson, W. S., Jonas, A., Clayton, D. F. & George, J. M. 1998. Stabilization of α-synuclein secondary structure upon binding to synthetic membranes. *Journal of Biological Chemistry,* 273**,** 9443-9449.

Davis, M. 1992. The role of the amygdala in fear and anxiety. *Annual Review of Neuroscience,* 15**,** 353-375.

De Duve, C., Pressman, B., Gianetto, R., Wattiaux, R. & Appelmans, F. 1955. Tissue fractionation studies. 6. Intracellular distribution patterns of enzymes in rat-liver tissue. *Biochemical Journal,* 60**,** 604.

De Ruijter, J., Valstar, M. J. & Wijburg, F. A. 2011. Mucopolysaccharidosis type III (sanfilippo syndrome): Emerging treatment strategies. *Current Pharmaceutical Biotechnology,* 12**,** 923-930.

Demartino, G. N. & Gillette, T. G. 2007. Proteasomes: machines for all reasons. *Cell,* 129**,** 659-662.

Deng, H., Xiu, X. & Jankovic, J. 2015. Genetic convergence of Parkinson's disease and lysosomal storage disorders. *Molecular Neurobiology,* 51**,** 1554-1568.

Dennissen, F., Kholod, N. & Van Leeuwen, F. 2012. The ubiquitin proteasome system in neurodegenerative diseases: culprit, accomplice or victim? *Progress in Neurobiology,* 96**,** 190-207.

Dermentzaki, G., Dimitriou, E., Xilouri, M., Michelakakis, H. & Stefanis, L. 2013. Loss of β-Glucocerebrosidase Activity Does Not Affect Alpha-Synuclein Levels or Lysosomal Function in Neuronal Cells. *PloS One,* 8**,** e60674.

Devine, M. J., Gwinn, K., Singleton, A. & Hardy, J. 2011. Parkinson's disease and alpha-synuclein expression. *Movement Disorders,* 26**,** 2160-8.

Dirosario, J., Divers, E., Wang, C., Etter, J., Charrier, A., Jukkola, P., Auer, H., Best, V., Newsom, D. L. & Mccarty, D. M. 2009. Innate and adaptive immune activation in the brain of MPS IIIB mouse model. *Journal of Neuroscience Research,* 87**,** 978-990.

Drury, M. 2014. Freezing of Gait: What to do when the Parkinson's Medications do not work. *AJON,* 24**,** 52.

Dufty, B. M., Warner, L. R., Hou, S. T., Jiang, S. X., Gomez-Isla, T., Leenhouts, K. M., Oxford, J. T., Feany, M. B., Masliah, E. & Rohn, T. T. 2007. Calpain-cleavage of α-synuclein: connecting proteolytic processing to disease-linked aggregation. *The American journal of pathology,* 170**,** 1725-1738.

Duncan, F. J., Naughton, B. J., Zaraspe, K., Murrey, D. A., Meadows, A. S., Clark, K. R., Newsom, D. E., White, P., Fu, H. & Mccarty, D. M. 2015. Broad functional correction of molecular impairments by systemic delivery of scAAVrh74-hSGSH gene delivery in MPS IIIA mice. *Molecular Therapy,* 23**,** 638-647.

Ebrahimi-Fakhari, D., Cantuti-Castelvetri, I., Fan, Z., Rockenstein, E., Masliah, E., Hyman, B. T., Mclean, P. J. & Unni, V. K. 2011. Distinct roles in vivo for the ubiquitin–proteasome system

and the autophagy–lysosomal pathway in the degradation of α-synuclein. *The Journal of Neuroscience,* 31**,** 14508-14520.

Fan, Y., Limprasert, P., Murray, I. V., Smith, A. C., Lee, V. M.-Y., Trojanowski, J. Q., Sopher, B. L. & La Spada, A. R. 2006. β-synuclein modulates α-synuclein neurotoxicity by reducing α-synuclein protein expression. *Human Molecular Genetics,* 15**,** 3002-3011.

Felson, D. 2001. The metabolic and molecular bases of inherited disease. Taylor & Francis.

Fischer, A., Carmichael, K. P., Munnell, J. F., Jhabvala, P., Thompson, J. N., Matalon, R., Jezyk, P. F., Wang, P. & Giger, U. 1998. Sulfamidase deficiency in a family of Dachshunds: a canine model of mucopolysaccharidosis IIIA (Sanfilippo A). *Pediatric Research,* 44**,** 74-82.

Folch, J., Lees, M. & Sloane-Stanley, G. 1957. A simple method for the isolation and purification of total lipids from animal tissues. *Journal of Biological Chemistry,* 226**,** 497-509.

Fornai, F., Schlüter, O. M., Lenzi, P., Gesi, M., Ruffoli, R., Ferrucci, M., Lazzeri, G., Busceti, C. L., Pontarelli, F. & Battaglia, G. 2005. Parkinson-like syndrome induced by continuous MPTP infusion: convergent roles of the ubiquitin-proteasome system and α-synuclein. *Proceedings of the National Academy of Sciences of the United States of America,* 102**,** 3413-3418.

Fraldi, A., Annunziata, F., Lombardi, A., Kaiser, H. J., Medina, D. L., Spampanato, C., Fedele, A. O., Polishchuk, R., Sorrentino, N. C. & Simons, K. 2010. Lysosomal fusion and SNARE function are impaired by cholesterol accumulation in lysosomal storage disorders. *The EMBO journal,* 29**,** 3607-3620.

Fraldi, A., Hemsley, K., Crawley, A., Lombardi, A., Lau, A., Sutherland, L., Auricchio, A., Ballabio, A. & Hopwood, J. J. 2007. Functional correction of CNS lesions in an MPS-IIIA mouse model by intracerebral AAV-mediated delivery of sulfamidase and SUMF1 genes. *Human Molecular Genetics,* 16**,** 2693-2702.

Gaugler, M. N., Genc, O., Bobela, W., Mohanna, S., Ardah, M. T., El-Agnaf, O. M., Cantoni, M., Bensadoun, J.-C., Schneggenburger, R. & Knott, G. W. 2012. Nigrostriatal overabundance of α-synuclein leads to decreased vesicle density and deficits in dopamine release that correlate with reduced motor activity. *Acta Neuropathologica,* 123**,** 653-669.

George, S., Van Den Buuse, M., San Mok, S., Masters, C. L., Li, Q.-X. & Culvenor, J. G. 2008. α-Synuclein transgenic mice exhibit reduced anxiety-like behaviour. *Experimental Neurology,* 210**,** 788-792.

Ghosh, P., Dahms, N. M. & Kornfeld, S. 2003. Mannose 6-phosphate receptors: new twists in the tale. *Nature reviews Molecular cell biology,* 4**,** 202-213.

Gifford, S. R., Scheie, H. G., Hambrick, G. W. & Barness, L. A. 1962. A newly recognized forme fruste of Hurler's disease (gargoylism). *American Journal of Ophthalmology,* 53**,** 753-769.

Giugliani, R. 2012. Mucopolysacccharidoses: From understanding to treatment, a century of discoveries. *Genetics and Molecular Biology,* 35**,** 924-931.

Glickman, M. H. & Ciechanover, A. 2002. The ubiquitin-proteasome proteolytic pathway: destruction for the sake of construction. *Physiological Reviews,* 82**,** 373-428.

Gliddon, B. L. & Hopwood, J. J. 2004. Enzyme-replacement therapy from birth delays the development of behavior and learning problems in mucopolysaccharidosis type IIIA mice. *Pediatric Research,* 56**,** 65-72.

Gregg, T. R. & Siegel, A. 2001. Brain structures and neurotansmitters regulating aggression in cats: implications for human aggression. *Progress in Neuro-Psychopharmacology and Biological Psychiatry,* 25**,** 91-140.

Greten-Harrison, B., Polydoro, M., Morimoto-Tomita, M., Diao, L., Williams, A. M., Nie, E. H., Makani, S., Tian, N., Castillo, P. E. & Buchman, V. L. 2010. αβγ-Synuclein triple knockout mice reveal age-dependent neuronal dysfunction. *Proceedings of the National Academy of Sciences,* 107**,** 19573-19578.

Gureviciene, I., Gurevicius, K. & Tanila, H. 2007. Role of α-synuclein in synaptic glutamate release. *Neurobiology of Disease,* 28**,** 83-89.

Hall, C. & Ballachey, E. L. 1932. A study of the rat's behavior in a field. A contribution to method in comparative psychology. *University of California Publications in Psychology,* Vol 6, 1-12.

Hamano, K., Hayashi, M., Shioda, K., Fukatsu, R. & Mizutani, S. 2008a. Mechanisms of neurodegeneration in mucopolysaccharidoses II and IIIB: analysis of human brain tissue. *Acta Neuropathologica,* 115**,** 547-559.

Hamano, T., Gendron, T. F., Causevic, E., Yen, S. H., Lin, W. L., Isidoro, C., Deture, M. & Ko, L. W. 2008b. Autophagic‐lysosomal perturbation enhances tau aggregation in transfectants with induced wild‐type tau expression. *European Journal of Neuroscience,* 27**,** 1119-1130.

Hara, T., Nakamura, K., Matsui, M., Yamamoto, A., Nakahara, Y., Suzuki-Migishima, R., Yokoyama, M., Mishima, K., Saito, I. & Okano, H. 2006. Suppression of basal autophagy in neural cells causes neurodegenerative disease in mice. *Nature,* 441**,** 885-889.

Hassiotis, S., Beard, H., Luck, A., Trim, P. J., King, B., Snel, M. F., Hopwood, J. J. & Hemsley, K. M. 2014. Disease stage determines the efficacy of treatment of a paediatric neurodegenerative disease. *European Journal of Neuroscience,* 39**,** 2139-2150.

Haurigot, V., Marcó, S., Ribera, A., Garcia, M., Ruzo, A., Villacampa, P., Ayuso, E., Añor, S., Andaluz, A. & Pineda, M. 2013. Whole body correction of mucopolysaccharidosis IIIA by intracerebrospinal fluid gene therapy. *The Journal of clinical investigation,* 123**,** 3254-3271.

Hemsley, K., Beard, H., King, B. & Hopwood, J. 2008. Effect of high dose, repeated intra‐cerebrospinal fluid injection of sulphamidase on neuropathology in mucopolysaccharidosis type IIIA mice. *Genes, Brain and Behavior,* 7**,** 740-753.

Hemsley, K. M. & Hopwood, J. J. 2005. Development of motor deficits in a murine model of mucopolysaccharidosis type IIIA (MPS-IIIA). *Behavioural Brain Research,* 158**,** 191-199.

Hemsley, K. M., King, B. & Hopwood, J. J. 2007. Injection of recombinant human sulfamidase into the CSF via the cerebellomedullary cistern in MPS IIIA mice. *Molecular Genetics and Metabolism,* 90**,** 313-328.

Hemsley, K. M., Luck, A. J., Crawley, A. C., Hassiotis, S., Beard, H., King, B., Rozek, T., Rozaklis, T., Fuller, M. & Hopwood, J. J. 2009. Examination of intravenous and intra‐CSF protein delivery for treatment of neurological disease. *European Journal of Neuroscience,* 29**,** 1197-1214.

Hernandez, F. & Avila, J. 2007. Tauopathies. *Cellular and Molecular Life Sciences,* 64**,** 2219-2233.

Hers, H. 1963. α-Glucosidase deficiency in generalized glycogen-storage disease (Pompe's disease). *Biochemical Journal,* 86**,** 11.

Heuer, G. G., Passini, M. A., Jiang, K., Parente, M. K., Lee, V. M. Y., Trojanowski, J. Q. & Wolfe, J. H. 2002. Selective neurodegeneration in murine mucopolysaccharidosis VII is progressive and reversible. *Annals of Neurology,* 52**,** 762-770.

Higashi, Y., Murayama, S., Pentchev, P. & Suzuki, K. 1993. Cerebellar degeneration in the Niemann-Pick type C mouse. *Acta Neuropathologica,* 85**,** 175-184.

Hopwood, J. & Brooks, D. 1997. An introduction to the basic science and biology of the lysosome and storage diseases. *Applegatrh, DA, Dimmick, JE, Hall, JG, eds. Organelle diseases. New York: Chapman & Hall Medical 1977; 7,* 35.

Hopwood, J. J. & Morris, C. P. 1990. The mucopolysaccharidoses. Diagnosis, molecular genetics and treatment. *Molecular Biology and Medicine,* 7**,** 381-404.

Hopwood, J. J., Vellodi, A., Scott, H., Morris, C., Litjens, T., Clements, P., Brooks, D., Cooper, A. & Wraith, J. 1993. Long-term clinical progress in bone marrow transplanted mucopolysaccharidosis type I patients with a defined genotype. *Journal of Inherited Metabolic Disease,* 16**,** 1024-1033.

Hunter, C. 1917. A rare disease in two brothers. *Proceedings of the Royal Society of Medicine,* 10**,** 104.

Hurler, G. 1920. Über einen Typ multipler Abartungen, vorwiegend am Skelettsystem. *European Journal of Pediatrics,* 24**,** 220-234.

Imundo, L., Leduc, C. A., Guha, S., Brown, M., Perino, G., Gushulak, L., Triggs-Raine, B. & Chung, W. K. 2011. A complete deficiency of Hyaluronoglucosaminidase 1 (HYAL1) presenting as familial juvenile idiopathic arthritis. *Journal of Inherited Metabolic Disease,* 34**,** 1013-1022.

Inzelberg, R. & Korczyn, A. 1994. Parkinsonism in adult‐onset GM2 gangliosidosis. *Movement Disorders,* 9**,** 375-377.

Isaac, E. L., Karageorgos, L. E., Brooks, D. A., Hopwood, J. J. & Meikle, P. J. 2000. Regulation of the lysosome-associated membrane protein in a sucrose model of lysosomal storage. *Experimental Cell Research,* 254**,** 204-209.

Iwai, A., Masliah, E., Yoshimoto, M., Ge, N., Flanagan, L., De Silva, H. R., Kittel, A. & Saitoh, T. 1995. The precursor protein of non-Aβ component of Alzheimer's disease amyloid is a presynaptic protein of the central nervous system. *Neuron,* 14**,** 467-475.

Jakes, R., Spillantini, M. G. & Goedert, M. 1994. Identification of two distinct synucleins from human brain. *FEBS Letters,* 345**,** 27-32.

Jeyakumar, M., Dwek, R. A., Butters, T. D. & Platt, F. M. 2005. Storage solutions: treating lysosomal disorders of the brain. *Nature Reviews: Neuroscience,* 6**,** 713-725.

Jeyakumar, M., Smith, D. A., Williams, I. M., Borja, M. C., Neville, D. C., Butters, T. D., Dwek, R. A. & Platt, F. M. 2004. NSAIDs increase survival in the Sandhoff disease mouse: Synergy with N‐butyldeoxynojirimycin. *Annals of Neurology,* 56**,** 642-649.

Ji, H., Liu, Y. E., Jia, T., Wang, M., Liu, J., Xiao, G., Joseph, B. K., Rosen, C. & Shi, Y. E. 1997. Identification of a breast cancer-specific gene, BCSG1, by direct differential cDNA sequencing. *Cancer Research,* 57**,** 759-764.

Johnson, D. E., Ostrowski, P., Jaumouillé, V. & Grinstein, S. 2016. The position of lysosomes within the cell determines their luminal pH. *The Journal of cell biology,* 212**,** 677-692.

Jolly, R., Allan, F., Collett, M., Rozaklis, T., Muller, V. & Hopwood, J. 2000. Mucopolysaccharidosis IIIA (Sanfilippo syndrome) in a New Zealand Huntaway dog with ataxia. *New Zealand Veterinary Journal,* 48**,** 144-148.

Kaidonis, X., Byers, S., Ranieri, E., Sharp, P., Fletcher, J. & Derrick-Roberts, A. 2016. N-butyldeoxynojirimycin treatment restores the innate fear response and improves learning in mucopolysaccharidosis IIIA mice. *Molecular Genetics and Metabolism,* 118**,** 100-110.

Kalivendi, S. V., Yedlapudi, D., Hillard, C. J. & Kalyanaraman, B. 2010. Oxidants induce alternative splicing of α-synuclein: Implications for Parkinson's disease. *Free Radical Biology and Medicine,* 48**,** 377-383.

Karageorgos, L. E., Guo, X.-H., Blanch, L., Weber, B., Anson, D. S., Scott, H. S. & Hopwood, J. J. 1996. Structure and sequence of the human sulphamidase gene. *DNA Research,* 3**,** 269-271.

Karageorgos, L. E., Isaac, E. L., Brooks, D. A., Ravenscroft, E. M., Davey, R., Hopwood, J. J. & Meikle, P. J. 1997. Lysosomal biogenesis in lysosomal storage disorders. *Experimental Cell Research,* 234**,** 85-97.

Kasai, T., Tokuda, T., Yamaguchi, N., Watanabe, Y., Kametani, F., Nakagawa, M. & Mizuno, T. 2008. Cleavage of normal and pathological forms of α-synuclein by neurosin in vitro. *Neuroscience Letters,* 436**,** 52-56.

Keatinge, M., Bui, H., Menke, A., Chen, Y.-C., Sokol, A. M., Bai, Q., Ellett, F., Da Costa, M., Burke, D. & Gegg, M. 2015. Glucocerebrosidase 1 deficient Danio rerio mirror key pathological aspects of human Gaucher disease and provide evidence of early microglial activation preceding alpha-synuclein-independent neuronal cell death. *Human Molecular Genetics,* 24**,** 6640-6652.

Kim, T.-H., Choi, J., Kim, H.-G. & Kim, H. R. 2014. Quantification of neurotransmitters in mouse brain tissue by using liquid chromatography coupled electrospray tandem mass spectrometry. *Journal of analytical methods in chemistry,* 141, 12, 3686–3695.

King, B., Savas, P., Fuller, M., Hopwood, J. & Hemsley, K. 2006. Validation of a heparan sulfate-derived disaccharide as a marker of accumulation in murine mucopolysaccharidosis type IIIA. *Molecular Genetics and Metabolism,* 87**,** 107-112.

Kiselyov, K., Jennings Jr, J. J., Rbaibi, Y. & Chu, C. T. 2007. Autophagy, mitochondria and cell death in lysosomal storage diseases. *Autophagy,* 3**,** 259-262.

Kjellén, L. & Lindahl, U. 1991. Proteoglycans: structures and interactions. *Annual Review of Biochemistry,* 60**,** 443-475.

Kokhan, V., Afanasyeva, M. & Van'kin, G. 2012. α-Synuclein knockout mice have cognitive impairments. *Behavioural Brain Research,* 231**,** 226-230.

Komatsu, M., Waguri, S., Chiba, T., Murata, S., Iwata, J.-I., Tanida, I., Ueno, T., Koike, M., Uchiyama, Y. & Kominami, E. 2006. Loss of autophagy in the central nervous system causes neurodegeneration in mice. *Nature,* 441**,** 880-884.

Korolchuk, V. I., Mansilla, A., Menzies, F. M. & Rubinsztein, D. C. 2009. Autophagy inhibition compromises degradation of ubiquitin-proteasome pathway substrates. *Molecular Cell,* 33**,** 517-527.

Kowalewski, B., Lamanna, W. C., Lawrence, R., Damme, M., Stroobants, S., Padva, M., Kalus, I., Frese, M.-A., Lübke, T. & Lüllmann-Rauch, R. 2012. Arylsulfatase G inactivation causes loss of heparan sulfate 3-O-sulfatase activity and mucopolysaccharidosis in mice. *Proceedings of the National Academy of Sciences,* 109**,** 10310-10315.

Kresse, H. 1973. Mucopolysaccharidosis III A (Sanfilippo A disease): Deficiency of a heparin sulfamidase in skin fibroblasts and leucocytes. *Biochemical and Biophysical Research Communications,* 54**,** 1111-1118.

Kresse, H. & Neufeld, E. F. 1972. The Sanfilippo A Corrective Factor: PURIFICATION AND MODE OF ACTION. *Journal of Biological Chemistry,* 247**,** 2164-2170.

Langford-Smith, A., Langford-Smith, K. J., Jones, S. A., Wynn, R. F., Wraith, J., Wilkinson, F. L. & Bigger, B. W. 2011. Female mucopolysaccharidosis IIIA mice exhibit hyperactivity and a reduced sense of danger in the open field test. *PloS One,* 6**,** e25717.

Lashuel, H. A., Overk, C. R., Oueslati, A. & Masliah, E. 2012. The many faces of α-synuclein: from structure and toxicity to therapeutic target. *Nature Reviews Neuroscience,* 14**,** 38-48.

Lau, A. A., Crawley, A. C., Hopwood, J. J. & Hemsley, K. M. 2008. Open field locomotor activity and anxiety-related behaviors in mucopolysaccharidosis type IIIA mice. *Behavioural Brain Research,* 191**,** 130-136.

Lau, A. A., Hannouche, H., Rozaklis, T., Hassiotis, S., Hopwood, J. J. & Hemsley, K. M. 2010. Allogeneic stem cell transplantation does not improve neurological deficits in mucopolysaccharidosis type IIIA mice. *Experimental Neurology,* 225**,** 445-454.

Lavedan, C. 1998. The synuclein family. *Genome Research,* 8**,** 871-880.

Lee, B. R. & Kamitani, T. 2011. Improved immunodetection of endogenous α-synuclein. *PloS One,* 6**,** e23939.

Lee, H.-J., Khoshaghideh, F., Patel, S. & Lee, S.-J. 2004. Clearance of α-synuclein oligomeric intermediates via the lysosomal degradation pathway. *The Journal of neuroscience,* 24**,** 1888-1896.

Lesage, S., Anheim, M., Condroyer, C., Pollak, P., Durif, F., Dupuits, C., Viallet, F., Lohmann, E., Corvol, J.-C. & Honoré, A. 2011. Large-scale screening of the Gaucher's disease-related glucocerebrosidase gene in Europeans with Parkinson's disease. *Human Molecular Genetics,* 20**,** 202-210.

Lesage, S., Anheim, M., Letournel, F., Bousset, L., Honoré, A., Rozas, N., Pieri, L., Madiona, K., Dürr, A. & Melki, R. 2013. G51D α - synuclein mutation causes a novel Parkinsonian – pyramidal syndrome. *Annals of Neurology,* 73**,** 459-471.

Levine, B. & Klionsky, D. J. 2004. Development by self-digestion: molecular mechanisms and biological functions of autophagy. *Developmental Cell,* 6**,** 463-477.

Limongelli, G. & Fratta, F. 2011. S1.4 Cardiovascular involvement in Pompe disease. *Acta Myologica,* 30**,** 202-203.

Lowe, J., Blanchard, A., Morrell, K., Lennox, G., Reynolds, L., Billett, M., Landon, M. & Mayer, R. J. 1988. Ubiquitin is a common factor in intermediate filament inclusion bodies of diverse type in man, including those of Parkinson's disease, Pick's disease, and Alzheimer's disease, as well as Rosenthal fibres in cerebellar astrocytomas, cytoplasmic bodies in muscle, and mallory bodies in alcoholic liver disease. *The Journal of pathology,* 155**,** 9-15.

Lozano, M. M., Liu, Z., Sunnick, E., Janshoff, A., Kumar, K. & Boxer, S. G. 2013. Colocalization of the ganglioside GM1 and cholesterol detected by secondary ion mass spectrometry. *Journal of the American Chemical Society,* 135**,** 5620-5630.

Machiya, Y., Hara, S., Arawaka, S., Fukushima, S., Sato, H., Sakamoto, M., Koyama, S. & Kato, T. 2010. Phosphorylated α-synuclein at Ser-129 is targeted to the proteasome pathway in a ubiquitin-independent manner. *Journal of Biological Chemistry,* 285**,** 40732-40744.

Macúchová, E., Ševčíková, M., Hrebíčková, I., Nohejlová, K. & Šlamberová, R. 2016. How various drugs affect anxiety-related behavior in male and female rats prenatally exposed to methamphetamine. *International Journal of Developmental Neuroscience,* 51**,** 1-11.

Mahalingam, K., Janani, S., Priya, S., Elango, E. & Sundari, R. M. 2004. Diagnosis of mucopolysaccharidoses: how to avoid false positives and false negatives. *The Indian Journal of Pediatrics,* 71**,** 29-32.

Mak, S. K., Mccormack, A. L., Manning-Bog, A. B., Cuervo, A. M. & Di Monte, D. A. 2010. Lysosomal degradation of alpha-synuclein in vivo. *Journal of Biological Chemistry,* 285**,** 13621-9.

Malinowska, M., Wilkinson, F. L., Bennett, W., Langford-Smith, K. J., O'leary, H. A., Jakobkiewicz-Banecka, J., Wynn, R., Wraith, J. E., Wegrzyn, G. & Bigger, B. W. 2009.

Genistein reduces lysosomal storage in peripheral tissues of mucopolysaccharide IIIB mice. *Molecular Genetics and Metabolism,* 98**,** 235-242.

Manning-Boğ, A. B., Mccormack, A. L., Purisai, M. G., Bolin, L. M. & Di Monte, D. A. 2003. α-Synuclein overexpression protects against paraquat-induced neurodegeneration. *The Journal of neuroscience,* 23**,** 3095-3099.

Maroteaux, L., Campanelli, J. T. & Scheller, R. H. 1988. Synuclein: a neuron-specific protein localized to the nucleus and presynaptic nerve terminal. *Journal of Neuroscience,* 8**,** 2804-2815.

Maroteaux, L. & Scheller, R. 1991. The rat brain synucleins; family of proteins transiently associated with neuronal membrane. *Molecular brain research,* 11**,** 335-343.

Maroteaux, P., Leveque, B., Marie, J. & Lamy, M. 1963. [A new dysostosis with urinary elimination of chondroitin sulfate B.]. *La Presse medicale,* 71**,** 1849-1852.

Martin, D. D., Ladha, S., Ehrnhoefer, D. E. & Hayden, M. R. 2015. Autophagy in Huntington disease and huntingtin in autophagy. *Trends in Neurosciences,* 38**,** 26-35.

Martins, C., Hůlková, H., Dridi, L., Dormoy-Raclet, V., Grigoryeva, L., Choi, Y., Langford-Smith, A., Wilkinson, F. L., Ohmi, K., Dicristo, G., Hamel, E., Ausseil, J., Cheillan, D., Moreau, A., Svobodová, E., Hájková, Z., Tesařová, M., Hansíková, H., Bigger, B. W., Hrebícek, M. & Pshezhetsky, A. V. 2015. Neuroinflammation, mitochondrial defects and neurodegeneration in mucopolysaccharidosis III type C mouse model. *Brain,* 138**,** 336-355.

Mata, I. F., Samii, A., Schneer, S. H., Roberts, J. W., Griffith, A., Leis, B. C., Schellenberg, G. D., Sidransky, E., Bird, T. D. & Leverenz, J. B. 2008. Glucocerebrosidase gene mutations: a risk factor for Lewy body disorders. *Archives of Neurology,* 65**,** 379.

Mazzulli, J. R., Xu, Y.-H., Sun, Y., Knight, A. L., Mclean, P. J., Caldwell, G. A., Sidransky, E., Grabowski, G. A. & Krainc, D. 2011. Gaucher disease glucocerebrosidase and α-synuclein form a bidirectional pathogenic loop in synucleinopathies. *Cell,* 146**,** 37-52.

Mcglynn, R., Dobrenis, K. & Walkley, S. U. 2004. Differential subcellular localization of cholesterol, gangliosides, and glycosaminoglycans in murine models of mucopolysaccharide storage disorders. *Journal of Comparative Neurology,* 480**,** 415-426.

Meikle, P. J. & Hopwood, J. J. 2003. Lysosomal storage disorders: emerging therapeutic options require early diagnosis. *European Journal of Pediatrics,* 162**,** S34-S37.

Meikle, P. J., Hopwood, J. J., Clague, A. E. & Carey, W. F. 1999. Prevalence of lysosomal storage disorders. *JAMA,* 281**,** 249-54.

Meredith, G. E. & Kang, U. J. 2006. Behavioral models of Parkinson's disease in rodents: a new look at an old problem. *Movement Disorders,* 21**,** 1595-1606.

Miller, T., Goude, M. C., Mcdevitt, T. C. & Temenoff, J. S. 2014. Molecular engineering of glycosaminoglycan chemistry for biomolecule delivery. *Acta biomaterialia,* 10**,** 1705-1719.

Mollenhauer, B., Locascio, J. J., Schulz-Schaeffer, W., Sixel-Döring, F., Trenkwalder, C. & Schlossmacher, M. G. 2011. α-Synuclein and tau concentrations in cerebrospinal fluid of patients presenting with parkinsonism: a cohort study. *The Lancet Neurology,* 10**,** 230-240.

Moraitou, M., Hadjigeorgiou, G., Monopolis, I., Dardiotis, E., Bozi, M., Vassilatis, D., Vilageliu, L., Grinberg, D., Xiromerisiou, G. & Stefanis, L. 2011. β-Glucocerebrosidase gene mutations in two cohorts of Greek patients with sporadic Parkinson's disease. *Molecular Genetics and Metabolism,* 104**,** 149-152.

Morris, R. 1984. Developments of a water-maze procedure for studying spatial learning in the rat. *Journal of Neuroscience Methods,* 11**,** 47-60.

Muenzer, J. 2004. The mucopolysaccharidoses: a heterogeneous group of disorders with variable pediatric presentations. *Journal of Pediatrics,* 144**,** S27-34.

Muenzer, J. 2011. Overview of the mucopolysaccharidoses. *Rheumatology,* 50**,** v4-v12.

Muntane, G., Dalfo, E., Martinez, A. & Ferrer, I. 2008. Phosphorylation of tau and α-synuclein in synaptic-enriched fractions of the frontal cortex in Alzheimer's disease, and in Parkinson's disease and related α-synucleinopathies. *Neuroscience,* 152**,** 913-923.

Natowicz, M. R., Short, M. P., Wang, Y., Dickersin, G. R., Gebhardt, M. C., Rosenthal, D. I., Sims, K. B. & Rosenberg, A. E. 1996. Clinical and biochemical manifestations of hyaluronidase deficiency. *New England Journal of Medicine,* 335**,** 1029-1033.

Nemani, V. M., Lu, W., Berge, V., Nakamura, K., Onoa, B., Lee, M. K., Chaudhry, F. A., Nicoll, R. A. & Edwards, R. H. 2010. Increased expression of α-synuclein reduces neurotransmitter release by inhibiting synaptic vesicle reclustering after endocytosis. *Neuron,* 65**,** 66-79.

Neufeld, E. F. 1991. Lysosomal storage diseases. *Annual Review of Biochemistry,* 60**,** 257-280.

Neufeld, E. F. & Muenzer, J. 2001. *The mucopolysaccharidoses. In: The Metabolic and Molecular Bases of Inherited Disease,* McGraw-Hill.

Neumann, J., Bras, J., Deas, E., O'sullivan, S. S., Parkkinen, L., Lachmann, R. H., Li, A., Holton, J., Guerreiro, R., Paudel, R., Segarane, B., Singleton, A., Lees, A., Hardy, J., Houlden, H., Revesz, T. & Wood, N. W. 2009. Glucocerebrosidase mutations in clinical and pathologically proven Parkinson's disease. *Brain,* 132**,** 1783-94.

Nidiffer, F. & Kelly, T. 1983. Developmental and degenerative patterns associated with cognitive, behavioural and motor difficulties in the Sanfilippo syndrome: an epidemiological study. *Journal of Intellectual Disability Research,* 27**,** 185-203.

Nijssen, P. C., Brusse, E., Leyten, A., Martin, J.-J., Teepen, J. L. & Roos, R. A. 2002. Autosomal dominant adult neuronal ceroid lipofuscinosis: parkinsonism due to both striatal and nigral dysfunction. *Movement Disorders,* 17**,** 482-487.

Ninkina, N., Connor-Robson, N., Ustyugov, A. A., Tarasova, T. V., Shelkovnikova, T. A. & Buchman, V. L. 2015. A novel resource for studying function and dysfunction of α-synuclein: mouse lines for modulation of endogenous Snca gene expression. *Scientific Reports,* 5, 16615.

Nishioka, K., Ross, O. A., Vilariño-Güell, C., Cobb, S. A., Kachergus, J. M., Mann, D. M. A., Snowden, J., Richardson, A. M. T., Neary, D., Robinson, C. A., Rajput, A., Papapetropoulos, S., Mash, D. C., Pahwa, R., Lyons, K. E., Wszolek, Z. K., Dickson, D. W. & Farrer, M. J. 2011.

Glucocerebrosidase mutations in diffuse Lewy body disease. *Parkinsonism & Related Disorders,* 17**,** 55-57.

Novikoff, A., Runling, B., Drucker, J. & Kaplan, S. Uptake of proteins and their intracellular fate-a cytochemical and electron microscopic study Journal of Histochemistry and Cytochemistry, 1960. Histochemical soc inc Univ Washington, Dept biostructure, box 357420, Seattle, Wa 98195 319-320.

Oaks, A. W. & Sidhu, A. 2011. Synuclein modulation of monoamine transporters. *FEBS Letters,* 585**,** 1001-1006.

Obeso, J. A., Rodriguez-Oroz, M. C., Goetz, C. G., Marin, C., Kordower, J. H., Rodriguez, M., Hirsch, E. C., Farrer, M., Schapira, A. H. & Halliday, G. 2010. Missing pieces in the Parkinson's disease puzzle. *Nature Medicine,* 16**,** 653-661.

Ohmi, K., Greenberg, D. S., Rajavel, K. S., Ryazantsev, S., Li, H. H. & Neufeld, E. F. 2003. Activated microglia in cortex of mouse models of mucopolysaccharidoses I and IIIB. *Proceedings of the National Academy of Sciences,* 100**,** 1902-1907.

Ohmi, K., Kudo, L. C., Ryazantsev, S., Zhao, H. Z., Karsten, S. L. & Neufeld, E. F. 2009. Sanfilippo syndrome type B, a lysosomal storage disease, is also a tauopathy. *Proceedings of the National Academy of Sciences of the United States of America,* 106**,** 8332-7.

Ohmi, K., Zhao, H. Z. & Neufeld, E. F. 2011. Defects in the medial entorhinal cortex and dentate gyrus in the mouse model of Sanfilippo syndrome type B. *PloS One,* 6**,** e27461.

Outeiro, T. F., Putcha, P., Tetzlaff, J. E., Spoelgen, R., Koker, M., Carvalho, F., Hyman, B. T. & Mclean, P. J. 2008. Formation of toxic oligomeric α-synuclein species in living cells. *PloS One,* 3**,** e1867.

Park, J. S., Mehta, P., Cooper, A. A., Veivers, D., Heimbach, A., Stiller, B., Kubisch, C., Fung, V. S., Krainc, D., Mackay-Sim, A. & Sue, C. M. 2011. Pathogenic effects of novel mutations in the P-type ATPase ATP13A2 (PARK9) causing Kufor-Rakeb syndrome, a form of early-onset parkinsonism. *Human Mutation,* 32**,** 956-64.

Pastores, G. M. 2011. Lysosomal storage diseases. *Neurochemical Mechanisms in Disease.* Springer New York, 785-797.

Patterson, M. C., Vecchio, D., Jacklin, E., Abel, L., Chadha-Boreham, H., Luzy, C., Giorgino, R. & Wraith, J. E. 2010. Long-term miglustat therapy in children with Niemann-Pick disease type C. *Journal of Child Neurology,* 25**,** 300-305.

Paxinos, G. & Franklin, K. B. 2004. *The mouse brain in stereotaxic coordinates*, Gulf Professional Publishing, English Book; Illustrated, 1.

Pchelina, S., Nuzhnyi, E., Emelyanov, A., Boukina, T., Usenko, T., Nikolaev, M., Salogub, G., Yakimovskii, A. & Zakharova, E. Y. 2014. Increased plasma oligomeric alpha-synuclein in patients with lysosomal storage diseases. *Neuroscience Letters,* 583**,** 188-193.

Pelkonen, A. & Yavich, L. 2011. Neuromuscular pathology in mice lacking alpha-synuclein. *Neuroscience Letters,* 487**,** 350-353.

Pellow, S., Chopin, P., File, S. E. & Briley, M. 1985. Validation of open: closed arm entries in an elevated plus-maze as a measure of anxiety in the rat. *Journal of Neuroscience Methods,* 14**,** 149-167.

Peña-Oliver, Y., Buchman, V. L. & Stephens, D. N. 2010. Lack of involvement of alpha-synuclein in unconditioned anxiety in mice. *Behavioural Brain Research,* 209**,** 234-240.

Peters, C. & Steward, C. 2003. Hematopoietic cell transplantation for inherited metabolic diseases: an overview of outcomes and practice guidelines. *Bone Marrow Transplantation,* 31**,** 229-239.

Petersen, G. M., Rotter, J. I., Cantor, R. M., Field, L. L., Greenwald, S., Lim, J., Roy, C., Schoenfeld, V., Lowden, J. A. & Kaback, M. M. 1983. The Tay-Sachs disease gene in North American Jewish populations: geographic variations and origin. *American Journal of Human Genetics,* 35**,** 1258.

Poorthuis, B. J., Wevers, R. A., Kleijer, W. J., Groener, J. E., De Jong, J. G., Van Weely, S., Niezen-Koning, K. E. & Van Diggelen, O. P. 1999. The frequency of lysosomal storage diseases in The Netherlands. *Human Genetics,* 105**,** 151-156.

Pringsheim, T., Jette, N., Frolkis, A. & Steeves, T. D. 2014. The prevalence of Parkinson's disease: A systematic review and meta‐analysis. *Movement Disorders,* 29**,** 1583-1590.

Qiao, L., Hamamichi, S., Caldwell, K. A., Caldwell, G. A., Yacoubian, T. A., Wilson, S., Xie, Z.-L., Speake, L. D., Parks, R., Crabtree, D., Liang, Q., Crimmins, S., Schneider, L., Uchiyama, Y., Iwatsubo, T., Zhou, Y., Peng, L., Lu, Y., Standaert, D. G., Walls, K. C., Shacka, J. J., Roth, K. A. & Zhang, J. 2008. Lysosomal enzyme cathepsin D protects against alpha-synuclein aggregation and toxicity. *Molecular Brain,* 1**,** 17.

Qiao, L. & Zhang, J. 2009. Inhibition of lysosomal functions reduces proteasomal activity. *Neuroscience Letters,* 456**,** 15-19.

Ravikumar, B., Duden, R. & Rubinsztein, D. C. 2002. Aggregate-prone proteins with polyglutamine and polyalanine expansions are degraded by autophagy. *Human Molecular Genetics,* 11**,** 1107-1117.

Ravikumar, B., Vacher, C., Berger, Z., Davies, J. E., Luo, S., Oroz, L. G., Scaravilli, F., Easton, D. F., Duden, R. & O'kane, C. J. 2004. Inhibition of mTOR induces autophagy and reduces toxicity of polyglutamine expansions in fly and mouse models of Huntington disease. *Nature Genetics,* 36**,** 585-595.

Reizes, O., Lincecum, J., Wang, Z., Goldberger, O., Huang, L., Kaksonen, M., Ahima, R., Hinkes, M. T., Barsh, G. S. & Rauvala, H. 2001. Transgenic expression of syndecan-1 uncovers a physiological control of feeding behavior by syndecan-3. *Cell,* 106**,** 105-116.

Richard, M., Arfi, A., Rhinn, H., Gandolphe, C. & Scherman, D. 2008. Identification of new markers for neurodegeneration process in the mouse model of Sly disease as revealed by expression profiling of selected genes. *Journal of Neuroscience Research,* 86**,** 3285-3294.

Rivers, R. C., Kumita, J. R., Tartaglia, G. G., Dedmon, M. M., Pawar, A., Vendruscolo, M., Dobson, C. M. & Christodoulou, J. 2008. Molecular determinants of the aggregation behavior of α‐and β‐synuclein. *Protein Science,* 17**,** 887-898.

Roberts, A. L., Howarth, G. S., Liaw, W. C., Moretta, S., Kritas, S., Lymn, K. A., Yazbeck, R., Tran, C., Fletcher, J. M. & Butler, R. N. 2009. Gastrointestinal pathology in a mouse model of mucopolysaccharidosis type IIIA. *Journal of Cellular Physiology,* 219**,** 259-264.

Roberts, A. L., Thomas, B. J., Wilkinson, A. S., Fletcher, J. M. & Byers, S. 2006. Inhibition of glycosaminoglycan synthesis using rhodamine B in a mouse model of mucopolysaccharidosis type IIIA. *Pediatric Research,* 60**,** 309-314.

Robertson, D. C., Schmidt, O., Ninkina, N., Jones, P. A., Sharkey, J. & Buchman, V. L. 2004. Developmental loss and resistance to MPTP toxicity of dopaminergic neurones in substantia nigra pars compacta of γ - synuclein, α - synuclein and double α / γ - synuclein null mutant mice. *Journal of Neurochemistry,* 89**,** 1126-1136.

Rockenstein, E., Nuber, S., Overk, C. R., Ubhi, K., Mante, M., Patrick, C., Adame, A., Trejo-Morales, M., Gerez, J. & Picotti, P. 2014. Accumulation of oligomer-prone α-synuclein exacerbates synaptic and neuronal degeneration in vivo. *Brain,* 137**,** 1496-1513.

Rodgers, R. & Dalvi, A. 1997. Anxiety, defence and the elevated plus-maze. *Neuroscience and Biobehavioral Reviews,* 21**,** 801-810.

Rose, C., Menzies, F. M., Renna, M., Acevedo-Arozena, A., Corrochano, S., Sadiq, O., Brown, S. D. & Rubinsztein, D. C. 2010. Rilmenidine attenuates toxicity of polyglutamine expansions in a mouse model of Huntington's disease. *Human Molecular Genetics,* 19**,** 2144-2153.

Rubinsztein, D. C. 2006. The roles of intracellular protein-degradation pathways in neurodegeneration. *Nature,* 443**,** 780-786.

Saftig, P. & Klumperman, J. 2009. Lysosome biogenesis and lysosomal membrane proteins: trafficking meets function. *Nature reviews Molecular cell biology,* 10**,** 623-635.

Saito, Y., Suzuki, K., Hulette, C. M. & Murayama, S. 2004. Aberrant Phosphorylation of α - Synuclein in Human Niemann - Pick Type C1 Disease. *Journal of Neuropathology and Experimental Neurology,* 63**,** 323-328.

Samii, A., Nutt, J. G. & Ransom, B. R. 2004. Parkinson's disease. *The Lancet,* 363**,** 1783-1793.

Sandi, C., Loscertales, M. & Guaza, C. 1997. Experience - dependent facilitating effect of corticosterone on spatial memory formation in the water maze. *European Journal of Neuroscience,* 9**,** 637-642.

Sanfilippo, S. J., Podosin, R., Langer, L. & Good, R. A. 1963. Mental retardation associated with acid mucopolysaccharidurie (heparitin sulfate type). *The Journal of Pediatrics,* 63**,** 837-838.

Sardi, S. P., Clarke, J., Kinnecom, C., Tamsett, T. J., Li, L., Stanek, L. M., Passini, M. A., Grabowski, G. A., Schlossmacher, M. G. & Sidman, R. L. 2011. CNS expression of glucocerebrosidase corrects α-synuclein pathology and memory in a mouse model of Gaucher-related synucleinopathy. *Proceedings of the National Academy of Sciences,* 108**,** 12101-12106.

Sardi, S. P., Clarke, J., Viel, C., Chan, M., Tamsett, T. J., Treleaven, C. M., Bu, J., Sweet, L., Passini, M. A. & Dodge, J. C. 2013. Augmenting CNS glucocerebrosidase activity as a

therapeutic strategy for parkinsonism and other Gaucher-related synucleinopathies. *Proceedings of the National Academy of Sciences,* 110**,** 3537-3542.

Savas, P. S., Hemsley, K. M. & Hopwood, J. J. 2004. Intracerebral injection of sulfamidase delays neuropathology in murine MPS-IIIA. *Molecular Genetics and Metabolism,* 82**,** 273-285.

Schaefer, L. 2014. Proteoglycans, key regulators of cell–matrix dynamics. *Matrix Biology,* 35**,** 1-2.

Schiffmann, R., Fitzgibbon, E. J., Harris, C., Devile, C., Davies, E. H., Abel, L., Van Schaik, I. N., Benko, W. S., Timmons, M. & Ries, M. 2008. Randomized, controlled trial of miglustat in Gaucher's disease type 3. *Annals of Neurology,* 64**,** 514-522.

Scott, H. S., Blanch, L., Guo, X., Freeman, C., Orsborn, A., Baker, E., Sutherland, G., Morris, C. & Hopwood, J. 1995. Cloning of the sulphamidase gene and identification of mutations in Sanfilippo A syndrome. *Nature Genetics,* 11.

Selkoe, D., Dettmer, U., Luth, E., Kim, N., Newman, A. & Bartels, T. 2014. Defining the native state of α-synuclein. *Neurodegenerative Diseases,* 13**,** 114-117.

Senior, S. L., Ninkina, N., Deacon, R., Bannerman, D., Buchman, V. L., Cragg, S. J. & Wade‐Martins, R. 2008. Increased striatal dopamine release and hyperdopaminergic‐like behaviour in mice lacking both alpha‐synuclein and gamma‐synuclein. *European Journal of Neuroscience,* 27**,** 947-957.

Settembre, C., Fraldi, A., Jahreiss, L., Spampanato, C., Venturi, C., Medina, D., De Pablo, R., Tacchetti, C., Rubinsztein, D. C. & Ballabio, A. 2008. A block of autophagy in lysosomal storage disorders. *Human Molecular Genetics,* 17**,** 119-129.

Settembre, C., Fraldi, A., Medina, D. L. & Ballabio, A. 2013. Signals from the lysosome: a control centre for cellular clearance and energy metabolism. *Nature reviews Molecular cell biology,* 14**,** 283-296.

Sevlever, D., Jiang, P. & Yen, S.-H. C. 2008. Cathepsin D Is the Main Lysosomal Enzyme Involved in the Degradation of α-Synuclein and Generation of Its Carboxy-Terminally Truncated Species†. *Biochemistry,* 47**,** 9678-9687.

Shachar, T., Bianco, C. L., Recchia, A., Wiessner, C., Raas‐Rothschild, A. & Futerman, A. H. 2011. Lysosomal storage disorders and Parkinson's disease: Gaucher disease and beyond. *Movement Disorders,* 26**,** 1593-1604.

Shen, H.-M. & Mizushima, N. 2014. At the end of the autophagic road: an emerging understanding of lysosomal functions in autophagy. *Trends in Biochemical Sciences,* 39**,** 61-71.

Sidhu, N. S., Schreiber, K., Propper, K., Becker, S., Usón, I., Sheldrick, G. M., Gartner, J., Kratzner, R. & Steinfeld, R. 2014. Structure of sulfamidase provides insight into the molecular pathology of mucopolysaccharidosis IIIA. *Acta Crystallographica Section D: Biological Crystallography,* 70**,** 1321-1335.

Sidransky, E., Nalls, M. A., Aasly, J. O., Aharon-Peretz, J., Annesi, G., Barbosa, E. R., Bar-Shira, A., Berg, D., Bras, J. & Brice, A. 2009. Multicenter analysis of glucocerebrosidase mutations in Parkinson's disease. *New England Journal of Medicine,* 361**,** 1651-1661.

Siebert, M., Sidransky, E. & Westbroek, W. 2014. Glucocerebrosidase is shaking up the synucleinopathies. *Brain***,** 1304-1322

Singleton, A., Farrer, M., Johnson, J., Singleton, A., Hague, S., Kachergus, J., Hulihan, M., Peuralinna, T., Dutra, A. & Nussbaum, R. 2003. α-Synuclein locus triplication causes Parkinson's disease. *Science,* 302**,** 841-841.

Sivakumur, P. & Wraith, J. 1999. Bone marrow transplantation in mucopolysaccharidosis type IIIA: a comparison of an early treated patient with his untreated sibling. *Journal of Inherited Metabolic Disease,* 22**,** 849-850.

Sly, W. S., Quinton, B. A., Mcalister, W. H. & Rimoin, D. L. 1973. Beta glucuronidase deficiency: report of clinical, radiologic, and biochemical features of a new mucopolysaccharidosis. *The Journal of pediatrics,* 82**,** 249-257.

Smith, D., Wallom, K.-L., Williams, I. M., Jeyakumar, M. & Platt, F. M. 2009. Beneficial effects of anti-inflammatory therapy in a mouse model of Niemann-Pick disease type C1. *Neurobiology of Disease,* 36**,** 242-251.

Smith, P. K., Krohn, R. I., Hermanson, G., Mallia, A., Gartner, F., Provenzano, M., Fujimoto, E., Goeke, N., Olson, B. & Klenk, D. 1985. Measurement of protein using bicinchoninic acid. *Analytical Biochemistry,* 150**,** 76-85.

Sohar, I., Sleat, D., Chang-Gong, L., Ludwig, T. & Lobel, P. 1998. Mouse mutants lacking the cation-independent mannose 6-phosphate/insulin-like growth factor II receptor are impaired in lysosomal enzyme transport: comparison of cation-independent and cation-dependent mannose 6-phosphate receptor-deficient mice. *Biochemical Journal,* 330**,** 903-908.

Sorrentino, N. C., D'orsi, L., Sambri, I., Nusco, E., Monaco, C., Spampanato, C., Polishchuk, E., Saccone, P., De Leonibus, E. & Ballabio, A. 2013. A highly secreted sulphamidase engineered to cross the blood‐brain barrier corrects brain lesions of mice with mucopolysaccharidoses type IIIA. *EMBO Molecular Medicine,* 5**,** 675-690.

Sorrentino, P., Barbato, A., Del Gaudio, L., Rucco, R., Varriale, P., Sibilio, M., Strazzullo, P., Sorrentino, G. & Agosti, V. 2016. Impaired gait kinematics in type 1 Gaucher's Disease. *Journal of Parkinson's Disease***,** 1-5.

Specht, C. G. & Schoepfer, R. 2001. Deletion of the alpha-synuclein locus in a subpopulation of C57BL/6J inbred mice. *BMC Neuroscience,* 2**,** 11.

Spencer, B., Potkar, R., Trejo, M., Rockenstein, E., Patrick, C., Gindi, R., Adame, A., Wyss-Coray, T. & Masliah, E. 2009. Beclin 1 gene transfer activates autophagy and ameliorates the neurodegenerative pathology in α-synuclein models of Parkinson's and Lewy body diseases. *The Journal of Neuroscience,* 29**,** 13578-13588.

Spillantini, M. G., Schmidt, M. L., Lee, V. M.-Y., Trojanowski, J. Q., Jakes, R. & Goedert, M. 1997. α-Synuclein in Lewy bodies. *Nature,* 388**,** 839-840.

Staba, S. L., Escolar, M. L., Poe, M., Kim, Y., Martin, P. L., Szabolcs, P., Allison-Thacker, J., Wood, S., Wenger, D. A. & Rubinstein, P. 2004. Cord-blood transplants from unrelated donors in patients with Hurler's syndrome. *New England Journal of Medicine,* 350**,** 1960-1969.

Staretz-Chacham, O., Lang, T. C., Lamarca, M. E., Krasnewich, D. & Sidransky, E. 2009. Lysosomal storage disorders in the newborn. *Pediatrics,* 123**,** 1191-1207.

Steinberg, H., Sykes, E. A., Mcbride, A., Terry, P., Robinson, K. & Tillotson, H. 1989. Computer analysis, using a digitizer, of ataxic mouse gait due to drugs. *Journal of Pharmacological Methods,* 21**,** 103-113.

Sui, Y.-T., Bullock, K. M., Erickson, M. A., Zhang, J. & Banks, W. A. 2014. Alpha synuclein is transported into and out of the brain by the blood–brain barrier. *Peptides,* 62**,** 197-202.

Tan, J., Zhang, T., Jiang, L., Chi, J., Hu, D., Pan, Q., Wang, D. & Zhang, Z. 2011. Regulation of intracellular manganese homeostasis by Kufor-Rakeb syndrome-associated ATP13A2 protein. *Journal of Biological Chemistry,* 286**,** 29654-62.

Tardieu, M., Zérah, M., Husson, B., De Bournonville, S., Deiva, K., Adamsbaum, C., Vincent, F., Hocquemiller, M., Broissand, C. & Furlan, V. 2014. Intracerebral administration of adeno-associated viral vector serotype rh. 10 carrying human SGSH and SUMF1 cDNAs in children with mucopolysaccharidosis type IIIA disease: results of a phase I/II trial. *Human Gene Therapy,* 25**,** 506-516.

Thayanidhi, N., Helm, J. R., Nycz, D. C., Bentley, M., Liang, Y. & Hay, J. C. 2010. α-Synuclein delays endoplasmic reticulum (ER)-to-Golgi transport in mammalian cells by antagonizing ER/Golgi SNAREs. *Molecular Biology of the Cell,* 21**,** 1850-1863.

Tobe, T., Nakajo, S., Tanaka, A., Mitoya, A., Omata, K., Nakaya, K., Tomita, M. & Nakamura, Y. 1992. Cloning and Characterization of the cDNA Encoding a Novel Brain‐Specific 14‐kDa Protein. *Journal of Neurochemistry,* 59**,** 1624-1629.

Tomás-Zapico, C., Díez-Zaera, M., Ferrer, I., Gómez-Ramos, P., Morán, M. A., Miras-Portugal, M. T., Díaz-Hernández, M. & Lucas, J. J. 2012. α-Synuclein accumulates in huntingtin inclusions but forms independent filaments and its deficiency attenuates early phenotype in a mouse model of Huntington's disease. *Human Molecular Genetics,* 21**,** 495-510.

Trim, P. J., Hopwood, J. J. & Snel, M. F. 2015. Butanolysis derivatization: improved sensitivity in LC-MS/MS quantitation of heparan sulfate in urine from mucopolysaccharidosis patients. *Analytical Chemistry,* 87**,** 9243-9250.

Trim, P. J., Lau, A. A., Hopwood, J. J. & Snel, M. F. 2014. A simple method for early age phenotype confirmation using toe tissue from a mouse model of MPS IIIA. *Rapid Communications in Mass Spectrometry,* 28**,** 933-938.

Uéda, K., Fukushima, H., Masliah, E., Xia, Y., Iwai, A., Yoshimoto, M., Otero, D., Kondo, J., Ihara, Y. & Saitoh, T. 1993. Molecular cloning of cDNA encoding an unrecognized component of amyloid in Alzheimer disease. *Proceedings of the National Academy of Sciences,* 90**,** 11282-11286.

Usenovic, M., Tresse, E., Mazzulli, J. R., Taylor, J. P. & Krainc, D. 2012. Deficiency of ATP13A2 leads to lysosomal dysfunction, α-synuclein accumulation, and neurotoxicity. *The Journal of Neuroscience,* 32**,** 4240-4246.

Valstar, M., Ruijter, G., Van Diggelen, O., Poorthuis, B. & Wijburg, F. 2008. Sanfilippo syndrome: a mini-review. *Journal of Inherited Metabolic Disease,* 31**,** 240-252.

Valstar, M. J., Neijs, S., Bruggenwirth, H. T., Olmer, R., Ruijter, G. J., Wevers, R. A., Van Diggelen, O. P., Poorthuis, B. J., Halley, D. J. & Wijburg, F. A. 2010. Mucopolysaccharidosis type IIIA: Clinical spectrum and genotype ‐ phenotype correlations. *Annals of Neurology,* 68**,** 876-887.

Vellodi, A., Young, E., Cooper, A., Lidchi, V., Winchester, B. & Wraith, J. 1999. Long-term follow-up following bone marrow transplantation for Hunter disease. *Journal of Inherited Metabolic Disease,* 22**,** 638-648.

Venda, L. L., Cragg, S. J., Buchman, V. L. & Wade-Martins, R. 2010. α-Synuclein and dopamine at the crossroads of Parkinson's disease. *Trends in Neurosciences,* 33**,** 559-568.

Villani, G. R., Di Domenico, C., Musella, A., Cecere, F., Di Napoli, D. & Di Natale, P. 2009. Mucopolysaccharidosis IIIB: oxidative damage and cytotoxic cell involvement in the neuronal pathogenesis. *Brain Research,* 1279**,** 99-108.

Villani, G. R., Gargiulo, N., Faraonio, R., Castaldo, S., Gonzalez Y Reyero, E. & Di Natale, P. 2007. Cytokines, neurotrophins, and oxidative stress in brain disease from mucopolysaccharidosis IIIB. *Journal of Neuroscience Research,* 85**,** 612-622.

Vogiatzi, T., Xilouri, M., Vekrellis, K. & Stefanis, L. 2008. Wild type α-synuclein is degraded by chaperone-mediated autophagy and macroautophagy in neuronal cells. *Journal of Biological Chemistry,* 283**,** 23542-23556.

Võikar, V., Rauvala, H. & Ikonen, E. 2002. Cognitive deficit and development of motor impairment in a mouse model of Niemann-Pick type C disease. *Behavioural Brain Research,* 132**,** 1-10.

Volkow, N. D., Gur, R. C., Wang, G.-J., Fowler, J. S., Moberg, P. J., Ding, Y.-S., Hitzemann, R., Smith, G. & Logan, J. 1998. Association between decline in brain dopamine activity with age and cognitive and motor impairment in healthy individuals. *American Journal of Psychiatry,* 155**,** 344-349.

Volpicelli-Daley, L. A., Luk, K. C., Patel, T. P., Tanik, S. A., Riddle, D. M., Stieber, A., Meaney, D. F., Trojanowski, J. Q. & Lee, V. M.-Y. 2011. Exogenous α-synuclein fibrils induce Lewy body pathology leading to synaptic dysfunction and neuron death. *Neuron,* 72**,** 57-71.

Wada, R., Tifft, C. J. & Proia, R. L. 2000. Microglial activation precedes acute neurodegeneration in Sandhoff disease and is suppressed by bone marrow transplantation. *Proceedings of the National Academy of Sciences,* 97**,** 10954-10959.

Walkley, S. U. Secondary accumulation of gangliosides in lysosomal storage disorders. Seminars in Cell and Developmental Biology, 2004. Elsevier, 433-444.

Walkley, S. U. & Suzuki, K. 2004. Consequences of NPC1 and NPC2 loss of function in mammalian neurons. *Biochimica et Biophysica Acta (BBA)-Molecular and Cell Biology of Lipids,* 1685**,** 48-62.

Wang, W., Perovic, I., Chittuluru, J., Kaganovich, A., Nguyen, L. T., Liao, J., Auclair, J. R., Johnson, D., Landeru, A. & Simorellis, A. K. 2011. A soluble α-synuclein construct forms a dynamic tetramer. *Proceedings of the National Academy of Sciences,* 108**,** 17797-17802.

Wang, X. H., Lu, G., Hu, X., Tsang, K. S., Kwong, W. H., Wu, F. X., Meng, H. W., Jiang, S., Liu, S. W. & Ng, H. K. 2012. Quantitative assessment of gait and neurochemical correlation in a classical murine model of Parkinson's disease. *BMC Neuroscience,* 13**,** 1.

Webb, J. L., Ravikumar, B., Atkins, J., Skepper, J. N. & Rubinsztein, D. C. 2003. α-Synuclein is degraded by both autophagy and the proteasome. *Journal of Biological Chemistry,* 278**,** 25009-25013.

Wei, H., Kim, S.-J., Zhang, Z., Tsai, P.-C., Wisniewski, K. E. & Mukherjee, A. B. 2008. ER and oxidative stresses are common mediators of apoptosis in both neurodegenerative and non-neurodegenerative lysosomal storage disorders and are alleviated by chemical chaperones. *Human Molecular Genetics,* 17**,** 469-477.

Whitley, C. B. 1993. The mucopolysaccharidoses. *McKusick s Heritable Disorders of Connective Tissue. St Louis: Mosby***,** 367-498.

Wilkinson, F. L., Holley, R. J., Langford-Smith, K. J., Badrinath, S., Liao, A., Langford-Smith, A., Cooper, J. D., Jones, S. A., Wraith, J. E., Wynn, R. F., Merry, C. L. R. & Bigger, B. W. 2012. Neuropathology in Mouse Models of Mucopolysaccharidosis Type I, IIIA and IIIB. *PloS One,* 7**,** e35787.

Winder-Rhodes, S. E., Garcia-Reitböck, P., Ban, M., Evans, J. R., Jacques, T. S., Kemppinen, A., Foltynie, T., Williams-Gray, C. H., Chinnery, P. F., Hudson, G., Burn, D. J., Allcock, L. M., Sawcer, S. J., Barker, R. A. & Spillantini, M. G. 2012. Genetic and pathological links between Parkinson's disease and the lysosomal disorder Sanfilippo syndrome. *Movement Disorders,* 27**,** 312-315.

Winner, B., Jappelli, R., Maji, S. K., Desplats, P. A., Boyer, L., Aigner, S., Hetzer, C., Loher, T., Vilar, M. & Campioni, S. 2011. In vivo demonstration that α-synuclein oligomers are toxic. *Proceedings of the National Academy of Sciences,* 108**,** 4194-4199.

Winner, L. K., Beard, H., Hassiotis, S., Lau, A. A., Luck, A. J., Hopwood, J. J. & Hemsley, K. M. 2016. A preclinical study evaluating AAVrh10-based gene therapy for Sanfilippo syndrome. *Human Gene Therapy,* 27**,** 363-375.

Woloszynek, J. C., Coleman, T., Semenkovich, C. F. & Sands, M. S. 2007. Lysosomal dysfunction results in altered energy balance. *Journal of Biological Chemistry,* 282**,** 35765-35771.

Woloszynek, J. C., Kovacs, A., Ohlemiller, K. K., Roberts, M. & Sands, M. S. 2009. Metabolic adaptations to interrupted glycosaminoglycan recycling. *Journal of Biological Chemistry,* 284**,** 29684-29691.

Wong, K., Sidransky, E., Verma, A., Mixon, T., Sandberg, G. D., Wakefield, L. K., Morrison, A., Lwin, A., Colegial, C. & Allman, J. M. 2004. Neuropathology provides clues to the pathophysiology of Gaucher disease. *Molecular Genetics and Metabolism,* 82**,** 192-207.

Wu, G., Lu, Z.-H., Kulkarni, N., Amin, R. & Ledeen, R. W. 2011. Mice lacking major brain gangliosides develop parkinsonism. *Neurochemical Research,* 36**,** 1706-1714.

Xilouri, M., Brekk, O. R. & Stefanis, L. 2013. Alpha-synuclein and protein degradation systems: a reciprocal relationship. *Molecular Neurobiology,* 47**,** 537-551.

Zcharia, E., Metzger, S., Chajek-Shaul, T., Aingorn, H., Elkin, M., Friedmann, Y., Weinstein, T., Li, J.-P., Lindahl, U. & Vlodavsky, I. 2004. Transgenic expression of mammalian heparanase uncovers physiological functions of heparan sulfate in tissue morphogenesis, vascularization, and feeding behavior. *The FASEB Journal,* 18**,** 252-263.

Zhang, L., Sheng, R. & Qin, Z. 2009. The lysosome and neurodegenerative diseases. *Acta biochimica et biophysica Sinica,* 41**,** 437-445.

Zhou, W., Hurlbert, M. S., Schaack, J., Prasad, K. N. & Freed, C. R. 2000. Overexpression of human α-synuclein causes dopamine neuron death in rat primary culture and immortalized mesencephalon-derived cells. *Brain Research,* 866**,** 33-43.